Surface Engineering of Hybrid Joints for Sub-Assembly

A thesis submitted by

Mahsa Esfahani, B. SC. Eng., M.Sc. Eng.

To

Faculty of Science, Engineering and Technology

In total fulfilment of the requirements for the degree of

Doctor of Philosophy

Swinburne University of Technology

Victoria 3122, Australia

2017

Abstract

Greenhouse emissions and global warming are major issues around the world and have motivated the automotive industry to reduce the weight of vehicles in order to reduce fuel consumption. Therefore, the application of light materials such as Al and Mg have increased within vehicles in recent years, and led to the development of self-pierce riveting which has been a promising technique for joining dissimilar materials in the automotive industry. However, the life cycle of self-pierce riveted joint is at risk without the application of a suitable coating to the rivet.

In this thesis a benchmarking of commercially available self-piercing rivets with various coatings such as mechanically plated Zn-Sn, Almac and electroplated Al coatings were used for joining Mg sheets. Evaluation of the joints showed that Al coatings remain intact under the joining process. However, thickness of Zn-Sn and Almac coatings increased at the top sheet and decreased at the bottom sheets due to the exertion of joining force.

Nanocrystalline zinc-tin coatings have been fabricated as an advanced coating with improved mechanical and corrosion properties for the protection of self-piercing rivets. Electrodeposition of nanocrystalline zinc from environmental friendly electrolyte (sulfate-gluconate) were performed as an introduction to the deposition of nanocrystalline zinc-tin coatings and provided fundamental understandings of electroplating of zinc alloys. Electrodeposition of zinc from sulfate and sulfate-gluconate electrolytes in the presence and absence of additives was investigated. Simulation of equilibrium distribution of zinc (II) species in both sulfate and sulfate-gluconate electrolytes showed that $ZnSO_4$ was the main species in both sulfate and sulfate-gluconate electrolytes. Voltammetric analysis and potentiostatic experiments showed that although $ZnSO_4$ had high concentration in both sulfate and sulfate-gluconate electrolytes, zinc-gluconate ($Zn(GH_4)^+$) species played a significant role in the reduction process. Effects of gluconate complex agent on the deposition of zinc was confirmed by evaluation of the surface morphology and the texture of electrodeposited zinc on mild steel substrate. Synergistic effects of additives resulted in the formation of zinc coatings with nano grain sizes for both sulfate and sulfate-gluconate electrolytes with the same preferred orientation. X-ray diffraction patterns indicated that the effects of ligands from which zinc deposition occurred became negligible in the presence of all additives.

Electrodeposition of zinc-tin alloy coatings from acidic sulfate and sulfate-gluconate bath in the presence of various additives was investigated by cyclic voltammetry, scanning electrode microscopy and X-ray diffraction. Gluconate as a complex agent changed the deposition potential of tin and moved it to more negative values and deposition potential of zinc to more positive values and thereby facilitate deposition of zinc-tin alloy. Effects of pulse plating parameters such as current on-time (T_{ON}) and current off-time (T_{OFF}) on the surface morphology of the deposits was investigated. The optimum plating conditions (T_{ON}= 5 ms, T_{OFF} = 7 ms and j = 0.046 A/cm^2) was chosen for the continuation of the experiments. Effects of various additives such as thiourea, hexadecyltrimethylammonium bromide (CTAB) and polyethylene glycol (PEG) with various molecular weights ($\bar{M}_n$= 400 and $\bar{M}_n$= 2050 g mol^{-1}) were investigated on the morphology and grain refinement of electrodeposited zinc-tin coatings. Nanocrystalline zinc-tin coatings with low content tin were only fabricated from gluconate electrolytes under the optimum plating parameters and in the presence of PEG ($\bar{M}_n$= 2050 g mol^{-1}) and CTAB.

In order to evaluate effects of grain refinement down to nano levels on mechanical and corrosion properties of coatings, nanocrystalline (NC) (average grain size = 79.99 ± 18.70 nm) and ultra-fine-grained (UFG) (average grain size = 423.35 ± 46.88 nm) Zn-Sn coatings were compared. Surface profile parameters such as mean roughness improved by grain refinement down to nano level. NC coatings exhibited superior mechanical properties such as hardness, lower coefficient of friction and lower wear volume than UFG coatings.

Corrosion properties of nanocrystalline and ultra-fine-grained coatings were studied. Corrosion of Zn-Sn alloys in this study started with the selective dissolution of zinc. Although nanocrystalline coating exhibited lower corrosion potential than ultra-fine-grained coatings they corroded with a smaller rate than ultra-fine-grained coatings. Corrosion products of nanocrystalline coatings have better barrier properties than ultra-fine-grained coatings as they are more compact and can prevent corrosion more effectively.

“The whole of science is nothing more than a refinement of everyday thinking”

Albert Einstein (1879 – 1955)

Dedication

This dissertation is dedicated to

The loving memory of my Father, who always lives in my heart

My Mother, the greatest symbol of love

My Daughter, the sweat meaning of my life

And

My patient Husband, the hero of my heart

Acknowledgments

I would like to express my sincere gratitude and my deep appreciation to various people who supported me during the past years of my PhD research work.

I wish to take this opportunity to bring my appreciation to all my Supervisors Dr. Yat Choy Wong, Dr. Yvonne Durandet, Dr. James Wang and Dr. Jie Zhang for their academic guidance. Also, once more my sincere thanks to Dr. Jie Zhang from Monash University who provided me an opportunity to join his research team, and who gave me access to his laboratory and his research facilities. Without his precious support and academic guidance it would not be possible to conduct this research.

My sincere thanks go to Dr. Peter Mahon and Dr. Aimim Yu who gave me access to the laboratory and research facilities in School of science at Swinburne University of Technology.

My deep gratitude to Prof. Cuie Wen and her PhD student Mr Khurram Shahzad Munir from RMIT University who helped me for conducting all nanoindentation analysis.

I would like to thank technical staff of the department, Mr Andrew Moore and Mr Brain Dempster, for their help in resolving my technical issues and making all my required stuff.

This research was financially supported by Excellerate Australia (previously known as Auto CRC), I would like to thank them for let me be part of their research team.

I thank my fellow labmates at Monash University for the stimulating discussions and for the knowledge they shared with me. I am a material engineer and had a little knowledge of electrochemistry, all members of Dr. Jie Zhang research group helped me to get through electrochemistry and taught me any necessary skills that I needed for performing my electrochemistry experiments. Also I would like to thank my office mates Dr. Scott Daniel and Dr. Alaa Al-Mosawe who always encouraged me during the hard times of my PhD research work.

Last but not the least, I would like to thank my family: my decedent father who always lives in my hearth, my beloved mother, my sisters and my brother for supporting me spiritually throughout this thesis. I have to specially appreciate my beautiful daughter

who missed the joy of having a fulltime mum in early stages of her life and most importantly, I appreciate my husband deeply from my soul and my heart. My thesis would never be possible without his unconditional love, support, encouragement and understanding.

Declaration

I **Mahsa Esfahani,** declare that this dissertation does not contain any material which has been accepted for the award to the candidate of any other degree or diploma, except where due reference has been made. To the best of my knowledge, this dissertation contains no material previously published or written by another person except where due reference has been made. I warrant that I have obtained, where necessary, permission from the copyright owners to use any third party copyright material reproduced in the thesis (such as artwork, images, unpublished documents), or to use any of my own published work (such as journal articles) in which the copyright is held by another party (such as publisher, co-author).

This thesis has been written by me and any help that I have received throughout my study has been gratefully acknowledged.

Mahsa Esfahani

2017

Table of Contents

List of Figures

List of Tables

Chapter 1

Introduction

Global warming is a major issue all around the world and it simply means the rise in the annual average global surface temperature of the Earth in the range of 1.5°C to 4°C. The most important reason for global warming is carbon dioxide (CO_2) and greenhouse gases emissions. These gases prevent the release of thermal radiations from the Earth and lead to increase of its temperature [1]. The transportation system is highly dependent on petroleum-based fuels (a major contributor to CO_2 emissions) and products. The global transportation system consumes 40% of oil, close to 75 million barrels per day. Furthermore, the annual average growth rate of vehicle ownership is increasing by 5% around the globe. Consequently, a reduction of the weight of the automobile is necessary in order to reduce fuel consumption [2].

The automotive industry has been considered the application of light materials such as Al and Mg in automobile. For example, Al has been used instead of steel in the chassis of a car to provide fuel efficiency. Also, great attention has been paid to weight reduction of the body of the car as it stands for 30% of the total weight of a vehicle [3]. However, introduction of such light materials and their applications was not free from difficulties. In some cases, traditional manufacturing process was not applicable to new materials. The most important issue was the joining process as the traditional spot welding was not applicable to Al alloys and dissimilar materials. The response of the industry to this problem was self-pierce riveting (SPR) which was introduced half a century ago. Self-pierce riveting is a mechanical joining technique in which two or more sheets of materials are fasten together by a rivet. Life time of the joints is affected by corrosion and fretting. For example, joining Al sheets by high-strength steel rivets can cause galvanic corrosion. Also, the joint overlap and the gap between the rivet and the pierced sheet can lead to crevice corrosion [3]. Fretting leads to crack initiation and can reduce fatigue life of a SPR joint [4, 5]. Application of a coating with advanced mechanical and chemical properties would increase the service life of a SPR joint. In this regard, zinc-tin coatings are considered as a choice for steel rivets as these coatings offer sacrificial properties of zinc and barrier protection of tin to the steel rivet at the same time. Also these coatings provide good frictional properties and ductility which will fulfil the requirements of the riveting process.

Nanocrystalline materials are produced by controlling the microstructure at nanometric levels. These materials have grain sizes less than 100 nm in which more than 50 vol. % of atoms belong to grain boundaries or interfacial boundaries. Nanocrystalline materials and coatings exhibit different properties in comparison with microcrystalline materials. In most cases nanocrystalline materials show advanced mechanical properties than microcrystalline materials. For example, nanocrystalline materials show higher yield strength and hardness, and reduced tensile elongation in comparison with microcrystalline materials [6, 7].

Corrosion properties of the materials also vary with grain size. However, no general relationships between the grain size and corrosion properties have been established. Grain boundaries which are considered as high energy areas with high degree of disorder are considered as the potential points of the corrosion initiation. Therefore, in general view a deterioration of corrosion properties of materials with grain refinements down to nano scales are expected. However, the improvements of corrosion properties of nanocrystalline materials with the nano structure in comparison with their microcrystalline counterpart has been reported [8-14].

Nanocrystalline materials can be produced by various methods from vapor, solid and liquid routes. Electrodeposition [12, 15-24] is from the liquid route in which high purity and high density nanocrystalline material could be produced by this method.

The aim of this thesis is to investigate and improve mechanical and corrosion properties of the coating of steel self-piercing rivets with a general application for joining steel, Al, Mg and etc, sheets.

Nanocrystalline, ultra-fine-grained and microcrystalline zinc-tin coatings were fabricated successfully by an electrodeposition method from environmental friendly electrolytes. Chemical responses of the electrolytes were examined by cyclic voltammetry. The surface morphology of the coatings were examined by scanning electron microscopy and their chemical compositions were studied by energy dispersive spectroscopy (EDS). X-ray diffraction was conducted to study phase identification and preferred orientation. Effects of grain refinements on the corrosion and mechanical properties of the coatings were evaluated specifically by comparison of nanocrystalline and ultra-fine-grained coatings.

The thesis is organized as follows:

- A literature review in Chapter 2 is presented and explains a general view of self-piercing rivets, their application and the challenges involved in their use. Various methods of the production of coatings as a means of protecting the SPR joints are presented. Nanocrystalline materials are introduced and their advanced properties in comparison with microcrystalline material are presented.
- Experimental methods used in this thesis are described in Chapter 3. This Chapter introduces all the chemicals and materials used in this study; providing explanation of electrode preparation methods, coating synthesis method, electrochemical characterization methods and also include physical, chemical and structural characterization methods.
- Chapter 4 is a benchmarking of rivets with Zn-Sn, Almac and Al coatings. These coatings have been used to join magnesium sheets by laser assisted self-pierce riveting (LSPR). The microstructure, surface topography and roughness of the rivet’s coatings have been characterized by optical microscopy, scanning electron microscopy (SEM), energy-dispersive X-ray spectroscopy (EDS) and surface profilometry. The effects of the joining process on the coatings of the rivets have been evaluated.
- In Chapter 5 electrodeposition of zinc from sulfate and sulfate-gluconate electrolytes in the presence and absence of additives such as Polyethylene glycol (PEG), hexadecyltrimethylammonium bromide (CTAB) and thiourea has been investigated. Equilibrium distribution of zinc (II) species was evaluated in both sulfate and sulfate-gluconate electrolytes. The effects of gluconate ligand on the initial stages of zinc deposition were evaluated on glassy carbon electrode by means of cyclic voltammetry and chronoamperometry. The effects of the gluconate anions on surface morphology and texture of the zinc deposits on steel substrate were

characterized and compared with zinc deposit from sulfate bath without gluconate anions. The combined effects of gluconate ligand and additives on zinc electrodeposition was investigated by evaluating electrochemical responses of these electrolytes, and by characterizing the surface morphology and preferred orientation of the deposits.

- The main focus of Chapter 6 was on the production of nanocrystalline zinc-tin coatings with low content of Sn (less than 30 wt. %) by using additives and pulse electrodeposition from environmental friendly complex agents such as gluconic acid. CTAB, PEG (various molecular weights) and thiourea were used as additives individually and in a mixture for the modification of the structure. Effects of additives were discussed in terms of cyclic voltammetry of the plating bath on glassy carbon electrode, surface morphology, composition of the deposit and in some cases texture of the deposits on mild steel substrates have been evaluated.
- Chapter 7 presents a study of the effects of grain size on the mechanical properties of the coatings, two types of coatings with different grain sizes are presented and compared in this chapter. Nanocrystalline zinc-tin coatings with the average grain size of 79.99± 18.7 nm and ultra-fine-grained zinc-tin coatings with the average grain size of 423.35± 46.88 nm were produced. Characteristics of the coatings such as surface morphology, grain size and chemical composition are presented. In the next stage, surface profile and mechanical properties of both coatings are presented and discussed in terms of the effects of grain size.
- In Chapter 8 corrosion properties of nanocrystalline and ultra-fine-grained Zn-Sn coatings have been evaluated by the means of electrochemical corrosion analysis. Open circuit potential, polarization resistance, potentiodynamic polarization were performed as parts of the study.
- Chapter 9 present conclusions and summarizes the findings of this study and explains suggestions for the future work.

Chapter 2

Literature Review

2.1 Introduction

As carbon emission and global warming are major concerns all around the world, car makers tend to utilize lightweight and strong materials in their products, especially the body panel in order to decrease fuel consumption. As a result, the use of lightweight materials such as aluminium and magnesium have been considered by car makers. Fuel efficiency has been investigated over the life cycle of a car for the application of lightweight materials in power-trains and vehicle structure. Greater fuel efficiencies have been achieved by the application of aluminium in the chassis of a car instead of conventional steel. The average passenger vehicle weight has reduced by 29.66 % from 1980 to 1991. Today the average vehicle weights about 1400 kg with majority of the weight devoted to steel [2, 25-27]. A pie chart in Fig. 2.1, shows materials distribution of total vehicle curb weight in kg.

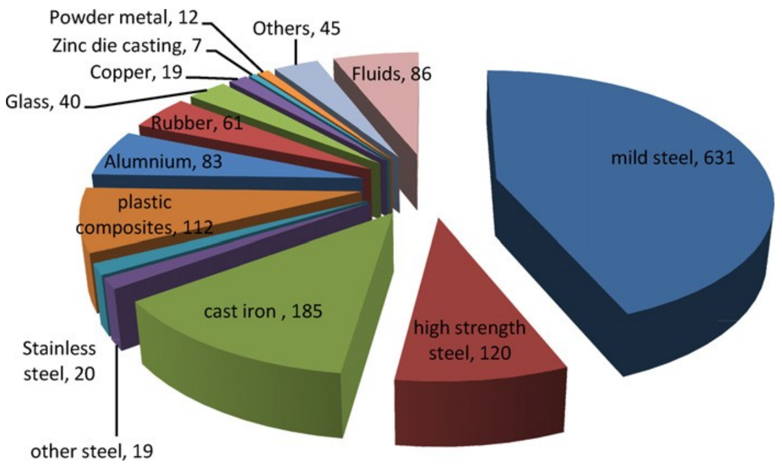

Fig. 2.1 A pie chart showing material distribution of total vehicle curb weight in kg [2].

The main issue arising from using different types of materials for body structure is joining methodology. Conventional spot welding is not an appropriate method for joining dissimilar materials such as aluminium and steel sheets because of their different melting points [28]. Moreover, spot welding is not a suitable method for joining aluminium sheets due to the high thermal conductivity and low melting temperature of aluminium alloys in comparison to steel, and their tendency to form an oxide surface layer [29-31].

Over the years, different joining techniques such as structural adhesives, laser beam welding and mechanical joining have been developed to overcome the difficulties of joining dissimilar or advanced materials [32, 33]. Among these methods self-pierce riveting (SPR) has attracted the most attention. SPR was introduced many years ago for application in the construction industries. Gradually it was applied to domestic products such as washing machines and ventilation systems [34]. During the last 20 years it has been considered as a promising alternative method for spot welding [35]. The Audi A8 was the first automotive assembly in which the SPR technique was employed for joining its aluminium space frames. It has almost 500 spot welds and 110 self-pierced rivets. In the Audi AL2, 1500 spot welded joints have been substituted by self-pierce riveted joints [36]. Other manufacturers such as Mackenzie, Jaguar and Volvo also utilized this method [37]. SPR is a fast and environmentally safe method that can be applied to a variety of materials with different thicknesses and/or surface finishes such as high strength steel, aluminium alloys, composites and coated materials [35, 38]. This chapter provides an overview of the self-pierce riveting process and discusses the properties of the joint which are effected by wear and corrosion. Due to the fact that coatings can overcome these deficits and prolong the working life of a material, this chapter continues with explaining methods to apply the coatings, and specific properties of the coatings used for fasteners. Finally, it describes how changes in the grain size of the coatings could lead to enhancement of the properties of the coatings.

2.2 Joint formation

Self-pierce riveting is a mechanical technique for joining two or more sheets together. Fig. 2.2 is a schematic of the SPR process [39]. It is a cold process in which a semi-tubular rivet is fed into the riveting module and is pushed by a punch into the sheets that are clamped by the riveting tool in advance (clamping) (step 1 in Fig. 2.2). The rivet pierces the top and any intermediate sheet (piercing) (step 2 in Fig. 2.2) and its shank flares into the upsetting die (flaring). At the same time the bottom sheets flares into the die and an interlock joint is formed (step 3 in Fig. 2.2) and the punch is released (step 4 in Fig. 2.2) [40]. Fig. 2.3 shows a load-displacement curve of the above mentioned steps. The process normally takes from 1 to 4 seconds [30] and there is no requirement for pre-drilling or pre-punching and even no need for precise alignment between the sheets and the riveting tool [29]. For joining steel sheets the combined joint thickness is up to about 6 mm and each sheet can have a thickness in the range of 0.5 to 3 mm [35].

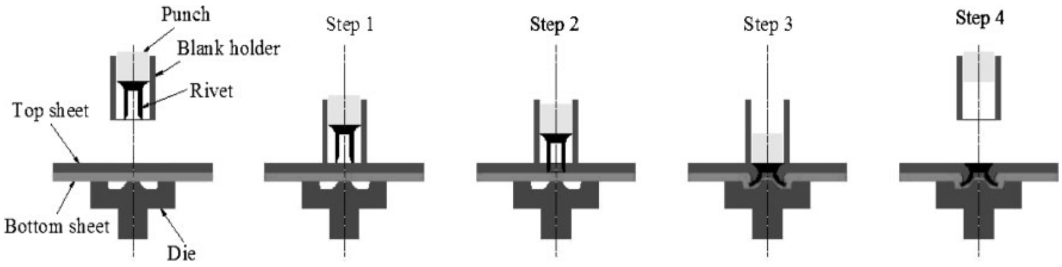

Fig. 2.2 Self-pierce riveting process [39].

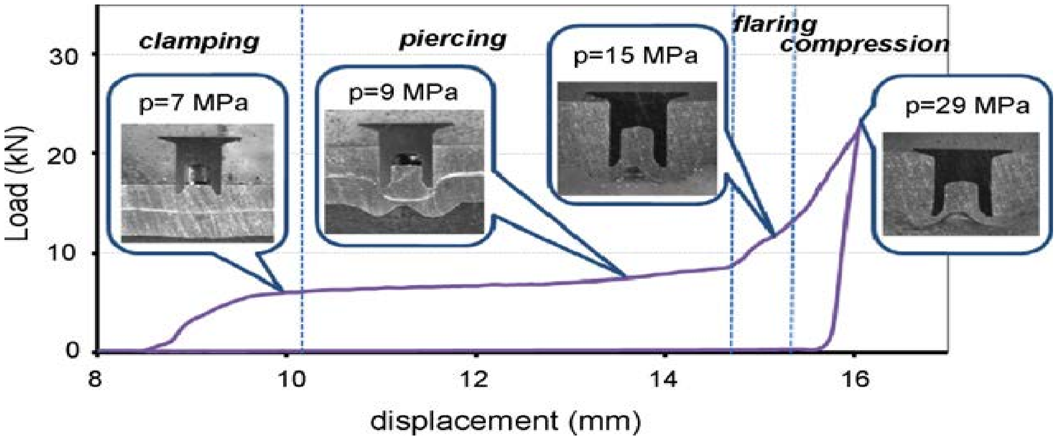

Fig. 2.3 Load-displacement curve of self-pierce riveting steps [30].

Main parameters of the self-pierce riveting process are: setting force, rivet dimension, profile and dimension of the upsetting die [41]. These parameters should be optimised depending on the application. Setting force depends on the die profile, sheet materials and thickness of the combined sheets which is called the joint stack height. Rivet length is defined by the joint stack height. The die profile is characterized by the internal diameter, depth and height of the central pin and is selected according to the process requirements. It should be considered that joint strength depends on the flares of the rivet leg into the locking sheet [38]. It was shown that a large diameter rivet and a high setting force leads to a strong joint [34]. It has to be considered that SPR involves a high degree of localized plastic deformation especially at the bottom sheet which makes this process challenging for the material such as Mg which has low formability at room temperature. Application of a laser beam as an add-on machine tool (laser-assisted SPR) can resolve the problem as it quickly increase the temperature of the sheets and lead to the production of a crack-free joint [42].

Rivets are made of different types of materials such as steel, copper and aluminium. They have a variety of head and countershunk, head dimensions and a wide diversity of coatings are applied to the rivets for corrosion protection or decorative purposes. Rivet materials should not only have sufficient hardness to pierce the top layer sheet but also the ductility to flare into the bottom sheet [28].

2.3 Properties of the joint

2.3.1 Fatigue properties

The fatigue strength of SPR joints has been compared to spot welded joints for different types of materials. The fatigue strength of a SPR joint is superior to that of a spot welded joint [35, 43]. Generally, SPR joints exhibit fatigue strength that is twice as high as the resistance of spot welding joints [44]. This difference has been attributed to the consequences of the welding and piercing processes. It has been stated that the metal adjacent to the spot weld area becomes softer during welding process as a result of heating, however work hardening occurs to the material around the rivet [45].

Investigation of different process parameters such as rivet diameter, rivet length, rivet hardness, sheet thickness and die shape on the static and fatigue properties of SPR joints in aluminium alloys AA5754, showed that the die tip height has the most important effect on the static strength of the joint. Sheet thickness and the cyclic load level were the effective parameters for the fatigue performance [46]. Moreover, it has been reported [47] that the fatigue behaviour of SPR joints for similar and dissimilar sheet materials, is a function of different elements such as the configuration of the joint coupons, the thicknesses of the base metals and different piercing directions.

2.3.2 Corrosion properties

Corrosion is one of the major problems for every joining technique. For a self-pierce riveted joint, different types of corrosion such as uniform, galvanic, crevice and fretting corrosion may occur. Galvanic corrosion [48] is the most possible one. However, the possibility of galvanic corrosion between the rivet and sheets will be eliminated if the rivet material is the same as the sheet material. This is not the solution for many self-pierced riveted joints, because the essential mechanical properties of rivets cannot be supplied by all types of sheet materials.

A brief description of the fundamental theory behind the corrosion of self-piercing rivets is discussed below.

2.3.2.1 Uniform Corrosion

Uniform corrosion is considered as a corrosive attack occurring evenly over the entire or a large fraction of the surface area of a material. A simple case is the rusting of steel in air. This type of corrosion may happen in a variety of environments like dry, damp or wet atmosphere, industrial environment, atmospheric contaminants, etc. Tarnishing of silver in the presence of H_2S in dry air is an example of dry corrosion. Humidity over 70% can cause corrosion since it provides an invisible layer of water over the surface of materials and this layer can act as an electrolyte in a corrosion cell. However there is a critical level of humidity for the onset of corrosion of every metal [49].

2.3.2.2 Galvanic Corrosion

Galvanic corrosion arises when two metals with different electrochemical potentials are in contact with each other in a corrosive media and form an electrochemical cell. Propensity of a metal to be corroded in a galvanic cell is related to its position in the galvanic series of metals and alloys (see Table 2.1). In accordance to this table a metal will corrode (anode) when it is in contact with a more noble metal (cathode) in the presence of corrosive media (electrolyte). As metals or alloys getting far from each other in the galvanic series the tendency of galvanic corrosion increases, and as they come closer the possibility decreases [49].

Table 2.1 Galvanic series of some commercial metals and alloys in seawater (adapted from [48]).

↑ Nobel or cathodic

Platinum
Gold
Graphite
Titanium
Silver
18-8 stainless steel (passive)
Inconel (passive) (80 Ni- 13 Cr-7 Fe)
Silver solder
Monel (70 Ni-30 Cu)
Cupronickels (60-90 Cu-40-10 Ni)
Bronzes (Cu-Sn)
Copper
Brasses (Cu-Zn)
Inconel (active)
Nickel (active)
Tin
Lead
Lead-tin solders
18-8Mo stainless steel (active)
18-8 stainless steel (active)
Ni-Resist (high Ni cast iron)
Chromium stainless steel, 13% Cr (active)
Cast iron
Steel or iron
2024 aluminium (4.5Cu, 1.5Mg, 0.6Mn)
Cadmium
Commercially pure aluminium (1100)
Zinc
Magnesium and magnesium alloys

↓ Active or anodic

The magnitude of a galvanic corrosion is affected by the ratio of anode to cathode area. At a constant current, the intensity of corrosion increases with decreasing the anode area and decreases with increasing the anode area. As a result the small ratio of anode to cathode area leads to severe galvanic corrosion [49].

A common and simple equation which is used for evaluating galvanic corrosion is as follows [50, 51]:

$$I = \frac{E_c - E_a}{R_c + R_a + R_e + R_m} \tag{2.1}$$

Where:

I= galvanic current between anode and cathode

E_c and E_a = cathodic and anodic open circuit potentials, respectively

R_a = anodic polarisation resistance

R_c = cathodic polarisation resistance

R_e = electrolyte resistance

R_m = metal resistance from the anode surface to the cathode surface through a metallic path

In order to suppress the galvanic corrosion, the current in Equation (2.1) should be very low. This could be provided by appropriate material selection, design assembly and the usage of coatings and insulation materials [50, 51].

The potential difference between the anode and cathode (E_c-E_a) should be as low as possible. For steel fasteners, such as self-pierce rivets, zinc and tin plating is used to prevent corrosion of the steel rivet and increase the compatibility of the fastener to aluminium and magnesium sheets.

The cathodic reaction should have a large polarization resistance, R_c, to decrease the cathodic rate reaction and slow down the anodic reaction [50, 51].

Electrolyte resistance (R_e) is defined by Equation 2.2. Any increase in R_e leads to a reduction of corrosion according to Equation 2.1.

$$R_e = \frac{1}{r_e} . \frac{l}{A} \tag{2.2}$$

Where

r_e = electrolyte conductivity

l = electrolyte path length

A = electrolyte cross section

Design of assembly should be in a way that the electrolyte drains efficiently. The electrolyte path length can be raised by inserting a washer of a non-conductive material between the anode and cathode [51].

The application of an insulating coating or caps on the fastener leads to the increase of R_e [50, 51]. However, while an insulating coating may decrease the galvanic corrosion drastically, it cannot eradicate the corrosion completely. An isolator coating only enhances the resistance of the electrolyte, and decelerates the galvanic current. Whereas, it does not block the electrical path in the solution. Song et al [51] showed that the effect of isolator thickness on the galvanic corrosion is not linear for a magnesium-steel cell; galvanic corrosion decreases rapidly with the increase of isolator thickness to 1 cm and then the reduction slows down as the thickness increases.

In a comprehensive survey conducted by Schlitt and Eschebach [52] on materials selection and corrosion protection for bi-metallic systems in the automotive environments, it was found that a thin layer of zinc rich and electrodeposited epoxy coatings (10-20 µm) reduced galvanic corrosion. Generally, one way to diminish corrosion in a galvanic cell is to apply a coating to the cathode. In this way the galvanic cell can shift, so that the anode becomes the cathode and coating acts as an anode [52].

2.3.2.3 Crevice Corrosion

Crevice corrosion is a localized type of corrosion which initiates in voids, holes and cavities between adjoining surfaces or on a metallic surface by the deposition of mud, dust or dirt. The most important factor for initiation of crevice corrosion is differential aeration cell formation. Any geometrical circumstances which lead to high oxygen concentration on one part of a metal surface and a low concentration (or zero concentration) on another cause the former to act as a cathode and the latter as an anode in a corrosion cell [48].

For those metals and alloys which are corrosion resistant due to the stability of a passive film, crevice corrosion should be considered seriously, because these films are not stable in the existence of high concentrations of Cl^- and H^+ ions [48].

The mechanism of the crevice corrosion is very complicated but a unified mechanism was given by Fontana and Greene [48]. The mechanism is explained here by an example.

Consider a riveted stainless steel section immersed in aerated sea water (pH 7).

Corrosion starts with metal oxidation and proceeds by reduction of oxygen:

Oxidation: $$M \rightarrow M^{+} + e^{-} \tag{2.3}$$

Reduction: $$O_2 + 2H_2O + 4e^{-} \rightarrow 4OH^{-} \tag{2.4}$$

Fig. 2.4 shows the initial and later stages of crevice corrosion.

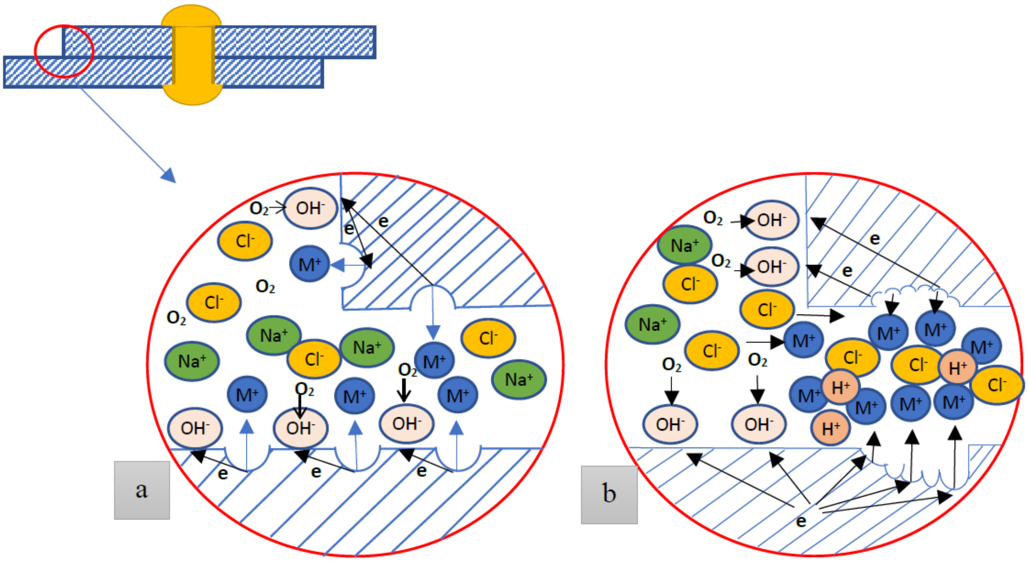

Fig. 2.4 Schematic representation of (a) initial and (b) later stages of crevice corrosion process.

The amount of dissolved oxygen decreases rapidly in the crevice, as a result, oxygen reduction is suppressed, while metal oxidation continues, which leads to the accumulation of (M^{+}). An increase in metal cation concentration in the crevice attracts negative charges such as OH^{-} and lots of Cl^{-} anions into the crevice. Chlorine anions concentration increases up to several times the mean value in the solution. Metallic chlorides compose and hydrolyse in the crevice and lead to the decrease of the pH and an increase of the acidity of the electrolyte.

$$M^{+}Cl^{-} + H_2O = MOH \downarrow + H^{+}Cl^{-} \tag{2.5}$$

H^+ and Cl^- promote the dissolution reaction in the crevice and oxygen reduction reaction becomes localized on the external surfaces close to the crevice. This "autocatalytic" process accelerates rapidly, even if several days or weeks were necessary to onset [48].

2.3.2.4 Corrosion in self-pierce riveted joints

Corrosion performance of steel self-piercing rivets for joining aluminium components have been investigated by Howard and Sunday [53]. Aluminium sheets were galvanically corroded when in contact with steel rivet heads in 3.5 wt.% NaCl water solution and crevice corrosion was observed between the rivet heads and aluminium sheets. Fig. 2.5 shows the aforementioned corrosion.

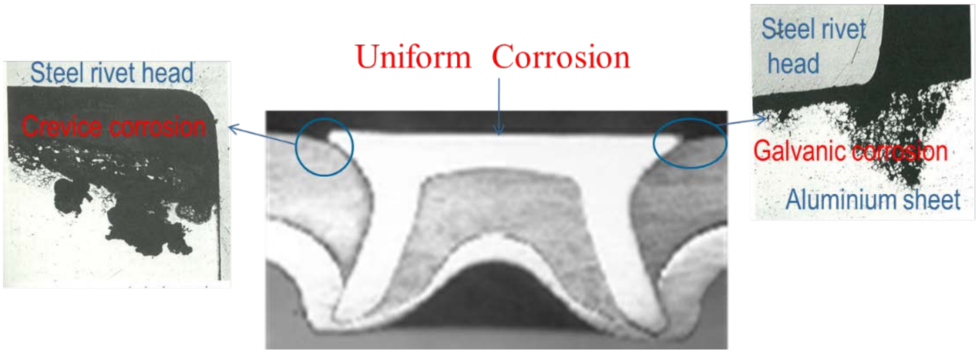

Fig. 2.5 Micrograph of a SPR joint showing galvanic and crevice corrosion of an aluminium sheet by steel rivet head “Reprinted with Permission from SAE International” [53].

The application of coatings such as Stalgard (registered trademark of Elco Industries Inc) and cadmium improved corrosion properties of the joint. Stalgard coating reduced the amount of galvanic corrosion, while the cadmium plated coating improved corrosion protection and showed a small amount of galvanic defects in comparison to stalgard coating and bare steel [53].

Fig. 2.6 shows the progress of corrosion of a steel sheet in contact with a steel rivet. Both the steel sheet and steel rivet are covered by Sn-Zn protective coating.

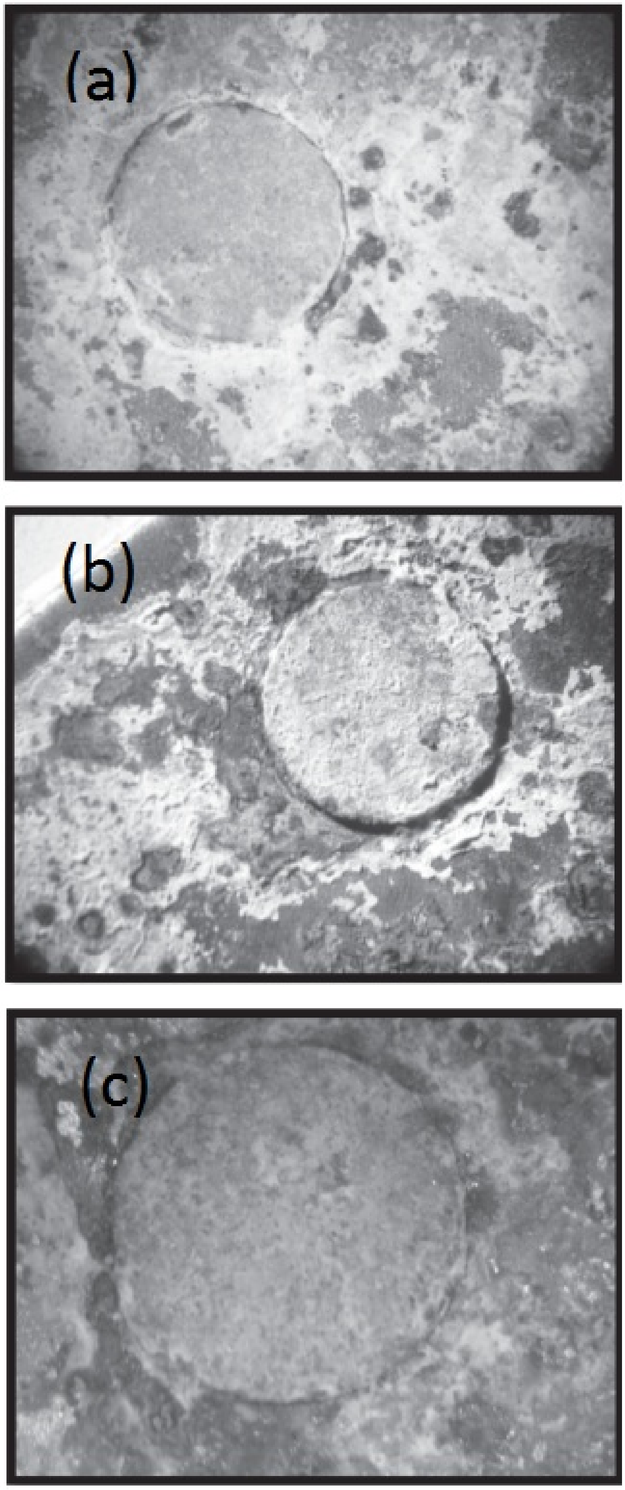

Fig. 2.6 Optical micrograph showing progress of corrosion of SPR joint (steel sheet in contact with steel rivet). (a) After 351 hours, (b) after 510 hours, and (c) after 850 hours of the exposure to 5 wt.% NaCl at 35 °C (±1.5 °C) in a salt-spray chamber [54].

In addition to the consumption of the coatings in an aggressive corrosive media, which eventually expose the sheet and the rivet to the corrosive environment, the effects of stress cell have to be considered. During the piercing step the area close to the head of the rivet are stressed while, the areas far from the head are not affected. Therefore, due to the high concentration of stress, the deformed area may act as the anode and the undeformed area as the cathode under the corrosion condition and accelerate the corrosion rate [54] .

2.3.3 Fretting Properties

Fretting fatigue is considered as a wear and corrosion process that happens when two contacting elements are under an oscillatory load [55].

In general when two sheets are clamped together and have nominal static contact, under a low movement in the range of 1 to 100 µm, they become affected by fretting [56]. Fretting leads to crack initiation and can reduce fatigue life of a SPR joint [4, 5]. Fatigue failure of a SPR joint is shown in Fig. 2.7.

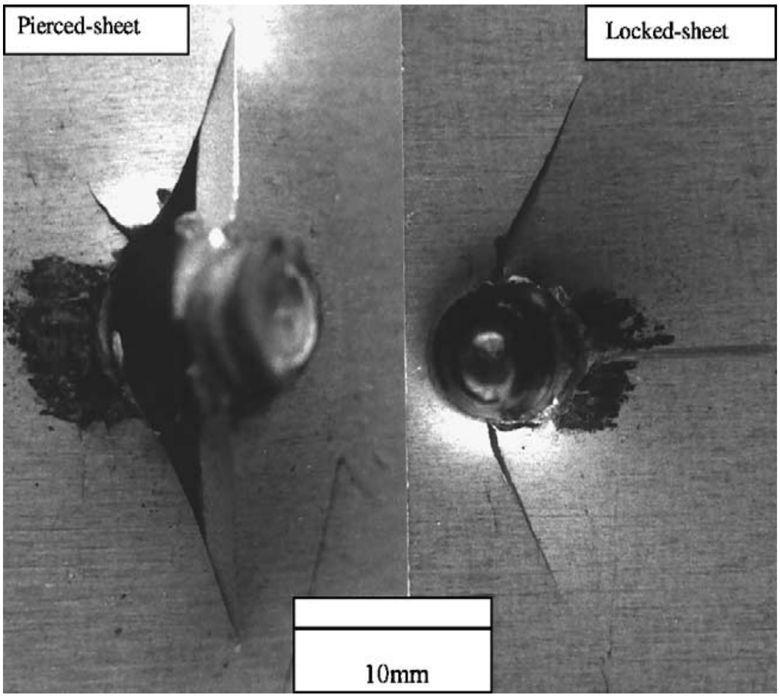

Fig. 2.7 Micrograph of fractured SPR joints with fretting scars formed on the interface between riveted sheets for 4.9×10^5 loading cycles at 3.6 kN [57].

Chen and Han [57] evaluated fretting wear in aluminium alloy AA5754 joined by SPR. Fretting was found in three different positions in a joint (Fig. 2.8) [55, 57].

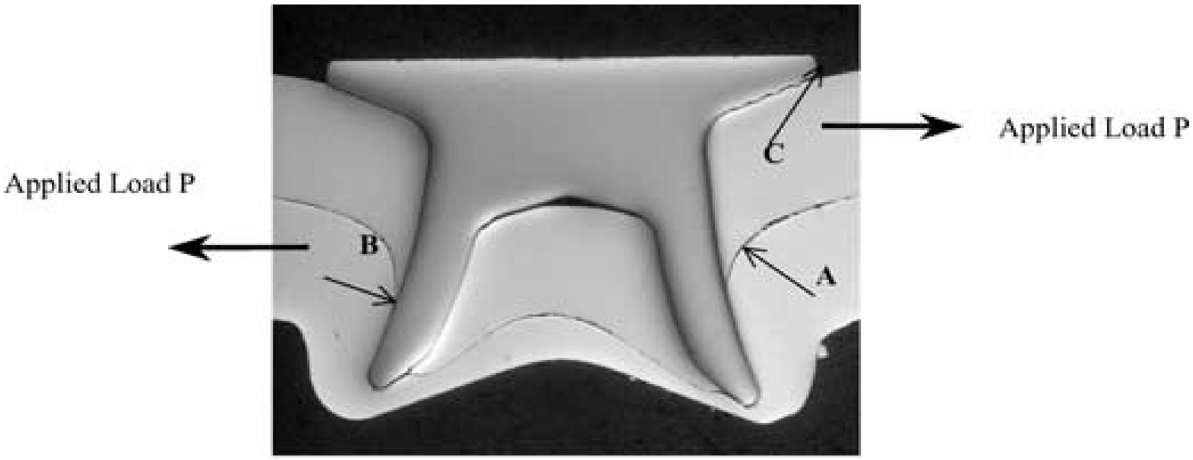

A: Interface between the two riveted sheets
B: Interface between the rivet shank and the locked sheet
C: Interface between the edge of the rivet head and the pierced sheet

Fig. 2.8 Micrograph showing cross-section of a self-piercing riveted joint [55].

Fretting in position A occurred due to load repetition, caused by movement of riveted sheets [55]. Fig. 2.9 represents fretting at this region. Fretting zones are black in colour and consist of oxidised wear debris [57].

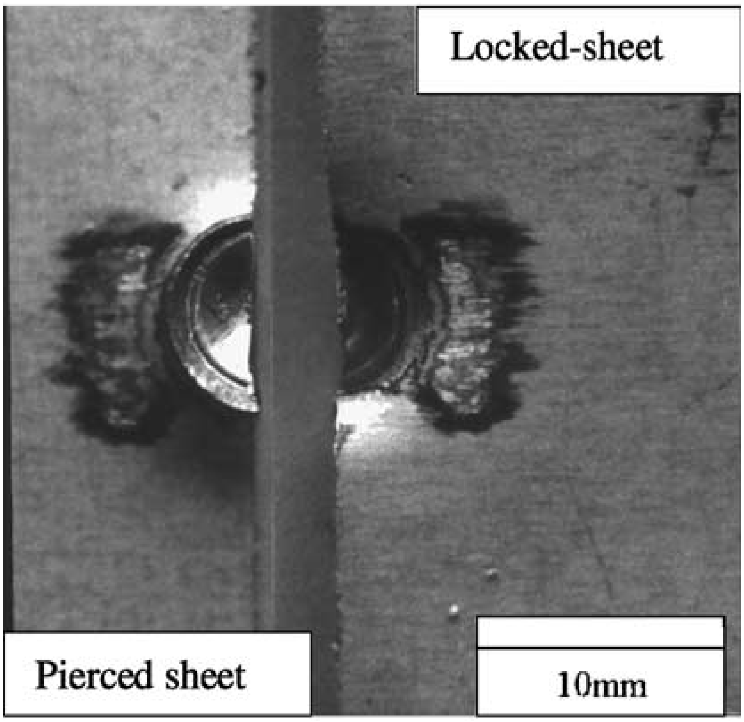

Fig. 2.9 Micrograph showing fretting regions at the interface between two sheets after fracture at for 2.1×10^4 cycles [57].

Fig. 2.10 shows a micrograph of a bottom sheet which failed after 489300 cycles at a maximum load of 3.6 kN. The rivet failed and cracks are visible in the picture [55].

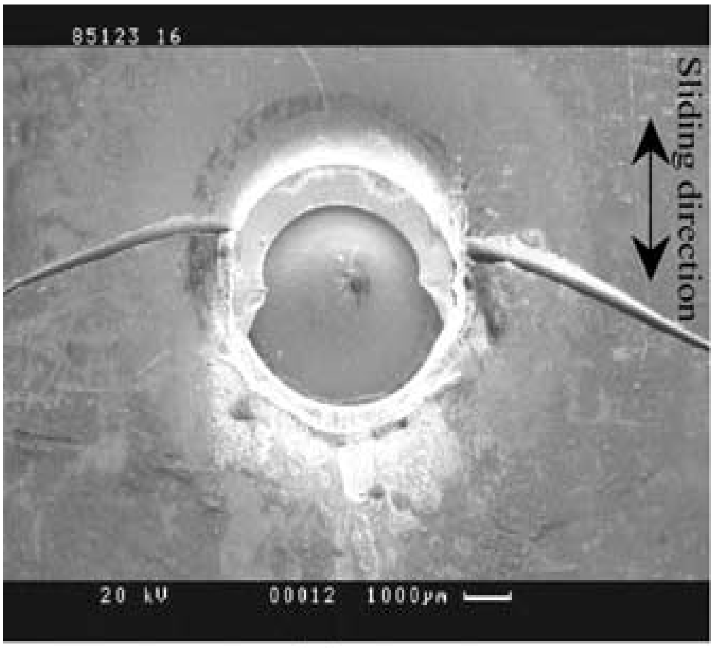

Fig. 2.10 Micrograph showing the locked sheet after 489 300 cycles at a peak load of 3.6 kN with a part of broken rivet [55].

Basically the rivet flares into the bottom sheet and die to form a mechanical interlock, so tilting of the rivet leads to relative movements between the rivet shank and locked sheets and causes fretting at point B (see Fig. 2.8). EDX analysis revealed a great amount of aluminium at the fretting scar of the rivet [57].

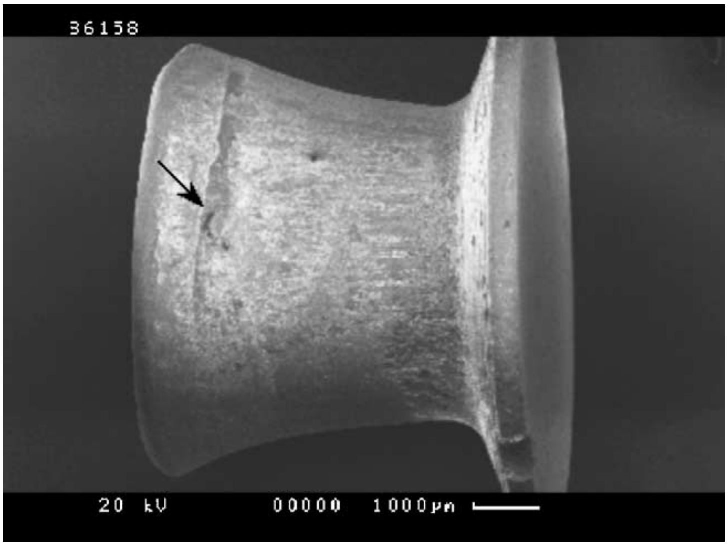

Fig. 2.11 Micrograph showing fretting zone for the interface marked B in Fig. 2.8 [57].

Due to rivet secondary bending and tilting, the rivet head applied pressure to the upper sheet and caused fretting at the interface between the edge of the rivet head and the pierced sheet (point C of Fig. 2.8). Fig. 2.12 [55] shows crack initiation and propagation resulting from fretting on the surface of the pierced sheet.

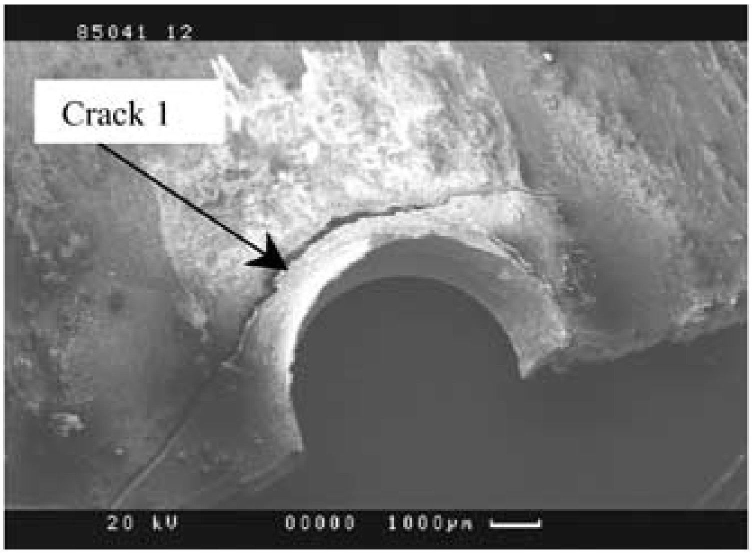

Fig. 2.12 Micrograph showing cracks formed at the pierced sheet after 133 800 cycles at a maximum load of 4.5 kN [55].

According to Chen and Han's [57] observations fretting leads to two macro-degradation models: surface fretting microcracks and fretting fatigue cracks. Multi-microcracks which have formed near an alloy surface may lead to delamination and detachment of the material and produce debris as can be seen in Fig. 2.13.

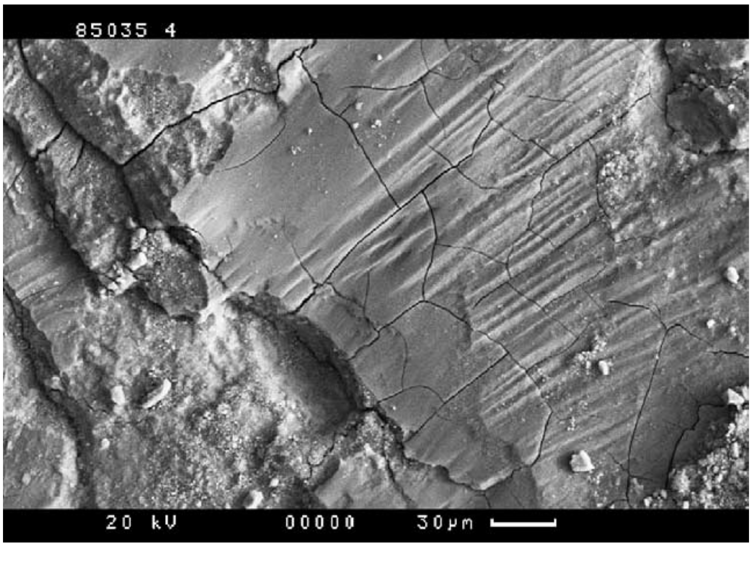

Fig. 2.13 Micrograph showing fatigue damage in an SPR fretting sheet at a 2.7kN load for 6.5× 10^6 cycles [57].

It was found that some microcracks altered their propagation mode and became macrocracks. Fig. 2.14 shows fretting fatigue microcracks which can lead to fatigue failure.

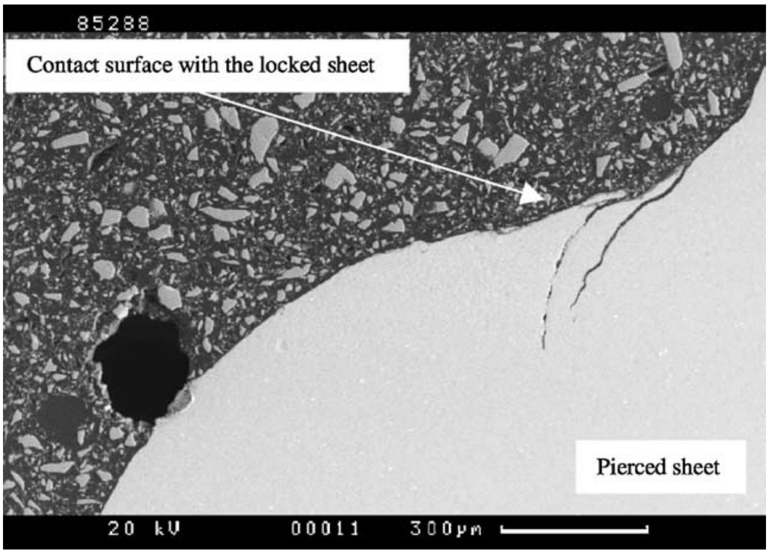

Fig. 2.14 Micrograph showing the fretting fatigue microcracks at 3.6 kN for 4.9×10^5 cycles [57].

Investigation of the fretting behavior of aluminum SPR joints with different interfacial conditions showed that the presence of a waxbased solid surface lubricant or a PTFE tape could decrease or inhibit the fretting damage, and may change the fatigue failure locations from the sheets to the rivet [37].

2.4 Rivet material and surface treatment

Rivet material should be chosen properly in order to provide various characteristics. In a very general view rivet material should be hard enough to pierce the upper sheet and ductile enough to flare into the bottom sheet. If the rivet material is softer than the sheet materials, formation of a joint will be impracticable. Yield strength of the materials also needs to be considered, a high yield strength may lead to deformation of the rivet during the joint formation. The formation of the joint would also rely on elongation and formability of the rivet. A low elongation or formability reduce the ability of forming a robust joint [3].

Depending on the application, rivets are mainly made of austenitic stainless steel, martensitic stainless steel, aluminum and copper. Ductile stainless steel sheets could be joined by austenitic stainless steel, for tougher sheets martensitic stainless steel are used. Aluminum and copper have specific applications. Aluminum is used in joining soft grades of aluminum, and copper is used for copper, brass and plastics. Rivets are coated either to provide corrosion protection or decorative purposes. Zinc, Almac, and zinc-tin are the three main categories of rivet coatings [58]. Rivets with a secondary layer such as organic and paint are also available. A few examples of the organic and top layer coatings for fasteners such as rivets are mentioned below:

- Aluminium and its alloys are joined by titanium or titanium alloy fasteners in aircrafts. In such an assembly, because of electrochemical coupling effect and tendency of aluminium to be galvanically corroded in contact with titanium, existence of a promising coating seems essential. A coating made of a mixture of aluminium powder and molybdenum disulfide (MoS_2), suspended in a phenol-formaldehyde thermosetting resin, dissolved in a volatile solvent carrier like, methyl, ethyl, propyl or isopropyl alcohol could provide corrosion protection to the joint. Metallic chromate such as strontium or zinc chromate may be added to the coating. Either polytetrafluoroethylene (Teflon) or a cation-type wetting agent such as fatty amino diamine is also included. For a steel or alloy steel components the latter one is used since it has a superior corrosion resistance especially in salt spray test. The coatings are applied by spraying, dipping or brushing and subsequent baking. The coating thickness varies between 5 to 12.7 µm. The coating does not cause embrittlement and has a good adherence, Teflon ingredients provide good lubricity and result in an abrasion resistant coating. These types of coatings are suitable for interference fit fasteners such as rivets [59, 60].
- A three-layer coating consisting of an inner metallic coat, a secondary epoxy base and a final top coat could provide enhanced corrosion protection to fasteners such as rivets. The epoxy base coat is preferably applied on the metallic core by cathodic electrodeposition. The composition of the top coating can comprise of sulphonates and sulfurized hydrocarbon fatty acid and ester and is deposited by dip-spin technique. Hydrocarbon fatty acid ester in the top coat can be derived from a polymer of ethylene, propylene or natural oil. Particularly preferred top

coat formulations additionally include a salt of sulfamic acid or a derivative and/or salts of barium such as barium carbonate and barium sulfate. Epoxy base coatings for cathodic electrodeposition are commercially available and are formulated with isocyanate cross linking agents. The finish coating is applied at a temperature between 37-65˚C [61].

- A possible problem during the insertion of a coated fastener such as a zinc plated nail, is damage to the coating. If the insertion process is done by a power tool the risk of damage will be higher. Scratched coatings show corrosion failure at early stages. A particular group of oil-free, cross linked polyester resins (a reaction product of one or more polyols such as pentaerythritol or trimethylopropane and diasic organic acids such as phthalic acid or isophthalic acid followed by heating between 100-180˚C for 2-8 hours) could be applied as a top coat. These top coats have good toughness and are non-brittle, therefore they can support the sub-layer corrosion protective coating from damage during the insertion process. The coating can be applied by immersion dipping and subsequent heating. The coating composition may have additives and modifiers such as clay, calcium carbonate, or amorphous silica. The solvent can be isopropyl alcohol or isobutylace. The solvent and modifier are added to adjust the viscosity [62].

2.5 Classification of coatings

2.5.1 Metallic coating

Metallic coatings create a barrier between a metal substrate and the environment. They are applied by different methods such as electroplating, electroless plating, spraying, hot dipping, chemical vapour deposition, ion vapour deposition and mechanical plating [63]. Electroplating and mechanical plating are mainly used in the fastener industry to provide protection to underlying material. Coatings should be free from pores in order to provide good corrosion properties. However, in practice coatings are not comprehensively pore free and scratches and other wear mechanisms may damage them. Depending on material selection and the table of electrochemical potential of the material under a different medium, a coating is nobler or more active than the substrate.

When there is a scratch or pore in the coating, in the case of a more noble coatings such as copper, nickel and chromium for a steel substrate, the corrosive medium reaches the substrate, and a galvanic cell is formed between the anodic substrate and cathodic coating (Fig. 2.15.a) which leads to severe localized corrosion of the substrate (small ratio of anode to cathode). If a coating cannot be deposited without defects, a fine and homogeneous distribution of the coating material decreases local corrosion. In other conditions, when coating material is more active than the substrate, the coating will protect the substrate sacrificially. Since there is a small cathode area the intensity of corrosion is low (Fig. 2.15.b). A less noble coating such as zinc and cadmium coatings protect steel fasteners sacrificially. Corrosion protection is almost provided since the coating material exists [64].

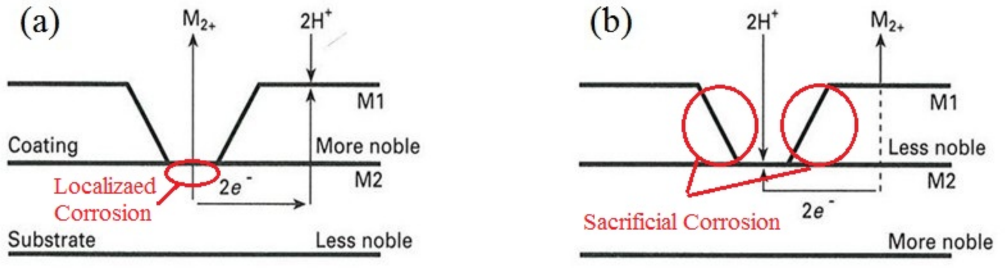

Fig. 2.15 Schematic illustration of corrosion mechanism of coating substrate system in the presence of defects (a) More noble coating on less noble substrate. (b) Less noble coating on nobler substrate [64].

2.5.2 Conversion coatings

Conversion coatings are defined as the coatings in which the ions of a substrate metal contribute to the production of a protective layer. A chemical or electrochemical process is required for the formation of these coatings on the metal substrate. They can be deposited anodically or can be deposited due to exposure of the substrate to a conversion bath. During the process of the deposition, part of the metallic surface converts to a metal oxide and provides better corrosion protection to its substrate cathodically.

Conversion coatings could be used for corrosion protection of different types of alloys and metals such as steel, zinc, aluminium, magnesium, copper, tin, silver, and nickel. They can also be used for decorative propose or as paint primers. Their categorisation is based on their main constituents and includes chromate conversion coatings, phosphate conversion coatings, and lanthanide-based conversion coatings. Their thickness varies in the range of 0.254 μm to 50.8 μm [61, 62].

Hexavalent chrome can be found in the conversion coating layer used to passivate zinc and zinc alloy plated surfaces. The amount of Cr (VI) changes from 5 to 400 mg/m^2, and is usually low for light blue coatings and high for yellow and olive green types. In the late 1990s the application of hazardous materials such as hexavalent chromium compounds were prohibited in the automotive industry by the European and American car industries. Therefore, the application of non-carcinogenic trivalent chrome passivation increased [65].

The process to apply a passive layer on zinc or zinc alloy coating is similar for both Cr^{+6} and Cr^{+3}, except for the solution. Zinc plated parts are immersed in hexavalent or tetravalent choromating solutions, zinc oxidized at the interface by Cr^{+6}, which is reduced to Cr^{+3} in a hexavalent chromium solution, to form zinc chromium oxide compounds. For Cr^{+3} the process relies on the direct reaction of Cr^{+3} [65].

For coatings consisting of 8 to 10% of leachable Cr^{+6}, if the film is scratched or mechanically damaged, moisture dissolves the leachable Cr^{+6}, restoring the conversion film and resealing the damaged area [65].

Sealers and topcoats are post passivation treatments, sealers such as silicate-based products, phosphates, silanes and transition metals reacts with the conversion coating film and leads to durable resistance finishes [62, 65].

2.5.3 Barrier coatings

Barrier coating provides protection to the substrate by providing a blocking layer which restricts the access of a corrosive media to the surface of the substrate providing corrosion protection. It can be categorized in 3 main forms [49, 63]:

2.5.3.1 Anodic oxide coatings

Anodic oxide coatings such as Al_2O_3. These coatings are deposited by pack cementation (aluminising) method. Generally, these coatings are porous and need a potassium dichromate sealer (health hazardous) to decrease the porosity [49,63].

2.5.3.2 Inorganic coatings

Inorganic coatings like ceramics and amorphous. Amorphous coatings do not have any crystalline structures such as grain boundaries or chemical defects and second phase particles which are considered as potential sites for corrosion, so they are expected to show better corrosion properties [49,63].

2.5.3.3 Organic coatings

Organic coatings such as epoxy, polyurethane, chlorinated rubber and polyvinyl chloride coatings are the third category of these coatings and are mainly served in the petroleum industry as a barrier to water and oxygen [49,63].

2.6 Coatings methods

There are a variety of processes to apply a coating on substrates such as brushing, spraying, dipping, flow coating, thermal spraying, pack cementation, fluidized-bed deposition, electrodeposition, etc. In this chapter some of the most common methods of applying a coating on fasteners are explained [49,63].

2.6.1 Sherardizing

Sherardizing is a process in which a layer of zinc is deposited on a metallic substrate. Components are packed in zinc powders and undergo a heat treatment process (380-400°C) in a furnace for a specific time. During the heat treatment, the coating substances atoms and substrate atoms diffuse into each other [63].

A post treatment process is usually a phosphate or chromate conversion coating that prohibits the zinc oxide formation in early stages. Sherardized coatings are composed of zinc-iron which is saturated in zinc at the top surface of the coating and its concentration decreases across the thickness in contrast to iron. The uniformity of sherardized coating is notable, which makes this method appropriate for irregular and complicated shapes such as threaded fasteners. The applied coating has a grey appearance that makes the surface ready for a post treatment process. Since the process is based on diffusion, and zinc diffuses into the crystal lattice of the steel substrate, a coating with good bond strength and abrasion resistance properties is provided. There are some other beneficial points for sherardizing; a very negligible amount of hydrogen gas is generated during the process so the possibility of hydrogen embrittlement is decreased drastically, and because of the low temperature of the heat treatment, mechanical properties of the substrate remains unaffected [66].

2.6.2 Mechanical plating

Mechanical plating, also known as impact plating or peen plating, is a process in which metal coatings are deposited on components by the use of kinetic energy at room temperature. Components to be coated are mixed with glass beads, water, surface preparation chemicals, promoter chemicals and metal powders in a lined barrel and are tumbled. Kinetic energy due to rotating barrel leads to the cold weld of metal particles, first on the surface of metal parts and then to advanced bonded particles. During the process metal particles undergo flattening plastic deformation, therefore the surface area to volume of each metal particle increases, and contamination-free active metal surfaces are produced, which result in a free exchange of electrons and atomic welding between parts and coating particles [67, 68].

Mechanical plating was introduced more than 50 years ago. During the past years the coating efficiency has improved from 20% for 10 hours of the process to above 90% for a duration of 30-60 minutes of the process [67, 68].

Various metals can be deposited by mechanical plating such as zinc, cadmium, tin, lead, copper, brass, aluminium, gold, silver, and indium. Predominant advantage of mechanical plating is its potential to deposit combined coatings, alloys, and layered or sandwich coatings. Combined coatings are achieved by using powders of different metals simultaneously. Sandwich or layered coatings are generated by addition of metal powders in sequence during the plating process. Alloy coatings are simply produced by using pre-alloyed metal powders. An example is the mixture of tin and zinc, which provides better corrosion properties in salt spray test due to the low galvanic potential of the mixed coating. The coefficient of friction and white corrosion products are reduced if a layer of tin is applied over zinc. Different materials can be coated by mechanical plating such as high carbon heat-treated spring steel, low-carbon steel, malleable iron, high strength low alloy steel, etc. Typical parts such as screws, bolts, nuts, clips, springs, stampings, washers, nails, and rivets are coated by this method. Thickness of the coating in this method is independent of the plating time, but relies on the amount of metal powder. Normally the total amount of metal powder is added in a small batch in order to provide better uniformity to the coating. The thickness of a coating is not uniform in on sharp edges. The commercial coating thickness is in the range of 5 to 12.5 µm. Higher thickness could also be achieved, usually mechanically deposited zinc coatings with more than 25 µm thickness are called mechanically galvanised coatings [67-69] .

The morphology or structure of the applied coating is different from hot dip or electrodeposition. Mainly the coating consists of distinct metal particles which look like a flat dish and are parallel to the substrate [67].

Hydrogen is produced during the mechanical plating process but because the rate of process is very slow and is not grain oriented it does not trap within the coating and release of hydrogen is more likely to happen than absorption into the base metal. Therefore, hydrogen embrittlement is not considered as a problem for mechanical plating [69].

2.6.3 Dip-spin technology

The dip/spin process is a bulk process so it is cost effective. It is a suitable method to apply coatings on small parts such as: fasteners, spring clamps, screws, bolts, motor mounts, O-rings, nails, clips, muffler hangers, body mounts, etc. In this method parts are placed into a basket and are submerged into a coating vat. The basket is then raised out of the coating solution, yet still remains in the vat, and spun up to 600 rpm. Depending upon the application, the coating viscosity, temperature, spin velocity and curing time can be varied to provide the desired thickness and consistent repeatability. Dip/spinning coatings are mainly used on parts that are pre-treated with a zinc-phosphate conversion coating. The dip-spin procedure does not need either acid pickling or electroplating, so it is hydrogen embrittlement-free and is applied to the fastener in a large amount [70] .

Zinc-aluminium-chromium (ZAC) coating, also named Dacromet [71-74] is an inorganic coating which is used by the automotive industry worldwide and is applied by dip/spin method. Dacromet is mainly composed of overlapping flakes of zinc and aluminium in an inorganic binder. It takes more than 1000 hours for a steel substrate which has been coated by 10 µm layer of Dacromet to show its first appearances of red rust in a neutral salt spray test. Dacromet with an organic top coat can be used in the marine industry. There are some disadvantages for Dacromet, such as carcinogenic chromium compounds and poor erosion-corrosion properties [72, 75].

2.6.4 Electroplating (electrodeposition)

Electrodeposition is the deposition of metallic coating to metallic or other conductive surfaces by electrochemical processes. It is achieved when an electrical current passes through an electrolyte which contains dissolved metal ions (coating material) and the substrate which serves as a cathode in an electrochemical cell [63].

The automotive industry owns the largest market (75%) in using zinc and zinc alloy electrodeposited steel parts. Recently, usage of zinc alloy like Zn-Fe, Zn-Co, Zn-Sn, and Zn-Ni is more widespread, because alloying elements increase the nobility of the composition and decrease the corrosion rate. If the alloy composition is low, the coating acts sacrificially to a steel substrate, and an equal thickness of an alloy coating protects the steel substrate for a longer time than conventional zinc [76].

2.6.4.1 Alloy electroplating

2.6.4.1.1 Zinc-Nickel

Zinc-Nickel alloy can be plated from acid or alkaline non-cyanide solutions. High nickel content (10 to 14% nickel versus 6-9%) can be achieved from an acid bath. Corrosion resistance of the deposit improves by increasing the Ni content up to 15%. Beyond 15% of Ni addition, the zinc-nickel coating becomes nobler than the substrate so it loses its protection. However, above 10% content of Ni, the coating is more passive, and, therefore not a suitable underlay for an effective chromate conversion process.

Although deposition from an alkaline bath is slower than an acid bath, it can produce a more uniform coating in terms of thickness and alloy composition [43, 45, 77-79].

2.6.4.1.2 Zinc-Cobalt

Sacrificial properties of zinc-cobalt alloy decreases with increasing the Co content in the alloy. At a high concentration of Co in the alloy, the coating may become nobler than steel and loses its sacrificial protection. On the other hand, with an increase in its concentration the barrier properties of the coating increases [80].

Zn-Co alloys with a low cobalt concentration have better corrosion resistance than pure zinc [58]. It is suggested that the type and composition of corrosion products that are formed during the corrosion process are the main reasons for this achievement. Zn-Co alloy is a solid solution of cobalt in the zinc matrix in which atoms of Co have been surrounded by zinc atoms. Co is a more positive metal than zinc leading to the formation of micro galvanic couples, and hence improving zinc dissolution. The interaction between the medium and the zinc can be expressed as follows:

$$Zn \rightarrow Zn^{2+} + 2e^{-} \tag{2.6}$$

The hydrogen ions react with the released electrons and cause hydrogen evolution.

$$2H^{+} + 2e^{-} \rightarrow H_2 \uparrow \tag{2.7}$$

Local pH value in the depth of corrosion damage increases due to this process and leads to the formation of zinc hydroxide chloride as a corrosion product in pits and their vicinity.

$$Zn^{2+} + 1.6OH^{-} + 0.4Cl^{-} \rightarrow Zn(OH)_{1.6}Cl_{0.4} \tag{2.8}$$

Pure galvanic coating is not thoroughly smooth and has so many protruded and concaved zones which can act as microgalvanic couples, as a result, zinc hydroxide chloride can be the corrosion product of a pure zinc coating in a treatment such as salt spray. The difference between pure zinc and Zn-Co coatings in the formation of zinc hydroxide chloride is that the process for pure zinc is much slower than Zn-Co coating and the formed zinc hydroxide chloride is more uniform in Zn-Co alloy because of uniform distribution of the alloying component in the zinc matrix [81].

2.6.4.1.3 Zinc-Tin

The co-deposition of zinc and tin was first introduced by Marino [82] in 1915. However, application of tin-zinc alloy coatings (containing more than 50 % tin) was only established commercially since 1940s [83]. Tin-zinc alloy coatings provide sacrificial and cathodic protection to the steel substrate. In addition to corrosion protection, these coatings provide anti-frictional properties, as well as enhanced ductility and solderability [83, 84].

Investigations have been reported [85-91] on the deposition and properties of tin-zinc alloy coatings with a high content of tin from different bath systems. The (80/20) tin-zinc alloy coatings were electrodeposited from an alkaline stannate/zincate bath with better corrosion properties than cadmium, zinc and (90/10) zinc-nickel alloy coatings of equal thickness [88]. Tin-zinc alloys with high tin content (70-80 wt. % tin) were investigated from sulphate-tartrate and sulphate-gluconate baths [89, 90]. Tin-20 wt.% zinc coatings were deposited from a non-cyanide alkaline bath and showed better corrosion resistance than cadmium and zinc-12 wt.% nickel coatings [85]. Vitkova et al. [92] electrodeposited Zn-Sn alloy with a low content of Sn from slightly acidic sulphate electrolytes and showed that Zn-Sn alloy coatings containing 10-20 wt.% tin resulted in better corrosion properties than zinc and Zn-Co coatings. Arici et al. [93] showed that zinc-tin coatings (22.73 wt. % Sn) deposited from an acidic bath protects steel substrates better than pure zinc. It has been reported that the alloy composition changed as a function of metal ion concentrations in the plating bath system and a large range of deposits were electrodeposited from citrate baths [94] and gluconate baths [95].

Zinc-tin alloy coatings provide barrier properties of tin and sacrificial properties of zinc to steel substrate. Different sources of electrolytes are available for alloy deposition, which include acid, alkaline, and neutral formulations [88, 89, 92, 95-99]. Mainly 25 to 30% zinc with 70 to 75% tin can provide optimum corrosion resistance. Such as other alloys of zinc, a chromate conversion coating is required to achieve the optimum corrosion performance.

Zn-Sn coatings have good frictional properties and excellent ductility for the application on parts that undergo deformation after plating (self-piercing rivet). Since, the coating is soft it is more prone to mechanical damage. These coatings are not susceptible to galvanic corrosion, and can be used on steel fasteners for aluminium alloy panels [100].

Zinc and tin exhibit very small mutual solubility based on their phase diagram (Fig. 2.16) [101]. Therefore, Zn-Sn is considered as a mechanical type of alloy in which zinc and tin do not show a solid-solution or an intermetallic compound.

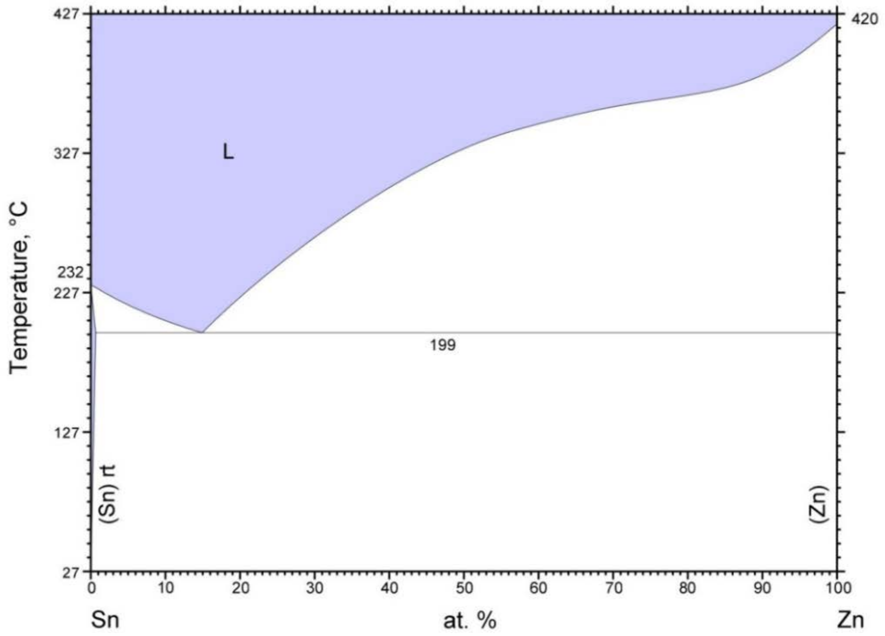

Fig. 2.16 Zinc-tin alloy phase diagram [101].

2.6.4.2 Hydrogen embrittlement and electrodeposition

A major problem arises from electroplating is hydrogen absorption by components during the process which may result in embrittlement. The mechanism of hydrogen evolution during electroplating is summarized below [102]:

$$H^+ + e^- \rightarrow H_{ads} \tag{2.9}$$

A great portion of adsorbed hydrogen will react with each other and evolve to the atmosphere.

$$2\ H_{ads} \rightarrow H_2 \tag{2.10}$$

On the other hand, a portion of them may diffuse to the steel substrate.

$$H_{ads} \leftrightarrow H_{adsorbed\ (in\ steel)} \tag{2.11}$$

Hydrogen can transfer through a substrate and concentrate at stress points and grain boundaries, the trapped hydrogens generate internal pressure and decrease the service life of the component under stressed condition. Hydrogen embrittlement can lead to crack initiation and propagation in highly stressed areas and end up with failure of the component or the assembly [69].

The possibility of hydrogen embrittlement increases for the components which the steel substrate is harder than Rockwell C32 or the component is used under cold work stress.

The different specifications to address this issue are published by ASTM [103], Chrysler [104], and Ford [105]. According to these specifications parts that are susceptible to hydrogen embrittlement are to be baked for the appropriate time and temperature [76].

2.6.4.3 Microstructure of electrodeposited coatings

Crystalline metals with various type of microstructures can be deposited by electroplating. Microstructure of electrodeposited metals could be categorized in columnar, fibrous, fine-grained and laminar (banded) structures. Fig. 2.17 shows each of these four microstructures [106].

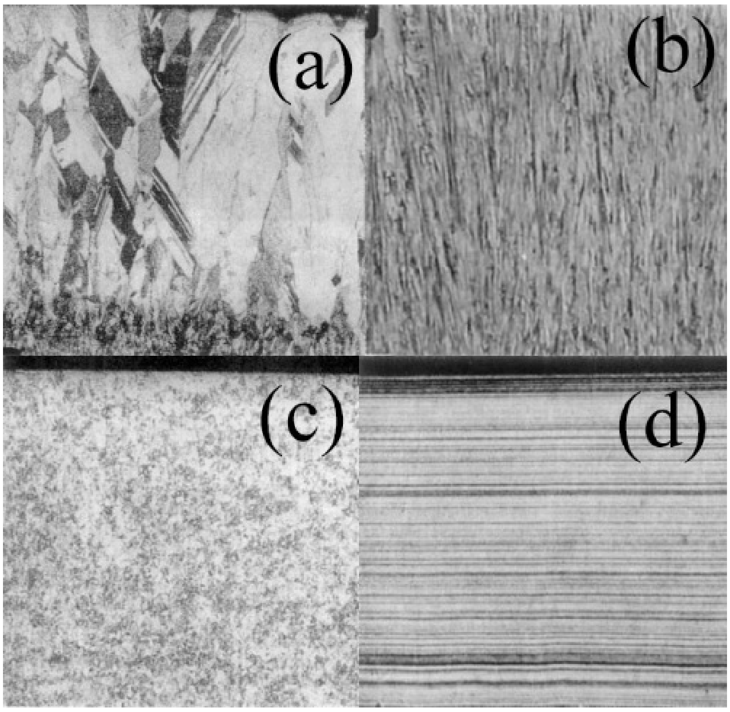

Fig. 2.17 SEM micrograph showing cross section of (a) columnar gold deposit (200 x) (b), fibrous nickel deposit (200 x) (c) fine grained copper deposit (200 x) (d) laminated (or banded) gold-copper deposit (250 x) [106].

Morphology of the electrodeposit is a function of metal ion concentration, addition agents, current density, temperature, agitation, and polarization. Fig 2.18 shows the effects of plating parameters on the microstructure.

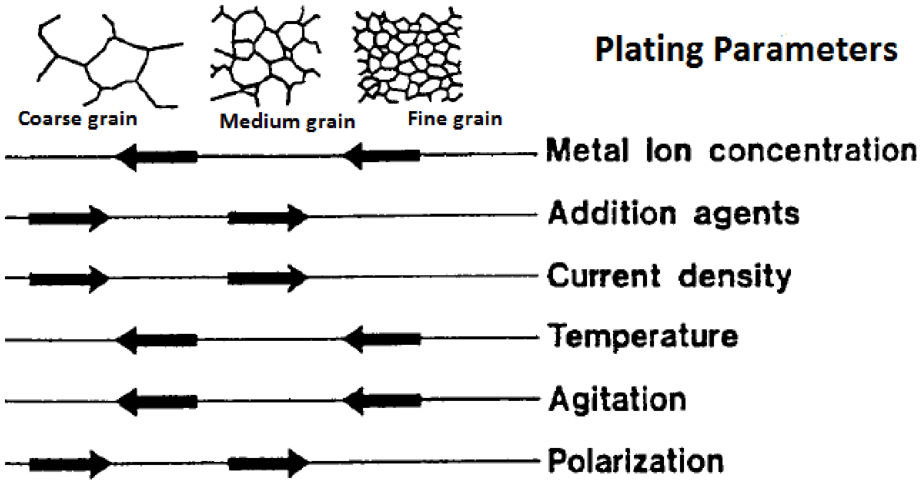

Fig. 2.18 Variation in microstructure of electrodeposit as a function of plating parameters. Tip of the arrows points to the direction in which the increase of the plating parameter leads to either grain coarsening or grain refinement [106] .

Generally metal electrodeposition starts with nucleation and formation of growth centers. The number of nuclei increases with the passage of time, up to a saturated condition. Saturation is a function of plating parameters and plating solution such as overvoltage, concentration of the electroactive species, adsorption/desorption of organic additives, temperature etc. The number of nuclei and saturation increases with the increase of current density and overvoltage. A high ratio of nucleation to growth rate leads to grain refinement. High current density would provide high nucleation rate and grain growth could be hindered by the application of additives [107, 108].

2.6.4.4. Constituent of the electroplating bath

Metal or alloy plating electrolytes have different constituents in addition to the source of plating metal, such as conducting salts, buffing agents, complex ions, and additives [109]. Conducting salts increase the conductivity of the bath and buffing agents prevent pH variation during the electrodeposition process.

2.6.4.4.1. Complex agent (Ligand)

Complex agents can play an important role in the electrodeposition of metals by modifying the kinetics and thermodynamics of these processes, thus affecting the performance of the bath and properties of the deposit. Electrodeposition of metals from electrolytes containing complex agents may also lead to grain refinement of the deposit [110].

2.6.4.4.1.1. Gluconic Acid

Organic acids such as gluconic acid and its salts are used as non-toxic and environmentally friendly complex agents for electrodeposition of different metals such as tin [111, 112], copper [113], cobalt [114] and zinc [115, 116]. They have also been used for the electrodeposition of alloys such as tin-zinc [89], zinc-copper [117], copper-tin [118], cobalt- nickel [119], and cobalt-manganese [120].

Gluconic acid ($HO\text{-}CH_2\text{-}(CH\text{-}OH)_4\text{-}COOH$) has been designated in some literature [121, 122] as HGH_4, in which the first H and the last H_4 refer to the carboxylic acid hydrogen and the four hydrogens on the secondary alcohol respectively, and the anion of gluconic acid has been shown as GH_4^- (gluconate). At acidic pH values gluconic acid undergoes lactonization and δ-lactone (pH>2.5) and γ-lactone (pH<2) are formed [121, 122]. Fig. 2.19 shows a schematic representation of the gluconic acid, gluconate, δ-lactone and γ-lactone. The same notations as the scheme have been used in this study.

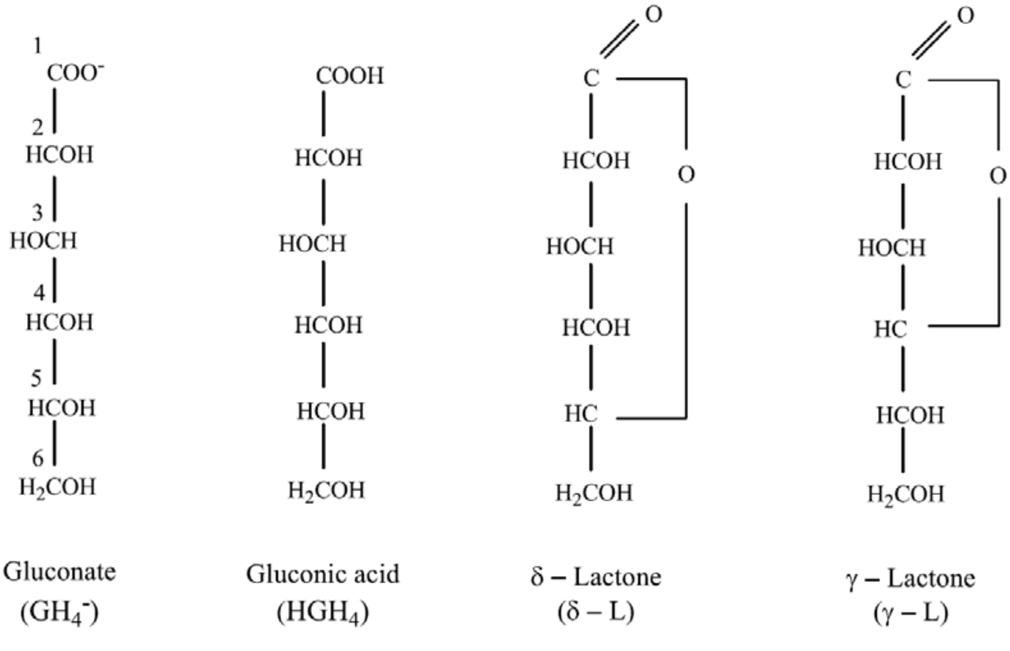

Fig. 2.19 Schematic presentation of gluconic acid, gluconate, δ-lactone and γ-lactone [122].

Zinc and gluconate coordinate by a carboxylate group of ligands in acidic systems and are assumed to be one to one complexes [121]. Gluconic acid salts in the zinc plating electrolyte have been shown to facilitate the electrodeposition of bright zinc at normal temperature (15 - 35°C) under high current densities without burning [115, 116]. Also a comparison of the corrosion properties of zinc deposits from acid sulfate, acid gluconate, acidic nitrilotriacetic, alkaline cyanide and alkaline tartarate showed that zinc coatings deposited using acidic gluconate electrolytes provided better corrosion resistance than those deposited using other types of plating baths [123].

2.6.4.4.1.2. Citric Acid

Citric acid (2-hydroxypropane-1, 2, 3-tricarboxylic) is a weak organic acid. It ($C_6H_7O_8$) has a hydroxyl group and three carboxylic groups in its structure. Fig. 2.20 shows a schematic representation of citric acid. In some literature citric acid has been designated by H_3Cit [124].

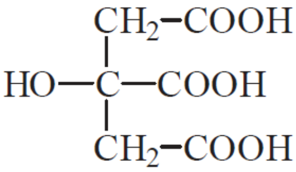

$$\begin{array}{c}
\qquad\quad CH_2-COOH \\
\qquad | \\
HO-C-COOH \\
\qquad | \\
\qquad\quad CH_2-COOH
\end{array}$$

Fig. 2.20 Schematic presentation of citric acid [124].

Due to its structure citric acid can work as a multidentate ligand and can make stable mononuclear and polynuclear complexes with various elements [124]. In electroplating, citric acid has been used as an environmentally friendly ligand for the deposition of different metals and alloys such as tin [125], zinc [126] and tin-zinc alloy [94].

2.6.4.4.2 Additives

Additives are used to improve the appearance and properties of a deposit since they can act as a leveller, brightener and/or grain refiner. Levelling is a property of a bath which can produce relatively thick deposits in recesses and relatively thin deposits on protrusions with final enhancements to surface regularities. Geometrical levelling is provided by uniform current distribution and additional true levelling is the result of specific organic additives with the ability to produce uniformly microdistributed deposits [127, 128]. Brightening is another property of the bath in production of deposits with orientated grain structure and crystalline size less than the wavelength of visible light i.e. smaller than 0.4 µm. Both the leveller and the brighter provide some degree of grain refinement to the deposits, however, a grain refiner interferes with nucleation and growth process of the deposits and leads to the decrease of the grain size. Some additives can play various roles in the plating bath [127]. In zinc electrodeposition PEG is mainly used as a brightener [102, 129-132], CTAB as a leveler and a grain refiner [20, 133-136] and thiourea as a grain refiner [20, 137, 138]. In some cases, a combination of additives and their synergistic effect have led to the production of zinc coatings with finer grains or even nanocrystalline structure [17, 20, 24, 137, 139, 140].

2.6.4.5. Pulsed-Electroplating

Pulse deposition has been used for controlling the electrocrystallization process and production of coatings with superior properties than the coatings deposited from direct electroplating [142,143].

Basically, in direct current electrodeposition current density is the only variable of importance. However, in pulse electroplating peak current density, current on-time ((T_{ON}) during which the current is applied) and current off-time ((T_{OFF}) zero current is applied) are the three main parameters of the plating process.

In pulse deposition the duty cycle is given by the following equation [141]:

$$Duty\ cycle = \frac{T_{ON}}{T_{ON}+T_{OFF}} \times 100 \qquad (2.12)$$

Duty cycle varies from 1 to 100% and on-off time from microseconds to milliseconds. Various combinations of square wave pulses can be used. Simple square wave pulses are mainly used for plating. Fig. 2.21 shows a schematic representation of different forms of pulses.

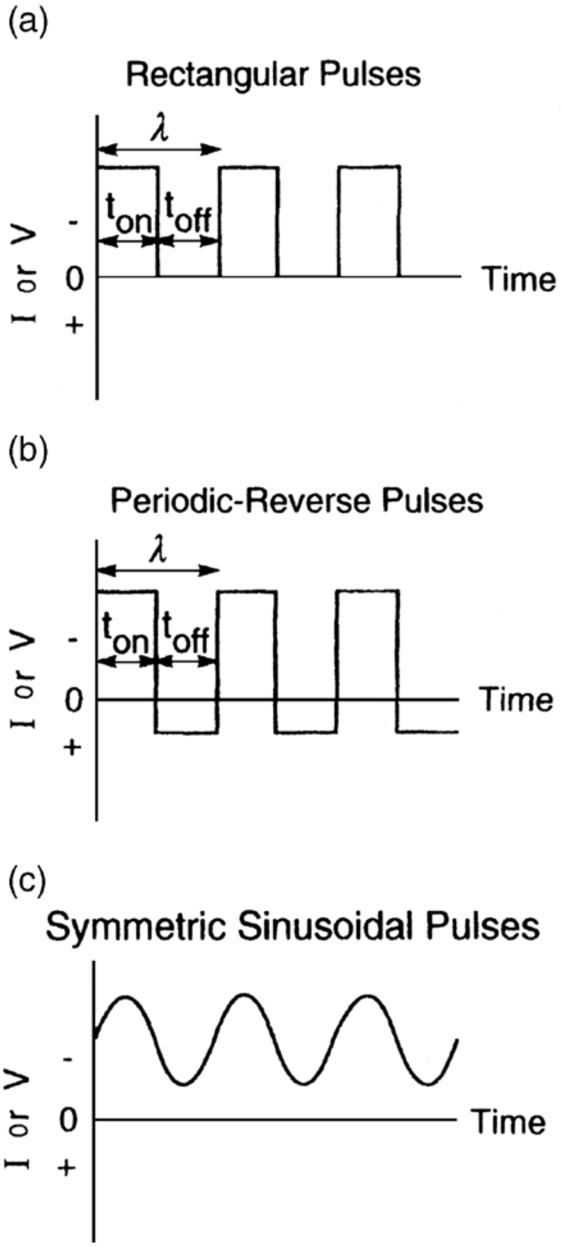

Fig. 2.21 Schematic representation of various types of pulses applied in pulsed deposition [141].

The average current density in pulse electrodeposition is defined as:

$$\text{Average current density} = \text{peak current} \times \text{duty cycle} \quad (2.13)$$

In pulse plating, pulse current density is higher than direct current plating thus more energy is available for the formation of new nuclei, as a result, nucleation and number of grains per unit area are increased which leads to refinement of the structure and production of finer deposits. Mechanical and physical properties of the coating could also improve by pulse deposition [142, 143].

Pulse deposition can be used for the deposition of single metals such as zinc and chromium with enhanced properties. Nanostructured zinc coatings deposited by pulse electrodeposition have improved hardness and corrosion properties [140]. Grain refinement and hardness improvement were observed for the deposition of chromium under pulse current deposition compared to the direct plated deposits. Corrosion resistance of the coating was also improved. Pulse electrodeposition is also used for the deposition of alloys [144]. In alloy pulse plating, changing the current density and on-off time can lead to the change of the composition and even multi-layered coating can be achieved [143]. For example in Zn-Co alloys cobalt content varied with the change of T_{ON} and the applied current density [145].

It should be considered that due to a large number of experimental variables, the complexity of the process and lack of standard procedure in evaluating a specific parameter, contradictory results for the same electroplating system using pulse deposition have been reported. An example is the result presented by Youssef et al. [137] and Chandrasekar et al. [17] on the electrodeposition of zinc. Youssef et al. stated that an increase in T_{ON} led to grain refinement. However, Chandrasekar et al. reported an increase in grain size with the increase in T_{ON}.

2.7 Nanostructured coatings

Nanocrystalline materials are produced by controlling the microstructure in nanometric levels. These materials have a grain size less than 100 nm in which more than 50 vol. % of atoms belong to the grain boundaries or interfacial boundaries. Fig. 2.22 shows a two-dimensional model of a nanostructured material. The black circles (atoms) showing the crystal and the white circles (atoms) showing the grain boundary [146, 147].

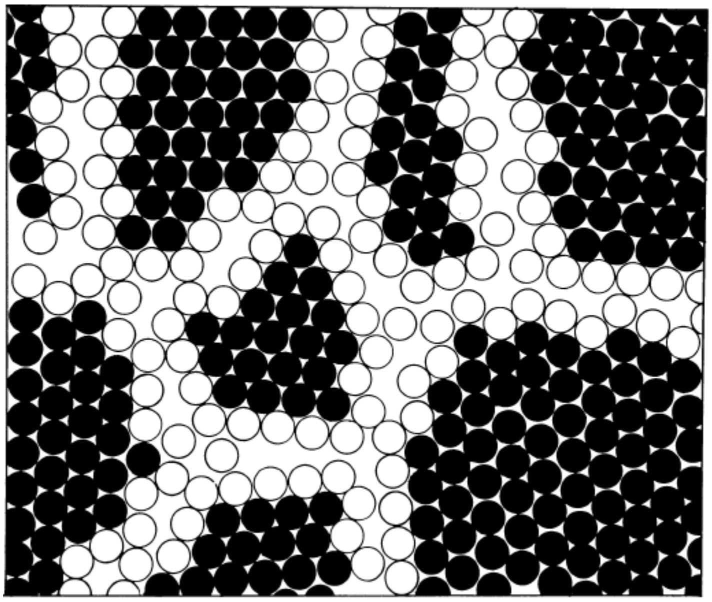

Fig. 2.22 A schematic diagram showing a two-dimensional model of a nanostructured material. The black circles (atoms) indicate the grains and the white circles (atoms) represent the grain boundary [146].

Nanocrystalline materials based on the shape of the crystal are categorized in layer shaped, rod-shaped and equiaxed crystallite groups as it is presented in Fig. 2.23 [147, 148].

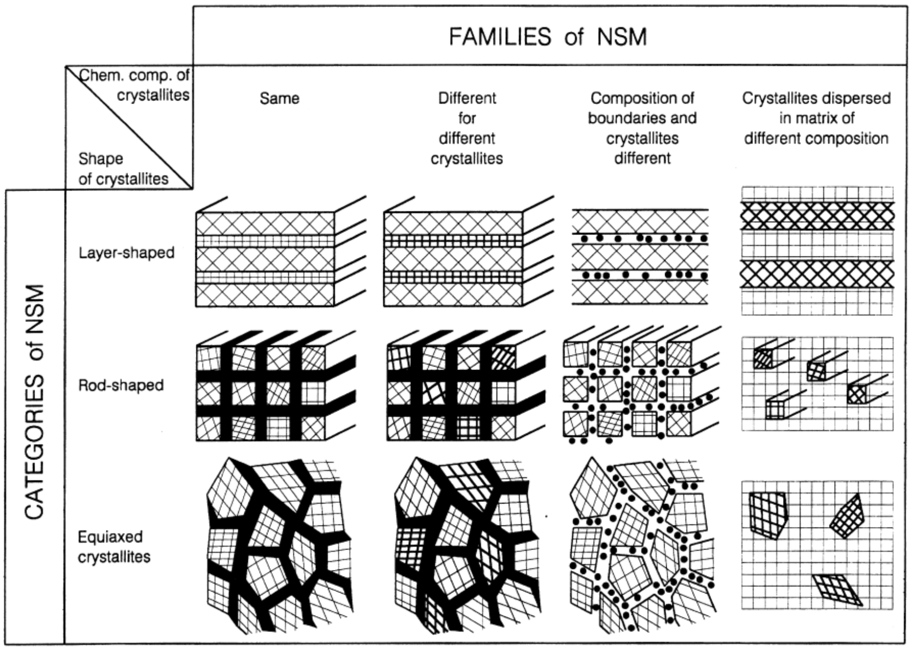

Fig. 2.23 Classification of nanostructured materials (NSM) based on their geometrical shape [149].

2.7.1 Nanocrystalline material; methods of fabrication

Nanocrystalline materials can be produced by various methods from the vapour, solid and liquid route. Physical vapour deposition (PVD), chemical vapour deposition (CVD), spray conversion processing, gas-phase condensation of particulates and consolidation [146, 150, 151] are methods from vapour route. Among these methods, CVD has some advantages as a pure, dense and uniform film at a high deposition rate and can be deposited on complex shape components. Metallic, ceramic and semiconducting thin films can be deposited by this method [6].

Mechanical alloying and compaction [152-155] and severe plastic deformation [156] are methods from the solid route mainly for the production of bulk nanocrystalline material.

Electrodeposition [12, 15-24] and sol-gel are from the liquid route. Sol-gel has been used for the production of metal oxides, ceramic powders and coatings in nano scale [157-160].

Each of these methods have advantages and disadvantages. Mechanical alloying is able to produce reasonable size billets of material, but it is not able to control material purity and obtain full density. Highly dislocated grains are produced under severe plastic deformation which are not uniform in size. Gas-phase condensation suffers from lack of complete densification. It is limited by the volume and control of the grain size during the consolidation process. During the electrodeposition of metals from aqueous solution hydrogen absorption and desorption may result in the formation of nano size voids in the electrodeposited metal. However, high purity and high density nanocrystalline material could be produced by this method. TEM images of electrodeposited nanocrystalline nickel (average grain size 30 nm) is presented in Fig. 2.24.

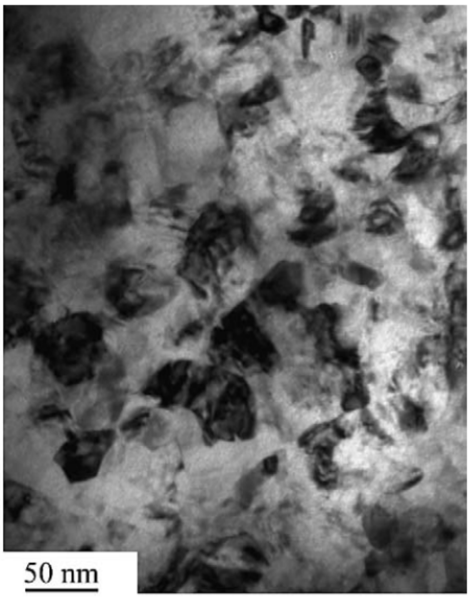

Fig. 2.24 Bright field TEM images of electrodeposited Ni [11].

Nowadays, more efforts are focused on the production of nanocrystalline material by electrodeposition. Electrodeposition is a low cost and industrial applicable process. Grain refinement is achievable by modification of the plating bath and plating parameters. Various types of conducting materials can be coated by this method under a high production rate [142, 143].

However, due to the variation of the properties of the material produced by aforementioned methods, there is no single process or method based on the application to produce a perfect coating.

Nanocrystalline materials and coatings exhibit different properties than those microcrystalline ones. Some of the properties of these materials are discussed below.

2.7.2 Mechanical properties

Nanocrystalline material shows high yield strength and hardness, and reduced tensile elongation in comparison to the microcrystalline material. Hardness and yield strength increases with decreasing grain size down to 15 nm [6, 7]. Fig. 2.25 [11] is a plot showing hardness as a function of grain size .

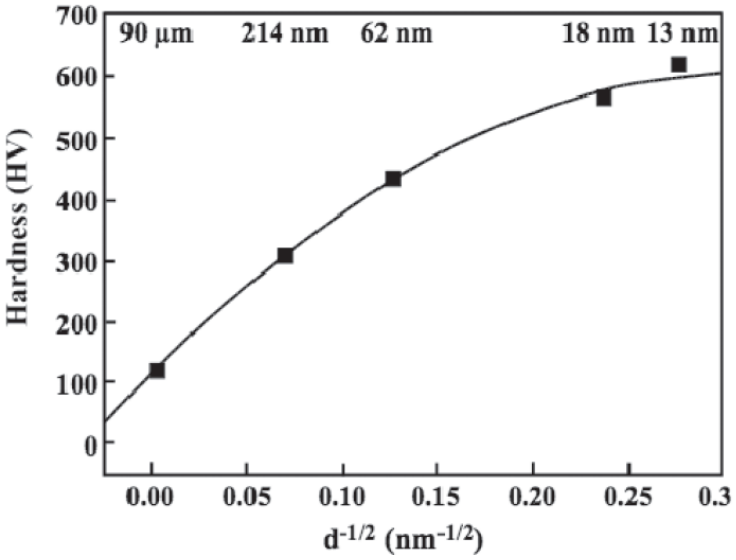

Fig. 2.25 Plot showing a variation of hardness as a function of grain size [11] .

When grain size is below 10 nm the strength decreases and the Hall-Petch relationship (based on Hall–Petch relationship, yield stress increases with the inverse of the square root of the grain size) is no longer valid. The exact reason for this phenomena is still a matter of controversy as the behavior of dislocations at this grain size is not exactly clear and conventional dislocation mechanisms do not apply to grain sizes below a critical value which may prohibit the pile-up of dislocations against grain boundaries [6]. Fig. 2.26 [7] is a plot showing a reduction of the flow stress at the grain sizes less than 10 nm.

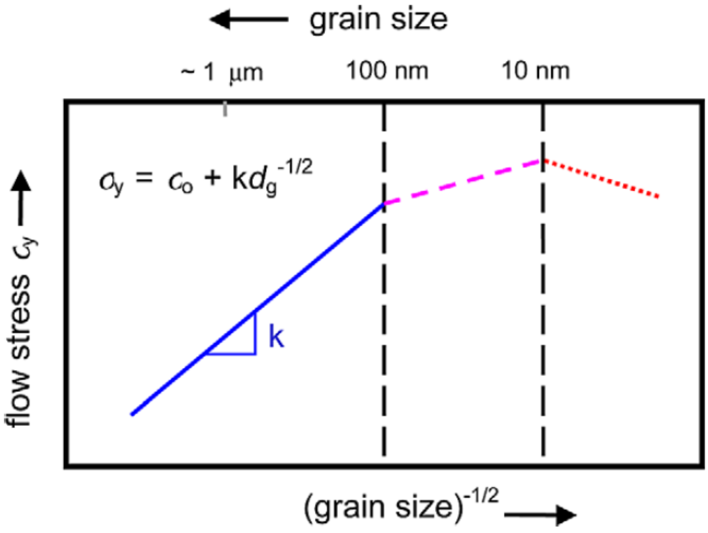

Fig. 2.26 Plot showing a variation of flow stress as a function of grain size [7].

Ductility of microcrystalline materials increase with grain refinement. However, ductility of metals decrease in grain sizes less than 25 nm. Defects such as porosities, tensile instability and crack nucleation or shear instability are the three main reasons explaining the inverse effects of grain refinements and ductility under 25 nm [161-163].

Superplasticity of nanocrystalline metals depends on the homologous temperatures (ratio of the test temperature to the melting point) and the strain rate. At low homologous temperature and high strain rates these materials show more superplasitsity than the microcrystalline ones [6]. Superplasticity has been reported in nanocrystalline Ni, Ni_3Al and aluminum alloy (1420Al; Al-Mg-Li) at 350, 300 and 725 °C, respectively [164-167].

Under stress controlled conditions, high cycle fatigue behavior of materials depends on the mechanical strength of the material and low cycle fatigue behavior depends on the tensile ductility. A study of the high cycle fatigue behavior of nanocrystalline and macro crystalline Ni under stress-controlled conditions showed that these materials possess better properties (high endurance limit) than microcrystalline ones [168]. On the other hand, low cyclic fatigue behavior deteriorated with grain refinement [169].

2.7.3 Corrosion Properties

Corrosion properties of the materials change with altering or different types of microstructure. There is no common or general relationship between grain size and corrosion properties of materials and the exact relationship is still under debate. Literatures show a wide variation of the corrosion properties of materials based on their grain size and demonstrated that for a material improvement or degradation depend on not only to the grain refinement, but also to the corrosive environment and fabrication method. In some cases there is even controversy surrounding properties of a material with the same trend of grain refinement in the same corrosive media [170] .

For example, it has been reported that corrosion properties of ferrous alloy increase with the decrease of the grain size [8, 171-177], and some other literatures reported that the susceptibility to corrosion increases with the reduction of grain size [178-180].

It has been reported that zinc corrosion rate decreases as the grain size decreases to nanometre scale in NaOH and NaCl corrosive media [181]. In contrast, degradation of the corrosion properties of zinc with grain refinement down to nano scale has been reported [181].

2.8 Summary

Self-pierce riveting is a promising technique for joining dissimilar material and light weight metals such as Al and Mg. SPR joints may suffer defects such as fretting and corrosion. Application of a coating with advanced mechanical and chemical properties would increase the service life of a SPR joint. Due to limitations arising from the process itself, the coating for the rivet should be hard and ductile at the same time in order to work under the piercing and flaring process of joining sheets. On the other hand, to satisfy the required mechanical properties of the joint, usually the rivet material is different to the sheet material and the possibility of galvanic corrosion arises. Using a compatible coating of the rivet with the sheet material could concur this problem. In this regard zinc-tin alloy sounds promising as these coatings offer the sacrificial properties of zinc and the barrier protection of tin to the steel rivet at the same time. Also these coatings provide good frictional and ductility which fulfil the requirements of the riveting process.

Microstructure of the coatings plays a predominant role in their mechanical and chemical properties of the coatings. Most of mechanical properties of the materials such as mechanical strength and hardness increase with nanocrystallisation. However, the corrosion properties of the coatings with the reduction of grain size down to nano scale is a matter of controversy. More studies are required in order to evaluate the effects of grain size on the corrosion properties of the alloy coatings such as zinc-tin. As these alloys are already used in the automotive industry and improvement in their properties would be considered as an advantage.

Chapter 3

Experimental Methods

3.1 Overview

Fig. 3.1 shows a schematic representation of the experiments and characterization method performed throughout each chapter. A detailed description of the process is presented accordingly in the current chapter or if necessary at the beginning of each individual chapter. Description of all the used instrument is presented in this chapter.

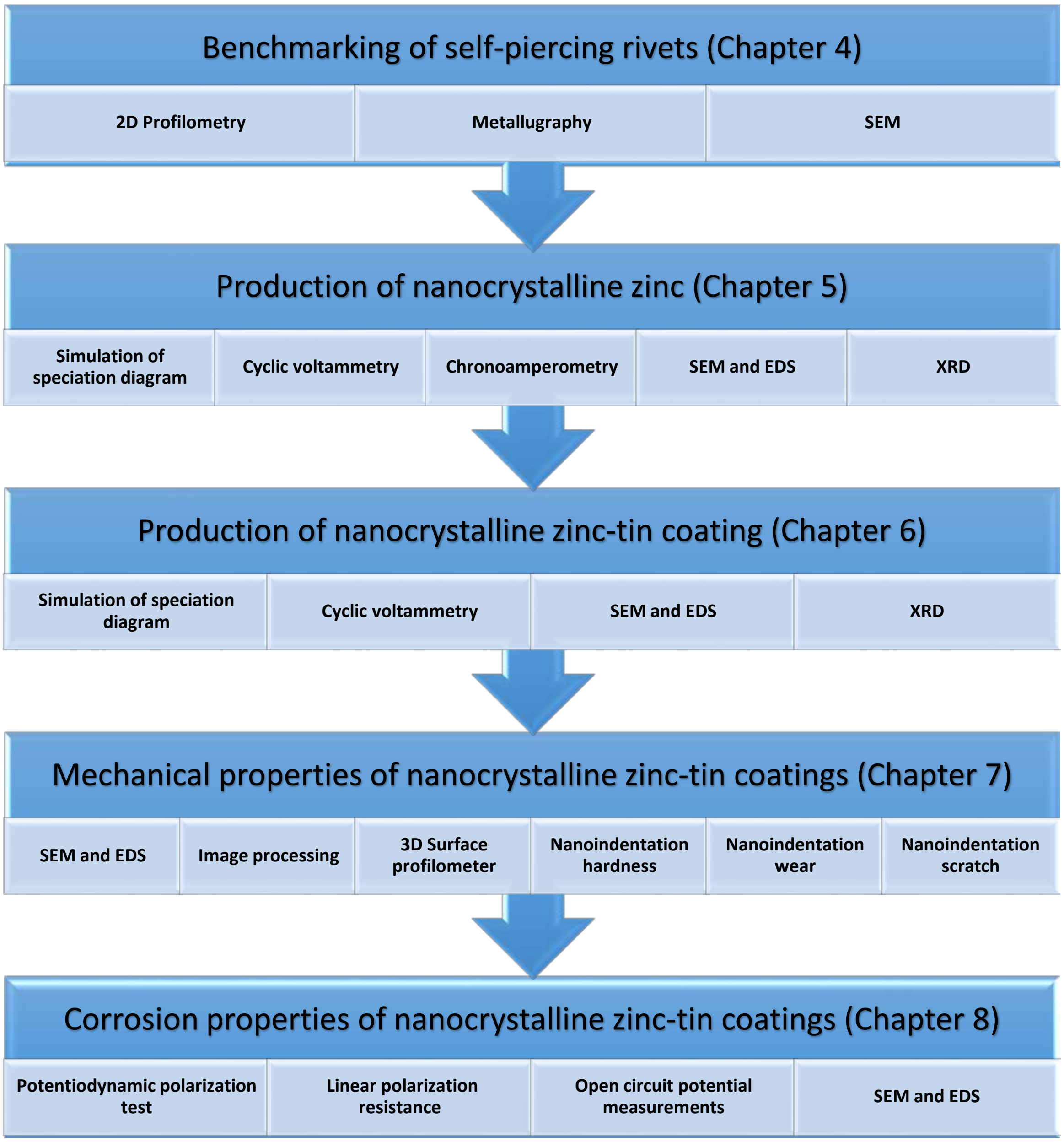

Fig. 3.1 Schematic representation of the experimental methods of each chapter.

3.2. Chemicals and materials

3.2.1 Rivet materials

Self-piercing rivets were provided by Henrob (part of the Atlas Copco group) company. Table 3.1 shows the characteristic of the rivets. Details of the joining process are presented in Chapter 4.

Table 3.1 Characteristics of the rivets.

Rivet Material	Rivet Coating	Top Coat	Nominal Hardness (Hv)	Nominal diameter of the rivet shank (mm)	Nominal effective length of the rivet shank (mm)
0.35% Carbon Steel	Almac	Gold chromate passivation	280	5	6
0.35% Carbon Steel	Zn-Sn	No passivation	280	5	6.5
0.35% Carbon Steel	Al	Clear chromate passivation	280	5	6.5

3.2.2 Chemical used in this study

Table 3.2 shows a detailed list of the chemicals and materials used in the present study for the production of nanocrystalline zinc and nanocrystalline zinc-tin coatings.

Table 3.2 List of the chemicals used in this study.

Chemical name	**Formula**	**Grade**	**Supplier**
Ethanol	C_2H_5OH	100%	Sigma- Aldrich
Acetone	$(CH_3)_2$ CO	100%	Sigma- Aldrich
Sodium hydroxide	NaOH	98.5%	AnalaR
Hydrochloric acid	HCl	32%	Sigma- Aldrich
Sodium sulfate anhydrous	Na_2SO_4	≥ 99%	Sigma- Aldrich
Zinc sulfate heptahydrate	$ZnSO_4$. 7 H_2 O	≥ 99%	Sigma- Aldrich
Tin (II) chloride	$SnCl_2$	≥ 99.99%	Sigma- Aldrich
Sodium D-gluconate	$HOCH_2[CH(OH)]_4CO_2Na$	97%	Sigma- Aldrich
Poly(ethylene glycol) Average M_n 400	$H(OCH_2CH_2)_nOH$	N/A	Sigma- Aldrich
Poly(ethylene glycol) Average M_n 2050	$H(OCH_2CH_2)_nOH$	N/A	Sigma- Aldrich
Thiourea	NH_2CSNH_2	≥99.0%	Sigma- Aldrich
Hexadecyltrimethylammonium bromide (CTAB)	$CH_3(CH_2)_{15}N(Br)(CH_3)_3$	≥99.0%	Sigma- Aldrich

3.2.3 Substrate material

3.2.3.1 Glassy carbon electrode

Glassy carbon electrode with 3 mm diameter were used as the working electrode (substrate) for all cyclic voltammetry and chronoamperometry experiments. Before each experiment surface of the glassy carbon electrode was polished with 0.3 micron alumina colloidal suspension followed by sonication in distilled water for 5 minutes. After sonication it was rinsed with acetone and dried with N_2 flux.

3.2.3.2 Steel substrate

Mild carbon steel (M 1030) were used as a working electrode (substrate) for the deposition of coatings. Table 3.3 shows the chemical composition of the steel. The alloy was supplied by Milltek Company and were cut to desired thickness. Fig 3.2 shows a schematic representation of the disc. The diameter of the disc was 12 mm and the thickness was 5 mm.

Table 3.3 Chemical composition of the M1030 mild carbon steel [182].

Alloying elements	C	Si	Mn	P	S
Weight %	0.25-0.35	0.35 max	0.3-0.9	0.05 max	0.05 max

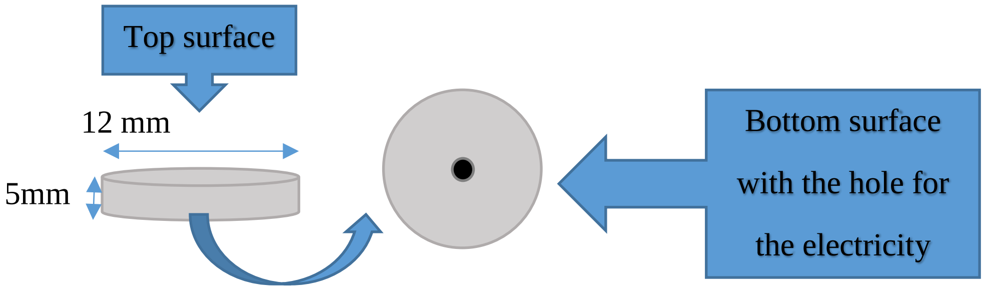

Fig. 3.2 Schematic representation of the steel substrate.

Surface of mild steel discs polished to mirror finish using emery paper (120-1200 grit sizes) and 0.3-micron alumina colloidal suspension sequentially, then sonicated in ethanol for 5 minutes followed by rinsing with distilled water. The polished discs were pickled in 10 % HCl for 10 s then rinsed with water and dried using N_2 flux. The disc was then placed in the plating electrolyte immediately after cleaning in order to avoid contamination.

3.3 Coatings deposition

Zinc and zinc-tin coating with various structures were synthetized by electrodeposition process. In this sub-chapter, electrodeposition technique has been explained further detail of the deposition process such as current density and time is presented in the following chapters.

3.3.1 Electrodeposition technique

Electrodeposition is a process in which ions of the depositing material in an electrolyte are moved by an electric field and deposit on the surface of the working electrode. Major component of the electroplating cell are two electrodes, the part to be coated (working electrode) is placed at the cathode and the coating material is placed as the anode (in case of consumable anodes). However, in some cases (also in this study) anodes are not consumable and the metallic ions of the deposit are fed into the electrolyte. Anodes and cathodes are connected to the positive and negative terminals of the external power supply respectively. A direct current or pulse current can flow between anode and cathode and consequently lead to oxidation and reduction to be proceed.

In this study, mild steel substrate after proper preparation used as the cathode (working electrode). A platinum mesh (2 cm × 2 cm) used as the counter electrode and Ag/AgCl (1M KCl) was used as the reference electrode. A schematic representation of the electroplating cell is presented in Fig. 3.3.

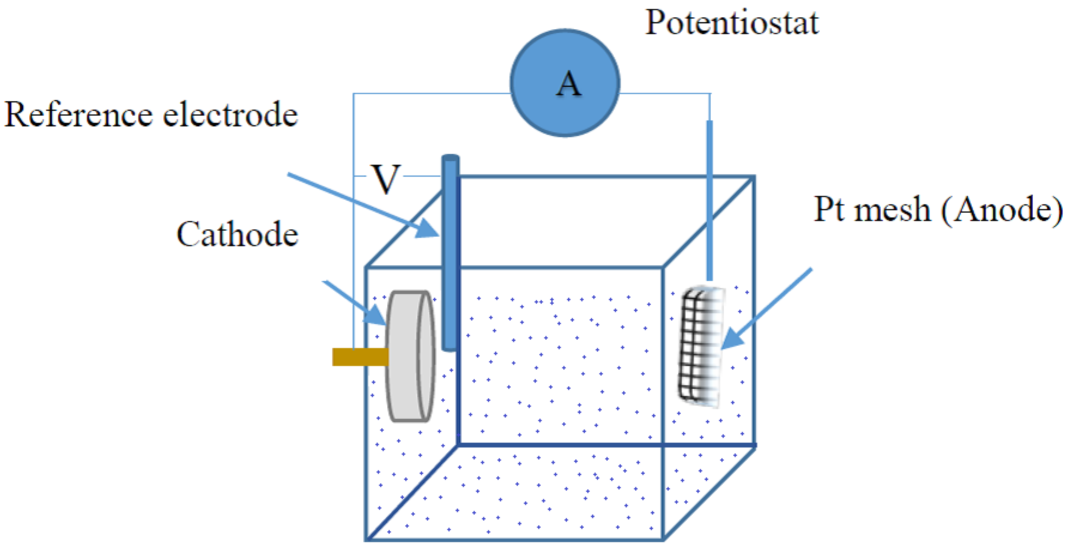

Fig. 3.3 Schematic representation of electroplating cell.

3.4 Electrochemical measurements

3.4.1 Cyclic Voltammetry

Cyclic voltammetry (CV) is an electrochemical technique which is used for the evaluation of the kinetics of the electron transfer process in an electrochemical cell. It is a popular technique for initial electrochemical studies of new systems and is very useful in obtaining information about fairly complicated electrode reactions. This technique is a type of potentiodynamic electrochemical measurements in which the potential of the working electrode is ramped linearly versus time and the resulting current is measured. Normally the potential is applied from an open circuit potential (OCP) or initial potential (E_i) up to the set values or final potential (E_f) (usually cathodic) following by sweeping (usually anodic) the potential to the initial values (such as OCP). In cathodic scan, deposition (reduction) peaks of the dissolved species and at the anodic scan dissolution (oxidation) peaks of the dissolved species in the electrolyte appear.

In this study cyclic voltammetry were performed in a 80 milliliter three electrodes glass cell. In a three electrodes cell, the potential is applied between a reference electrode and working electrode. The resulting current is measured between a working electrode and a counter electrode. In all measurements, glassy carbon was used as the working electrode, Ag/AgCl (1 M KCl) as the reference electrode and platinum wire was used as the counter electrode. All electrochemical measurements were performed using a CHI electrochemical analyser (CH Instruments, Texas, USA) at the scan rate of 50 mV/s at room temperature (21 ± 1 °C) without stirring. Fig. 3.4 shows a schematic representation of the cyclic voltammetry wave form.

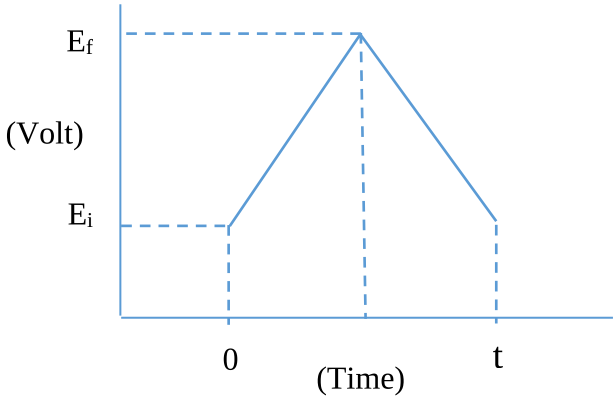

Fig. 3.4 Schematic representation of the cyclic voltammetry wave form.

3.4.2 Chronoamperometry

Chronoamperometry is an electroanalytical method in which the potential of working electrode is stepped to a set value and the corresponding current from faradic process occurring at the working electrode is measured as a function of time. Chronoamperometry gives quantitative information on nucleation process. The schematic representative of the potential step is presented in Fig. 3.5.

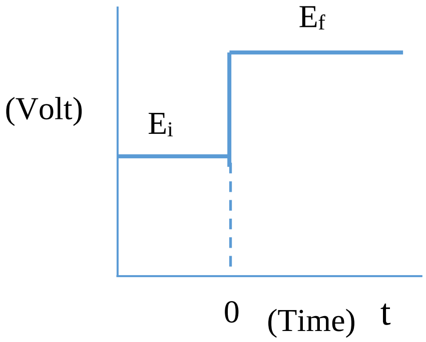

Fig. 3.5 Schematic representation of the wave form of a potential step experiment.

The same three electrode cell arrangement (Fig. 3.3) as discussed for the cyclic voltammetry was used for the chronoamperometric experiments.

3.4.3 Corrosion studies

In a corrosive environment, corrosion occurs between anodic and cathodic parts of a corroding system and leads to an electric current in metal and ionic current in the electrolyte at the metal-electrolyte interface. To evaluate the rate of corrosion, the amount of produced current of oxidation or reduction reaction should be measured.

Various electrochemical measurements were performed to examine corrosion properties of the Zn-Sn coatings. For all various methods a corrosion flat cell with 500 ml capacity (with similar structure to the cell in Fig. 3.3) was used. Zn-Sn coating on a steel substrate with the surface area of 1 cm^2 were used as the working electrode. Platinum mesh (2 cm ×2 cm) and a Saturated Calomel Electrode (SCE) were used respectively as the reference and counter electrode. All the measurements were performed in 0.63 M NaCl (pH = 6.2) as the corrosive media at room temperature (21 ± 1°C) without either aeration or deaeration. Electrochemical measurements were conducted using a PARSTAT 2273 electrochemical station through electrochemical PowerCorr software. Each measurement were performed minimum 3 times to ensure of reproducibility.

3.4.3.1 Open circuit potential (OCP) studies

Open circuit potential is the potential of a working electrode relative to the reference electrode in the absence of any applied potential or current. Usually the sacrificial properties of the metal coatings are evaluated by measuring the open circuit potential over time.

OCP of the Zn-Sn coatings were measured during 12 hours under free corroding condition in a 0.63 M NaCl solution.

3.4.3.2 Linear polarization resistance (LPR)

Linear polarization resistance (LPR) is a nondestructive technique to measure corrosion rate data. In this technique working electrode is polarized, very close to corrosion potential typically in the order of ± 25 mV, relative to its OCP and the potential is measured when no current is flowing. The polarization resistance of a material is defined as the slope of the potential-current density ($\Delta E/\Delta I$) curve at the free corrosion potential. Polarization resistance is related to corrosion current by the Stern-Geary equation [183].

$$R_P = \frac{B}{i_{corr}} = \frac{(\Delta E)}{(\Delta I)}\ (\Delta E) \to 0 \tag{3.1}$$

In which: R_p is the polarization resistance, i_{corr} is the corrosion current, B is the proportionality constant, and can be calculated according to the following equation from the anodic (b_a) and cathodic (b_c) of Tafel slopes.

$$B = \frac{b_a \times b_c}{2.3\ (b_a + b_c)} \tag{3.2}$$

For LPR measurements the potential was swept linearly from −20 mV to +20 mV vs. OCP at a scan rate of 0.166 mV/s. The scan was performed for 12 hours, after each one hour the polarization resistance was recorded.

3.4.3.3 Potentiodynamic polarization measurements

Potentiodynamic polarization is a technique where the potential of a electrode is varied at a selected rate by application of a current through the electrolyte. Passivation tendencies and effects of inhibitors or oxidizers on specimens are distinguished with this technique.

In anodic polarization, working electrode potential is scanned in an anodic direction (positive direction) causing the working electrode to become as the anode and corrodes.

In cathodic polarization, working electrode potential is scanned in an cathodic direction (negative direction) causing the working electrode to become more negative and electron are added to the surface.

Anodic potentiodynamic measurements were performed by sweeping the potential at a scan rate of 5 mV/s from -250 mV vs. OCP to 1600 mV (vs. SCE) after 1 hour of immersion in 0.63 M NaCl.

From the polarization curves, the corrosion current density and the corrosion potential were measured and fitted with PowerCorr Software.

3.5 Characterizations techniques

Corrosion properties of the coatings were characterized by various methods as explained earlier in sub-chapter 3.4.3. Physical and structural characterization methods of the coatings will be discussed in the following sub-chapters.

3.5.1 3 dimensional (3D) surface profilometry

3D surface profilometry is a non-contacting and non-destructive method for measuring the surface profile of the specimen. It produces a three dimensional representative of the surface by using the wavelength of light. Fig. 3.6 shows a schematic drawing of 3D profilometer.

Light is scattered by the upper beam splitter and is directed to the objective lens. The lower beam splitter splits the light into two separate beams. One beam goes to the sample and the other one goes to an internal reference mirror. Finally, the two beams recombined and directed to the detector. In this study, surface profile measurements were performed using a ContourGT-K, Bruker Nano, 3D profilometer (USA) coupled with SurfVision software.

Amplitude parameter which gives information about the height deviation in surface topography are measured in this study. Thes parameters include a) Sq; the root mean square value of the ordinate values within a sampling area, b) $S_{a;}$ the arithmetic mean of the absolute height, c) S_{Sk}; Skewness of topography height distribution and d) S_{ku}; Kurtosis of topography height distribution. The formulae for each of the parameters are presented in Table 3.4.

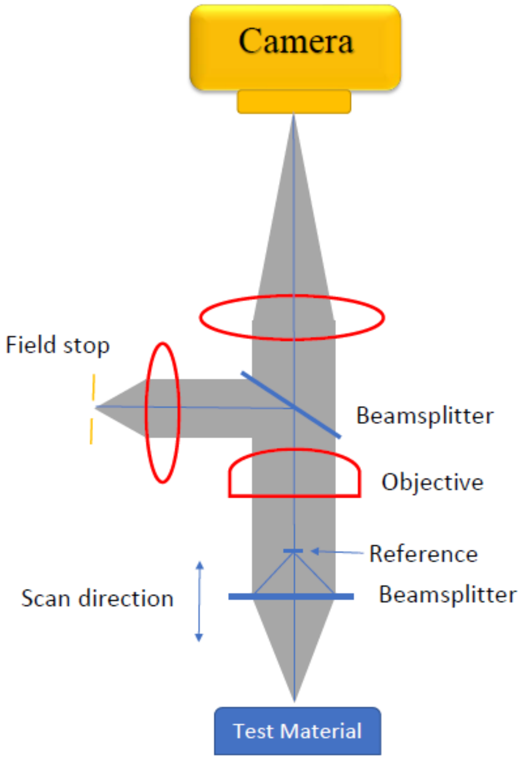

Fig. 3.6 Schematic representation of a 3D-surface profilometer.

Table 3.4 Formulae for surface amplitude parameters [184].

$S_q =$	$S_a =$	$S_{sk} =$	$S_{ku} =$
$\sqrt{\frac{1}{N}\frac{1}{M}\sum_{i=1}^{N}\sum_{j=1}^{M} z_{ij}^2}$	$\frac{1}{A}\int_A \lvert z(x,y)\rvert \; dx\,dy$	$\frac{1}{S_q^3}\left[\frac{1}{A}\iint_A z^3(x,y)\,dx\,dy\right]$	$\frac{1}{S_q^4}\left[\frac{1}{A}\iint_A z^4(x,y)\,dx\,dy\right]$
Where A is the sampling area, xy. Where *N* is the number of points in the *x* direction and *M* is the number of points in the *y* direction.			

3.5.2 X-ray Diffraction (XRD)

X-ray diffraction is a non-destructive technique. Chemical composition, crystallographic structure and orientation, phase identification, crystal size determination and unit cell dimension can be evaluated by XRD. In this method atoms of the test material are stroked by X-ray beams. The interaction of the incident rays with the test material produces constructive interference (and a diffracted ray) which follows Bragg's Law [185].

$$n\,\lambda = 2d \sin\theta \tag{3.3}$$

Where n is an integer, λ is the wavelength of the incident X-ray beam, d is the distance between atomic layers in a crystal, and θ is the angle of incident. Fig. 3.7 shows a schematic representation of the principles of the X-ray diffraction.

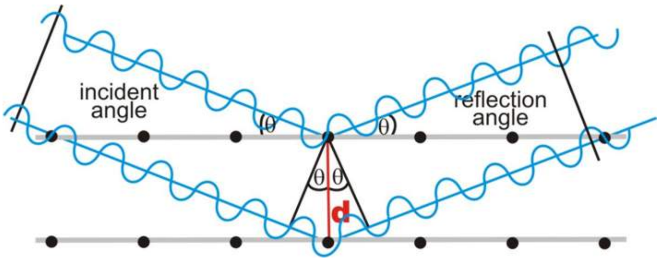

Fig. 3.7 Schematic representation of the principles of an X-ray diffraction (XRD).

In this study X-ray diffraction analysis was performed using a Bruker D8 Advance X-ray diffractometer with Cu Kα radiation (**λ**=0.15418 nm), working at 40 mA and 40 kV. The x-ray diffraction scan was performed at a rate of 0.2° min^{-1} for 2θ ranging from 20° to 90°.

Preferred crystallographic orientations of the grains were determined from the x-ray diffraction data based on the method described by Berube and Esperance [186]. In which texture coefficient (TC) is calculated from the following equation.

$$R_1 = \frac{I\ (hkl)deposit}{\sum_1^i I\ (h_i k_i l_i)deposit} \tag{3.4}$$

$$R_2 = \frac{I\ (hkl)standard\ sample}{\sum_1^i I\ (h_i k_i l_i)standard\ sample} \tag{3.5}$$

$$TC = \frac{R_1\ (hkl)\ deposit}{R_2\ (hkl)standard\ sample} \tag{3.6}$$

In which *I* is the intensity of the peak and *i* is the number of crystallographic plane.

3.5.3 Scanning Electron microscopy and Energy-dispersive X-ray Spectroscopy

The scanning electron microscope (SEM) scans the surface of test specimen by high-energy beams of electrons in a raster scan pattern. Interaction of the electron beams and atoms of the specimen can give information about surface morphology and composition of the samples. Specimens can be observed in high and low vacuum, in wet conditions (in environmental SEM), and at a wide range of cryogenic or elevated temperatures. Various signals can be produced by an SEM such as secondary electrons (SE), reflected or back-scattered electrons (BSE), photons of characteristic X-rays and light (cathodoluminescence) (CL), absorbed current (specimen current) and transmitted electrons. Backscattered electrons are used for chemical composition evaluation and secondary electron are used for the evaluation of surface morphology [187]. Fig. 3.8 shows a schematic drawing of a scanning electron microscope.

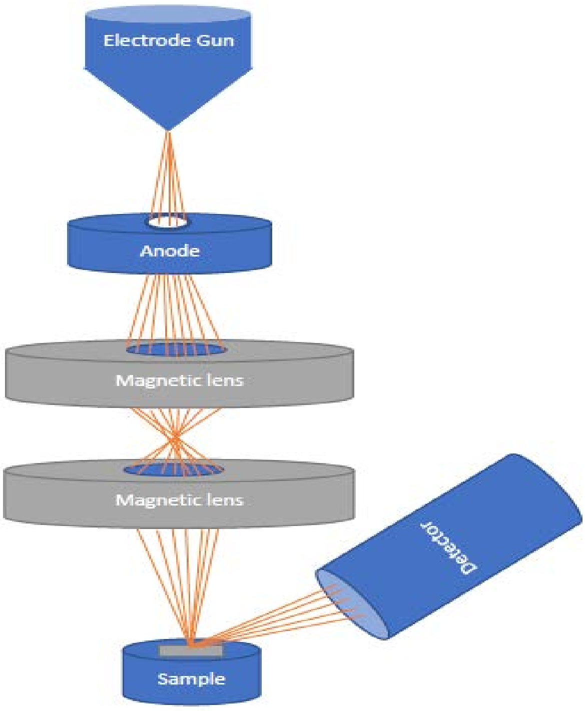

Fig. 3.8 Schematic representation of a scanning electron microscope.

Energy dispersive X-ray spectroscopy analyze the chemical composition of the specimen by using x-rays radiation emitted from the sample due to the bombardment of electron beams. The energy of the X-ray radiation is specific to each material therefore, leads to the identification of material.

In this study A Leica (MEF4M) Microsystem and a ZEISS Supra 40 VP field emission scanning electron microscope (FESEM) fitted with an energy dispersive X-ray spectrometer was used for surface morphology and chemical composition analysis.

3.5.4 Nanoindenting testing

Nanoindenting is the measurement of the mechanical properties of material on a very small scale. Mechanical properties of features less than 100 nm, and thin films less than 5 nm thick, can be evaluated. Test methods include hardness determination, scratch and wear evaluation. A three-sided, pyramid-shaped diamond probe tip is typically used for indenting.

3.5.4.1 Hardness testing

For nanoindentation, the tip is forced into the surface at a controlled rate and to a selected maximum force. Depth of penetration (h) is recorded versus the applied load. The generated load-displacement graph is plotted and is used to extract the nano-mechanical properties of material. Fig. 3.9 shows a typical load-displacement curve of a nanoindentation test.

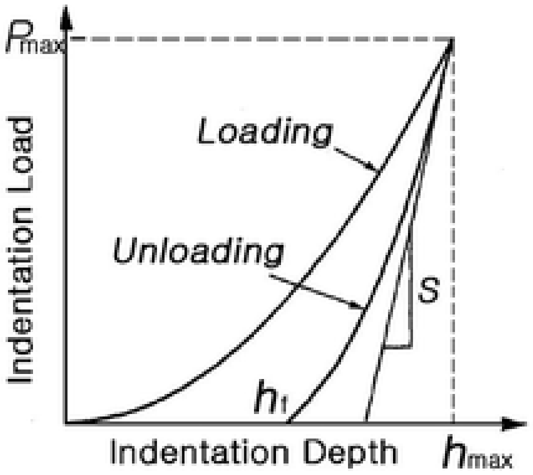

Fig. 3.9 Schematic representation of force-displacement curve of a nanoindentation.

The following procedure is used by the instrument according to Oliver and Pharr method [188] to calculate the reduced modulus and hardness from the load versus displacement curve:

- The curve is fit using the power law relation:

$$P = A\,(h - h_f)^m \tag{3-7}$$

- The derivative of the power law relation (with respect to *h*) is evaluated at the maximum load to calculate the contact stiffness, *S*.

- The contact depth, *hc*, is calculated with:

$$h_c = h_{max} - 0.75\times \frac{P_{max}}{S} \tag{3-8}$$

Where h_c is given as contact depth, h_{max} is given as maximum depth, P_{max} is given as maximum force and *S* is given as stiffness.

- The hardness is calculated with:

$$H = \frac{P_{max}}{A\,(h_0)} \tag{3-9}$$

Where *H* is given as hardness, P_{max} is given as maximum force and $A(h_c)$ is given as contact area.

- The reduced modulus is calculated with: where E_r is given as reduced modulus, $A(h_c)$ is given as contact area and *S* is given as stiffness.

$$E_r = \frac{\sqrt{\pi}}{2\sqrt{A\,(h_c)}} \times S \tag{3-10}$$

The reduced modulus (E_r) is related to Young' modulus (E_S) of the test specimen according to the following equation:

$$\frac{1}{E_r} = \frac{(1-\nu_i^2)}{E_i} + \frac{(1-\nu_s^2)}{E_s} \tag{3-11}$$

In which ν_i and ν_s are Poisson's ratio of the indenter and specimen respectively.

In this study, cyclic loading indentation were performed using a Hysitron TI-950 TriboIndenter with a Berkovich diamond tip (150 nm in diameter). Load was applied in a series of trapezoidal loading cycles with a total cycle of 20 on different positions (array of 5×4). Each load was applied linearly up to maximum load in 10 s with a dwell time of 10 s followed by unloading in 10 s. The maximum load for each cycle is incrementally increased with each loading cycle with the first cycle having a maximum load of 50 µN and last cycle having a maximum load of 1000 µN. For each coating twenty indentations were performed in the form of 5 × 4 array on 3 different positions. The indentations were separated by 20 µm. Thermal drift was set to be less than 0.05 nm/s. The nano hardness and elastic modulus of the coatings were evaluated by using Oliver and Pharr method as explained.

3.5.4.2. Nanoscratch

Tribological properties of the coatings can be determined by nanoscratch test.

The sample to be tested is moved perpendicular to the scratch probe whilst the contact is either held constant or ramped at a user-defined rate. Throughout the test the probe penetration depth and tangential (frictional) load are continuously monitored. Single and multi-pass tests are possible. Multi-pass tests allow the investigation of nano-wear as will be discussed later.

The nanoscratch test in this study was performed at the load controlled mode and at the constant load of 100 µN using the Hysitron TI-950 TriboIndenter with a Berkovich diamond tip (150 nm in diameter). The test was repeated for three times for each of the coatings. Fig. 3.10 shows a load function that was applied in this study.

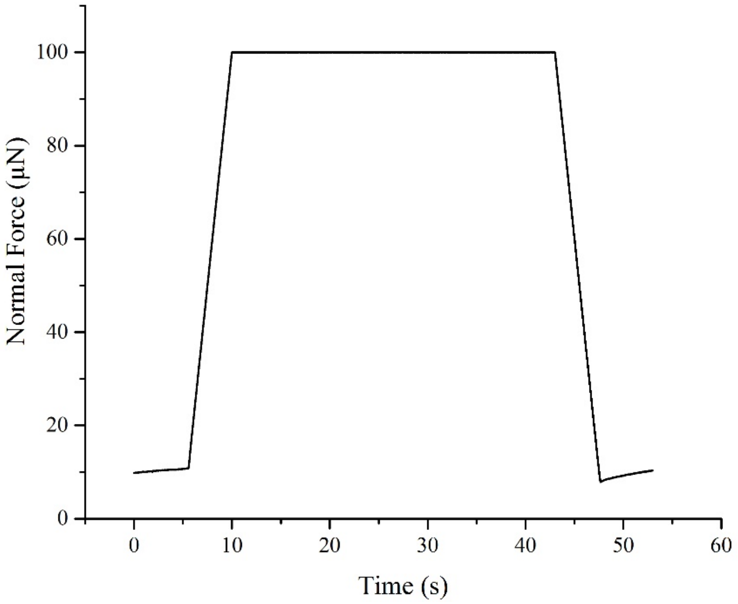

Fig. 3.10 Normal applied force versus time for performing the nanoscratch test.

3.5.4.3 Nanowear

A scanning wear test is performed by scanning an area at user defined number of passes at an elevated setpoint and then measuring the height difference from the surrounding area to calculate the amount of material worn away. Fig 3.11 shows a worn and a non-scanned area image taken by in-Situ Scanning Probe Microscopy (SPM) mode.

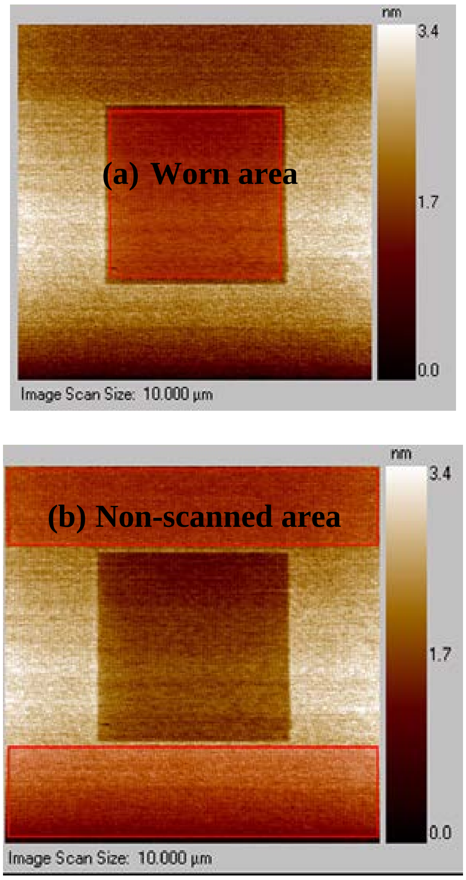

Fig. 3.2 SPM images showing a worn and a non-scanned area [189].

The wear volume is measured through the following relations [189].

|Height outside wear region [nm]| - |Height inside wear region [nm]| = Wear height [nm]

(Square of wear scan size [µm]) × (wear height [µm]) = Wear volume [μm^3]

In this study wear properties of coatings were analyzed with a constant load of 100 µN. The scan area was either 10×10 (μm^2) or 5×5 (μm^2), number of passes was 10 for both scan dimensions.

Chapter 4

Surface characterization of self-piercing rivets when used with Mg component

4.1 Introduction

Self-pierce riveting (SPR) is a mechanical joining technique that provides an alternative to resistance spot welding and is used for joining two or more sheets together. It is a solid state (non fusion) process which normally takes from 1 to 4 seconds. There is no requirement of pre-drilling or pre-punching, and even precise alignment between sheets and riveting tool is not necessary [35]. Life time of a SPR join may be affected by galvanic and crevice corrosion, hence coating of the rivet play a predominant role to stop or hinder corrosion [53]. Understanding the effects of joining process on the coating of a rivet and tailoring the relationships between structure and properties of coatings for SPR rivets are required not only for the protection of the rivet material itself, but also for galvanic compatibility with the parts to be assembled. The published scientific literature on coatings of SPR rivets is however limited [60]. In this study, rivets with Zn-Sn, Almac and aluminum coatings have been used to join magnesium sheets by laser assisted self-pierce riveting (LSPR). It has to be considered that SPR involves a high degree of localized plastic deformation especially at the bottom sheet which makes this process challenging for the materials such as Mg which has low formability at room temperature. Application of a laser beam as an add-on machine tool (laser-assisted SPR) can resolve the problem as it quickly increase the temperature of the sheets and lead to production of a crack-free join [42].

The microstructure, surface topography and roughness of the rivet’s coating have been characterized by optical microscopy, scanning electron microscopy (SEM), energy-dispersive X-ray spectroscopy (EDS) and surface profilometry. The effects of the joining process on the coating of the rivets have been evaluated.

4.2 Methodology

Magnesium has low formability at room temperature, therefore preheating of magnesium was required to prevent cracking during SPR joining. In this work, laser assisted SPR (LSPR) was applied using a 2.2 kW diode laser. Wrought 2.3 mm thick strips of AZ31B-H24 magnesium alloy were joined by LSPR using steel rivets with three different coatings: mechanical plated Zn-Sn (no passivation), mechanical plated Almac (gold chromate passivation), and electroplated aluminum (clear chromate passivation) coatings. Dial laser power was 700 W and preset pulse length was 3.5 seconds. Cross-sections of rivets, before and after joining, were prepared using standard metallographic techniques. Coating characterization was performed using a Leica (MEF4M) microsystem light optical microscope, ZEISS Supra 40 VP field emission scanning electron microscope, energy dispersive X-ray spectrometer analyzer and alpha-step D-120 Stylus Profiler. Characteristics of the rivets are shown in Table 3.1 (see Chapter 3).

4.3 Results and discussion

4.3.1 Characterization of the coatings before joining process

4.3.1.1 Surface Roughness

Roughness is one of the major properties of a surface. Wear and fretting properties are affected by roughness. Coefficient of friction at contact surfaces without lubricant increases with the increase of surface roughness [190]. Wear and friction inherently occurs during the joint formation process of self-pierce riveting. Therefore, surfaces with low roughness are more desirable for this purpose. Fig. 4.1 shows the surface profiles of three different rivets’ heads (see Fig. 4.11(c)) with Zn-Sn, Almac and aluminum coatings.

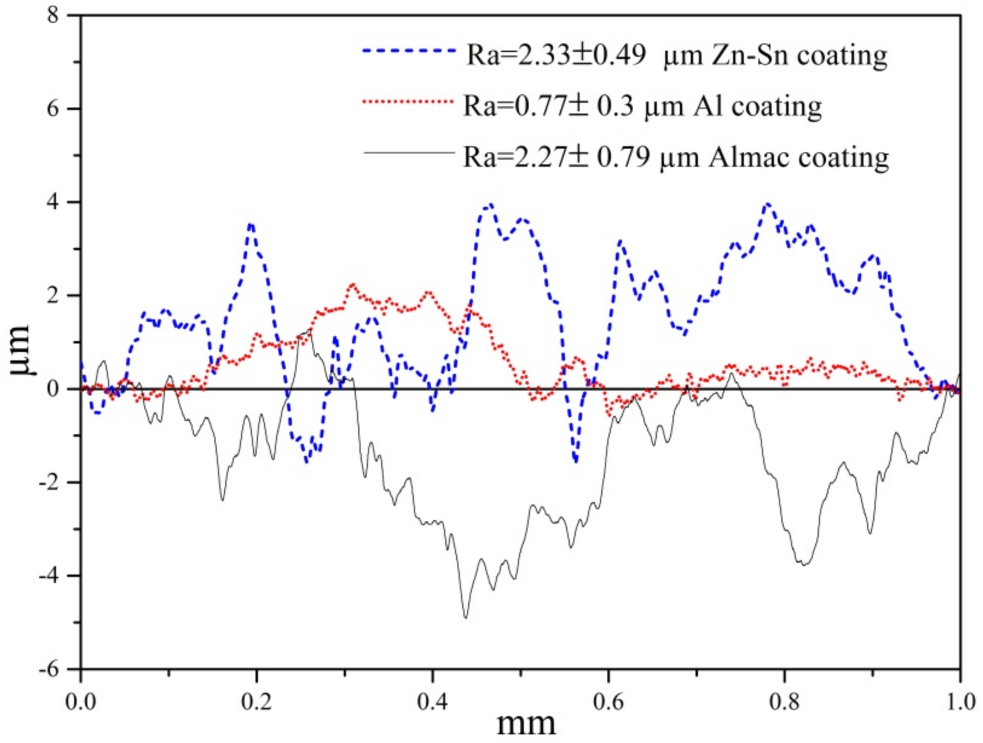

Fig. 4.1 Surface profiles of the rivet’s head with Zn-Sn, Almac and aluminum coatings.

The Ra values for Zn-Sn and Almac coatings are very close, while the Ra value for aluminum coating is three times lower. Several peaks were observed for Zn-Sn coating and valleys for Almac, while aluminum coating displayed neither large peaks nor deep valleys. Surface profiles reveal peaks and valleys which are related to the surface morphology of the coatings, as it is explained below.

4.3.1.2 Surface Morphology

Surface morphology of the coatings is presented in Fig. 4.2. The SEM images show a visibly rougher surface for Zn-Sn and Almac than aluminum coating as confirmed from the surface roughness analysis. Coating surfaces appeared porous, and displayed some protruding areas and holes (marked respectively by the blue and red circles in the higher magnification images in Fig. 4.2 (a′) to (c′).

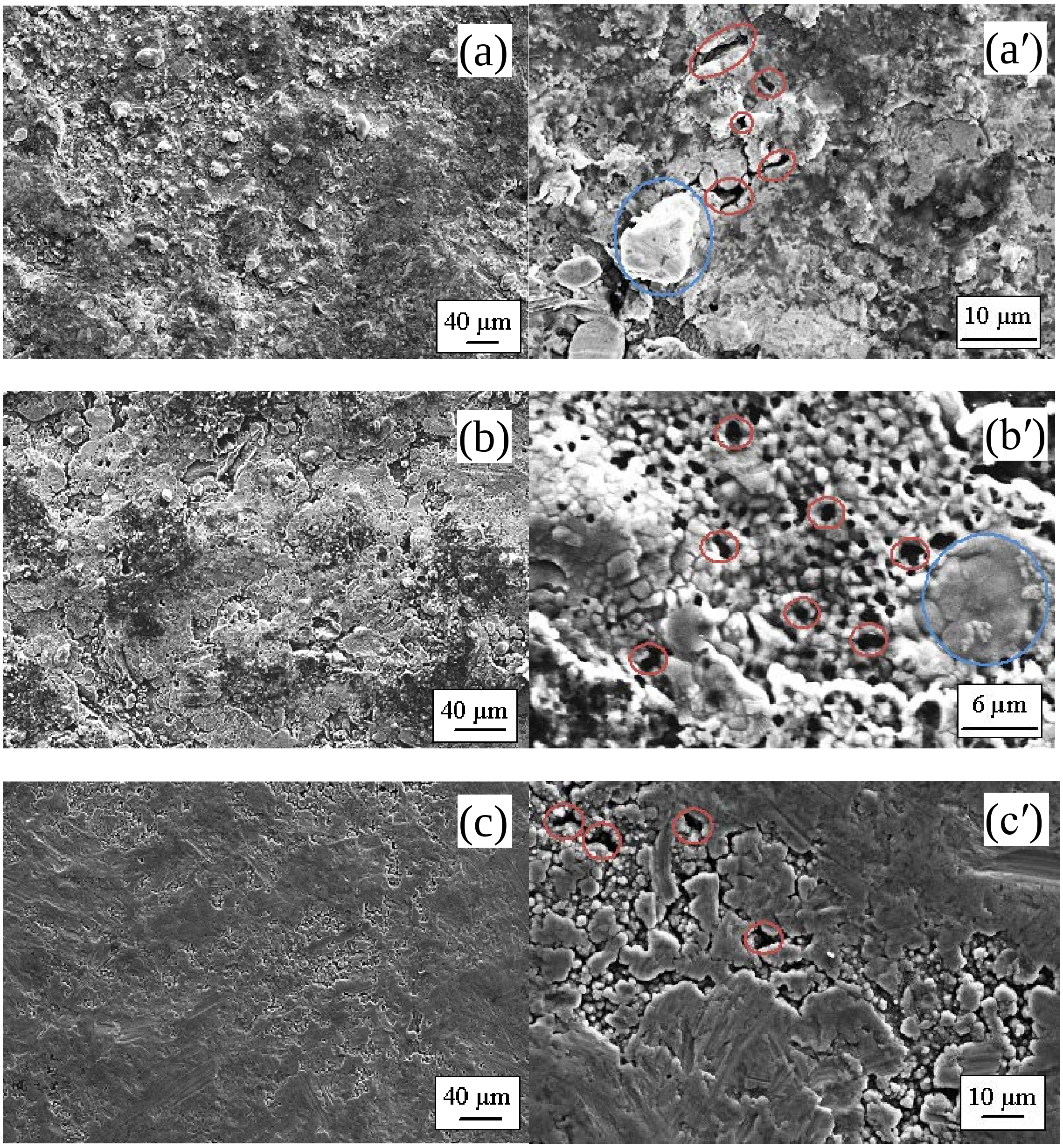

Fig. 4.2 Scanning electron micrographs of surface morphology of mechanically plated Zn-Sn (a, a′), Almac (b, b′) and electroplated Al (c, c′) coatings.

Coating in mechanical plating forms due to the cold welding and flattening of metal particles (with sizes in the range of 1 to 20 microns) to one another and to the surface of the work piece as a result of the generated kinetic energy of tumbling and some electromechanical process [191], while electrodeposition is based on add-atoms process. This difference in coating formation procedure between mechanical plating and electrodeposition would explain the difference between the Ra values of Zn-Sn, Almac and aluminum coatings.

4.3.1.3 Edge coverage analysis

Fig. 4.3 are SEM images showing the edge of a Zn-Sn, Almac and aluminum rivet's head as received, where part of the coating was missing for Zn-Sn and Almac, exposing the underlying steel substrate (see iron X-ray map of the same region in Fig. 4.3 (a′) and (b′)). This phenomenon was occasionally observed for the Zn-Sn and Almac coated rivets. The aluminum coating displayed more uniformity around the edge. In mechanical plating, the coating is more prone to build up in recesses rather than around the edges, whereas in electrodeposition, edge coating can be expected to be more uniform [192]. This defect may lead to crevice and galvanic corrosion which can happen near the edge of the rivet head and top sheet as discussed in sub-chapter 2.3.2.4 [53].

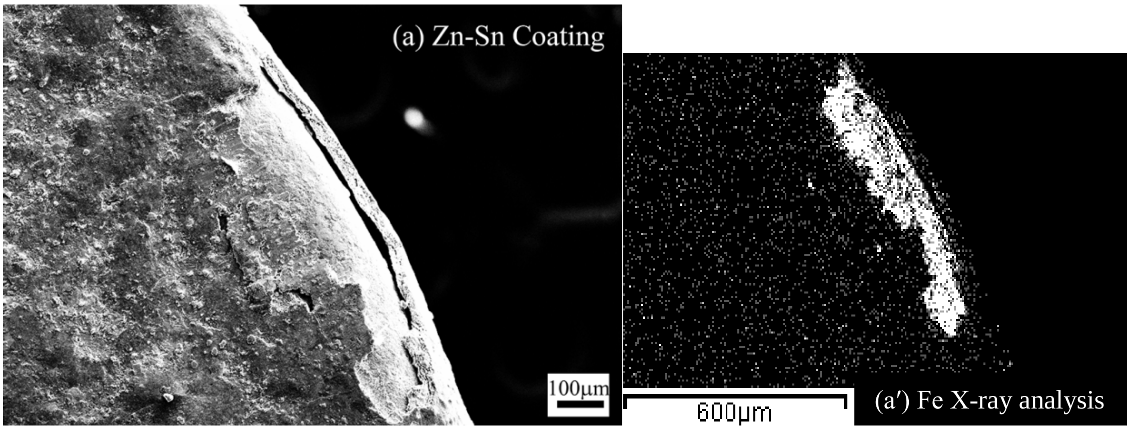

Fig. 4.3 (a) Scanning electron micrograph of the edge of the rivet with Zn-Sn coating and (a′) corresponding Fe elemental X-ray map for the same region.

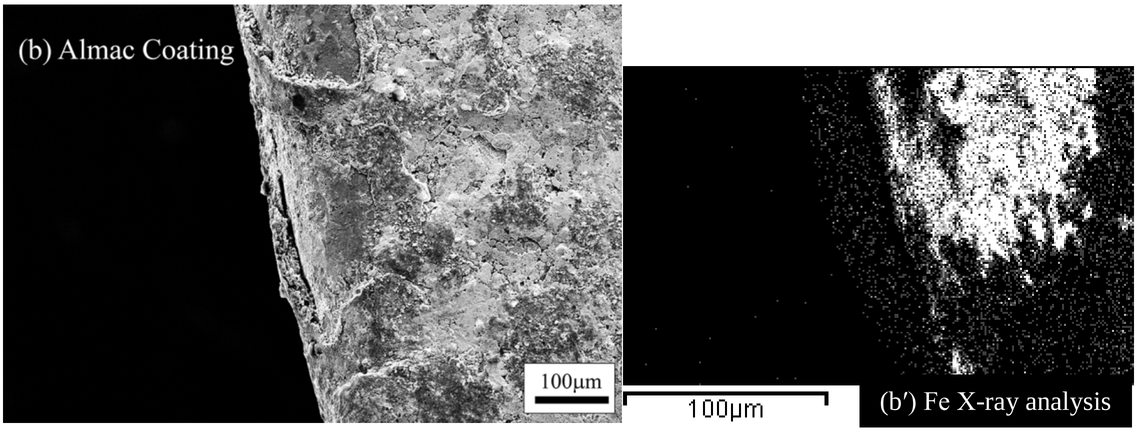

Fig. 4.3 (b) Scanning electron micrograph of the edge of the rivet with Almac coating and (b′) corresponding Fe elemental X-ray map for the same region.

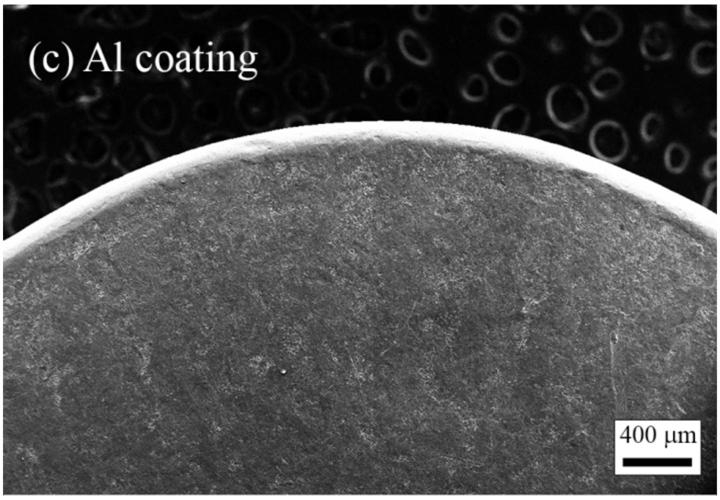

Fig. 4.3 (c) Scanning electron micrograph of the edge the rivet with aluminum coating.

4.3.1.4 Cross section analysis

Scanning electron micrograph of the cross section of the Zn-Sn coating on the rivet's head is presented in Fig. 4.4.

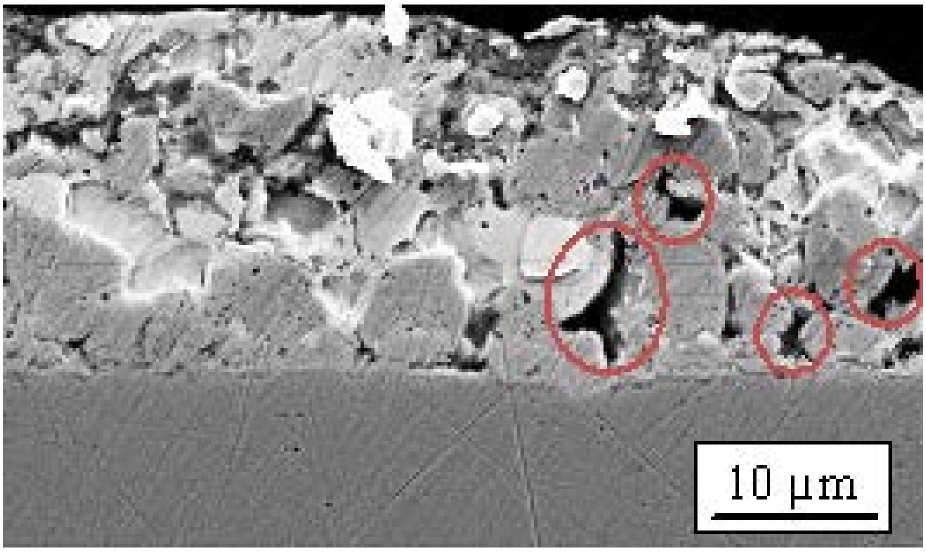

Fig. 4.4 Scanning electron micrograph of the cross section of the Zn-Sn coating on the rivet's head.

Similar to the surface of the Zn-Sn coating in Fig. 4.2 some porosities were observed at the cross section of the coating which are marked by red circles in Fig. 4.4.

X-ray elemental mapping of the Zn-Sn coating is presented in Fig.4.5. It shows that the grey and white regions in secondary electron micrographs correspond to zinc-rich and tin-rich phases respectively.

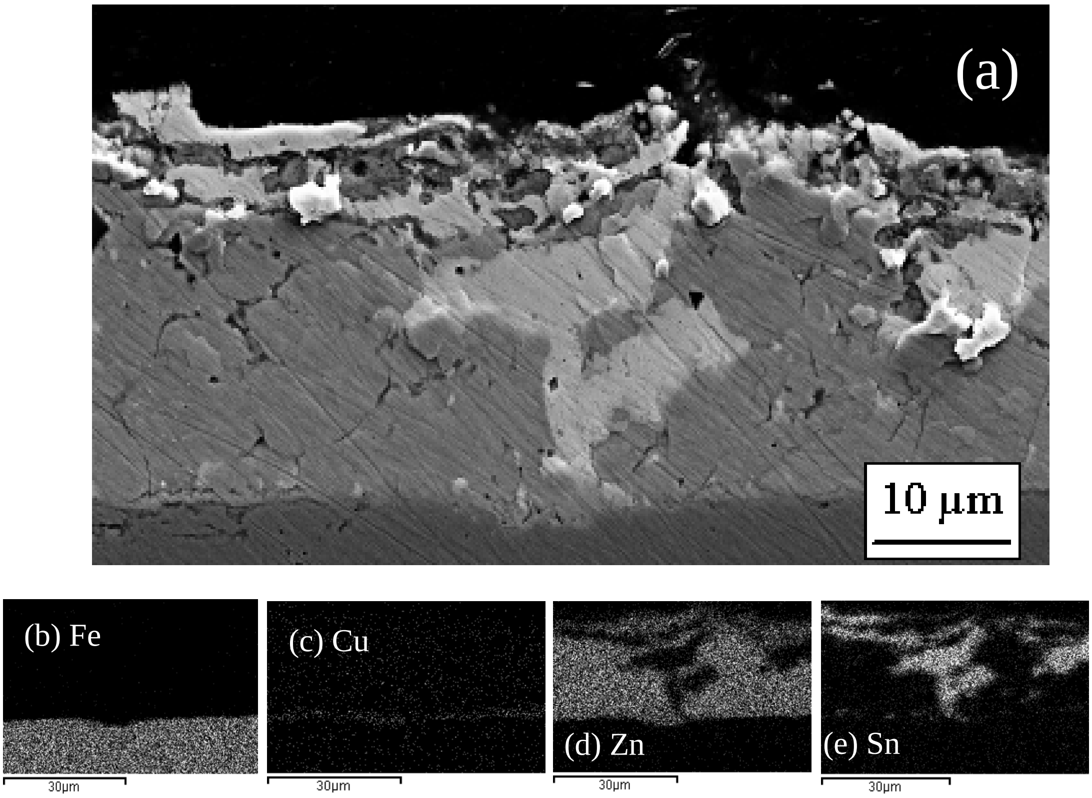

Fig. 4.5 (a) Secondary electron image of the cross section of the Zn-Sn coating on the rivet's head and corresponding elemental X-ray analysis of (b) iron, (c) copper, (d) zinc and (e) tin.

The co-deposition of Zn and Sn is viable galvanically, if a slurry of more anodically active metal (Zn) and salt of the noble metal (Sn) is provided. The active metal is considered as driving metal and the noble one is the plating metal [191]. The microstructure of the coating changed from the copper interface to the surface. The inner layers seem more compact and consist of bigger size particles. Boundaries between Zn particles are more visible in intermediate layers, whereas in the top layers near the surface, particles are more flattened and the concentration of Sn particles is higher. The particles at the outer layers have been tumbled and impacted for a relatively long time before deposition compare to the particles which deposited at inner layers. This could be the reason of changing the structure from bottom to the top layers.

A thin layer (around 1 µm), found at the interface between the coating and surface of the steel rivet, has been identified as a ‘copper strike’ coating. Such coating layer is usually applied after cleaning the substrate, by displacement plating and/or galvanomechanical technique, to protect the cleaned steel’s surface and facilitate the subsequent deposition of other metals such as zinc, aluminium and tin [193]. An interfacial copper layer was also observed in Almac coating, while in aluminum coating a Ni interfacial layer was found as will be discussed later in the next sub-chapter.

Scanning electron micrograph of the cross section of the Almac coating on the rivet’s head is presented in Fig. 4.6, showing porosities.

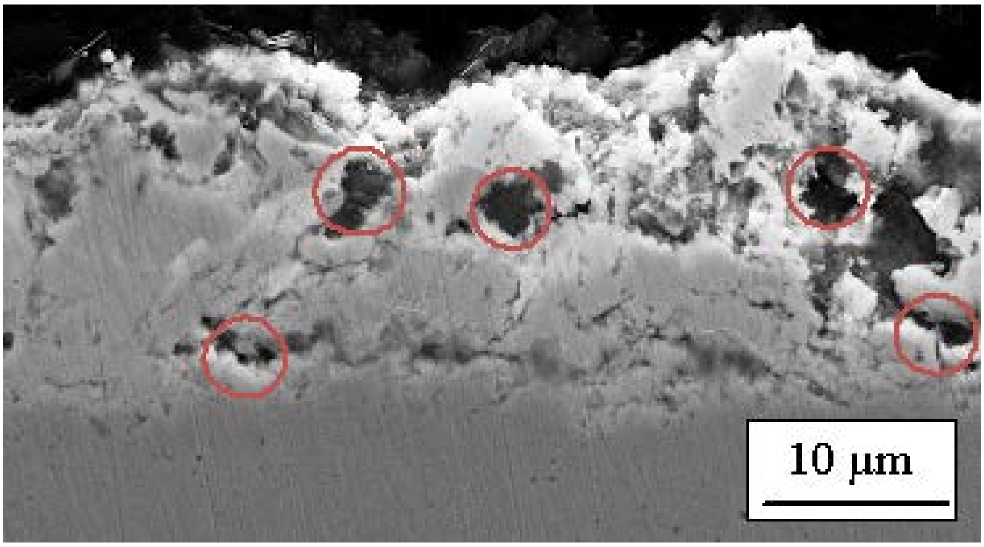

Fig. 4.6 Scanning electron micrograph of the cross section of the Almac coating on the rivet’s head showing porosities.

Porosities observed along the thickness of the Almac coating as was observed on the surface (Fig. 4.2 (b and b′)). Metal oxide layer which are formed during the plating process and also inorganic salt which exist in the plating solution may reduce the adhesion of the metal to metal. Although film former and chemical flux can prevent the oxide formation or removal of the organic salt layer respectively, the process shows poor efficiency [194]. Poor adhesion and cohesion of metal to substrate and to one another lead to porosity formation in the coating. Therefore porosities are seen not only on the surface of coating but also inside the Zn-Sn and Almac coatings.

X-ray elemental mapping of the Almac coating is presented in Fig.4.7.

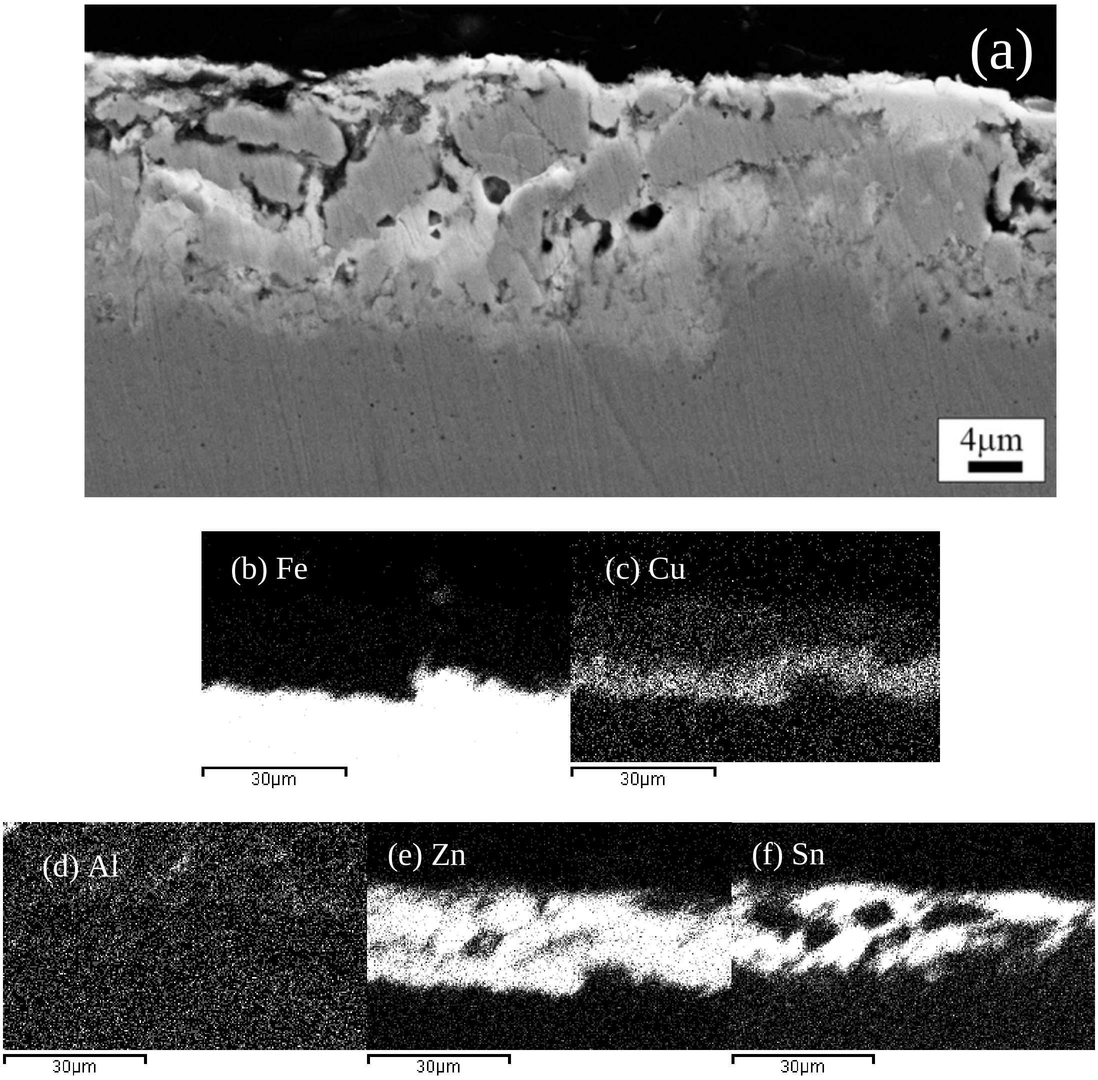

Fig. 4.7 (a) Secondary electron image of the cross section of the Almac coating on the rivet’s head and corresponding elemental X-ray analysis of (b) iron, (c) copper, (d) aluminium, (e) zinc and (f) tin.

In addition to the malleability of metal particles, recrystallization temperature is also a key parameter of coating formation through the mechanical plating procedure at room temperature. For those malleable metal such as zinc and tin which have a recrystallization temperature close to the ambient temperature, during the plating process at the point of metal to metal contact temperature rise up and reaches to recrystallization temperature because of released energy due to plastic deformation. As a result an atomic bond forms between the zinc and tin particles. In case of aluminium which has a recrystallization temperature of about 150˚C a very thin layer of aluminum may deposit at room temperature [195, 196]. Aluminium was not detected precisely in the EDS map and no aluminium peak was not detected in the EDS spectrum (see Fig. 4.8). These results explain the low concentration of aluminum in the Almac coating and suggest that possibly the coating has not been produced at temperature close to the aluminum recrystallization temperature which led to contribution of very small amount of aluminum to the coating.

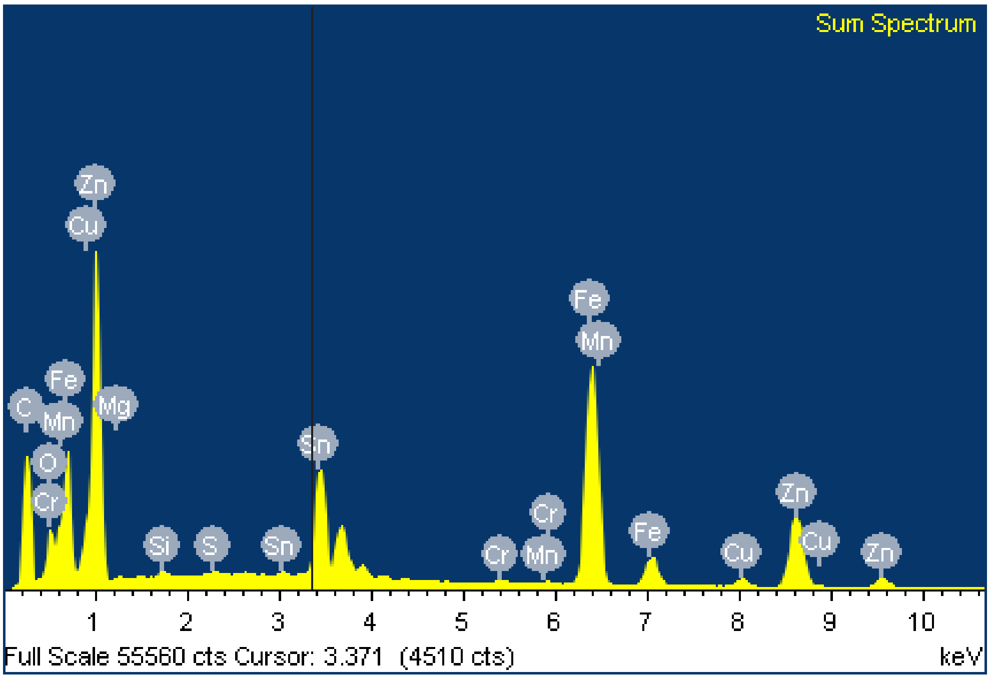

Fig. 4.8 EDS spectrum of Almac coating.

Scanning electron micrograph of the cross section of the aluminium coating on the rivet’s head is presented in Fig. 4.9. Coating is uniform and has deposited on a nickel layer which was identified by EDS map as presented in Fig. 4.10.

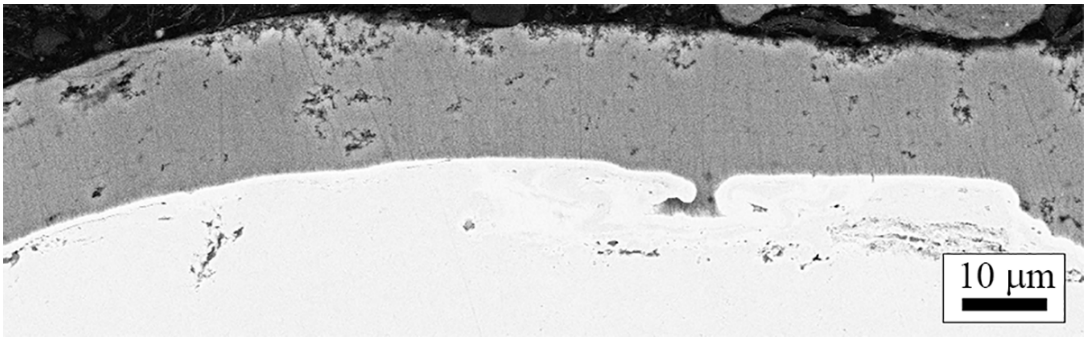

Fig. 4.9 Scanning electron micrograph of the cross section of the Almac coating on the rivet’s head showing a uniform coating.

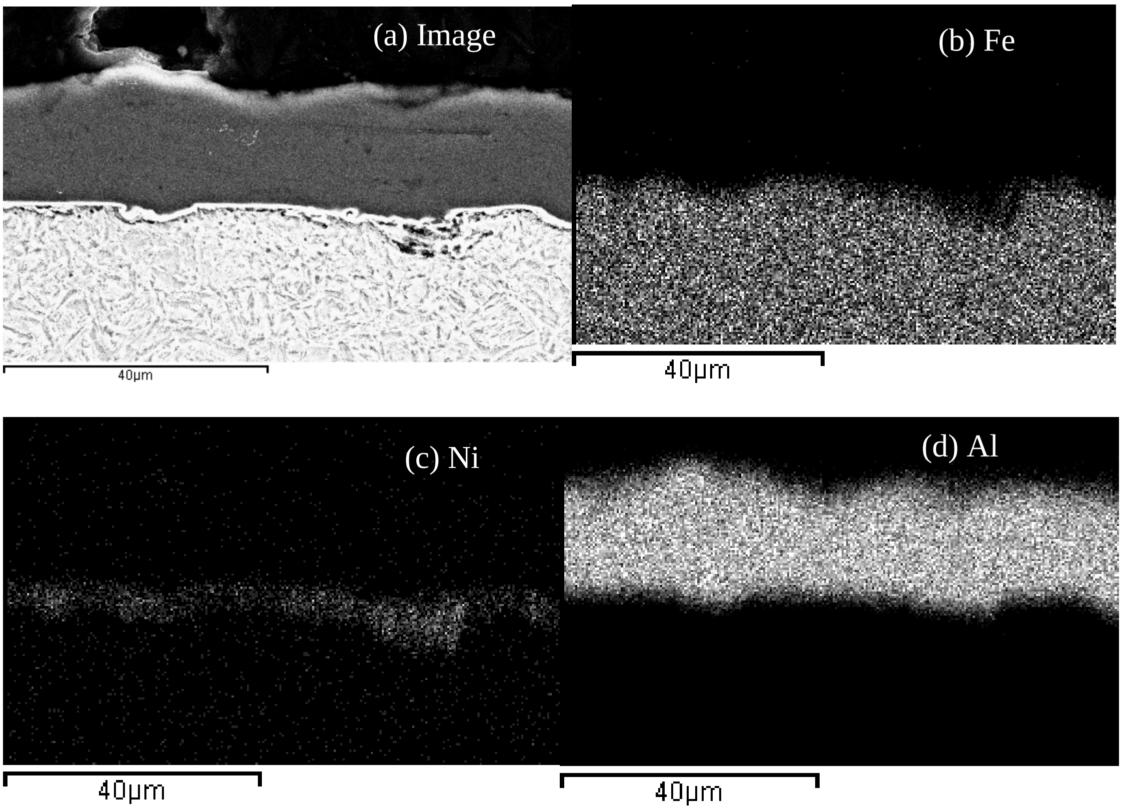

Fig. 4.10 (a) Back-scattered image of the cross section of the aluminum coating (etched) on the rivet’s head and corresponding elemental X-ray analysis of (b) iron, (c) nickel and (d) aluminium.

4.3.2 Characterization of the coatings after joining process

Fig. 4. 11 (a) and (b) show the produced joint of Mg sheets by laser assisted self-pierce riveting from the top sheet and bottom sheet view, respectively. The cross section view of the joint is shown in part (c) of Fig. 4. 11.

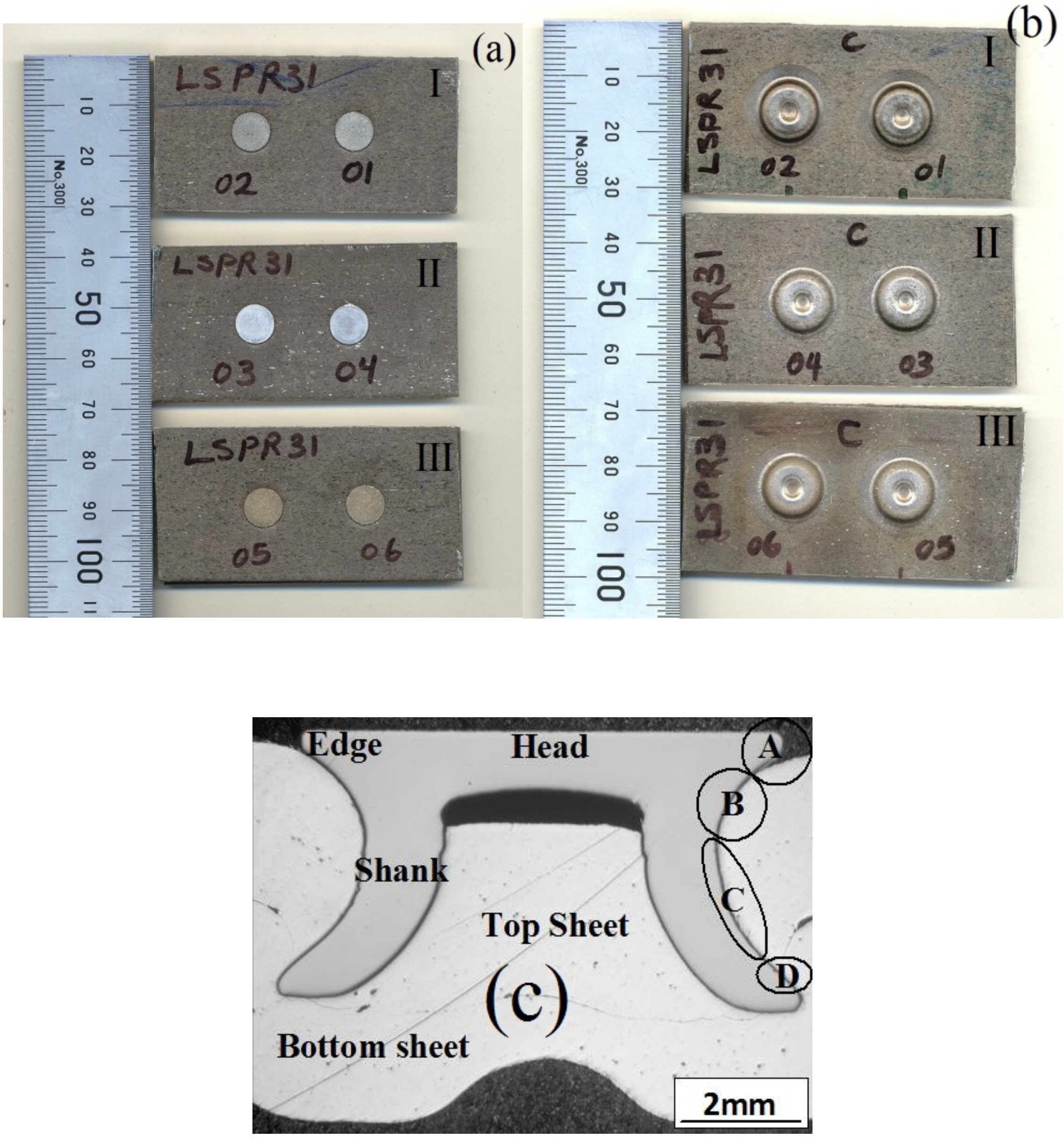

Fig. 4.11 Optical micrograph of Mg sheets joined by laser assisted self-pierce riveting (a) top sheet view (b) bottom sheet view of (I) Zn-Sn, (II) Aluminium, (III) Almac coated rivets and, (c) cross section view of a Zn-Sn joint.

Optical microscopy examination of the interface area between the edge of the rivet head with Zn-Sn coating and the top Mg sheet (region A in Fig. 4.11 (c)) reveals that; part of the coating is missing, as shown in Fig. 4. 12 (a). One possible reason is that a section of coatings was removed during the piercing or rivet setting process. Since the edge of the rivet head is not embedded in the top sheet, it is more likely that part of the rivet coating was already detached before joining as shown in Fig. 4.3. The positive point is that the coating has not been peeled off at the corner under the edge and along the shank of the rivet in the top sheet (regions B and C of Figure 4.11 (c)). When a steel rivet is used to join sheets rather than steel (as a top layer sheet), the galvanic corrosion between the steel rivet and non-ferrous sheets can be stopped or hinder by coatings of the rivet and the sheet. So the rivet coating not only protect the rivet from rusting it decrease the risk of galvanic corrosion and increase the life time of the joint. A failure like this as a pre-existing condition will lead to corrosion of the rivet and the sheet. Even if the top sheet is steel, the crevice corrosion which can occur around region A of Figure 4.11(c) will lead to failure of the joint.

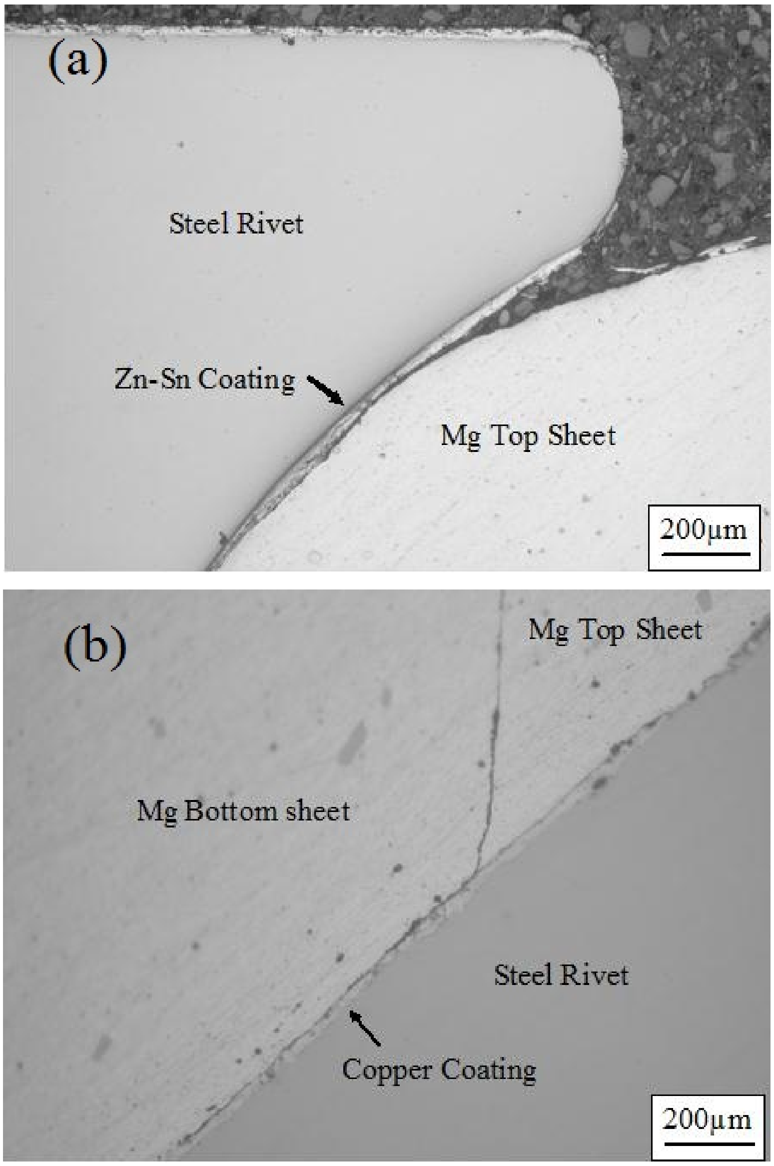

Fig. 4.12 SEM image showing cross section of the rivet with Zn-Sn (a) around edge and corner under the edge in the top sheet (b) shank of the rivet near to top and bottom sheet.

As the rivet penetrated through and flared into the bottom sheet (region D in Figure 4.11 (c)), the thickness of the coating decreased from 20 micron near the top sheet to 1 micron in the bottom sheet for Zn-Sn and Almac coating, as shown in Fig. 4. 12 (b). For both Zn-Sn and Almac coatings, it was found that the remaining coating is mostly copper flash and a very small amount of Zn-Sn. The remaining Zn-Sn coating confirmed the role of the tightly adhesive primer copper layer to ensure the adhesion of Zn and Sn to the rivet surface [193]. Results indicated that the thickness of aluminum coating remained unchanged after the joining process. Cross section of rivet with aluminum and Almac coatings around the edge and corner under the edge in the top sheet is presented in Fig. 4.13.

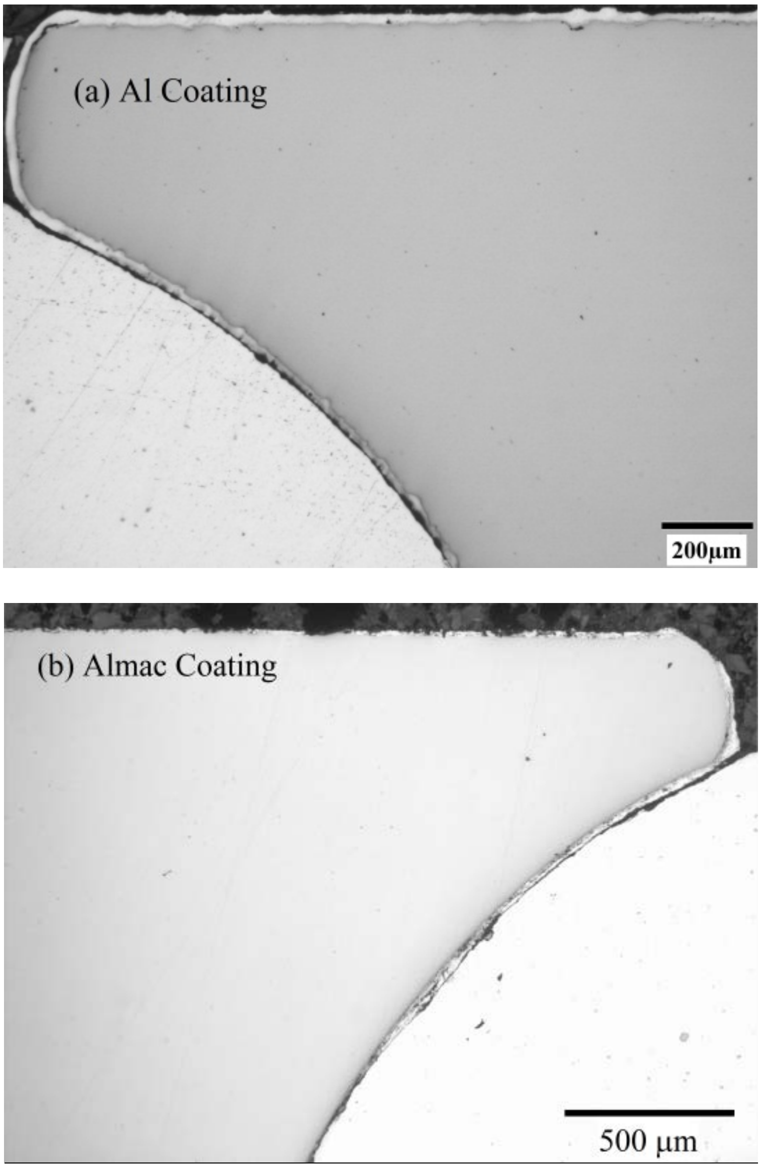

Fig. 4.13 SEM image showing cross section of the rivet showing around edge and corner under the edge in the top sheet (a) aluminum coating, (b) Almac coating.

A comparison of the rivets coating before and after joining showed that the Zn-Sn and Almac coatings in the top sheet deformed in the opposite direction to riveting. During joining, a process similar to rolling observed along the rivet shank in the top sheet, leading to the elongated and compacted structure as shown in Fig. 4.14. Regions of coating on the rivet’s tips and lower shank (regions D and C in Figure 4.11 (c)) were sheared during the piercing process and pushed upward of the rivet in the top sheet, so that the rivet coating in that part of the joint (region B of Fig. 4.11 (c)) ended up with a thicker coating than its original thickness. Zn-Sn coatings have good frictional properties and excellent ductility for applications where parts such as self-piercing rivets, undergo friction and deformation after plating [100]. Therefore they do not fail by cracking and tearing during the flaring process, and because of their low recrystallization temperature (-4˚C for tin and 10˚C for Zinc [197]), they deform easily at the joining condition (about 200°C [6]). On the other hand, Fig. 4.14 (c) suggests that the aluminum coating produced by electrodeposition was adherent to the substrate and coherent across the thickness, and was not affected by force and temperature conditions of LSPR joining process. This may be due to the low surface roughness of the aluminum coating (Fig. 4.1), generating less frictional contact between the Mg sheet and coating.

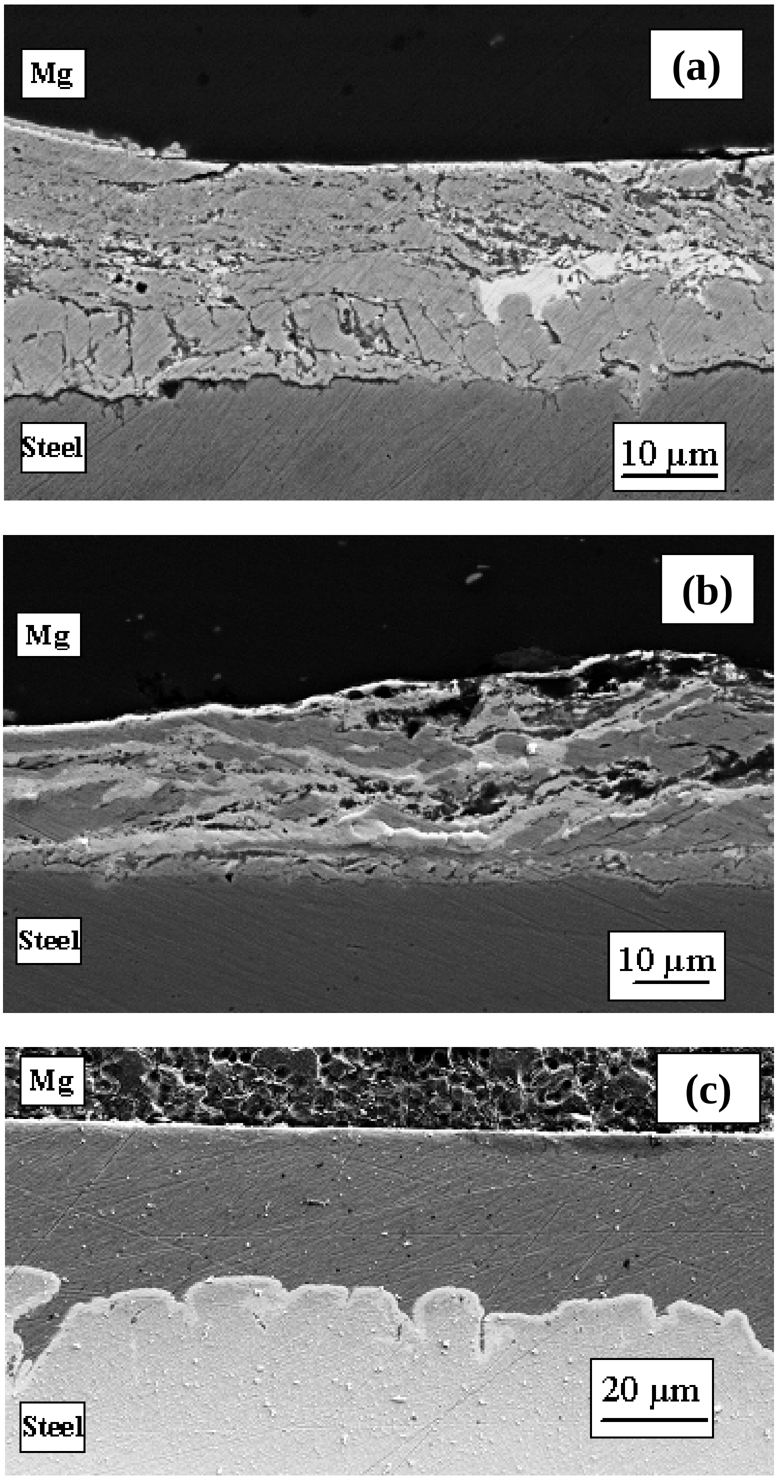

Fig. 4.14 Secondary electron micrograph of (a) Zn-Sn, (b) Almac and (c) aluminum coatings across the rivets' shank in the joints' top sheet.

4.4 Summary

This study examined possible effects of laser assisted self-pierce riveting on the rivet’s coating by characterising the rivets coating before and after joining of Mg sheets. It was found that:

- Failure such as peeling was not observed for Zn-Sn, Almac and aluminum coatings of the self- piercing rivets during the laser assisted self-pierce riveting.
- The thickness of the mechanically plated Zn-Sn and Almac coatings increased at the top sheet (25%-30% of the original thickness (20 µm)) and formed a compacted coating in the top sheet, and decreased at the bottom sheet (up to 75% reduction to the original thickness) due to the joining force.
- Electroplated aluminum coating appeared not to be affected by the joining process, thickness of the coating remained unchanged (20-25 µm) under the joining process.
- Although aluminium coating presented better properties than Zn-Sn and zinc coatings, they did not consider for the continuation of this thesis. The main reason is that; electroplating of aluminium on a steel substrate is only possible from hazardous non-aqueous solutions. Therefore, due to the safety issues involved in aluminium plating, this option was not considered.

Chapter 5

Electrodeposition of nanocrystalline zinc from sulfate and sulfate-gluconate electrolytes in the presence of additives

5.1 Introduction

In this chapter electrodeposition of zinc from sulfate and sulfate-gluconate electrolytes in the presence and absence of additives such as Polyethylene glycol (PEG), hexadecyltrimethylammonium bromide (CTAB) and thiourea has been investigated. Equilibrium distribution of zinc (II) species was evaluated in both sulfate and sulfate-gluconate electrolytes. The effects of gluconate ligand on the initial stages of zinc deposition was evaluated on glassy carbon electrode by means of cyclic voltammetry and chronoamperometry. Also the effects of the gluconate anions on the surface morphology and texture of the zinc deposits on steel substrate were characterized and compared with zinc deposit from sulfate bath without gluconate anions.

The combined effects of gluconate ligand and additives on zinc electrodeposition was investigated by evaluating electrochemical responses of these electrolytes, and by characterizing the surface morphology and preferred orientation of the deposits.

5.2 Experimental

Table 5.1 shows the compositions of the electrolytes used in this study. The pH value of the electrolytes was adjusted to 4.4 - 4.7 using 10 M NaOH. Polyethylene glycol (PEG, $(C_2H_4O)_n H_2O$) with a mean molecular weight of 400 g/mole, CTAB ($CH_3 (CH_2)_{15}N (CH_3)_3Br$) and thiourea ($NH_2CSNH_2$) were used as additives. In zinc electroplating PEG is mainly used as a brightener, CTAB as a leveller and thiourea as a grain refiner. Therefore, in this study brightener (PEG), leveller (CTAB) and finally grain refiner (thiourea) were added to the plating baths sequentially. Na_2SO_4 used as the supporting electrolyte and boric acid was used as a buffing agent to maintain pH during deposition. Chemical structure of these additives is presented at Table 5.2.

Table 5.1 Compositions of the electrolytes used in this study.

Bath	Constituents
Zn-S (SS)	0.7 M $ZnSO_4$,7 H_2O + 0.3 M Na_2SO_4 + 0.2 M H_3BO_3
Zn-SP	SS + 5 mM PEG $_{400}$
Zn-SPC	SS + 5 mM PEG $_{400}$ + 1 mM CTAB
Zn-SPCT	SS+ 5 mM PEG $_{400}$ + 1 mM CTAB + 0.015 M thiourea
Zn-G (SG)	SS + 0.7M Na-Gluconate (NaGH$_4$)
Zn-GP	SG + 5 mM PEG $_{400}$
Zn-GPC	SG + 5 mM PEG $_{400}$ + 1 mM CTAB
Zn-GPCT	SG + 5 mM PEG $_{400}$ + 1 mM CTAB+ 0.015 M thiourea

Table 5.2 Chemical structure of additives.

PEG	CTAB	Thiourea
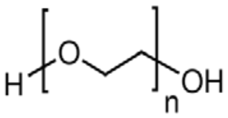	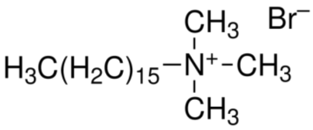 $H_3C(H_2C)_{15}-N^+(CH_3)_3\ Br^-$	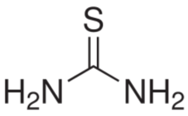

Cyclic voltammetry and chronoamperometric experiments were carried out in a three-electrode glass cell at room temperature (21 ± 1°C) without stirring on glassy carbon electrode. Cyclic voltammetry was carried out at the scan rate of 50 mVs^{-1} and chronoamperometric experiments were performed from 0 V to different overpotentials ranging from -1.35 V to – 1.6 V.

Pulse zinc electrodeposition (current density j = 0.02 A/cm^2, current on-time T_{ON} = 5 ms and current off-time T_{OFF} = 9 ms) was carried out in a 500 ml three-electrode cell for 1200 s without stirring using a CHI electrochemical workstation at room temperature (21 ± 1°C). Mild steel discs were used as the working electrodes, with a surface area of 1.13 cm^2.

5.3. Results and discussion

5.3.1 Distribution of zinc (II) species

Zinc (II) ions in the aqueous solution may present as free metal ions and/or metal complexes. The speciation of zinc in the electrolyte depends on the composition, pH and temperature of the electrolyte and can be studied by material balance equations [198].

Table 5.3 shows the reaction and equilibrium constant for species which were considered for material balance equation calculations in this study. Zinc cations and sulfate anions undergo ion pairing in solution. Therefore, the presence of the neutral $ZnSO_4$ complex was considered in the mass balance calculation. Based on preliminary studies, all the zinc hydroxide complexes were formed at alkaline pH values. Therefore, zinc hydroxide formation was not included in the material mass balance at pH range of 1 to 6. In sulfate-gluconate electrolyte, zinc and gluconate can coordinate by carboxylate group of ligand and produce carboxylic acid complex of zinc ion (II) with relatively low stability as presented in Table 5.3. In alkaline electrolytes, zinc (II) coordination by the secondary alcohol groups can also develop mainly at alkaline pH ranges according to the following equilibrium and a more stable complex can be formed [121, 199]. However, formation of this complex at pH range of 1 to 6 was not part of investigation in this study.

$$\mathrm{Zn(GH_4)^+ + (OH)^- \leftrightarrow ZnGH_4(OH)} \quad \mathrm{Log\,K_{eq}} = 8.14 \qquad (5.1)$$

Table 5.3 Equilibrium reaction and corresponding stability constants [200].

Equilibrium	Log K_{eq}
$\mathrm{Zn^{2+} + SO_4^{2-} \leftrightarrow ZnSO_4}$	2.38
$\mathrm{Zn^{2+} + GH_4^{-} \leftrightarrow Zn(GH_4)^{+}}$	1.7
$\mathrm{H^{+} + SO_4^{2-} \leftrightarrow HSO_4^{-}}$	1.99
$\mathrm{H^{+} + GH_4^{-} \leftrightarrow HGH_4}$	3.86
$Na^{+} + SO_4^{2-} \leftrightarrow NaSO_4^{-}$	0.7

Mass balance equation was solved for Zn^{2+}, SO_4^{2-} and GH_4^{+} ions by using HySS2009 software for Zn-S and Zn-G (listed in Table 5.3) electrolytes. Fig. 5.1 (a) and (b) show Zn (II) speciation as a function of pH at the range of 1 to 6 in sulfate and sulfate-gluconate electrolytes respectively. Speciation of GH_4^{-} in sulfate-gluconate electrolyte is presented in Fig. 5.1 (c).

Results showed that in sulfate solution the main species was $ZnSO_4$ and concentration of Zn^{2+} species was very small over a wide range of pH. In sulfate-gluconate electrolyte zinc (II) sulfate was a predominant complex formed under the studied electrolyte condition. Higher concentration of $ZnSO_4$ species than $Zn(GH_4)^{+}$ has also been reported for 0.01 M Zn(II) + 0.01 M Cu(II) solution containing 0.5 M Na_2SO_4 and with total concentration of 0.02 M gluconic acid [201]. $Zn(GH_4)^{+}$ concentration continuously increases with increasing pH and reached a steady state value (still lower than $ZnSO_4$ concentration) at pH 4.5. On the other hand, concentration of protonated ligands declined and concentration of free ligand increases with increasing pH. At pH =1 the total concentration of protonated ligand (HGH_4) and free ligand anion $(GH_4)^{+}$ is 0.7 M. However, the total concentration of these two species reached to 0.558 M at pH = 6. Whereas, $Zn(GH_4)^{+}$ concentration increased from zero at pH = 1 to 0.142 M at pH = 6. The variation of the species concentrations with pH showed that increase in $Zn(GH_4)^{+}$ occurred with the expenses of free ligand anions.

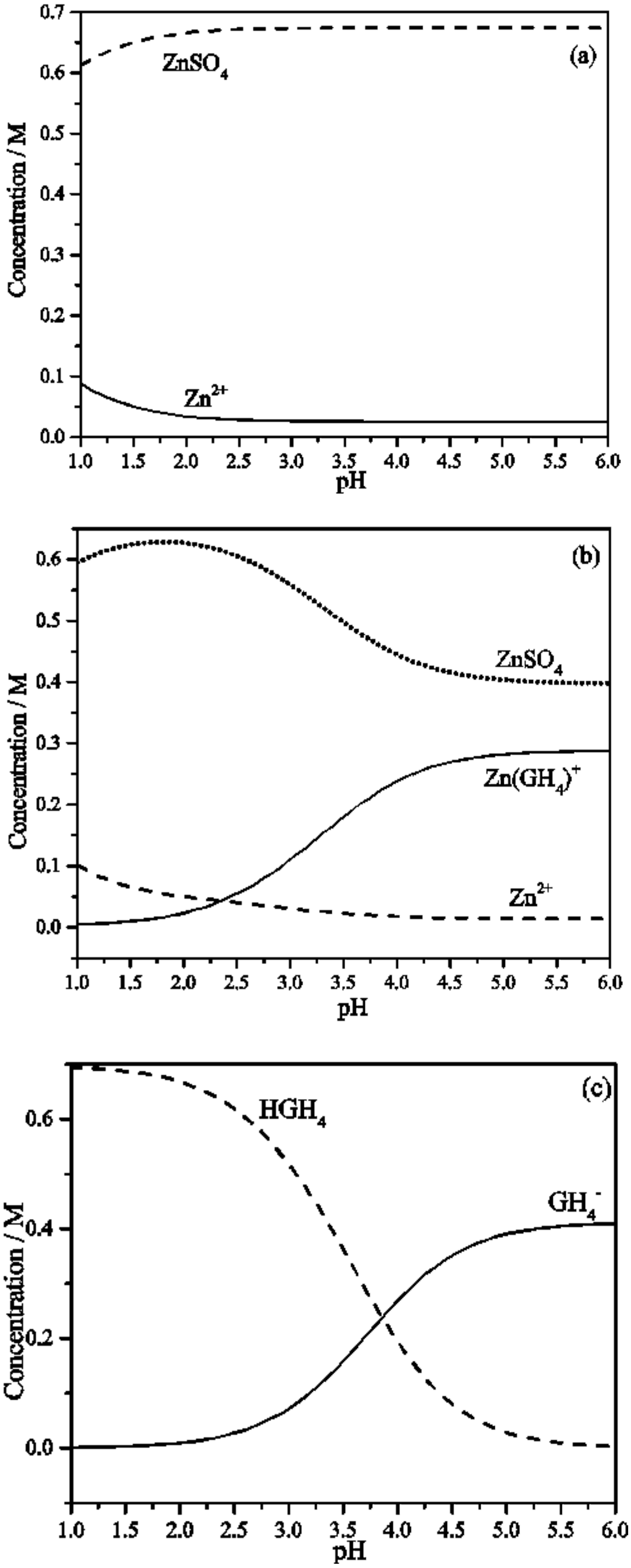

Fig. 5.1 Speciation diagrams as a function of pH for (a) Zn (II) in sulfate electrolyte (Zn-S), (b) Zn (II) in sulfate-gluconate electrolyte (Zn-G) and (c) GH_4^- in sulfate-gluconate electrolyte (Zn-G).

5.3.2 Voltammetric study

Voltammetric studies were carried out to evaluate the effects of gluconate anions and organic additives in the zinc reduction process. Figs. 5.2 (a) and (b) show the voltammograms obtained for zinc reduction and oxidation on glassy carbon electrode from sulfate and sulfate-gluconate electrolytes, in the absence and presence of additives, respectively. The arrows indicate the initial direction of potential sweep. Results are discussed in the following sub-chapters.

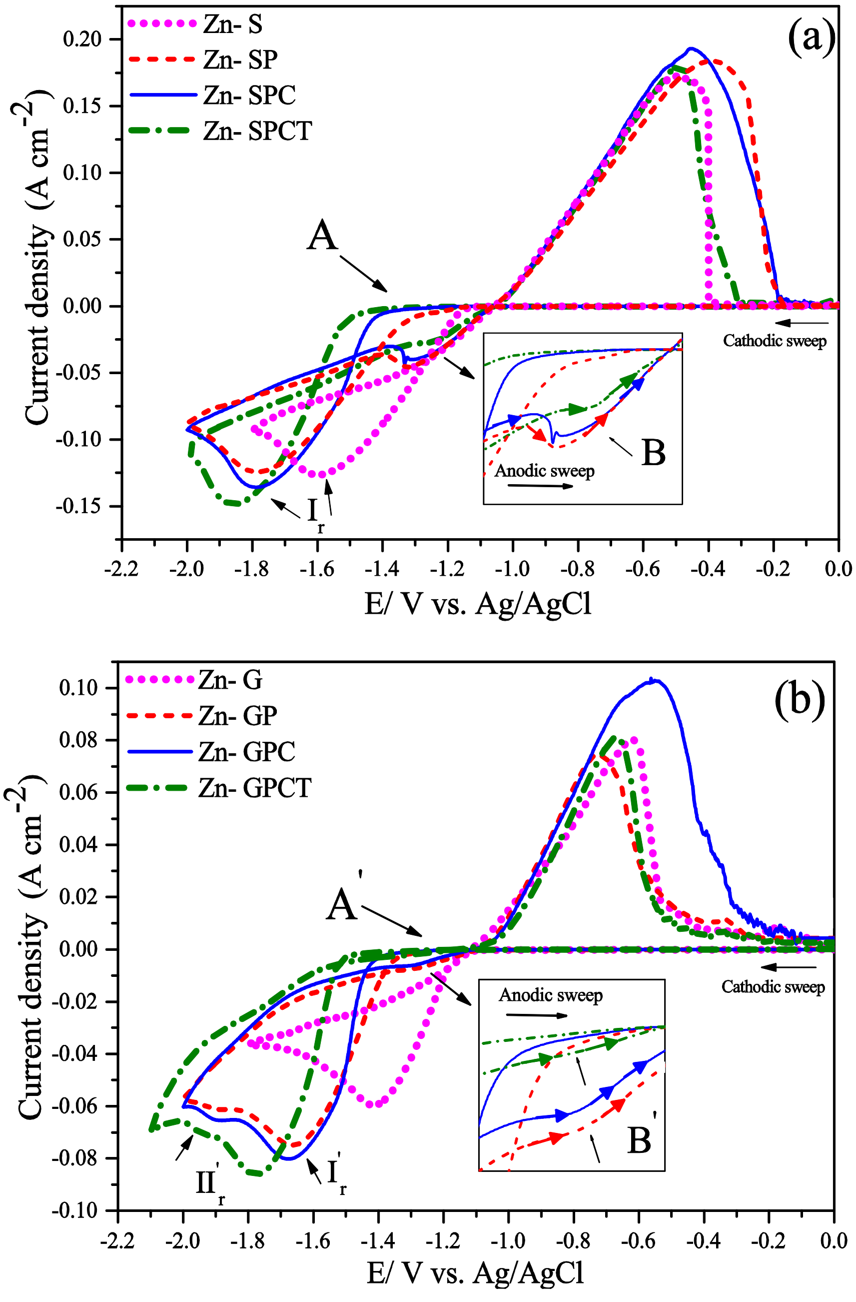

Fig. 5.2 Cyclic voltammograms of a glassy carbon electrode in (a) zinc sulfate and (b) zinc sulfate-gluconate electrolytes with and without additives.

5.3.2.1 Effects of gluconate anion

In the absence of additives, electrodeposition of zinc from sulfate solution started at -1.11 V and occurred through a reduction peak potential at -1.599 V. According to the speciation diagram of Zn (II) in gluconate free electrolyte (Fig. 5.1 (a)), zinc sulfate complex is the major contributor to the reduction of zinc from sulfate electrolyte as the concentration of free Zn (II) ions is very small at the pH range of this study (4.4 - 4.7), therefore the I_r reduction peak at the voltammograms corresponded to Zn (II) reduction from Zn-sulfate complexes.

In the gluconate electrolyte one peak was observed for the reduction of zinc from $ZnSO_4$ and $Zn(GH_4)^+$ complexes (Fig. 5.1(b)). The reduction started at -1.08 V (slightly more positive than Zn-S solution) and occurred at more positive values in comparison to sulfate solution (Zn-S) at -1.414 V.

According to the revised Nernst equation in the presence of complex ions [109] the reduction potential of Zn^{2+} from the sulfate complex and gluconate complex may be written as follows respectively.

$$E_{ZnSO_4/Zn} = E^0_{Zn^{2+}/Zn} - \frac{0.0591}{2}\log K_{eq} + \frac{0.0591}{2}\log\frac{a_{ZnSO_4}}{a_{SO_4^{2-}}} \qquad (5.2)$$

$$E_{Zn(GH_4)^+/Zn} = E^0_{Zn^{2+}/Zn} - \frac{0.0591}{2}\log K_{eq} + \frac{0.0591}{2}\log\frac{a_{Zn(GH_4)^+}}{a_{GH_4^-}} \qquad (5.3)$$

Where log K_{eq} is the stability constant for the complex and the activity of the species is denoted as (a). A simple approximation of the formula arises of cancelling out the activity coefficient and substituting the concentration for activities. The stability constant for $ZnSO_4$ is larger than $Zn(GH_4)^+$ (see Table 5.3), consequently a more negative potential is expected for the deposition and dissociation of zinc from sulfate complexes compared with gluconate complexes.

Thus, the positive shift of deposition potential in the presence of gluconate ions showed that although 0.4 M of Zn (II) ions are in coordination with sulfate anions (Fig. 5.1 (b)), $Zn(GH_4)^+$ cations (at around 0.28 M) (peak I'_r in Fig. 5.2 (b)) play a predominant role in zinc deposition. The magnitude of deposition current density decreased drastically from 0.127 A/cm^2 (absolute value) in sulfate solution to 0.059 A/cm^2 (absolute value) in gluconate containing electrolyte. Decrease in deposition current density is expected due to several reasons such as decreasing the switching potential and/or total concentration of depositing ions and/or addition of organic additives to the electrolyte. Total concentration of Zn (II) was similar for sulfate and sulfate-gluconate electrolytes, no additives existed in the electrolytes and switching potential was -1.8 V for both experiments, therefore the observed reduction in deposition current density is explained by selective deposition of zinc ions from $Zn(GH_4)^+$ which had a lower concentration than $ZnSO_4$ complexes at the pH of (4.4 - 4.7) based on speciation diagram (Fig. 5.1 (b)). This is evident from the results of surface morphology of the deposits and XRD evaluations which are discussed in sub-chapter 5.3.4 and 5.3.5.

In a study conducted by Vasantha et al. [202] for the deposition of zinc on glassy carbon electrode from a zinc sulfate electrolyte (0.05 M $ZnSO_4$, 0.1 M Na_2SO_4) in the presence of gluconate complex anion (0.05 M sodium gluconate) and the pH range of 3.5 to 5, reduction of zinc from gluconate complex has been considered as the rate determining step of the deposition, however no specific change to the electrochemical spectrum was reported.

5.3.2.2 Effects of additives

With the addition of organic additives, zinc reduction potentials moved to more negative values (Fig. 5.2 (a) and (b)) for both sulfate and sulfate-gluconate electrolytes. In addition to the potential displacement, a second reduction peak appeared for the deposition of zinc from sulfate-gluconate electrolytes. A peak (I'_r in Fig. 5.2 (b)) was recorded at around -1.6 V to -1.8 V and another small reduction peak (II'_r in Fig. 5.2 (b)) at around -1.8 V to -2 V. These two reduction peaks were attributed to the reduction of Zn^{2+} from a gluconate complex (I'_r) and from sulfate complex (II'_r) respectively.

Shifts of metal reduction potential to more negative values in the presence of additives have been reported in the literature [134, 135]. It has mostly been explained by the absorption of organic additives on the cathode surface and partial blockage of active sites which lead to decrease in nucleation rate and increase of overpotential. Moreover, inhibition of electrocrystallization process with the adsorption of organic additives on the growing deposit could interfere with the growth process

Table 5.4 shows cathodic peak potential (E_{CP}) and current efficiency (ratios of total anodic to cathodic charge calculated from the integration of anodic and cathodic part of cyclic voltammograms) in all sulfate and sulfate-gluconate electrolytes respectively.

Addition of PEG (a non-ionic surfactant) to the electrolytes resulted in an increase of reduction potential and slight decrease of current efficiency in both sulfate and sulfate-gluconate electrolytes.

PEG can change the mechanism of zinc reduction and affects current density. It is reported [133] that the addition of non-ionic surfactant affects metal reduction process by changing the mass transfer rate. Also depending on the concentration, PEG can form complexes with depositing metal ions and change the mechanism of metal deposition [203, 204]. PEG can also form a layer on metallic surfaces due to its strong surface active properties [203]. Any of these activities can interfere with zinc nucleation and growth process and impose changes to electrochemical responses of the electrolyte.

Table 5.4 Cathodic peak potential (E_{CP}) and current efficiency values, associated with the reduction of zinc from all sulfate and sulfate-gluconate electrolytes on glassy carbon electrode.

Solution	E_{CP} vs. Ag/AgCl (V)	Current efficiency (%)
Zn-S	-1.599	98.63
Zn-SP	-1.783	93.03
Zn-SPC	-1.789	93.38
Zn-SPCT	-1.857	65.8
Zn-G	-1.414	66.52
Zn-GP	-1.663	64.36
Zn-GPC	-1.683	89.65
Zn-GPCT	-1.779	43.54

CTAB is a cationic surfactant and could electrostatically interact with the surface of electrode. Thus a negative shift of deposition potential upon addition of CTAB to the electrolyte is expected. It was also reported [20] that the adsorption of PEG increased by Br^- ions from CTAB. However, results showed that negligible increment in reduction potential was observed from Zn-SPC and Zn-GPC electrolytes due to addition of CTAB. The starting point of deposition moved to more negative potential (region A and A′ in Fig. 5.2 (a) and (b) respectively) from -1.15 V in Zn-SP to -1.25 V in Zn-SPC and from -1.32 V in Zn- GP to -1.39 V in Zn-GPC electrolytes. The results suggested that adsorption of CTAB on the surface of electrode and its interaction with PEG may depend on the potential. At the beginning of the process and at potentials that zinc deposition started, CTAB were absorbed on the surface of electrode and interacted with PEG and led to an increase in deposition at starting potential. It is probable that as the potential moved to more negative values and towards valley of the deposition peak desorption of CTAB occurred and as a result the reduction process was only affected by PEG molecules and no significant increase in deposition potential was observed. In a study conducted by Nayana and Venkatesha [135] absorption of CTAB on the surface of glassy carbon electrode was potential dependent. Current efficiency hardly changed in Zn-SPC bath but a large increase was observed in Zn-GPC bath. Evaluation of the cathodic and anodic charges of the Zn-GPC voltammogram showed that anomalous increase in current efficiency of this deposit mainly raised from the anodic charge. In the presence of CTAB zinc dissolution moved to more positive values in comparison to other types of gluconate electrolytes, and high anodic charge density was calculated for the zinc dissolution. Increase in current efficiency and anodic charge showed that zinc reduction occurred at a higher rate than hydrogen evolution and a greater portion of cathodic current density was devoted to zinc deposition. Therefore, combination of CTAB and PEG worked as a barrier for hydrogen absorption and even might shifted the hydrogen overpotential to more negative values as explained by Gomes [134] on the effects of CTAB on the electrodeposition of zinc .

Addition of thiourea to PEG and CTAB containing electrolytes imposed high negative shifts to deposition potential values. It was reported that adsorption of thiourea to the surface of electrode occurred through the sulphur atoms [138], and the competition of PEG and thiourea in the process of adsorption led to a decrease in overall adsorption phenomena [20]. Current efficiency decreased drastically and more negative values of deposition potential were achieved upon addition of thiourea to the electrolytes. Results suggested that the synergic effect of additives led to the increase in their inhibitive effect and altered the required activation energy for deposition either by reducing the available sites for electron transfer or by increasing the distance for electron transfer.

5.3.3 Current-time transients

Nucleation and initial stages of zinc deposition on glassy carbon electrode from sulfate (Zn-S) and sulfate-gluconate (Zn-G) bath with no additives was evaluated by chronoamperometric method. Potential was stepped from the initial value of 0 V to some constant potentials of -1.5 V to -2 V in sulfate bath (Fig. 5.3 (a)) and -1.35 V to -1.6 V in sulfate-gluconate bath (Fig. 5.3 (b)).

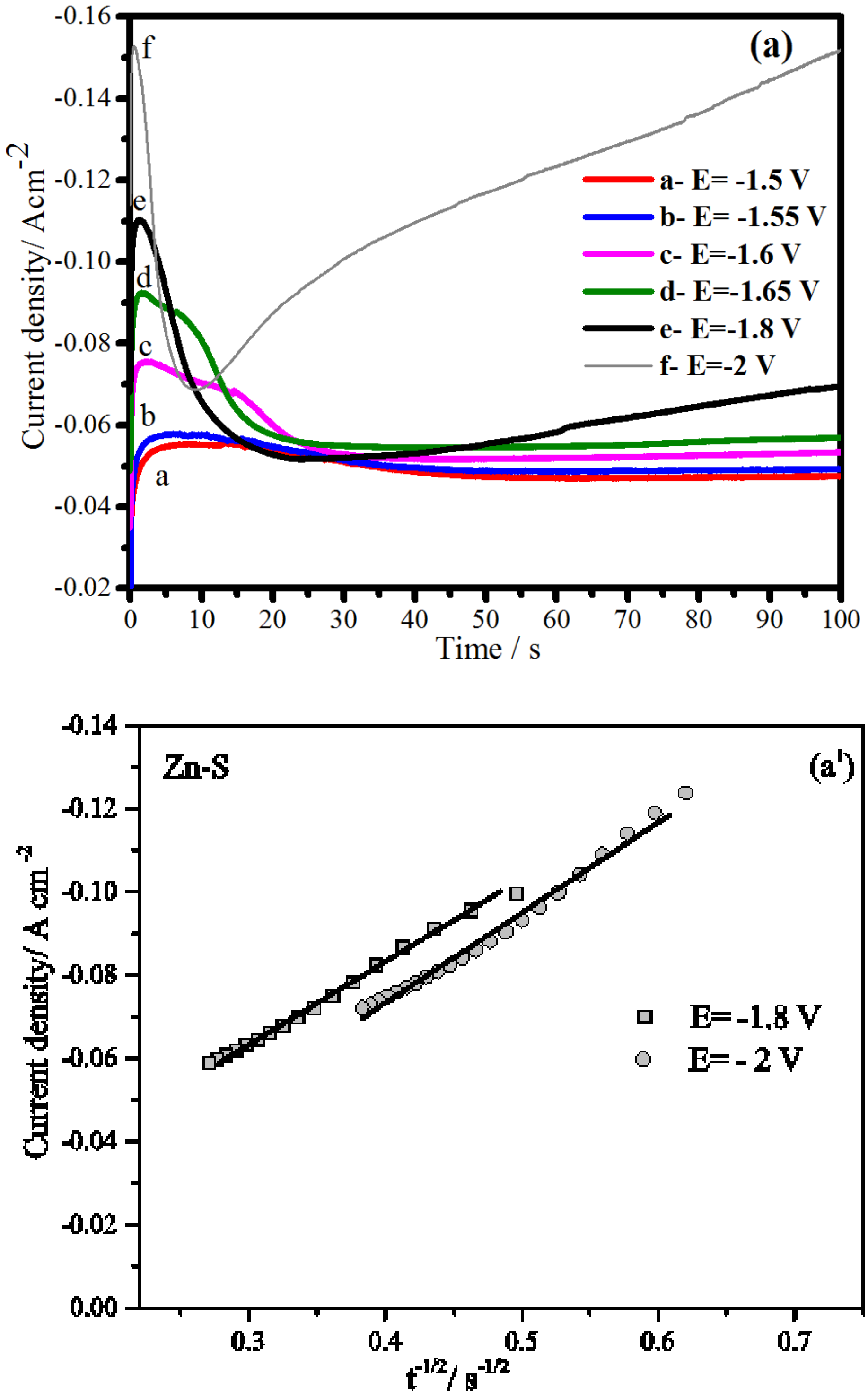

Fig. 5.3 (a) Choronoamperometric curves for zinc deposition on glassy carbon electrode from zinc sulfate (Zn-S) electrolytes at different overpotentials. (a′) Corresponding variation of current density versus $t^{-1/2}$ plot for the descending part of the choronoamperometric curves of Zn-S at E = -1.8 V and -2 V.

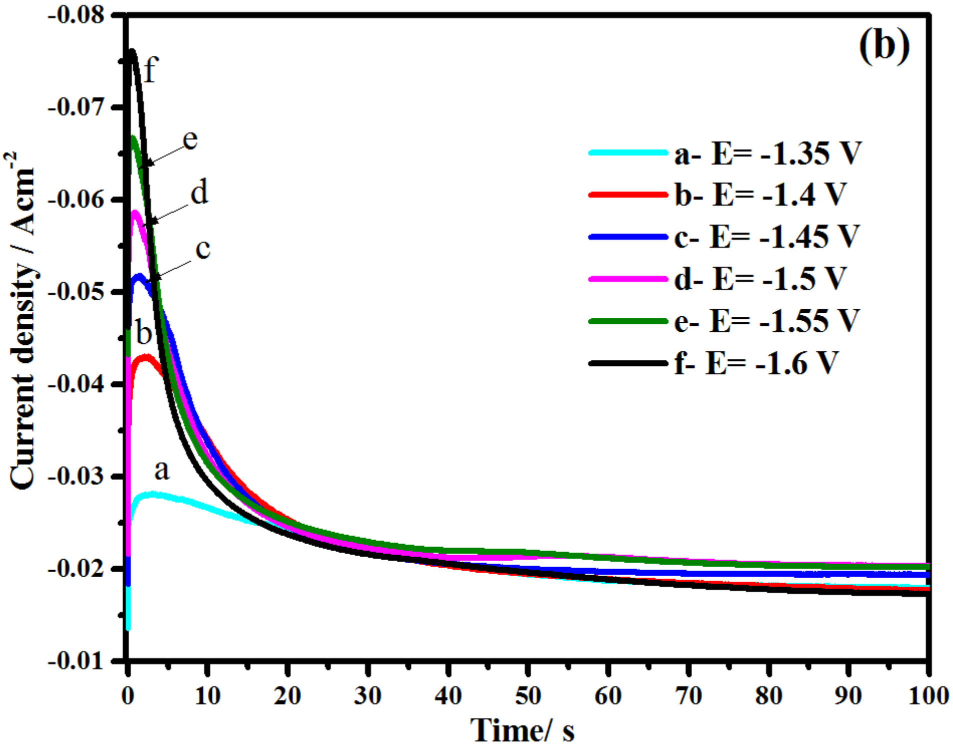

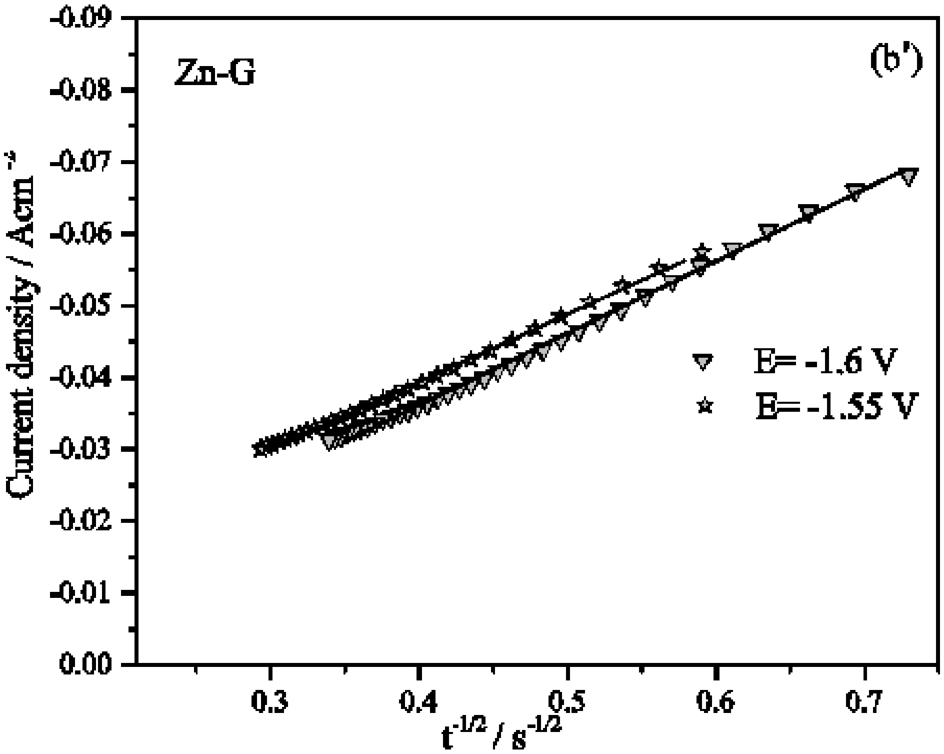

Fig. 5.3 (b) Choronoamperometric curves for zinc deposition on glassy carbon electrode from zinc sulfate (Zn-G), electrolytes at different overpotentials. (b′) Corresponding variation of current density versus t$^{-1/2}$ plot for the descending part of the choronoamperometric curves of Zn-G at E = -1.6 V and -1.55 V.

In all cases, current density increased rapidly with time and reached its maximum. High current densities were achieved in a relatively short time upon increase of overpotential. It is known that at initial stages of electrodeposition, two or three dimensional nucleation process occurs. Rate of nucleation and number of nuclei depend on overpotential values. In current-transition curves, the rising part corresponds to the increase in electroactive area due to the growth of an established nuclei or as the new nuclei are formed [205]. At high overpotential high activation energy was provided for nucleation of new nuclei. As a result, an increase in current maxima was obtained at current-transition curve.

After the maxima at current-transient curves, a gradual decrease in current density to a limiting value was observed. In aqueous metal solution, rate of charge transfer is usually considered fast and mass transfer of electrodepositing ions to the growth centre determines the growth rate of a mature nuclei. Under diffusion controlled system, growth of nuclei is either controlled by spherical or planar diffusion [205]. It is assumed that at the rising part of the current-transient curve, zinc nuclei are randomly distributed on the surface of glassy carbon electrode and grow under localized hemispherical diffusion model. With increase in time the nuclei sizes start to grow, and consequently result in overlap of diffusion zones which restrict displacement of zinc ions to the planes near the surface of electrode. The deposition is viable through the linear diffusion down to the surface of electrode. Thus, hemispherical mass transfer changes to planar mass transfer and a planar diffusion layer forms and a linear mass transfer is observed at the descending part of the current-transient curve [205, 206].

For planar electrodes, under linear diffusion control, the descending part of the current-transient follows the Cottrell equation (equation 5.4), in which the current density (j) changes linearly with the inverse of the square root of time, and the diffusion coefficient can be calculated from the slope of j vs. $t^{-1/2}$ [207].

$$j(t) = \frac{nFAD^{1/2}c}{\pi^{1/2}t^{1/2}} \qquad (5.4)$$

Where *n* is stoichiometric number of electrons involved in the electron transfer reaction; *F* is Faraday’s constant, *A* is the electrode area, *D* is diffusion coefficient and *C* is bulk concentration of redox species.

The linear dependency was characterized at -1.8 V and -2 V for sulfate electrolyte and at

-1.6 V and -1.55 V for sulfate-gluconate electrolyte at the descending part of the curves. A linear relationship between i and $t^{-1/2}$ was noticed. The diffusion coefficients of 6.98×10^{-6} cm^2/s and 1.34×10^{-6} cm^2/s were determined for zinc in sulfate and sulfate-gluconate electrolytes, respectively.

Diffusion coefficient depends on different parameters such as temprature, viscosity and electrolyte, etc. Speciation of zinc in sulfate and sulfate-glucoante electolyte showed that apart from free Zn (II) ions, other complexes are possible either with sulfate and/or gluconate anion (Fig. 5. 1). Therefore the calculated diffusion coefficient could not be only derived from free Zn (II) ions, but should be considered as the average of various zinc species where specific complexation with large gluconate anion has limited the mobility of zinc species and diminished the diffusion coefficient of zinc.

The nucleation mechanism was evaluated based on the model developed by Scharifker and Hills [205] for three-dimensional nucleation under diffusion controlled growth. According to the model, instantaneous and progressive nucleation are expressed as in Equation 5.5 and 5.6 respectively.

$$(\frac{j}{j_m})^2 = 1.9542\,\{1 - \exp(-1.2564(\frac{t}{t_m})\}^2(\frac{t}{t_m})^{-1} \tag{5.5}$$

$$(\frac{j}{j_m})^2 = 1.254\,\{1 - \exp(-2.3367(\frac{t}{t_m})\}^2(\frac{t}{t_m})^{-1} \tag{5.6}$$

Where j stands for the current density at any instant of time t and j_m is the maximum current density with its corresponding time t_m. Experimental dimensionless curves were prepared (Fig. 5.4) and compared with the instantaneous and progressive limiting nucleation mechanism.

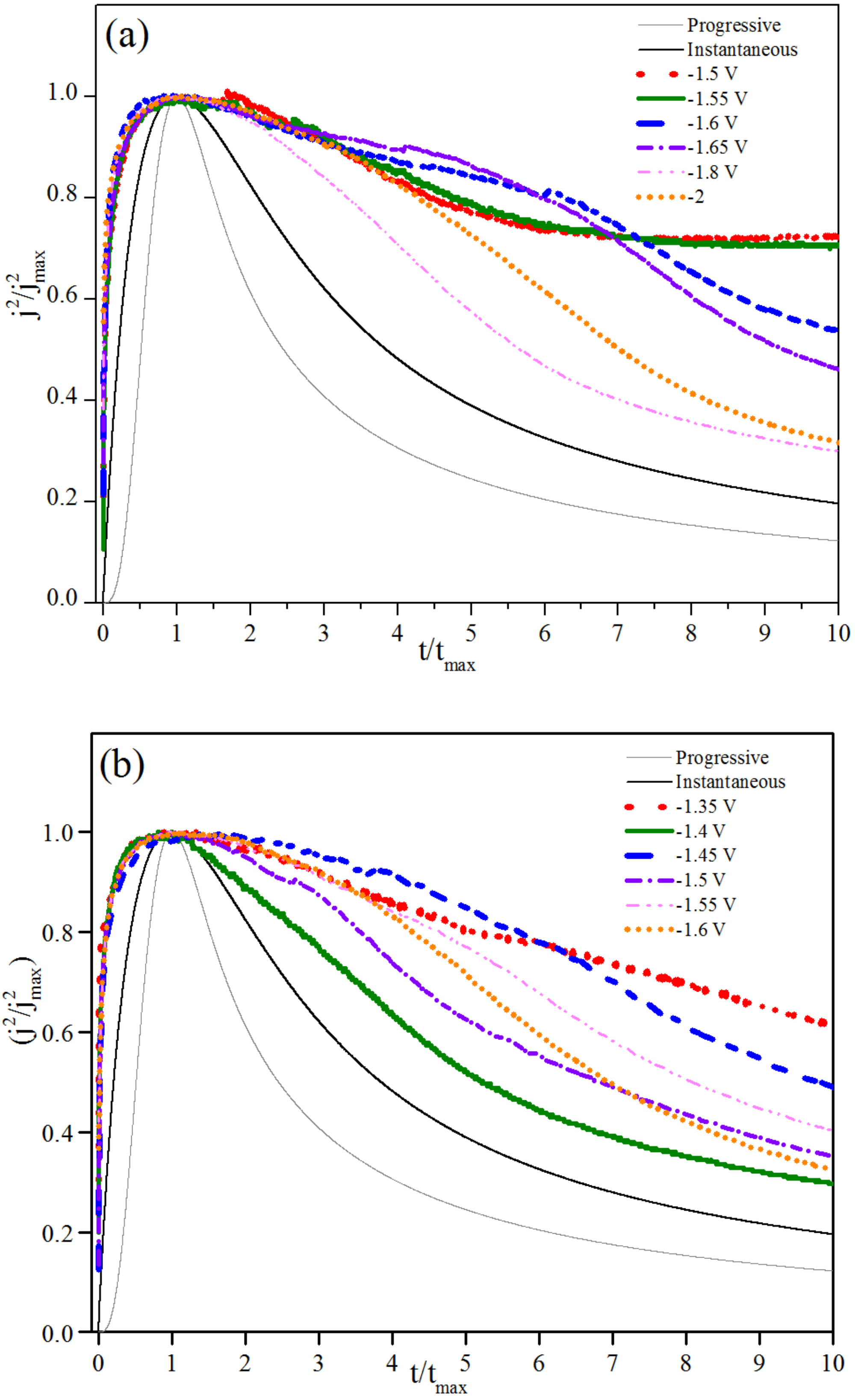

Fig. 5.4 Dimensionless plots of $(j/j_m)^2$ vs. t/tm using the data in Fig. 5.3: (a) Sulfate solution (b) sulfate-gluconate solution.

Under instantaneous nucleation mechanism, all nuclei are formed instantly after the potential step is applied, whereas under progressive nucleation, the number of nuclei continuously increases during the entire process of deposition.

For both sulfate (Zn-S) and sulfate-gluconate solutions (Zn-G) at various overpotentials, the experimental results did not match either simultaneous or progressive nucleation, nor did they lie between these two limiting cases. It is concluded that deposition of zinc from its complexes such as $ZnSO_4$ and $Zn(GH_4)^+$, and release of cation from the complex have imposed an additional step to nucleation and growth processes which inhibited the correlation between experimental and theoretical results.

5.3.4 Surface morphology characterization

The surface morphology of zinc deposits from the sulfate and sulfate-gluconate electrolytes with no additives (Zn-S in Fig. 5.5 (a) and Zn-G in Fig. 5.5 (a′)) shows two completely distinct microstructures which can be attributed to the selective deposition of zinc from $Zn(GH_4)^+$ species as discussed earlier.

Zinc deposit from sulfate solution usually displays a hexagonal structure in which planes have aligned parallel to the substrate [17, 134, 208]. However, the present Zn-S deposit shows a coarse structure in which grains are agglomerated in the form of irregular pyramids. These pyramids are not uniform in size and are covered by whiskers or fibre-like planes. Whiskers or fibre-like planes may represent ZnO, as oxygen was detected by EDS evaluation, and XRD patterns showed peaks of zinc oxides (sub-chapter 3.5). Formation of ZnO would occur during the electrodeposition due to hydrogen evolution and local change of pH [134]. Zinc deposition and hydrogen evolutions occur concurrently during the process of electroplating. Consequently, concentration of OH^- anions increases at the surface of the cathode and a layer of $Zn(OH)_2$ forms at the vicinity of electrode. Yan et al.[208] showed that under such condition deposition of zinc occurred from $Zn(OH)_2$ species. Based on the fact that zinc deposition and hydroxide formation reactions occurred at different rates, they proposed a cyclic depletion and replenishment of the OH^- anions at the vicinity of the electrode surface. They explained that at the time of depletion, $Zn(OH)_2$ layer dehydrated and led to deposition of ZnO as they observed an ultrathin ZnO layer on top of the zinc deposit [208].

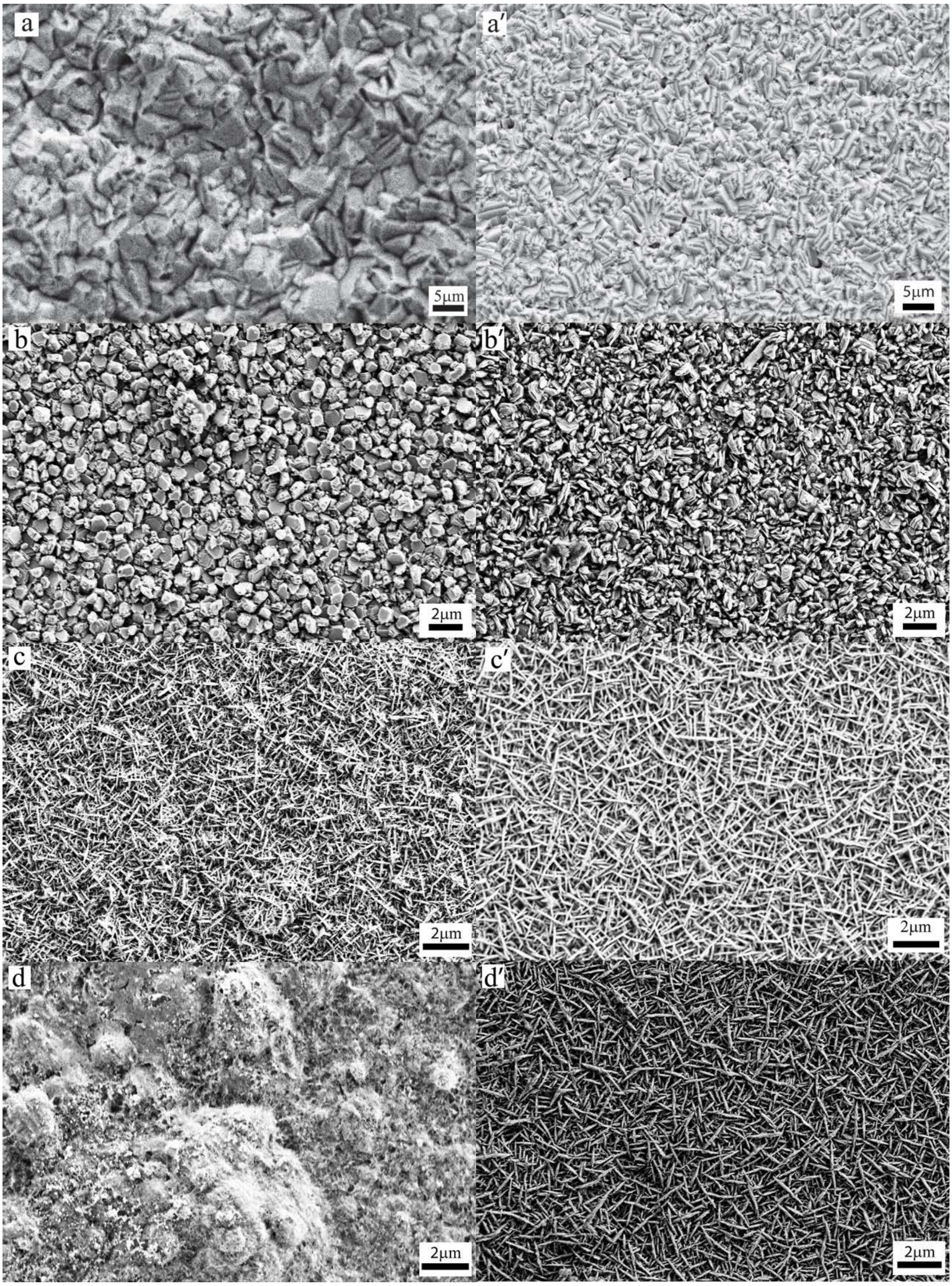

Fig. 5.5 SEM images of the surface morphology of zinc deposits from baths with no additives: (a) sulfate electrolyte (Zn-S), (a′) gluconate electrolyte (Zn-G); and with additives from sulfate bath (b) Zn-SP, (c) Zn- SPC, (d) Zn-SPCT; and from sulfate-gluconate bath: (b′) Zn-GP, (c′) Zn-GPC and (d′) Zn-GPCT.

Zinc deposits from sulfate-gluconate electrolyte (Fig. 5.5 (a′)) showed a finer structure compared with sulfate solution (Fig. 5.5 (a)). This structure consists of rectangular platelets which are piled together into agglomerate of grains. Although the coating looks very compact, it contains small voids or porosities probably due to absorption and desorption of hydrogen bubbles during the process of deposition. Usually complex ligands are added to the plating electrolytes to produce a smooth and fine structure. It was observed that morphology changed upon addition of gluconate to the bath and fine structure was achieved, but gluconic acid alone was not capable of producing homogeneous and significantly smooth microstructure.

The surface morphology of the zinc deposits changed with the addition of PEG to the plating electrolytes (Zn-SP and Zn-GP in Figs. 5.5 (b) and (b′)). Zinc deposits from Zn-SP displayed hexagonal shaped grains, and small stacks of hexagonal planes with an average size of less than 1 µm. The orientation of the hexagonal platelets was irregular; some of which were parallel to the substrate, while others piled together with a random orientation in relation to the substrate.

Addition of PEG to the sulfate-gluconate electrolyte caused a significant change in the surface morphology (Fig. 5.5 (b′)). The structure was composed of packets of hexagonal platelets with random orientation. The stack size decreased considerably down to less than 1 µm in comparison to Zn-G deposit. SEM images in Fig. 5.5 indicated that zinc deposits from sulfate and sulfate-gluconate electrolytes are refined to the same extent in the presence of PEG. The main difference between these two structures was related to the orientation of the hexagonal platelets. PEG acted as a physical barrier between adions and growth sites, and hence hindered the growth process leading to refinement of the structure. However, the blocking effects of PEG resulted in a non-compact structure for both sulfate and sulfate-gluconate electrolytes at the applied overpotential.

Figs. 5.5 (c) and 5.5 (c′) show the surface morphology of zinc deposits from sulfate and gluconate electrolytes in the presence of PEG and CTAB under pulse current condition. A porous needle-like structure was obtained for both deposition systems due to strong blocking effects of additives although the needles were long and thick from deposits of sulfate-gluconate electrolyte.

The change in surface morphology of deposit showed that CTAB interacted with PEG under the present plating condition, and their synergistic effect significantly changed the surface morphology of the zinc deposits from both sulfate and sulfate-gluconate electrolytes. It is speculated that CTAB with a cationic head group could absorb on the substrate surface electrostatically and inhibit the deposition of zinc by reducing the available surface area for electron transfer [134].

Zinc deposits from a Zn-SPCT electrolyte (Fig. 5.5 (d)) composed of tiny needles covered with a cloud of small grains. However, the needle-like surface morphology of the deposits from sulfate-gluconate electrolyte remained unchanged with the addition of thiourea to the plating electrolyte (Fig. 5.5 (d′)). A closer examination of the needles (Figs. 5.6 (c) and (d)) revealed that these needles consisted of nano grains with an average size of less than 100 nm. Figs. 5.6 (a) to (d) are SEM images showing the surface morphology and cross section microstructure of zinc deposits from sulfate and sulfate-gluconate electrolytes containing PEG, CTAB and thiourea.

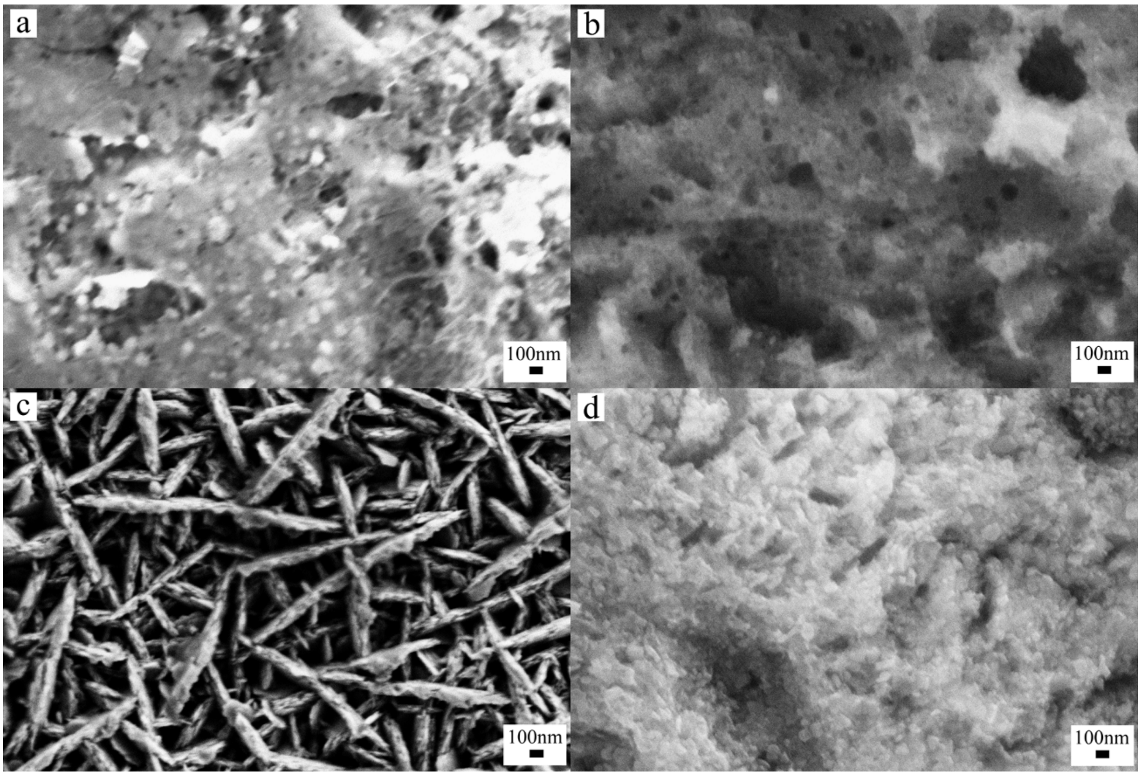

Fig. 5.6 SEM images of the zinc deposits from a Zn-SPCT bath (a) surface morphology (b) cross section; and of the zinc deposits from a Zn-GPCT bath (c) surface morphology (d) cross section.

It appeared from the surface morphology and cross section of zinc deposits from the Zn-SPCT (Figs. 5.6 (a) and (b)) that either an amorphous phase, oxide layer or a mossy zinc deposit might be present. However, XRD analysis of the deposit did not show any traces of an amorphous structure or any of oxide formation, also the coating was adherent and had a grey metallic appearance unlike to non-adherent black powdery mossy deposit [209]. Therefore, this structure might arise from nano grains that compacted together very closely.

A comparison of all surface morphologies achieved from various electrolytes showed that the effects of gluconate complex agent on modification of zinc deposits were mainly considerable in additive free bath. Both sulfate and sulfate-gluconate electrolytes can be modified to the same extent by the addition of organic additives. No significant morphological change was observed in the deposition of zinc from gluconate electrolytes with additive than the gluconate free electrolytes.

5.3.5 XRD analysis

X-ray diffraction pattern of zinc deposits from sulfate and sulfate-gluconate electrolytes and percentage of relative texture coefficient (RTC) as a function of crystallographic planes are presented in Fig. 5.7. The Fe peaks in the XRD patterns are attributed to the underlying steel substrate.

Zinc deposits from the sulfate electrolyte with no additives (Zn-S) showed narrow peaks with the preferred orientation of (112). ZnO peak was also detected for this deposit. Preferred orientation of the crystallites in electrodeposited metals has been explained by different theories such as internal strain theory [210], theory of geometrical selection [211] and two-dimensional nuclei theory [212]. Among them the proposed two-dimensional theory is widely adopted. This theory is based on the required work to form a two-dimensional nucleus of the type (h k l). The growth rate would be faster for a plane in which the required work formation is smallest (high atomic packing planes) than the planes with large work formation. Pangrov [211-213] calculated the formation energy for two-dimensional nuclei as a function of crystallization overvoltage and showed that in a h.c.p. lattice such as zinc, preferred orientation of deposit along basal plane (002) would occur at low overpotential values, and increase in overpotential leads to the formation of planes with low atomic packing which consume less energy of formation.

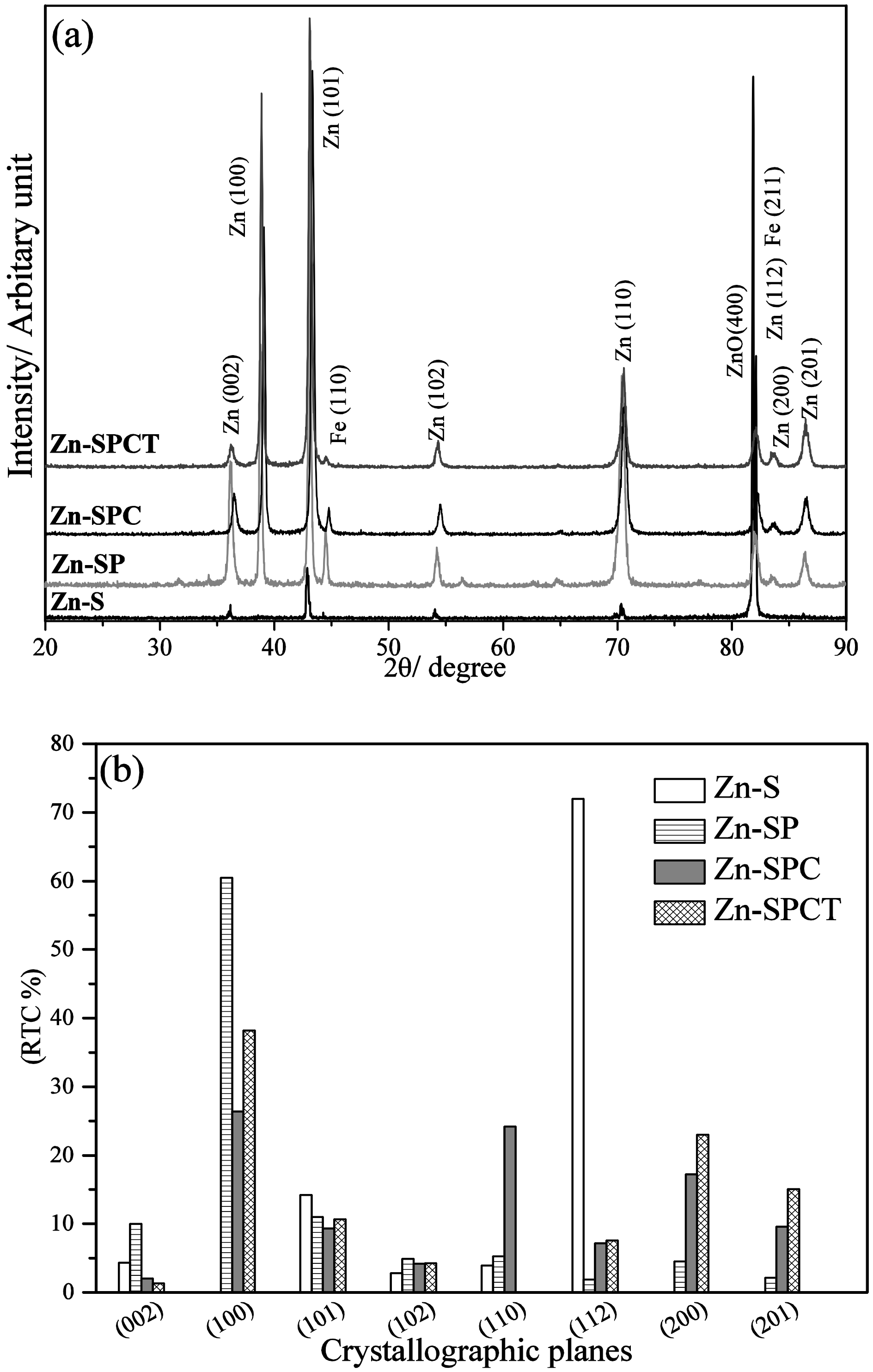

Fig. 5.7 (a) X-ray diffraction patterns of zinc deposit from sulfate electrolytes and (b) Percentage of relative texture coefficient (RTC) as a function of crystallographic plane of zinc deposit from sulfate electrolytes.

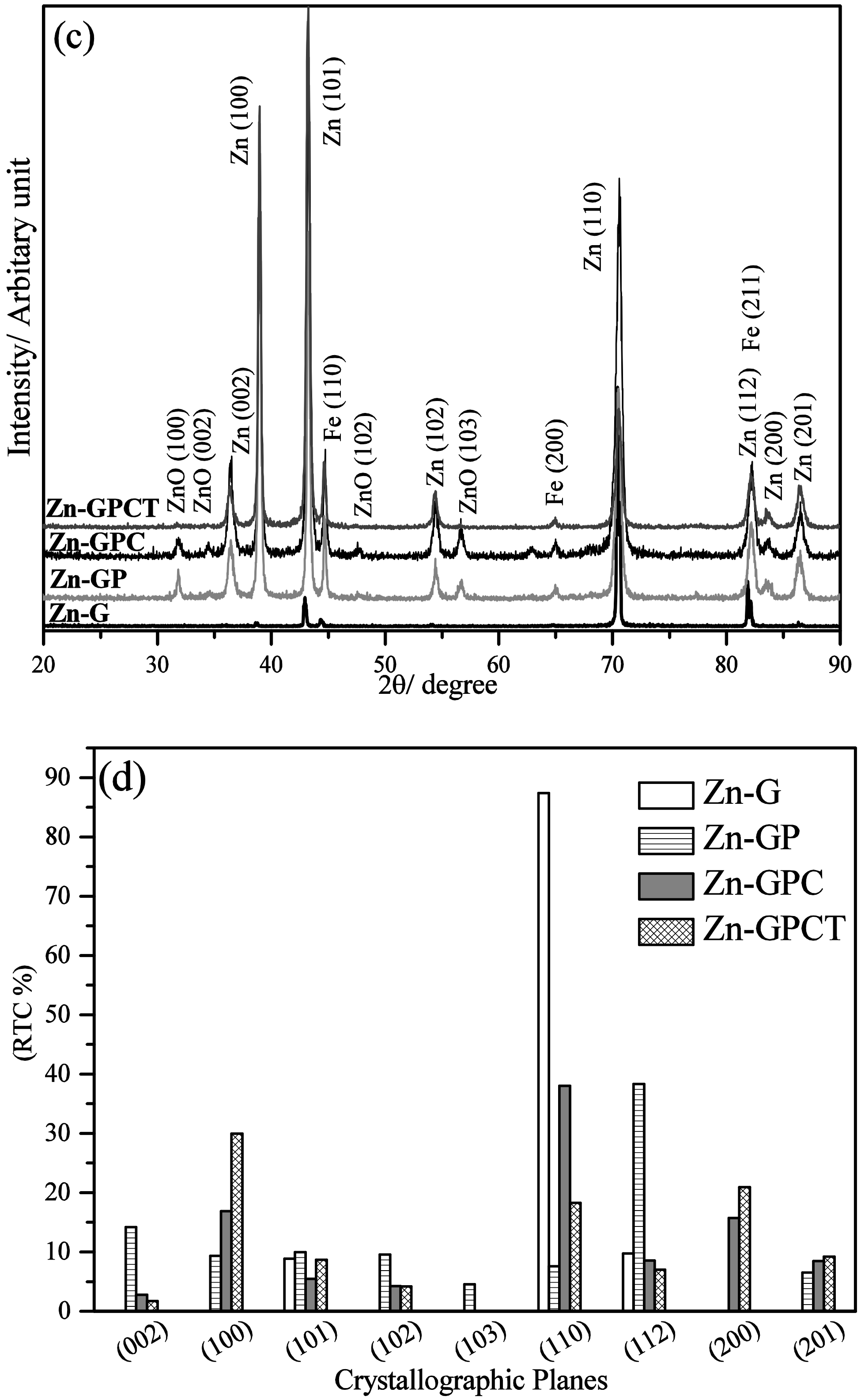

Fig. 5.7 (c) X-ray diffraction patterns of zinc deposit and (d) percentage of relative texture coefficient (RTC) as a function of crystallographic plane from sulfate-gluconate electrolytes.

In this study, the deposition current density was applied based on the preliminary cyclic voltammetry experiment on the surface of steel electrode in a way that the applied current density could provide sufficient deposition overpotentials for all kinds of solutions. As shown in Fig. 5.2, deposition potential in the presence of additives is more negative that in the electrolytes without additives. So an intermediate value of deposition overpotential for the electrolytes with additives may be considered as high for solutions without additives and it could be suggested that under the plating condition of the present experiments, the applied current density generated high deposition overpotential for the sulfate electrolyte and therefore the formation of low atomic packing plane of (112) emerged. In sulfate-gluconate bath, (110) was the preferred orientation which also is considered as a low atomic packing plane and could be formed under high deposition overpotential as observed by Youssef et al [214] for the deposition of zinc from sulfate solution .

Preferred orientation of the grains changed with inclusion of additives to the plating bath. In Zn-SP, 60% of the grain oriented along prismatic (100) plane. A dual orientations along (100) and (110) was observed for deposits from Zn-SPC electrolytes and most of the planes oriented along (100) and (200) planes in Zn-SPCT. (112) preferred orientation of Zn-GP changed to (110) in Zn-GPC, and similar dual orientation as for Zn-SPCT was formed for Zn-GPCT.

Epitaxial growth can only last for approximately 1000 Å and for the initial stages of metal deposition on substrate, then grain growth changes due to the effects of several factors such as electrolyte composition and plating conditions. Under different plating conditions and electrolyte composition, such as change in temperature, pH and additives concentration, specific crystal faces can grow faster onto the substrate surface [127, 213, 215]. Preferred orientation of metal deposit is also affected by the kinetics of hydrogen evolution and any change in surface energy can lead to change in preferred orientation. Additives can also change preferred orientation of grains by changing deposition overpotential or modifying nucleation mechanism [216-218].

As discussed above and in the previous sections, and based on the present results of cyclic voltammetry and surface morphology, additives and gluconate anion interfered with zinc nucleation and growth mechanism, which results in changes in preferred orientation. However, similar preferred orientation of the grains in Zn-SPCT and Zn-GPCT showed that at high concentration of additives, preferred orientation of grains was more affected by additive rather than by depositing ligand.

5.4. Summary

Electrodeposition of zinc from sulfate and sulfate-gluconate electrolytes with and without additives was investigated. The analysis of the distribution of zinc (II) species showed that $ZnSO_4$ was the main species in both sulfate and sulfate-gluconate electrolytes.

Cyclic voltammetry and chronoamperometry, along with surface morphology and XRD analyses confirmed that gluconate complex agent played a predominant role on the electrodeposition of zinc from sulfate-gluconate baths.

Additives changed the electrochemical responses of the electrolytes and the preferred orientation of the grains. Their synergistic effects produced porous nanocrystalline zinc plated structure from both sulfate and sulfate-gluconate electrolyte systems. However, the role of depositing ligand on the surface morphology and preferred orientation became negligible as the number of additives increased in the plating bath.

Chapter 6

Electrodeposition of nanocrystalline zinc-tin alloy from gluconate electrolyte in the presence of additives

6.1 Background

For alloy electrodeposition the individual deposition potentials of the alloying elements should be very close. For those alloying elements which their deposition potentials are very different, alloy deposition is possible by change of the activity of the elements (normally reducing the concentration of the noble metal) or introducing complex agent to the plating bath.

There is a large difference between the standard electrode potentials E_0 for Sn^{2+}/ Sn (-0.14 V) and that of Zn^{2+}/ Zn (-0.762 V). Thus the codeposition of these metals is viable through application of a proper complex agent.

In this study, the main focus is on the production of nanocrystalline zinc-tin alloy with low content of Sn (less than 30 wt.% tin) by using additives and pulse electrodeposition from environmental friendly complex agents such as gluconic acid, citric acid or tartaric acid. In a preliminary study, electrodeposition of zinc-tin alloy from citric acid electrolyte and tartaric acid electrolyte were not promising and in most cases powdery deposits were produced due to the low limiting current densities of these electrolytes for the production of zinc-low content tin alloy. However, by using gluconic acid as the complex agent, electroplating of zinc-low content tin alloy is viable. Therefore, this ligand is used in this study as an excellent choice for the synthetize of nanocrystalline zinc-tin coatings.

CTAB, PEG (various molecular weights) and thiourea used as additives individually and in combination for the modification of the structure. Effects of additives are discussed in terms of cyclic voltammetry of the plating bath on glassy carbon electrode, surface morphology, composition of deposits and in some cases texture of deposits on mild steel substrates have been evaluated.

6.2 Experimental

The chemical composition of the solutions used in this study is presented in Table 6.1. The pH of the electrolytes was adjusted to 4.3-4.7 using 10 M NaOH. For the preparation of a stable solution at the pH range of this study and avoiding precipitation of tin hydroxide, $SnCl_2$ was dissolved at concentrated HCl 32% and then solution was diluted with distilled water. Other elements of the bath added to the solution only after dissolution and dilution of $SnCl_2$ solution.

Table 6.1 List of the electrolytes

Solution	Constituents
S_{Base}	0.45 M Na-gluconate ($C_7H_{11}Na\,O_7$) + 0.56 M Na_2SO_4 + 0.18M HCl
S_{Sn}	S_{Base} + 0.04 M $SnCl_2$
S_{Zn}	S_{Base} + 0.4 M $ZnSO_4$,7 H_2O
S_{Sn+Zn} (Alloy bath)	S_{Base} + 0.04 M $SnCl_2$ + 0.4 M $ZnSO_4$,7 H_2O

In acidic gluconate electrolyte media, a range of zinc and tin species, including metal ions (Zn (II) and Sn (II)), metal complexes and ligand anions, are present. The speciation of zinc and tin in the electrolyte varies with the composition and pH of the electrolytes. To investigate the composition and pH dependent speciation, mass balance equations were solved for Zn^{2+}, Sn^{2+}, SO_4^{2-}, $GH_4^{-}$and Na^{+} ions using HySS2009 Software. Ion pairs of zinc and tin with sulfate and chloride anions were considered in the calculations. Equilibrium equations reactions and corresponding stability constants used in this thesis are presented in Table 6.2.

Table 6.2. Equilibrium reactions and corresponding stability constants [200].

Equilibrium reactions	Log K_{eq}
$Zn^{2+} + SO_4^{2-} \leftrightarrow ZnSO_4$	2.38
$Zn^{2+} + GH_4^- \leftrightarrow Zn(GH_4)^+$	1.7
$Zn^{2+} + Cl^- \leftrightarrow ZnCl^+$	0.43
$Zn^{2+} + 2Cl^- \leftrightarrow ZnCl_2$	0.61
$Zn^{2+} + 3Cl^- \leftrightarrow ZnCl_3^-$	0.53
$Zn^{2+} + 4Cl^- \leftrightarrow ZnCl_4^{2-}$	0.2
$Sn^{2+} + H_2O \leftrightarrow SnOH^+ + H^+$	-3.8
$Sn^{2+} + 2H_2O \leftrightarrow Sn(OH)_2(aq) + 2H^+$	-7.8
$Sn^{2+} + 3H_2O \leftrightarrow Sn(OH)_3^- + 3H^+$	-17.6
$Sn^{2+} + GH_4^- \leftrightarrow Sn(GH_4)^+$	3.01
$Sn^{2+} + 2GH_4^- \leftrightarrow Sn(GH_4)_2$	2.28
$Sn^{2+} + SO_4^{2-} \leftrightarrow SnSO_4$	1.29
$Sn^{2+} + 2(SO_4^{2-}) \leftrightarrow Sn(SO_4)_2$	1.65
$Sn^{2+} + Cl^- \leftrightarrow SnCl^+$	1.34
$Sn^{2+} + 2Cl^- \leftrightarrow SnCl_2(aq)$	2.13
$Sn^{2+} + 3Cl^- \leftrightarrow SnCl_3^-$	1.99
$Sn^{2+} + 4Cl^- \leftrightarrow SnCl_4^{2-}$	2.03
$H^+ + SO_4^{2-} \leftrightarrow HSO_4^-$	1.99
$H^+ + GH_4^- \leftrightarrow HGH_4$	3.86
$Na^+ + SO_4^{2-} \leftrightarrow NaSO_4^-$	0.7

6.3 Results and Discussion

6.3.1 Zinc electrolytes in the absence and presence of Na-gluconate

6.3.1.1 Distribution of Zn (II) species in the absence and presence of Na-gluconate

Zinc distribution diagram in the absence and presence of Na-gluconate is presented in Fig. 6.1 (a) and (b). Fig. 6.1 (c) shows speciation of gluconate in S_{Zn} solution.

$ZnSO_4$ is the predominant species in absence and presence of Na-gluconate. Survila [201] et al. reported $ZnSO_4$ as the main species in a sulfate-gluconate electrolyte at the pH range of 3 to 7. Concentration of $Zn(GH_4)^+$ increases with the increase in pH. This behaviour is also noticed for zinc speciation in the solution of study in Chapter 5. For more detail and discussion see sub-chapter 5.3.1.

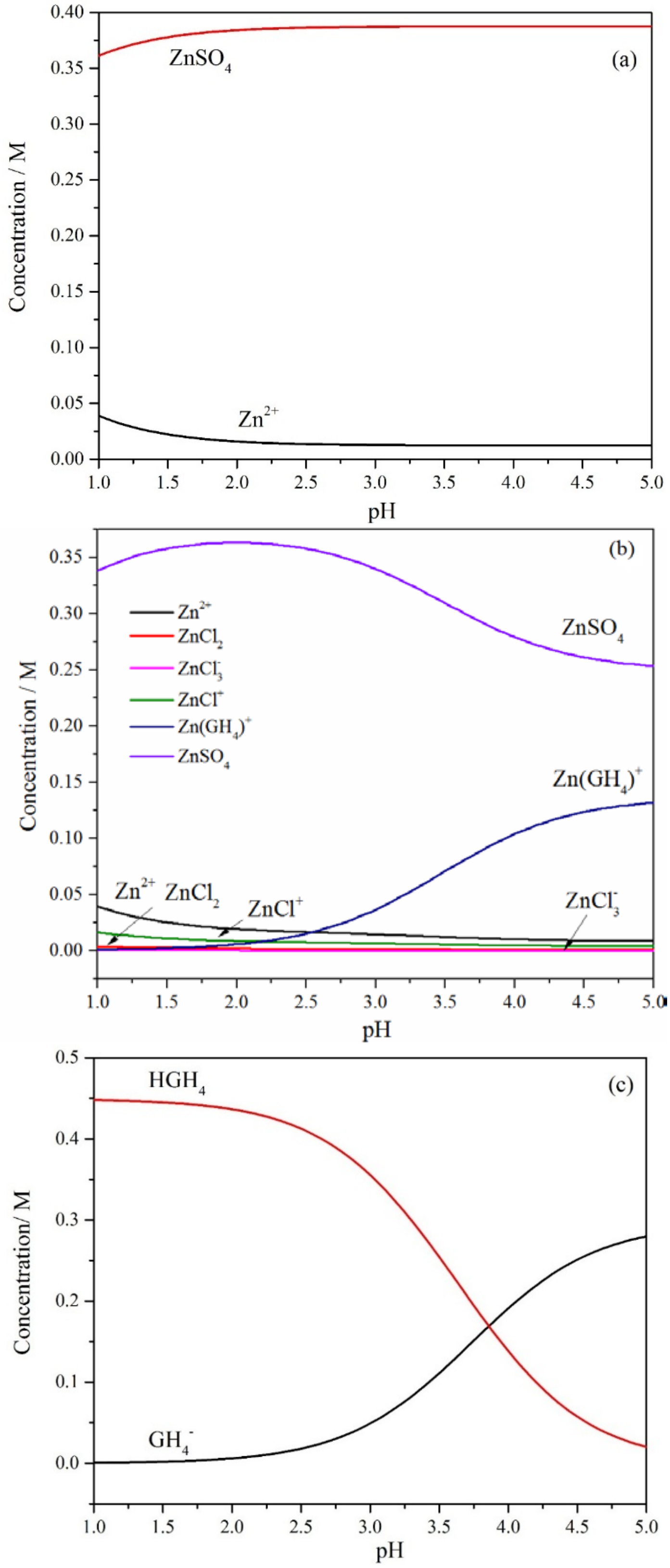

Fig. 6.1 Speciation diagram of zinc in (a) 0.4 M $ZnSO_4$, 7 H_2O + 0.56 M Na_2SO_4 solution (b) 0.4 M $ZnSO_4$, 7 H_2O + 0.56 M Na_2SO_4 + 0.45 M Na-gluconate (S_{Zn}) and (c) gluconate speciation in S_{Zn} as a function of pH.

6.3.1.2 Voltammetric evaluation of zinc in the absence and presence of Na-gluconate

Cyclic voltammetry of zinc in a solution containing 0.4 M $ZnSO_4$, 7 H_2O + 0.56 M Na_2SO_4 and in a 0.4 M $ZnSO_4$, 7 H_2O + 0.56 M Na_2SO_4 + 0.45 M Na-gluconate (S_{Zn}) solution at pH = 4.45 is presented in Fig. 6.2.(a) and (b) respectively.

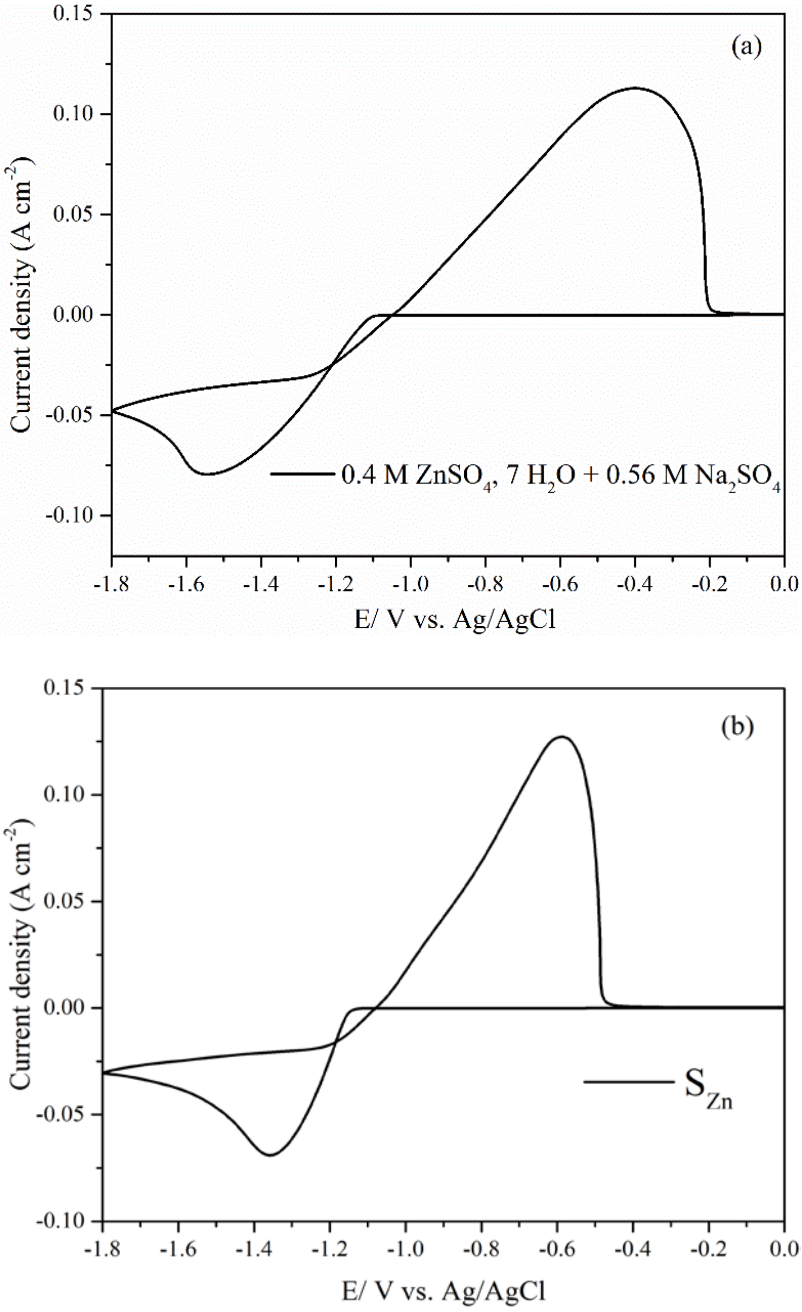

Fig. 6.2 Cyclic voltammetry of a glassy carbon electrode in (a) 0.4 M $ZnSO_4$, 7 H_2O + 0.56 M Na_2SO_4 solution at pH = 4.45 and (b) 0.4 M $ZnSO_4$, 7 H_2O + 0.56 M Na_2SO_4 + 0.45 M Na-gluconate (S_{Zn}) at pH = 4.45.

Zinc deposition in the absence of gluconate ions started at -1.11 V and occurred through a reduction peak at -1.54V. While with the addition of gluconate deposition started at -1.14 V and occurred through a reduction peak at -1.35 V. There was a negligible change in the onset of deposition potential (0.03V), however shifts of peak potential to more positive values was noticeable. Shift of zinc deposition potential to more positive values in the presence of Na-gluconate was observed and discussed in detail in sub-chapter 5.3.2.1.

6.3.2 Tin electrolytes in the absence and presence of Na-gluconate

6.3.2.1 Distribution of Sn (II) species in the absence and presence of Na-gluconate

Tin distribution diagram in the absence and presence of Na-gluconate is presented in Fig. 6.3 (a) and (b). Fig. 6.3 (c) shows speciation of gluconate in S_{Sn} solution.

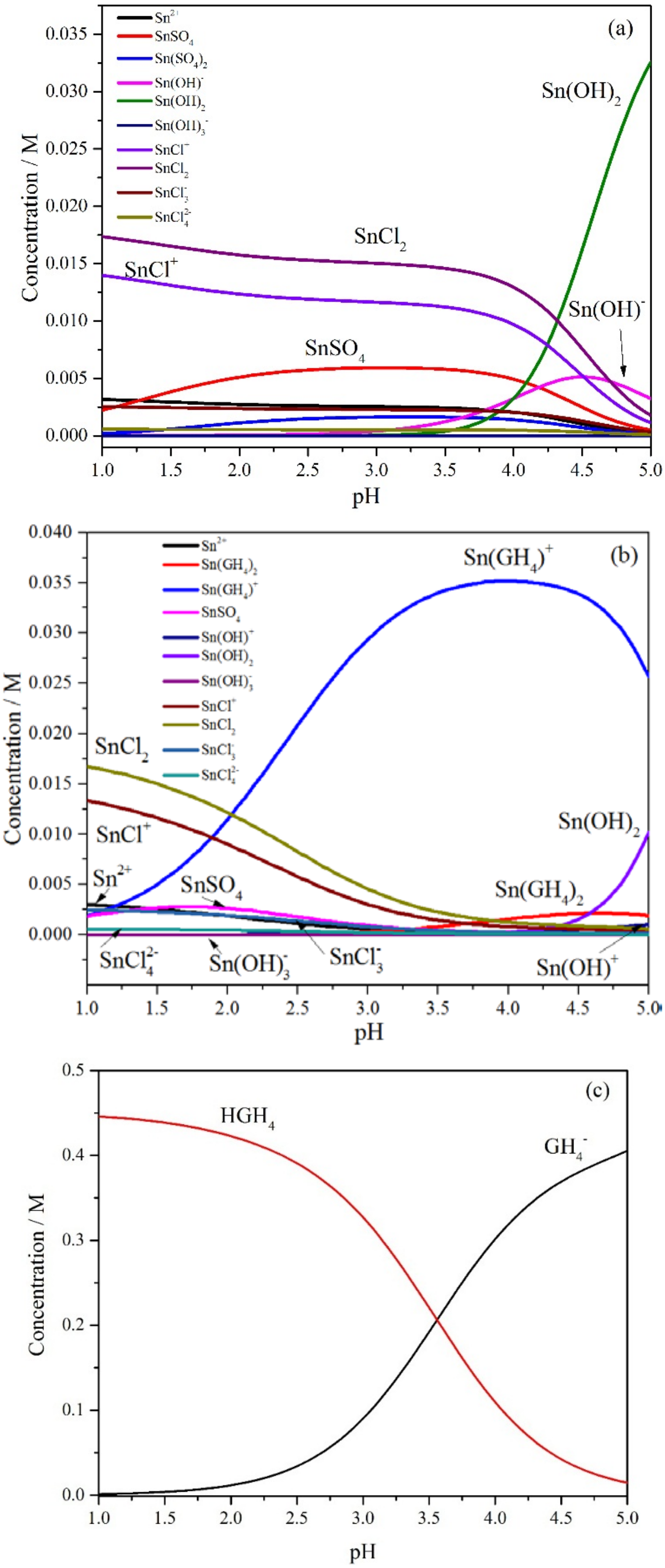

Fig. 6.3 Speciation diagram of tin in (a) 0.04 M $SnCl_2$ + 0.56 M Na_2SO_4 + 0.18 M HCl (b) 0.04 M $SnCl_2$ + 0.56 M Na_2SO_4 + 0.45 M Na-gluconate+ 0.18 M HCl (S_{Sn}) and (c) gluconate speciation in S_{Sn} as a function of pH.

In the absence of gluconate ions various complexes of tin (II) such as $SnCl_2$, $SnCl^+$ and $SnSO_4$ were stable over a wide range of pH (pH ≤ 4). With the increase in pH, concentration of these species declined and concentration of $Sn(OH)_2$ prevailed.

In the presence of gluconate other complexes of Sn with Cl^- and SO_4^{2-} were only stable at pH ≤ 2. At higher values of pH, $Sn(GH_4)^+$ became the predominant species in the solution. This occurred as a result of deprotonation of gluconic acid. At pH values lower than 2 most of GH_4^- anions were in protonated form and were not able to coordinate with Sn^{2+} cations. With increase in pH, deprotonation of gluconate occurred and concentration of free GH_4^- anions increased. At this stage the Sn^{2+} coordinate with the gluconate ligand cations and thus the increase in the concentration of $Sn(GH_4)^+$ was observed. At higher values of pH (≥4.57) concentration of $Sn(GH_4)^+$ decreased and on the other hand the concentration of $Sn(OH)_2$ increased due to the increase of concentration of free $(OH)^-$ anions. At the pH range of 3.9 - 4.57 most of Sn (II) cations are in coordination with GH_4^- anions either in form of $Sn(GH_4)^+$ or $Sn(GH_4)_2$.

6.3.2.2 Voltammetric evaluation of tin in the absence and presence of Na-gluconate

Cyclic voltammetry of tin in a solution containing 0.04 M $SnCl_2$ + 0.57 M Na_2SO_4 + 0.18 M HCl and in a solution containing 0.04 M $SnCl_2$ + 0.57 M Na_2SO_4 + 0.18 M HCl 0.45 M Na-gluconate (S_{Sn}) at pH = 3.5 is presented in Fig. 6.4 (a) and (b) respectively. In the absence of gluconate, tin deposition starts at -0.54 V. Based on the speciation diagram of Sn^{2+} in Fig. 6.4 (a) $SnCl_2$ is the predominant species of tin at pH value of 3.5. Therefore, peak I in Fig. 6.4 (a) was attributed to the dissociation and deposition of tin from $SnCl_2$ complexes. With the addition of gluconate, the onset deposition potential stayed unchanged and deposition started at - 0.54V and occurred through a reduction peak at - 0.72 V. Shifts of deposition potential to more negative values occurred due to the change of the ionic strength as the result of the addition of Na-gluconate to the solution. In addition to change in ionic strength, complexation of tin with gluconate anions and production of stable complexes of $Sn(GH_4)^+$ led to the change of deposition potential. Stability constant of $Sn(GH_4)^+$, (Log k = 3.01 [200]) is larger than $SnCl_2$ (Log k = 2.13 [200]) , therefore its dissociation requires application of high value of overpotentials.

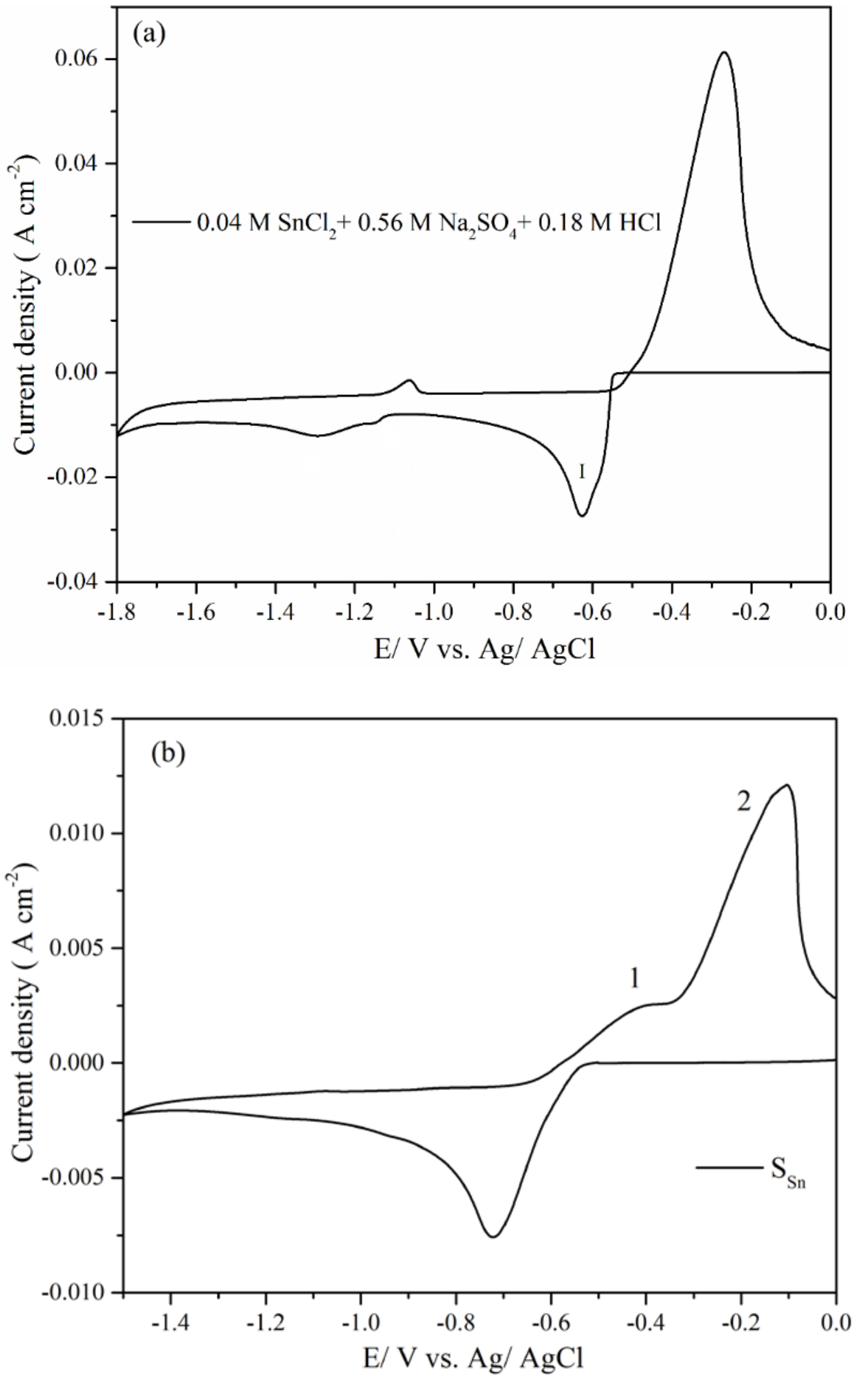

Fig. 6.4 Cyclic voltammetry of a glassy carbon electrode in (a) 0.04 M $SnCl_2$ + 0.56 M Na_2SO_4 + 0.18 M HCl solution at pH = 3.5 and (b) 0.04 M $SnCl_2$+ 0.56 M Na_2SO_4 + 0.18 M HCl + 0.45 M Na-gluconate (S_{Sn}) at pH = 3.5.

In the presence of gluconate, during the anodic scan small shoulder appeared as part of the tin oxidation peak and designated as 1 in Fig. 6.4 (b). Torrent-Burgues et al. [219] reported two peaks for the oxidation of Sn from sulfate-gluconate electrolyte. Based on their evaluation the height ratio of the peak at more negative values varied with the change in gluconate concentration and change in tin concentration only had effected on the height of the peak at more positive values. They concluded that the emergence of two oxidation peaks was due to the complexation of gluconate and tin ions at the time of oxidation, and contributed peak at more negative values to the complex products of tin and gluconate. Therefore, peak 1 attributed to the formation of a complex of tin and gluconate at the time of oxidation and peak 2 attributed to bulk oxidation of tin.

6.3.3 Alloy bath evaluation

6.3.3.1 Distribution of zinc (II) and tin (II) species in the alloy bath

The speciation of zinc and tin in the alloy bath (alloy bath in Table 6.1) is presented in Fig. 6.5 at the pH range of 1 to 5. Fig. 6.5 (c) also presents the speciation of gluconate.

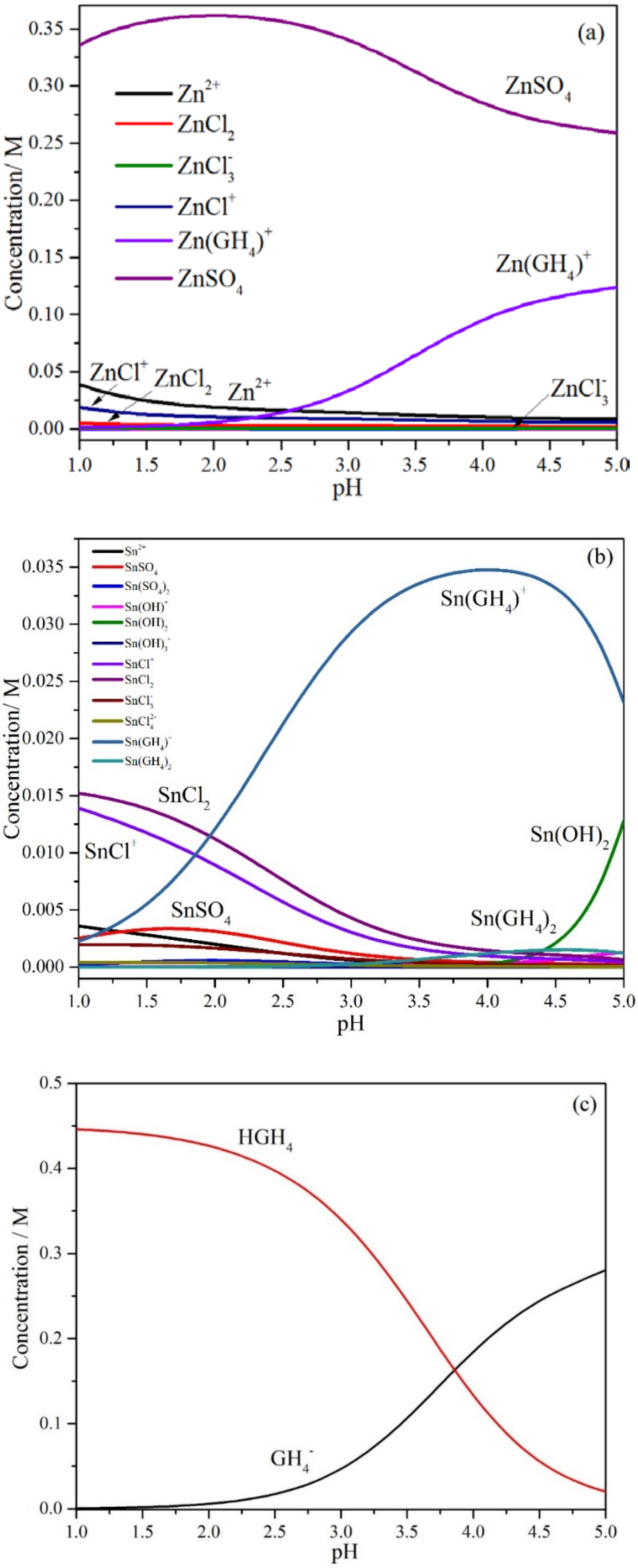

Fig. 6.5 Speciation diagrams as a function of pH for (a) Zn^{2+}, (b) Sn $^{2+}$, and (c) gluconate in S_{Sn+Zn} (alloy bath) electrolyte (see Table. 6.1).

Speciation of Zn^{2+} and Sn^{2+} in the alloy bath was close to the single bath of zinc and tin in the presence of gluconate ions. Only small variation in the concentration of species was observed.

Zinc (II) speciation diagram showed that $ZnSO_4$ was the main species over the pH range of 1.5 to 5. However, small amount of zinc complexes with chloride anions were composed.

At pH values over 2, $Sn(GH_4)^+$ was the predominant species of tin in the main electrolyte (Fig. 6.5 (b)). With the increase of pH the deprotonation of gluconic acid occurred (Fig. 6.5 (c)) and the concentration of GH_4^+ increased, which led to the increase in concentration of $Sn(GH_4)^+$.

6.3.3.2 Cyclic voltammetry of the alloy bath

The electrochemical response of the alloy bath and the supporting electrolyte (to validate the cathodic potential window available for electrodeposition of Zn and Sn metals is adequate) in the presence of gluconate is presented in Fig. 6.6 (a) and (b).

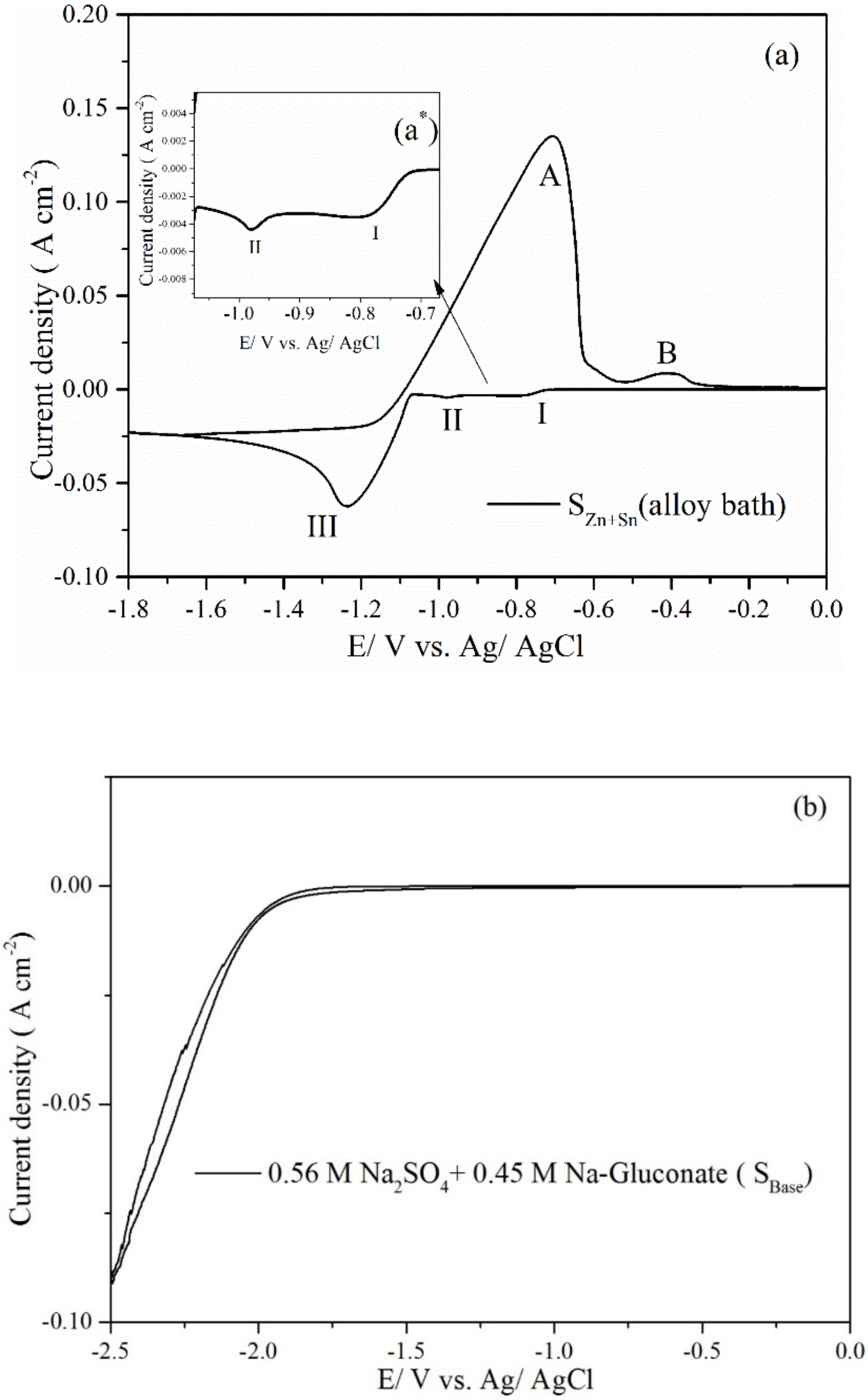

Fig. 6.6 Cyclic voltammetry of a glassy carbon electrode in a (a) S_{Zn+Sn} (alloy bath) and (b) S_{Base} solutions.

Cyclic voltammetry of the alloy bath (S_{Zn+Sn}) showed a pre-wave and two reduction peaks at -0.778 V (peak I in Fig. 6.6 (a)), -0.979 V (peak II in Fig. 6.6 (a)) and -1.237 V (peak III in Fig. 6.6 (a)), respectively, for the deposition of Zn-Sn on glassy carbon electrode. Comparison of the alloy voltammograms with that of individual Sn (S_{Sn} in Fig. 6.4 (b)) and individual Zn (S_{Zn} in Fig. 6.2 (b)) indicated that the pre-wave (I) and first reduction peak (II) could be assigned to tin deposition and the second reduction peak (III) could be analogous to the zinc reduction peak for the deposition of zinc from S_{Zn} solution.

In the alloy electrolyte due to complexation of gluconate with zinc ions the relative percentage of the tin complexes changed in the bath. This situation resembles the case of which the concentration of the ligand (gluconate) decreases in the electrolytes and the degree of the complexation declines. Under this circumstance and under steady state condition sudden changes in electrolyte composition could occurs at the surface of electrode and complexes of tin with chloride anions act as electroactive species despite their low concentration at the surface of electrode. In such a system imposing overvoltage could lead to a sudden decrease in concentration of electroactive species at the surface of electrode and a pre wave could emerge as a plateau of limiting current [220, 221]. Therefore, in this study peak I attributed to the deposition of tin from chloride complexes.

On the other hand, deposition from Sn-gluconate complex (peak II) moved to more negative potential in the alloy electrolyte in comparison to S_{Sn} bath. This could be due to variation in thermodynamics factors of the electrolyte such as ionic strength. The S_{Sn} solution and S_{Sn+Zn} solution with different ionic strength led to variation in tin ions activity in S_{Sn} and S_{Sn+Zn} electrolytes. Therefore, a different deposition potential for tin from these two electrolytes would be expected. Also interaction between ions and surface active charges were different in the alloy bath compared with the single tin bath, which also imposed variation to the deposition potential [110].

The third reduction peak at -1.234 V from the S_{Zn+Sn} solution is analogous to zinc deposition from the S_{Zn} solution (Fig. 6.2 (b)) with a small shift to positive potentials. During the cathodic scan of the S_{Zn+Sn} solution, Sn was deposited on glassy carbon substrate before zinc reduction. Therefore, zinc reduction occurred on a layer of Sn rather than on glassy carbon substrate which led to a shift of zinc reduction potential to more positive values as reported in literature [89].

Cyclic voltammetry of the supporting electrolyte (Fig. 6.6 (b)) showed a sharp decrease of current density starting at almost -1.9 V, which indicated that hydrogen evolution of the supporting electrolyte on glassy carbon electrode started at -1.9 V.

6.3.4 Pulse plating of the alloy bath on mild steel substrate

Based on the fundamental theories of pulse electrodeposition, morphology and composition of alloy deposit can be affected due to the variation in current density and current on-time and current off-time. The following experiments were performed to find the optimum duty cycle for the plating.

6.3.4.1 Effect of current off-time at constant current on-time

6.3.4.1.1 T_{ON} = 5 ms

Effects of the variation of T_{OFF} (5, 7, 9 and 11 ms) on the surface morphology of the Zn-Sn alloy deposits from the alloy bath (S_{Zn+Sn}) on the mild steel substrate is presented in Fig. 6.7. All the deposits prepared at constant pulse duration (T_{ON} = 5 ms) with constant pulse current density (0.047 A/cm^2).

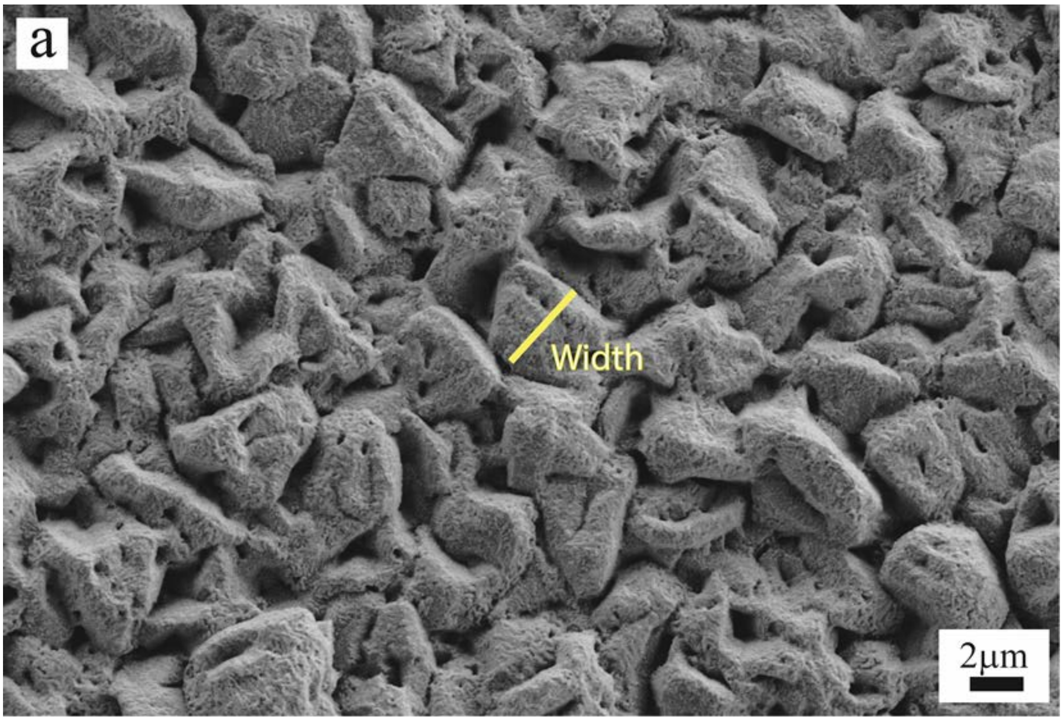

Fig. 6.7 (a) Zn-Sn alloy deposits (from alloy bath) at T_{ON} = 5ms, T_{OFF} = 5ms.

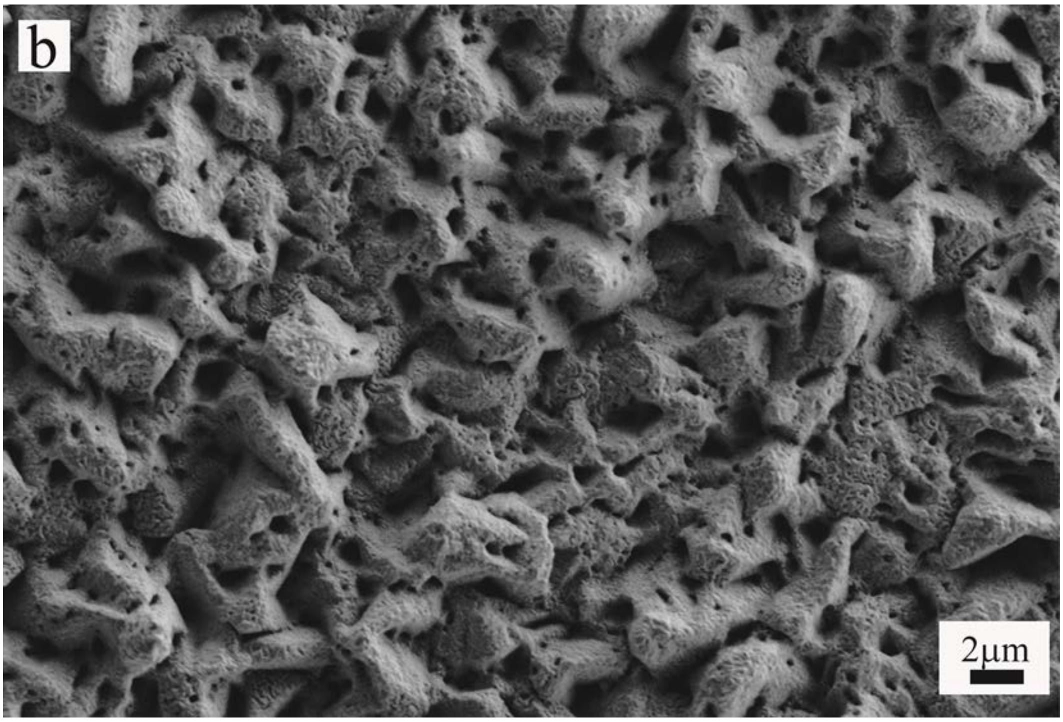

Fig. 6.7 (b) Zn-Sn alloy deposits (from alloy bath) at T_{ON} = 5ms, T_{OFF} = 9ms.

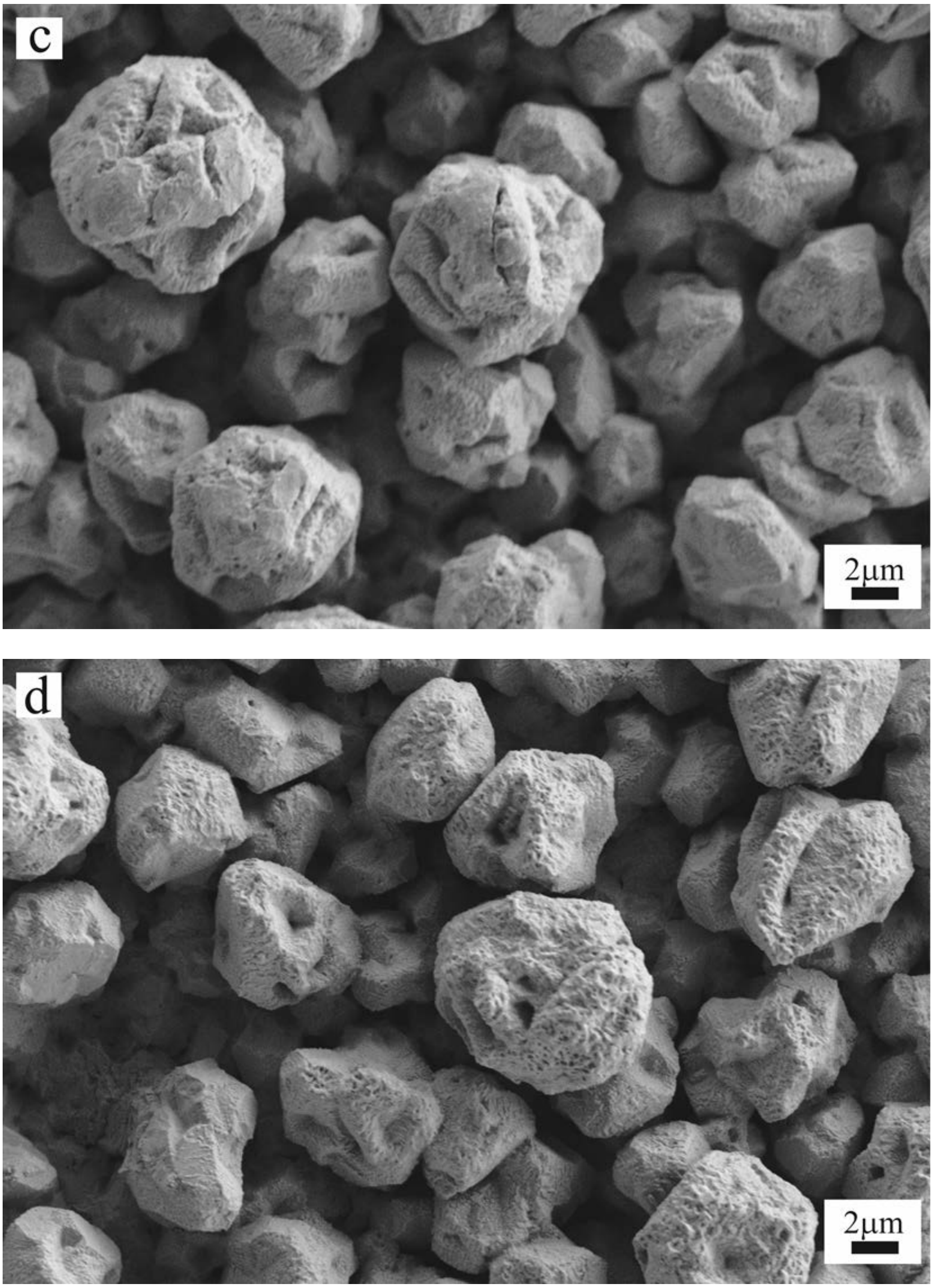

Fig. 6.7 FESEM micrographs of the surface morphology of the Zn-Sn alloy deposits (from alloy bath) prepared at constant current on-time (T_{ON} = 5ms) with constant pulse current density (0.047 A/cm^2) at different current off-times (c) 9 ms and (d) 11 ms.

Surface morphology of the alloy deposit at T_{OFF} = 5 ms and 7 ms, showed a pyramidal structure with voids. These pyramids are composed of agglomerate of small grains. Average width of pyramids decreased from 2.75 ± 0.8 µm (Fig. 6.7 (a)) at T_{OFF} = 5 ms to 1.74 ± 0.7 µm (Fig. 6.7 (b)) at T_{OFF} = 7 ms.

Nodular structure was observed at higher pulse off-time (T_{OFF} = 9 ms and 11 ms). These nodules also composed of agglomerate of small grains. The average nodule size increased from 5.73 ± 1.45 µm at T_{OFF} = 9 ms to 7.3 ± 1.5 µm at T_{OFF} = 11 ms.

The effects of T_{OFF} time on the surface morphology of the deposits was considerable. During the on-time of a pulse cycle, depletion of ions at the vicinity of the electrode occurs, refurbishment of the double layer at the vicinity of electrode occurs during the T_{OFF} of a pulse cycle. If the T_{OFF} is short the refurbishment of electrolyte at the vicinity of electrode does not fully occurs. Thus deposition would occur from a depleted electrolyte, in this case growth enhances in comparison to the nucleation and a coarse morphology is expected [152]. Therefore, the higher width of pyramids at 5 ms in comparison to 7 ms current off-time was due to insufficient duration of current off-time (T_{OFF} = 5 ms) which was not able to fully supply zinc and tin ions to the electrolyte at the vicinity of electrode surface.

Change of the morphology from a pyramidal to nodular structure with the increase of T_{OFF} was due to the migration of add-atoms during the off-time of the cycle and their tendency to join high energy area such as peaks (and not to the valleys) which promote production of a nodular structure. In pulse electrodeposition at constant current density and constant T_{ON}, duty cycle and consequently average current density decreases with the increase in T_{OFF} (see sub-chapter 2.6.4.5). Decrease in average current density from 0.017 A/cm^2 at T_{OFF} = 9 ms to 0.014 A/cm^2 at T_{OFF} = 11 ms led to production of smaller number of nuclei and increase in the diameter of the nodules.

Variation in zinc, tin and oxygen contents in the alloys of Fig. 6.7 as a function of current off-time is illustrated in Fig. 6.8.

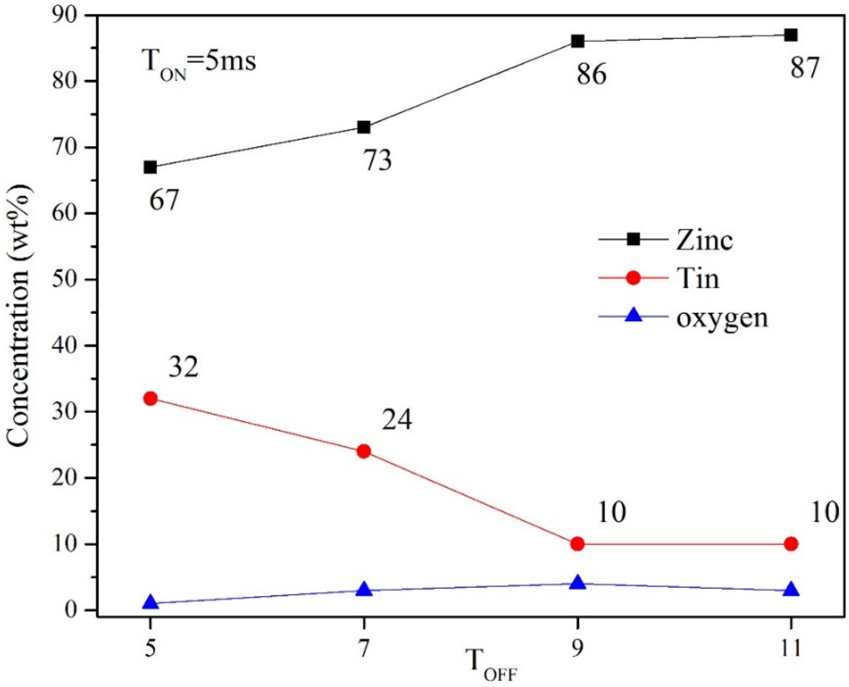

Fig. 6.8 Zinc, tin and oxygen contents of the alloy deposited at T_{ON} = 5ms and j = 0.047 A/cm^2 as a function of various T_{OFF} (morphology is presented in Fig. 6.7 as (a) 5 ms, (b) 7 ms, and (c) 9 ms (d) 11 ms.

With the increase of current off-time from 5 ms to 11 ms, concentration of zinc increased from 77 wt.% to 87 wt.%. While, Sn concentration reduced from 32 wt.% to only 10 wt.%. The oxygen content of the deposit which explains the possibility of oxide formation during the plating or after deposition is very negligible and at highest concentration is only 4 wt.% at deposits of Fig. 6.7 (c). Increase in zinc concentration with increase of T_{OFF}, means that more active metal (zinc) deposits than the more noble metal (tin). This situation may suggest the possibility of anomalous codeposition of zinc and tin with increasing the current off-time. However, as increase in T_{OFF} would result in the decrease of average current density, so the increase in zinc concentration is related to deposition of ions with high concentration at low current densities. Zinc to tin ratio is 10, therefore at low average current densities deposition of more zinc is favored due to the high concentration of zinc in the bath.

6.3.4.1.2 T_{ON} = 7 ms

The effects of variation of current off-time (5, 7, 9 and 11 ms) on the surface morphology of the Zn-Sn alloy deposits from the main solution (S_{Zn+Sn}) on the mild steel substrate is presented in Fig. 6.9. All the deposits prepared at constant pulse duration (T_{ON} = 7 ms) with constant pulse current density (0.047 A/cm^2).

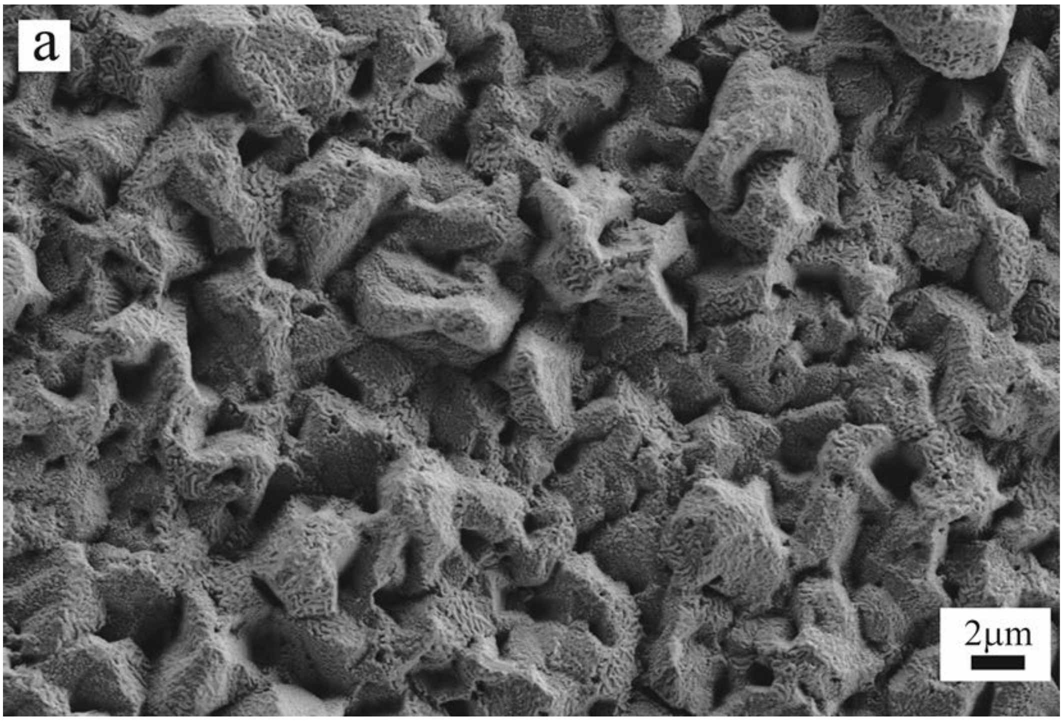

Fig. 6.9 (a) Zn-Sn alloy deposits (from alloy bath) at T_{ON} = 7 ms, T_{OFF} = 5ms.

Fig. 6.9 (b) Zn-Sn alloy deposits (from alloy bath) at T_{ON} = 7 ms, T_{OFF} = 7 ms.

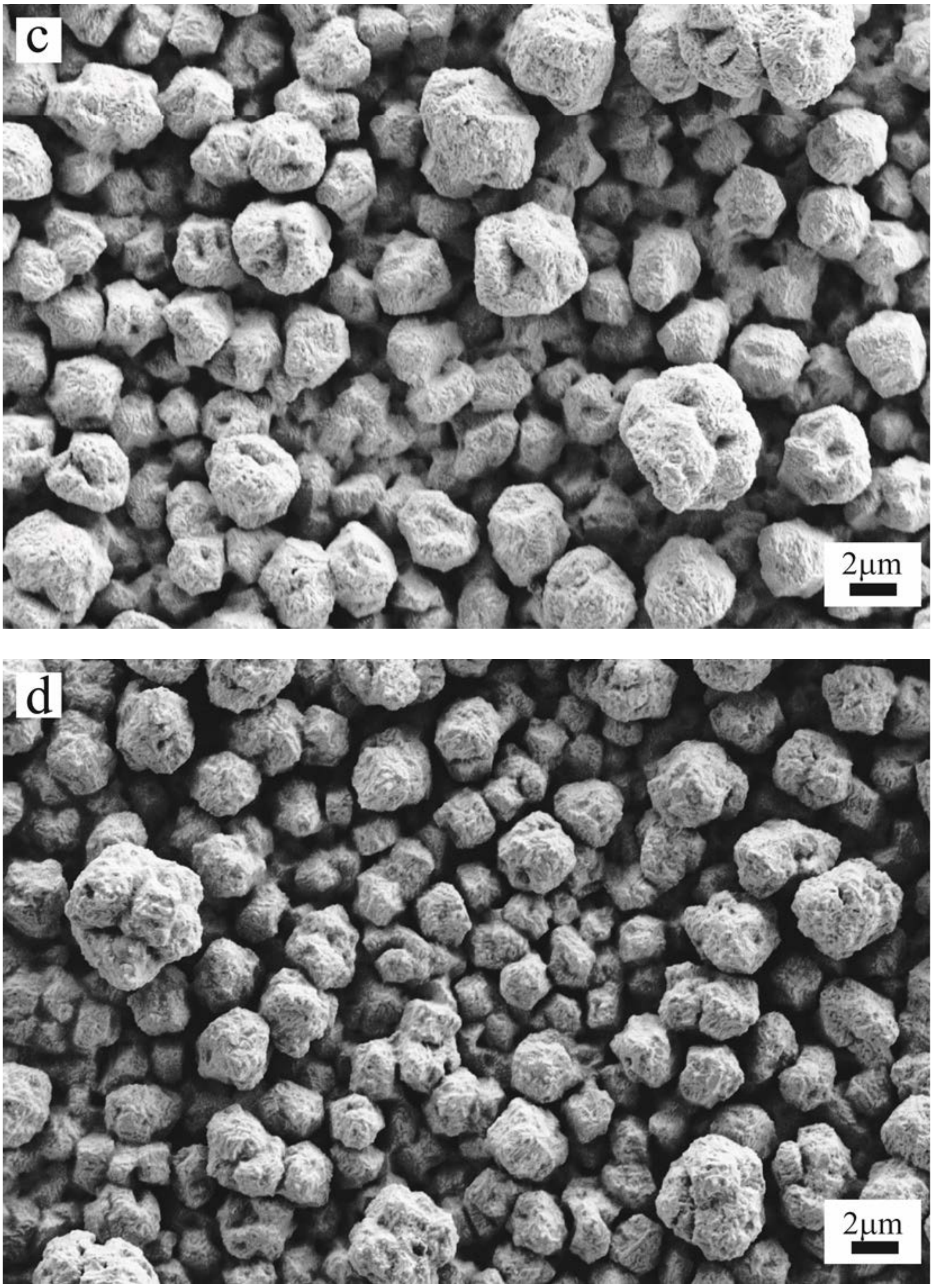

Fig. 6.9 FESEM micrographs of the surface morphology of the Zn-Sn alloy deposits prepared at constant current on-time (T_{ON} = 7ms) with constant pulse current density (0.047 A/cm^2) at different current off-times (c) 9 ms and (d) 11 ms.

Surface morphology of the deposits changed from a pyramidal structure to a nodular structure with an increase in current off-time from 5 ms to 7 ms. A decrease of the average nodule size was observed upon further increase of off-time from 7 ms to 9 ms and then to 11 ms. This trend in the reduction of nodule size was in contrast to the previous observation in constant T_{ON} = 5 ms, which showed the complexity of pulse electrodeposition process. Usually coarsening of the structure is expected due to increase of T_{OFF} as more time is provided for the refurbishment of the microstructure and due to the possible migration of add-atoms on the surface of the deposit as observed at T_{ON} = 5 ms. The result showed that T_{ON} = 7 ms imposed a high degree of depletion to the double layer, thus the concentration of the ions at double layer could be refurbished at high applied T_{OFF}. At small current off-time in relation to current on-time deposition of double layer occurred from a depleted layer which normally leads to the production of coarse structure as mentioned in sub-chapter 6.3.4.1.1 for the deposition at $T_{ON\,=}$ 5 ms and T_{OFF} = 5 and 7 ms respectively.

Comparison of the nodules' sizes of the deposits at T_{ON} = 5 ms with the deposits at T_{ON} $_{=}$7 ms for the same pulse off-time durations showed a reduction in the diameter of the nodules at longer T_{ON}. This was mainly due to the high value of overpotential applied at longer T_{ON} time at a fixed current density and current off-time.

Variation in zinc, tin and oxygen contents in the alloys of Fig. 6.9 as a function of current off-time is illustrated in Fig. 6.10.

Zinc concentration initially increased with the increase of current-off time from 79 wt.% at T_{OFF} = 5 ms to 85 wt.% at T_{OFF} = 7 ms. Then it gradually decreased to 80 wt.% and 77 wt.% at current off-time of 9 ms and 11 ms sequentially. Tin content followed a reversed procedure to zinc and decreased initially from 21 wt.% to 10 wt.% and then increased to 12 wt.% and 17 wt.% with the increase of current off-time. Concentration of oxygen in the deposit increased gradually with the increase of current-off time.

Composition of the deposit at T_{ON} = 7 ms did not follow the same behavior as T_{ON} = 5ms with variation of T_{OFF} which indicate that pulse deposition is complicated and any small change would have an effect on the deposit.

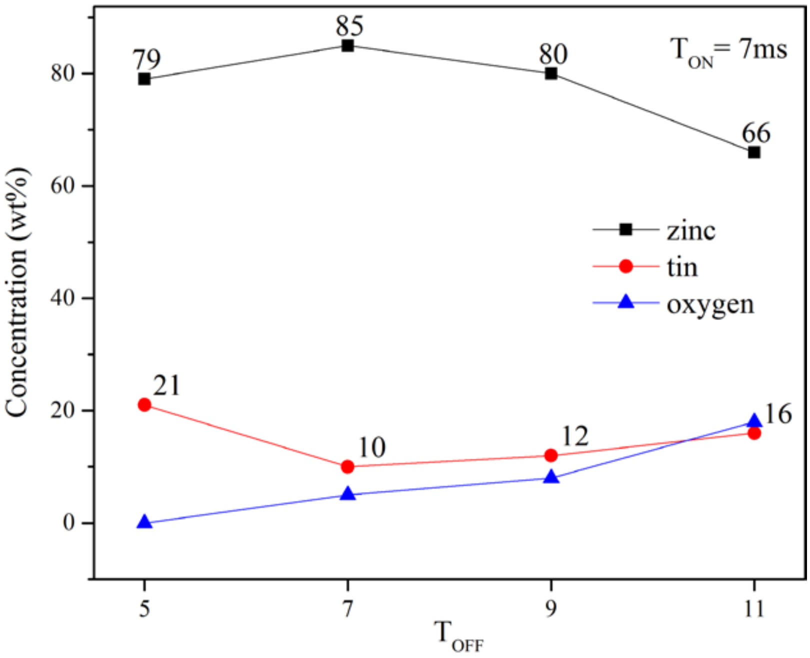

Fig. 6.10 Zinc, tin and oxygen contents of the alloy deposited at T_{ON} = 7 ms and j = 0.047 A/cm^2 as a function of various T_{OFF} (morphology is presented at Fig. 6.7as (a) 5 ms, (b) 7 ms, and (c) 9 ms (d) 11 ms.

In this study the first aim was to produce zinc-tin alloy with low content of tin at the range of 25 wt. % to 30 wt.%. Therefore, the plating parameters of the deposit of micrograph (b) in Fig. 6.7 was chosen for the rest of this study. Under this plating condition a non-nodular structure finer than the non-nodular structure of the deposits of micrographs of Fig. 6.7 (a) and Fig. 6.9 (a) deposited.

6.3.4.2 Effects of additives

Preliminarily trail experiments showed that production of nanocrystalline Zn-Sn alloy without using any additive was practically impossible. Study on the effect of various additives such as thiourea, CTAB and PEG (M_n = 400, 2050) were either carried out individually or in combination for the production of nanocrystalline Zn-Sn alloy.

6.3.4.2.1 Effects of thiourea

6.3.4.2.1.1 Cyclic Voltammetry

Cyclic voltammetry of the alloy bath in the presence of various concentration of thiourea is presented in Fig. 6.11. Tin and zinc deposition potential moved to more negative values in the presence of thiourea. The magnitude of the shift increased with the increase in thiourea concentration. The shifts of deposition potential to more negative value and reduction of the cathodic current density in the presence of thiourea was mainly due to its blocking effect. It has been reported [138] that adsorption of thiourea to the surface of electrode occurred through the sulphur atoms. Absorbed thiourea interferes with the nucleation and growth of tin and zinc ions. Due to the reduced electrode area zinc and tin deposition need more overpotentials for deposition.

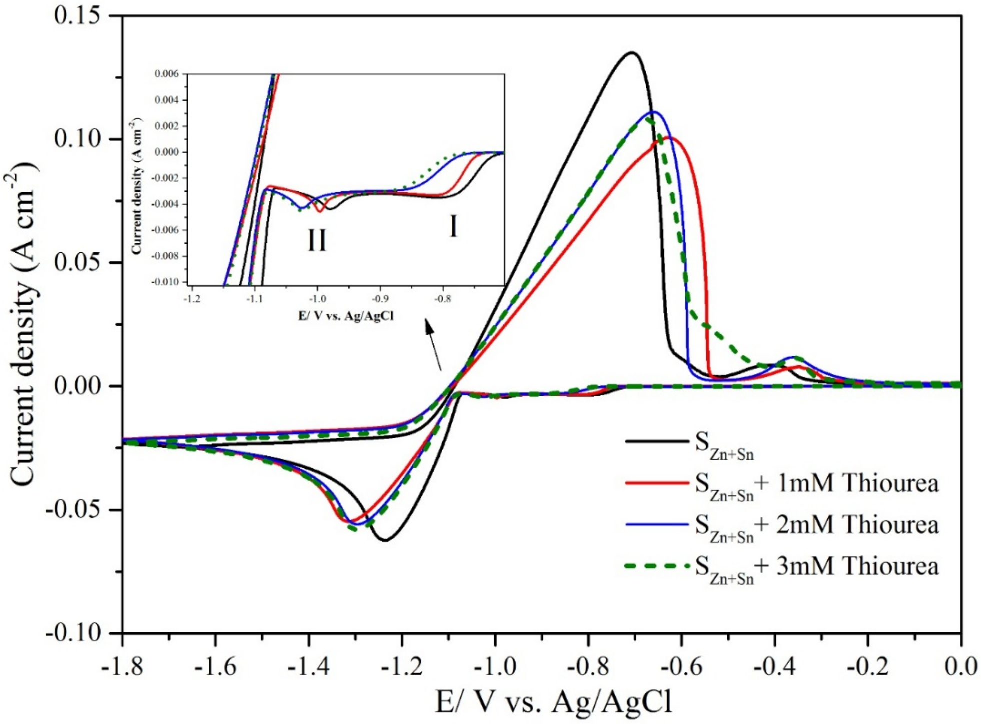

Fig. 6.11 Cyclic voltammetry of the alloy solution with no additives and in the presence of 1, 2, and 3 mM thiourea.

6.3.4.2.1.2 Surface morphology

Surface morphology of the zinc-tin alloy in the presence of various concentration of thiourea is presented in Fig. 6.12. Pyramid structure of the alloy deposit (Fig. 6.7 b) changed and a more porous structure observed in the presence of thiourea. Increase in thiourea concentration made the structure slightly compact with no specific change in the dimension of the deposit. Thiourea at the studied concentration was not able to refine structure of the alloy deposit. Table 6.3 shows the composition of the deposits.

Table 6.3 Composition of the Zn-Sn alloy in the presence of thiourea.

Thiourea Content	Zinc (wt. %)	Tin (wt. %)	Others (wt.%)
1 mM	73	24	3
2 mM	80	20	none
3 mM	74	25	1

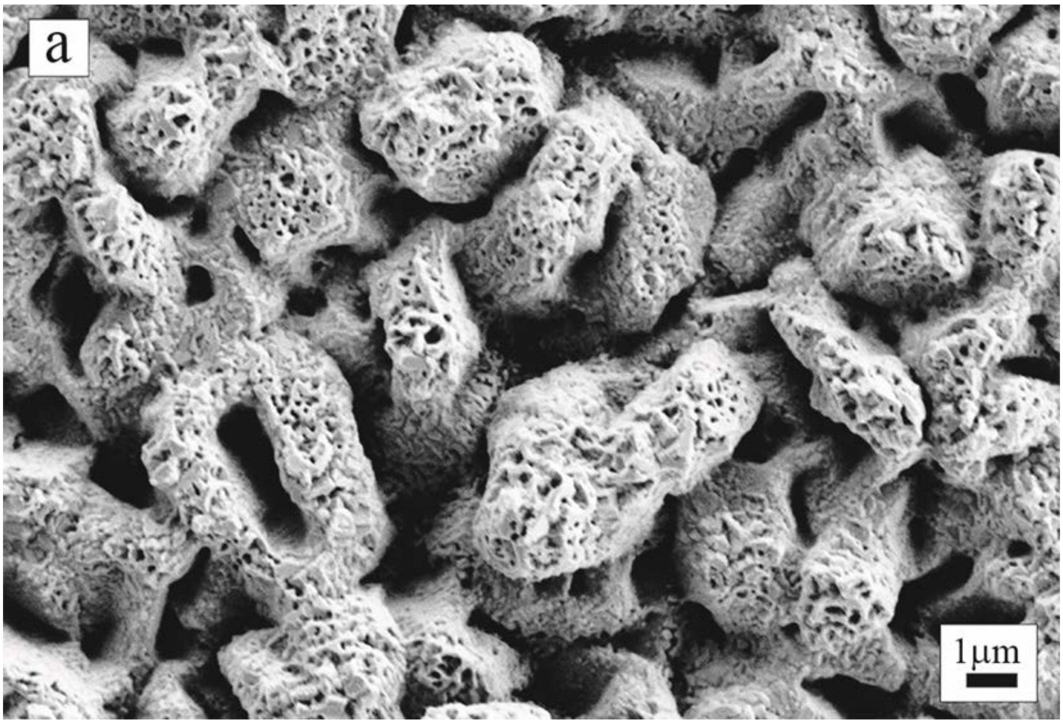

Fig. 6.12 (a) 1mM of thiourea $j = 0.046$ A/cm^2 $T_{ON} = 5$ ms, $T_{OFF} = 7$ ms.

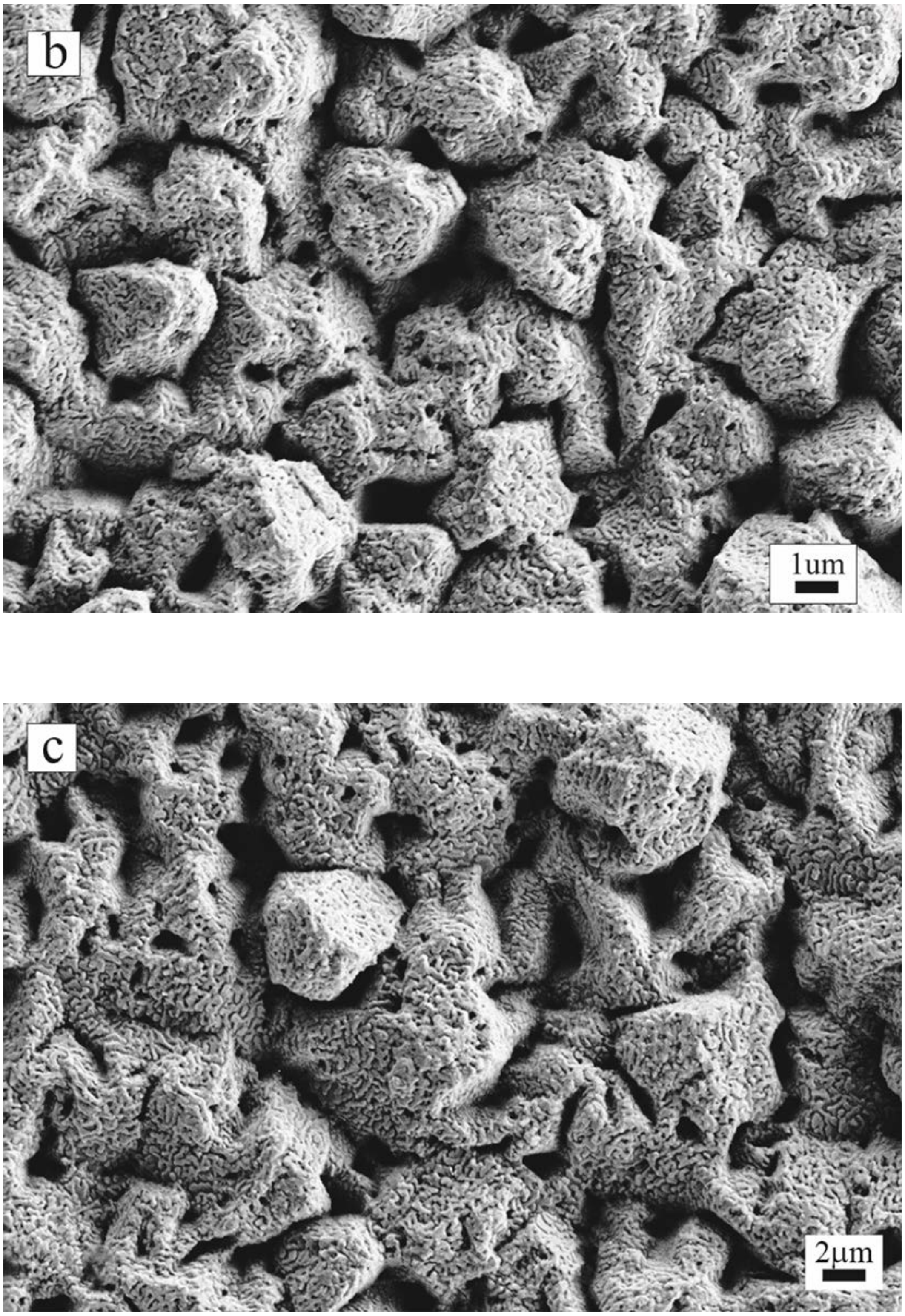

Fig. 6.12 Surface morphology of the alloy deposit on steel substrate in the presence of (b) 2mM and (c) 1mM of thiourea. j = 0.046 A/cm^2 T_{ON} = 5 ms, T_{OFF} = 7 ms.

6.3.4.2.2 Effects of PEG (400)

6.3.4.2.2.1 Cyclic Voltammetry

Cyclic voltammetry of the alloy bath in the presence of 1 gr/ lit PEG 400 is presented in Fig. 6.13. A large shift in zinc and tin deposition potential was observed due to addition of PEG to the electrolyte. PEG is a non-ionic surfactant and can change the mechanism of zinc and tin deposition by different means. It has been reported [133] that the addition of non-ionic surfactant affects metal reduction process by changing the mass transfer rate. Also depending on the concentration, PEG can form complexes with depositing metal ions and change the mechanism of metal deposition [203, 204]. PEG can form a layer on metallic surfaces due to its strong surface active properties [203]. Any of these reasons can interfere with zinc nucleation and growth process and impose changes to electrochemical responses of the electrolyte.

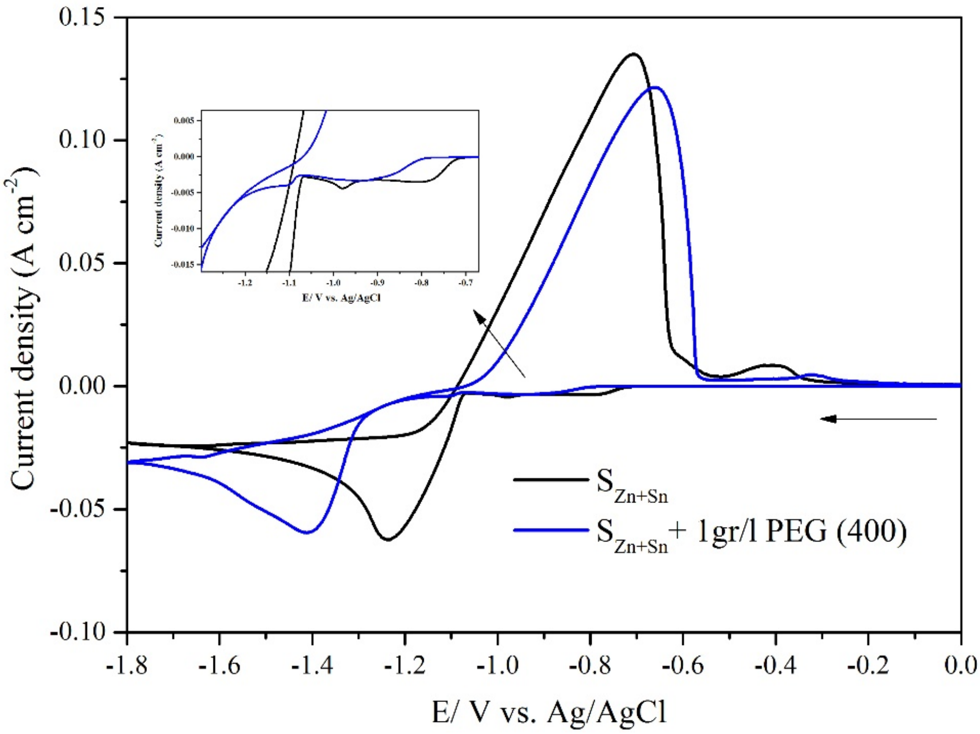

Fig. 6.13 Cyclic voltammetry of the alloy solution (S_{Zn+Sn}) in the absence and presence of 1gr/lit PEG (400).

6.3.4.2.2.2 Surface morphology

Effects of PEG on the surface morphology of the deposit were studied at various current densities. At j = 0.042, 0.046, 0.052 A/cm^2 deposits were burnt and black. Only at j = 0.03 A/cm^2 and low values such as j=0.025 A/cm^2 a bright deposit was produced. EDS examination of the deposits showed that bright deposit had more than 85 wt. % tin and up to 15% of zinc. Results indicated that PEG by itself cannot withstand high values of current densities in the electroplating bath. On the other hand, low current densities are not able to provide adequate voltage for the deposition of zinc (active metal). Surface morphology of the deposit at j = 0.052 and 0.02 A/cm^2 is presented in Fig. 6.14 (a) and (b).

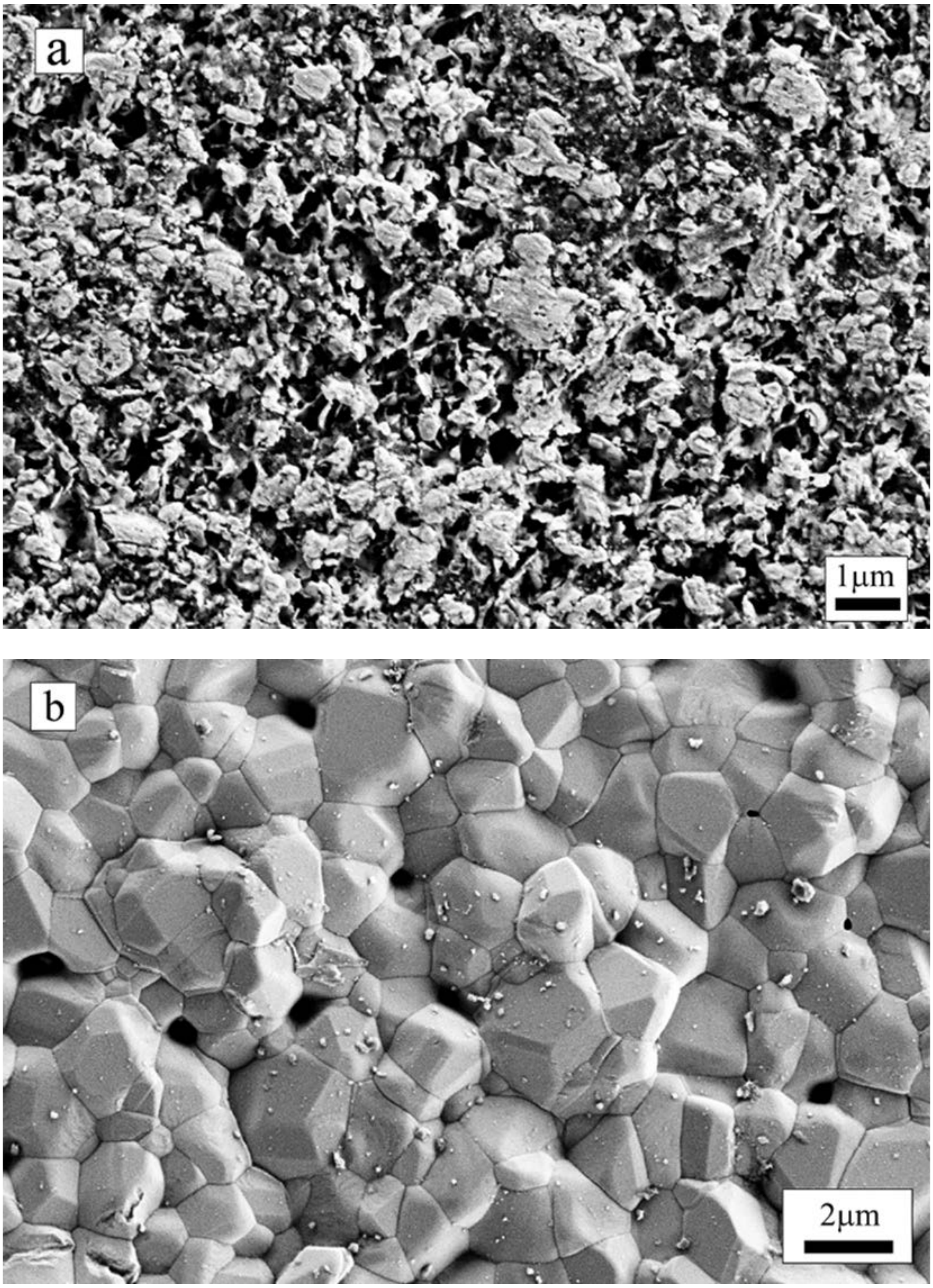

Fig. 6.14 SEM images showing surface morphology of the alloy deposit on steel substrate in the presence of 1 gr/lit PEG (400). (a) j = 0.052 A/cm^2 T_{ON} = 5 ms, T_{OFF} = 7 ms and (b) j = 0.02 A/cm^2 T_{ON} = 5 ms, T_{OFF} = 7 ms.

6.3.4.2.3 Effects of CTAB

6.3.4.2.3.1 Cyclic Voltammetry

Various concentration of CTAB (1, 5, 10 mM) was added to the plating electrolyte. Cyclic voltammetry of the alloy electrolyte in the absence and presence of CTAB is presented in Fig. 6.15. With the addition of 1mM CTAB zinc and tin deposition potential moved to more negative values. Upon further addition of CTAB (5 mM and 10 mM) zinc potential moved to more negative values and tin deposition potential stayed almost unchanged.

Quaternary ammonium salts (QAS) such as CTAB is used as inhibitor or catalyst in electroplating [222, 223]. This cationic surfactant could electrostatically interact with the surface of electrode. Small concentration of CTAB could adsorb on the active sites of the surface such as kinks and act as a deactivating inhibitor or could partially cover the surface and reduce the available geometrical area for electron transfer [224]. Therefore, they can impose negative shifts to tin and zinc deposition potential. It has to be noted that cations of CTAB act only act as blocking inhibitor for the deposition of electrostatically neutral depositing species. However, CTAB can also play either a catalyst or inhibitive role in metal deposition process. In case of anionic nature of depositing species, CTAB cations behave as ion pairing catalyst and reduce the energy barrier for the deposition of anionic species of the electrolyte which are not electrically interested to attract to a negatively charged surface of working electrode. On the other hand, in case of the cationic nature of depositing species, CTAB compete with cations of depositing species and hinder the deposition process [223, 225]. Accordingly, deposition of tin and zinc from $Sn(GH)_4^+$ and $Zn(GH)_4^+$ complexes not only was hindered by blocking effects of CTAB and but also these cations have to compete with CTAB cations at the time of deposition for the absorption to the negatively charged surface of glassy carbon electrode.

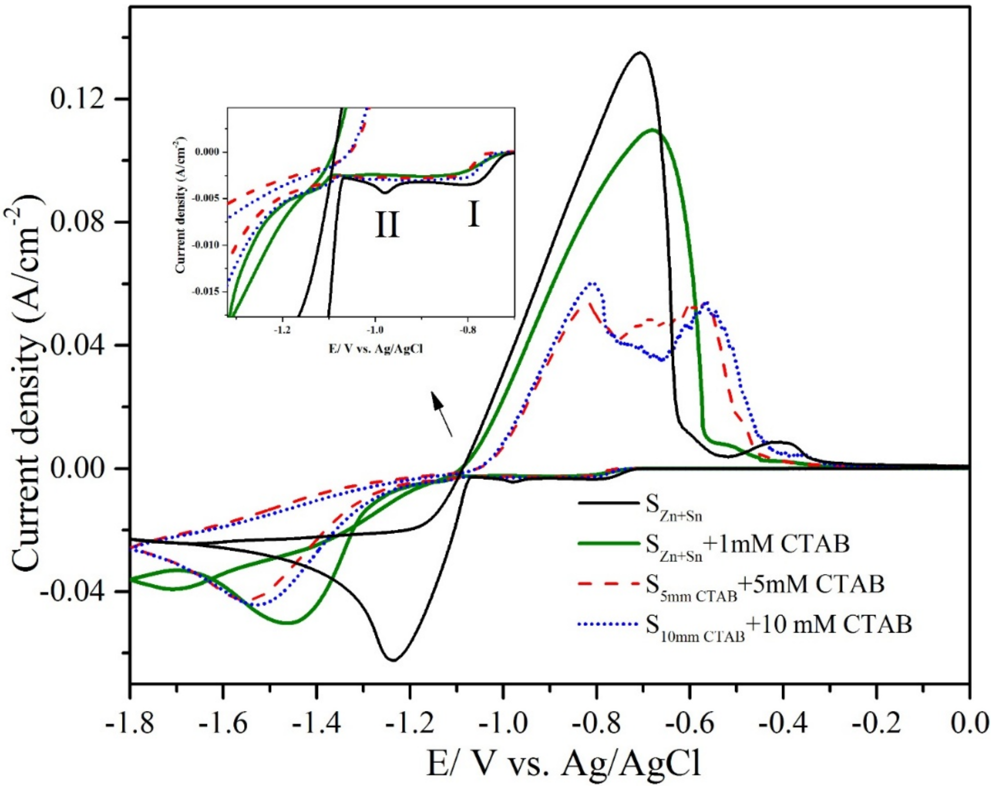

Fig. 6.15 Cyclic voltammetry of the alloy solution (S_{Zn+Sn}) in the absence and presence of 1mM, 5mM and 10 mM CTAB.

6.3.4.2.3.2 Surface morphology

Surface morphology of the alloy bath containing 1 mM (at j= 0.04 and 0.058 A/cm^2), 5 mM and 10 Mm (at j= 0.058 A/cm^2) of CTAB is presented in Fig. 6.16. Surface morphology of each alloy has been presented at two magnifications. Higher magnification of each morphology has a prime attached to the image name. For example, Fig. 6.16 (a) is taken at 10000X magnification and (a′) at 25000 X magnification.

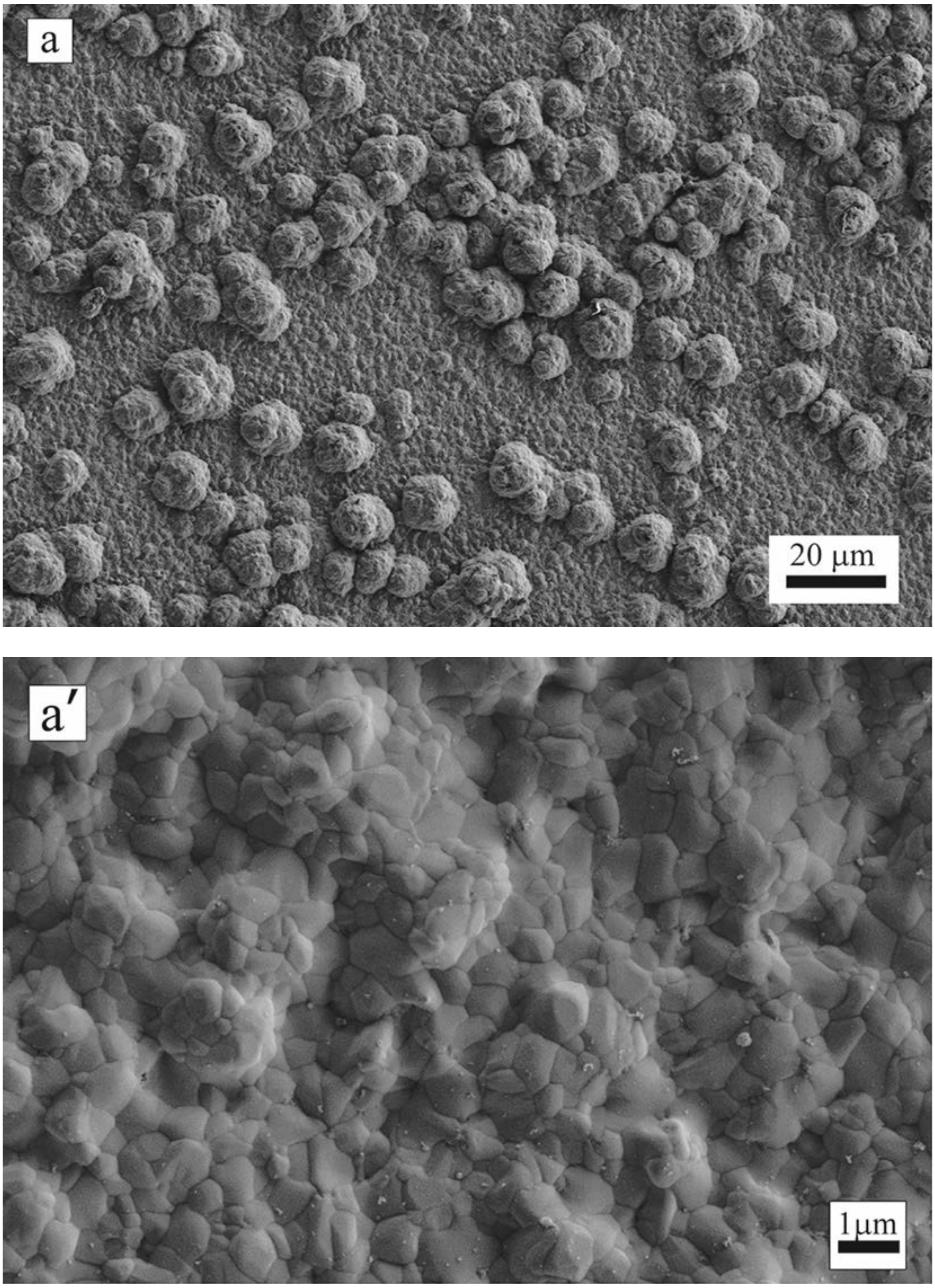

Fig. 6.16 (a) and (a$^{'}$) SEM images showing surface morphology of the alloy deposit on steel substrate in the presence of 1mM CTAB, j = 0.04 A/cm^2, T_{ON} = 5 ms and T_{OFF} = 7 ms.

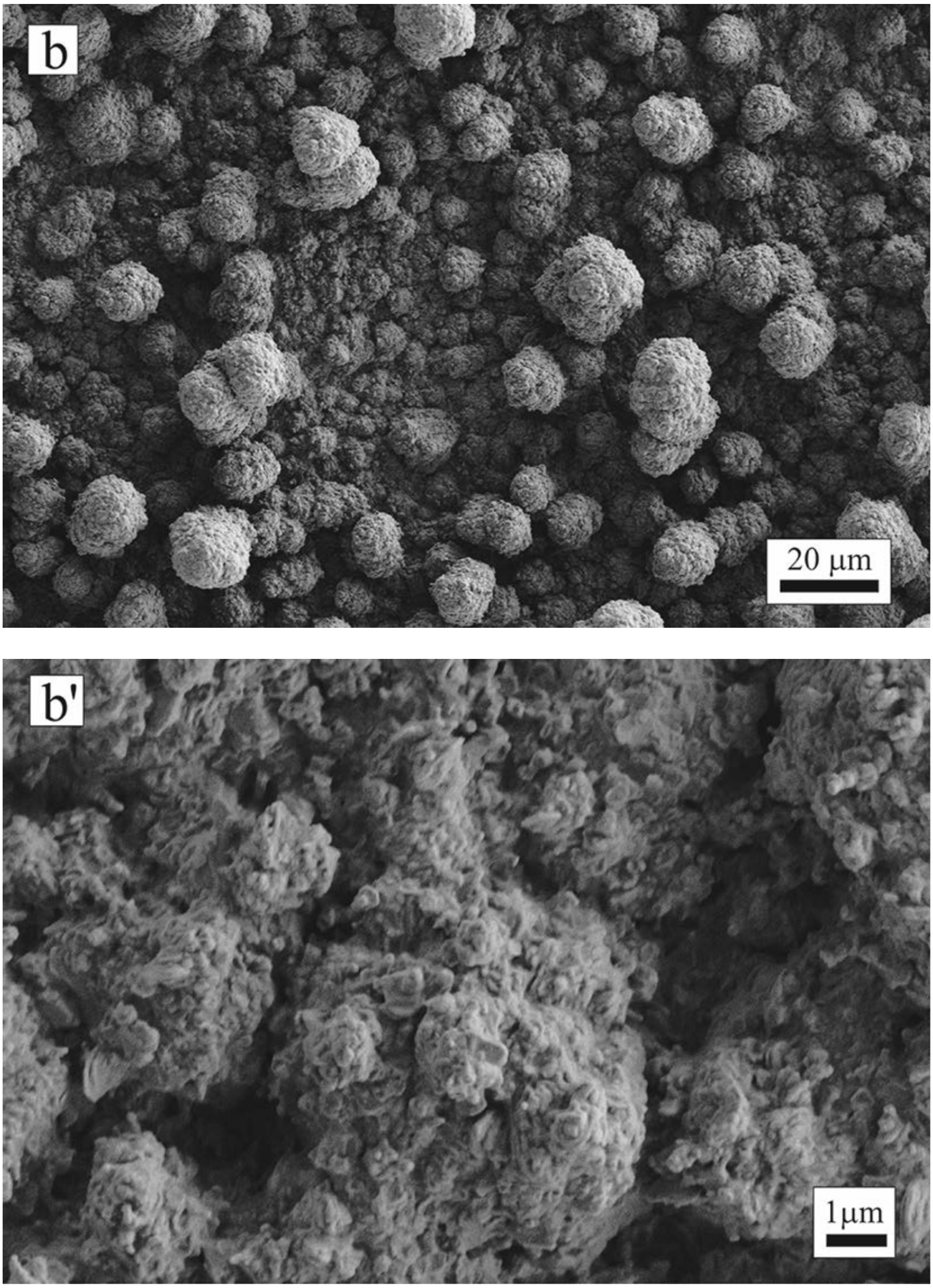

Fig. 6.16 (b) and (b′) SEM images showing surface morphology of the alloy deposit on steel substrate in the presence of 1mM CTAB, j = 0.058 A/cm^2, T_{ON} = 5 ms and T_{OFF} = 7 ms.

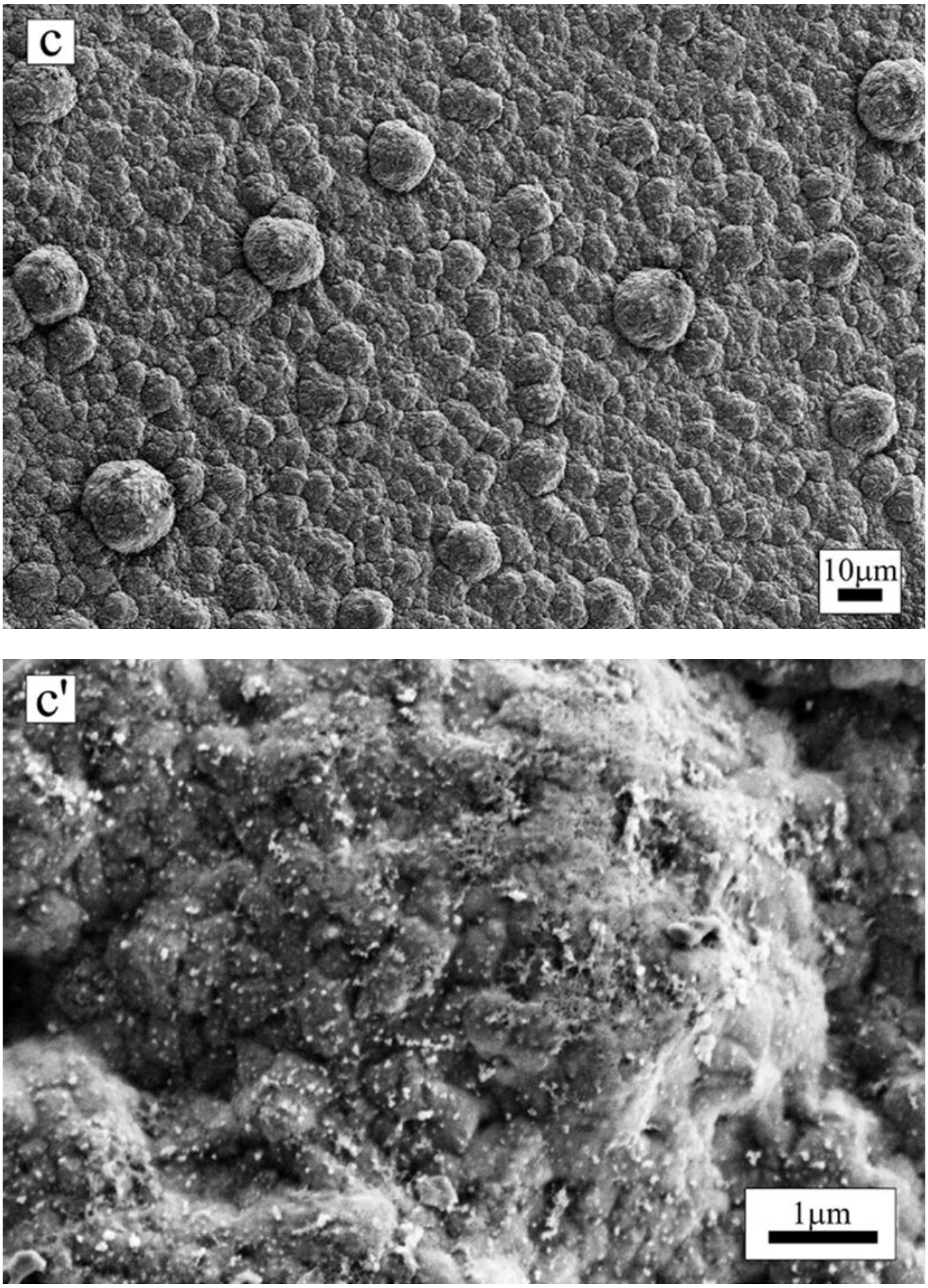

Fig. 6.16 (c) and (c′) SEM images showing surface morphology of the alloy deposit on steel substrate in the presence of 5mM CTAB, $j = 0.04$ A/cm^2, $T_{ON} = 5$ ms, $T_{OFF} = 7$ ms.

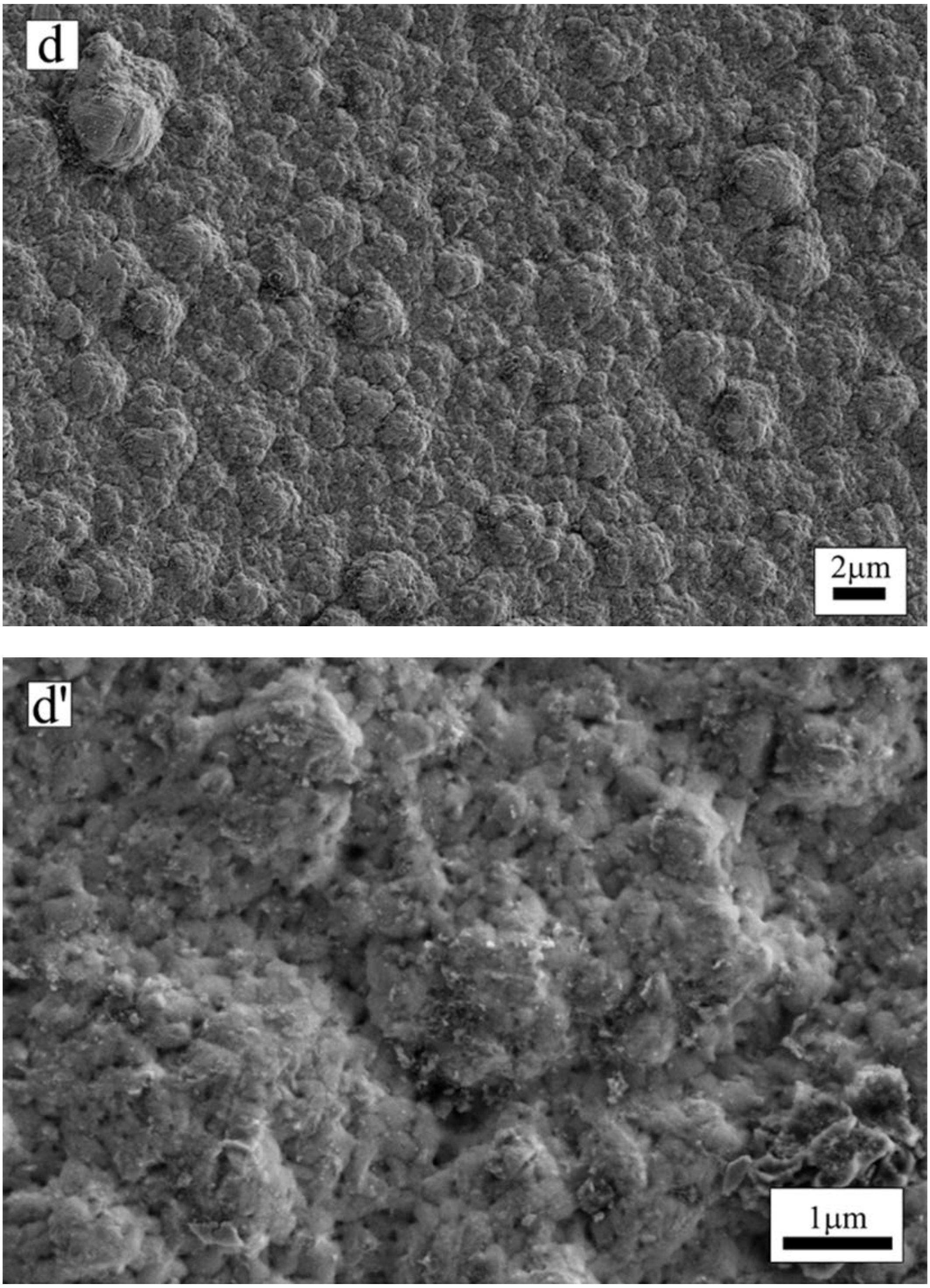

Fig. 6.16 (d) and (d′) SEM images showing surface morphology of the alloy deposit on steel substrate in the presence of 10 mM CTAB (j = 0.04 A/cm^2), T_{ON} = 5 ms, T_{OFF} = 7 ms.

Surface morphology of the deposit in the presence of 1 mM CTAB at j = 0.04 A/cm^2 (Fig. 6.16 (a) and (a′)) was a mixed combination of nodular and granular structure. The nodules also composed of grains with an average grain size of about 374 ± 32 nm. For the same composition increase in the current density from 0.04 A/cm^2 to 0.056 A/cm^2 led to production of a nodular structure (Fig. 6.16 (b) and (b′)). These nodules were irregular in size and had a mossy appearance. With the increase in CTAB concentration to 5mM (Fig. 6.16 (c) and (c′)) and 10 mM (Fig. 6.16 (d) and (d′)) the structure turned to a fully nodular structure. However, surface of the deposits was covered by a layer of mossy deposits.

6.3.4.2.4 Combination of CTAB, thiourea and PEG (400)

A combination of CTAB, thiourea and PEG were applied for the grain refinement. Based on the preliminary result 1mM CTAB was chosen for the rest of the experiments because, at concentration greater than 1 mM (5mM and 10 Mm) a layer of mossy deposit covered the surface of the zinc-tin alloy (see sub-chapter 6.3.4.2.3.2).

Increase in thiourea concentration (see sub-chapter 6.3.4.2.1.2) increased the compactness of the coating, however no specific change in the grain size was observed upon its addition. Therefore, high concentration of thiourea (90 mM and 120 Mm) were selected for the continuation of the study.

PEG (400) (1gr/lit) at low current densities refined the microstructure and produced a compact coating (see sub-chapter 6.3.4.2.2.2).

6.3.4.2.4.1 Cyclic Voltammetry

Cyclic voltammetry of the alloy bath in the absence and presence of additives is presented in Fig. 6.17.

1mM CTAB, 1 gr/li PEG 400 and various concentration of thiourea (90 mM and 120 mM) were used in combination as additives. In the presence of CTAB, PEG and thiourea, tin and zinc deposition potential moved to very negative values. Tin deposition started at -0.72 V in the absence of additives. In the presence of CTAB, PEG and 90 mM thiourea tin deposition started at -0.95 V and at 120 mM thiourea started at -0.98 V.

Also tin deposition from peak I and peak II (see inset A in Fig. 6.17) got close and appeared as shoulders as it is presented in inset B in Fig. 6.17.

Zinc deposition from alloy bath in the presence of additives moved from -1.23 V to -1.46 V and in the presence of 90 mM thiourea and moved to -1.48 V in the presence of 120 mM thiourea. Blocking effects of the additives increased by the synergic effects and moved the deposition potential to more negative values.

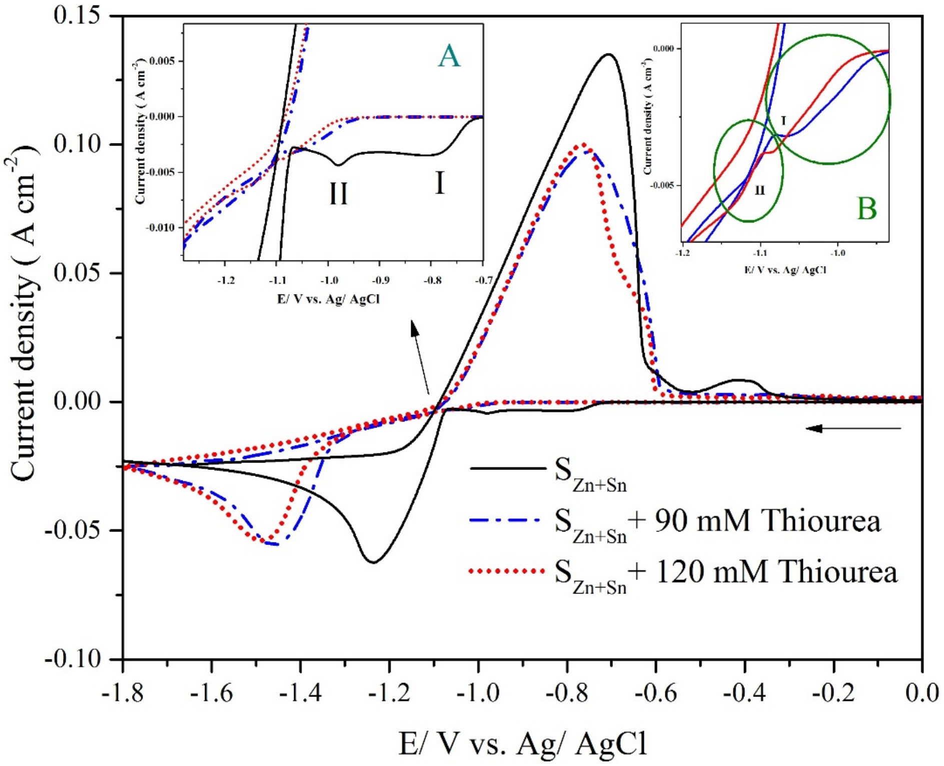

Fig. 6.17 Cyclic voltammetry of the alloy solution (S_{Zn+Sn}) in the absence of additives and in the presence of 1 mM CTAB, 1 gr/ lit PEG 400 at various concentration of thiourea (90 mM and 120 mM).

6.3.4.2.4.2 Surface Morphology

Surface morphology of the alloy bath in the presence of CTAB, PEG and thiourea is presented in Fig. 6.18. At 90 mM of thiourea surface of the deposit composed of nodules with average size of 4 µm. These nodules composed of grain with an average size of 209 ± 23 nm. Increase in thiourea concentration to 120 mM decreased the nodule size to less than 2 µm and average grain size of 131 ± 14 nm. Increase in thiourea concentration decreased the grain size, however further reduction of grain size was not possible due the production of burnt deposits at high concentration of thiourea.

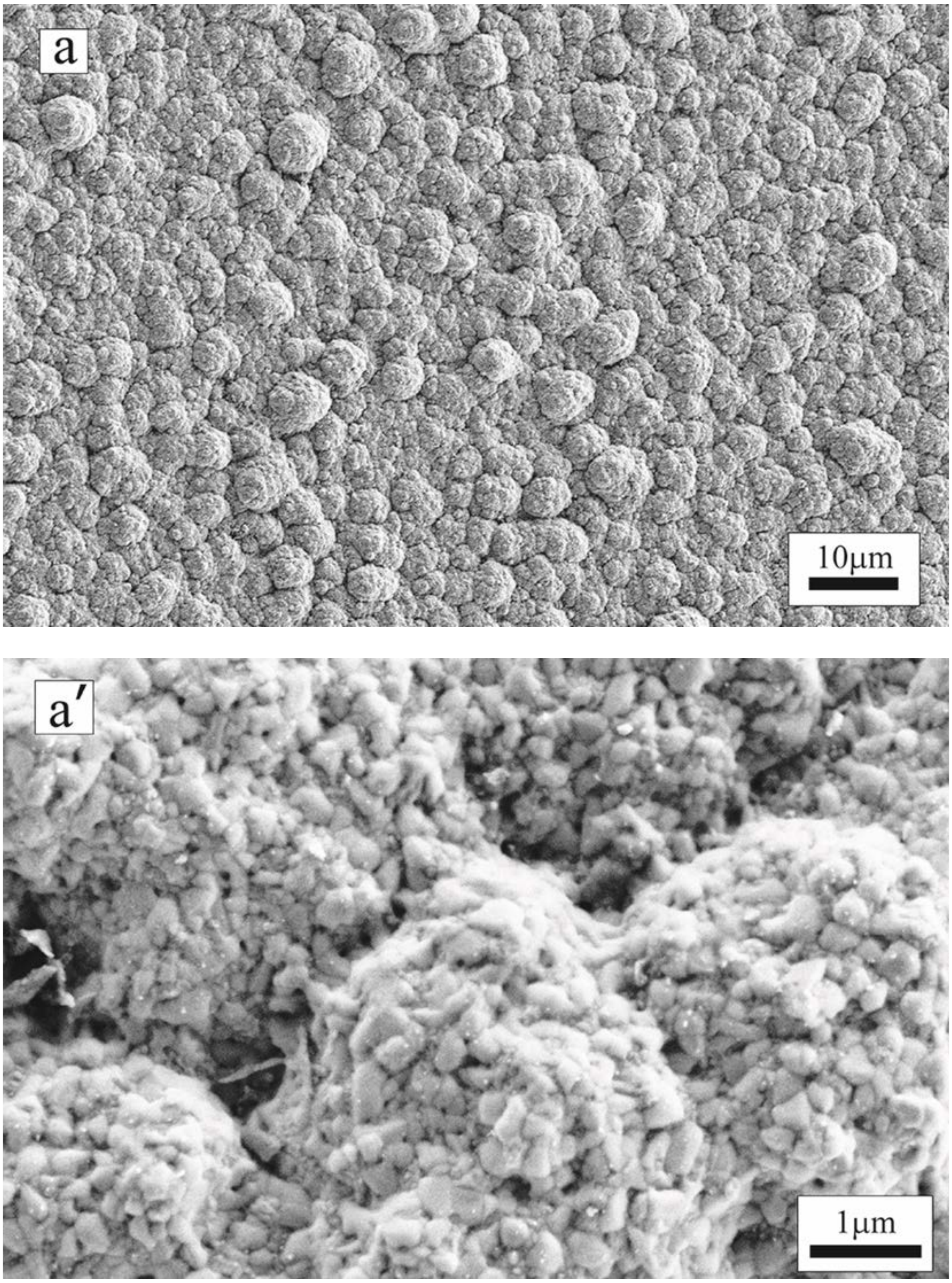

Fig. 6.18 (a) and (a$'$) 1mM CTAB + 1gr/lit PEG 400 + 90 mM thiourea. T_{ON} = 5 ms, T_{OFF} = 7 ms and j = 0.048 A/cm^2 (various magnifications).

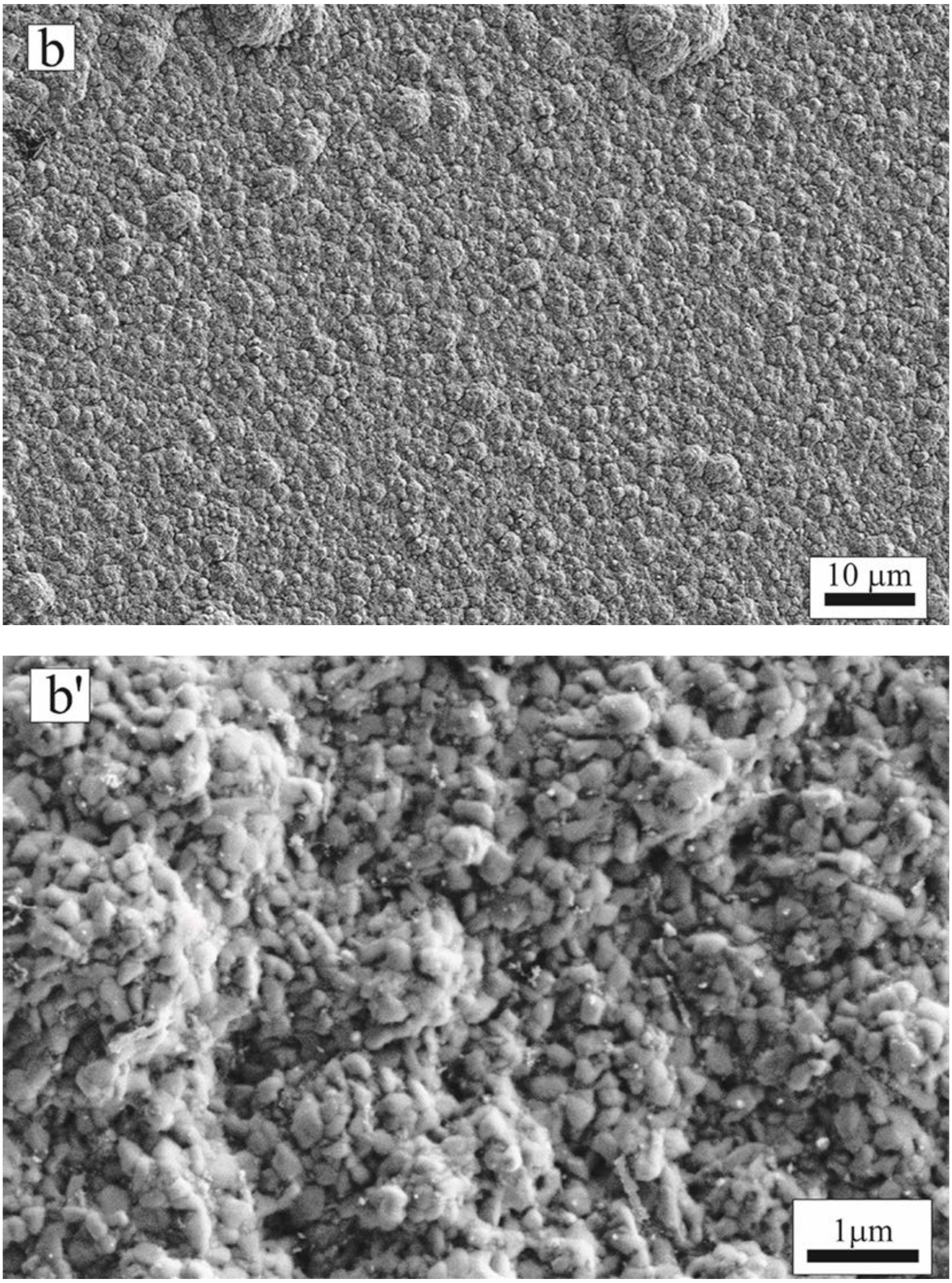

Fig. 6.18 (b) and (b′) SEM images (various magnifications) showing surface morphology of the alloy deposit on steel substrate in the presence of 1mM CTAB + 1gr/lit PEG 400 + 120 mM thiourea. $T_{ON} = 5$ ms, $T_{OFF} = 7$ ms and $j = 0.048$ A/cm^2.

6.3.4.2.5 Combination of CTAB and PEG (400)

Effects of various concentration of PEG 400 (1, 2 and 4 gr/lit) and CTAB 1mM on the cyclic voltammetry of the alloy bath is presented in Fig. 6.19.

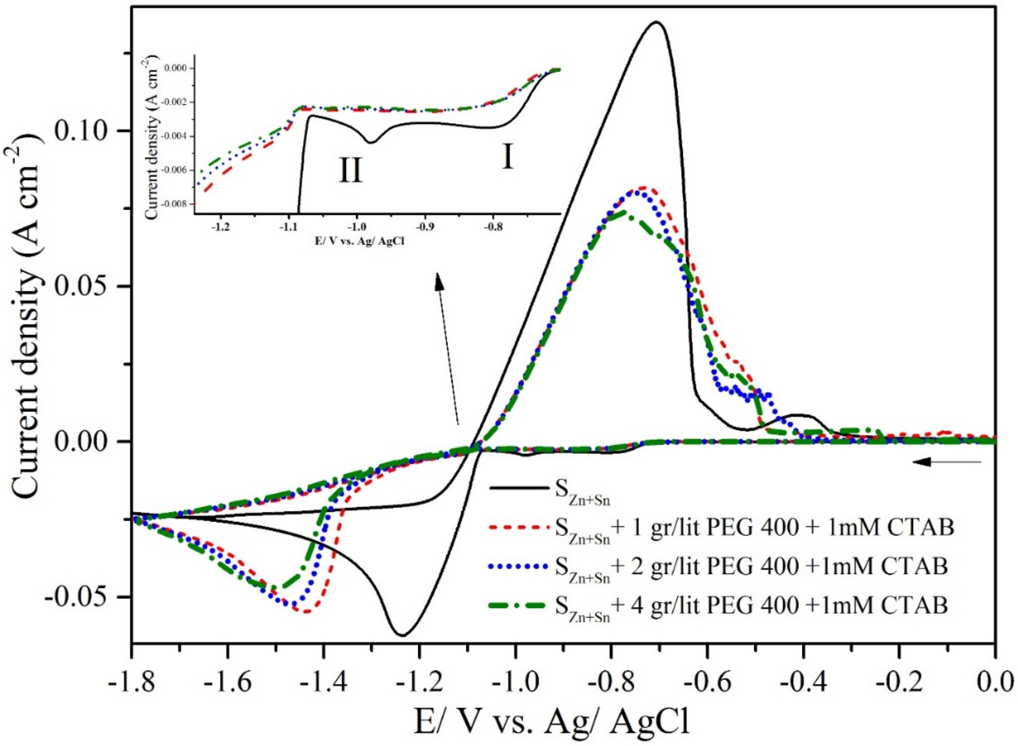

Fig. 6.19 Cyclic voltammetry of the alloy bath in the absence and presence of 1mM CTAB at various concentrations of PEG 400 (1, 2 and 4 gr/lit).

In the presence of PEG 400 and CTAB, tin reduction moved to negative values, and deposition of tin from gluconate complex appeared as a shoulder at the range of -1.08 V to -1.141 V (inset of Fig. 6.19). Increase in PEG 400 concentration imposed very negligible change to deposition potential of tin. While zinc deposition potential moved to more negative values sequentially with the increase of PEG 400 concentration.

As discussed previously (sub-chapter 6.3.4.2.3) CTAB is a cationic surfactant and is used as an inhibitor or catalyst in electroplating [222, 223]. PEG is a non-ionic surfactant which can absorb on the surface by lone pair of electrons from oxygen atoms [226]. These inhibitors decrease the charge transfer rate either by hindering or by prolonging the access of metallic ions or adions to the growing sites. They could also limit surface diffusion of adions. At any of these cases their inhibitive effect lead to the increase in deposition overvoltage and decrease in current efficiency.

It has been reported [227] that adsorption of PEG in the presence of Cl^- occurs through a layer of spherically packed molecules and Br^- ions from CTAB encourage adsorption of PEG [20]. In this study Cl^- anions were introduced in the bath by HCl (see sub-chapter 6.1) and CTAB excited at its critical micelle concentration. This provides a proper condition for absorption of PEG to the surface of glassy carbon electron.

Current efficiencies of the electrolytes were calculated from the ratios of total anodic to cathodic charges of cyclic voltammograms and results are presented in Fig. 6.20.

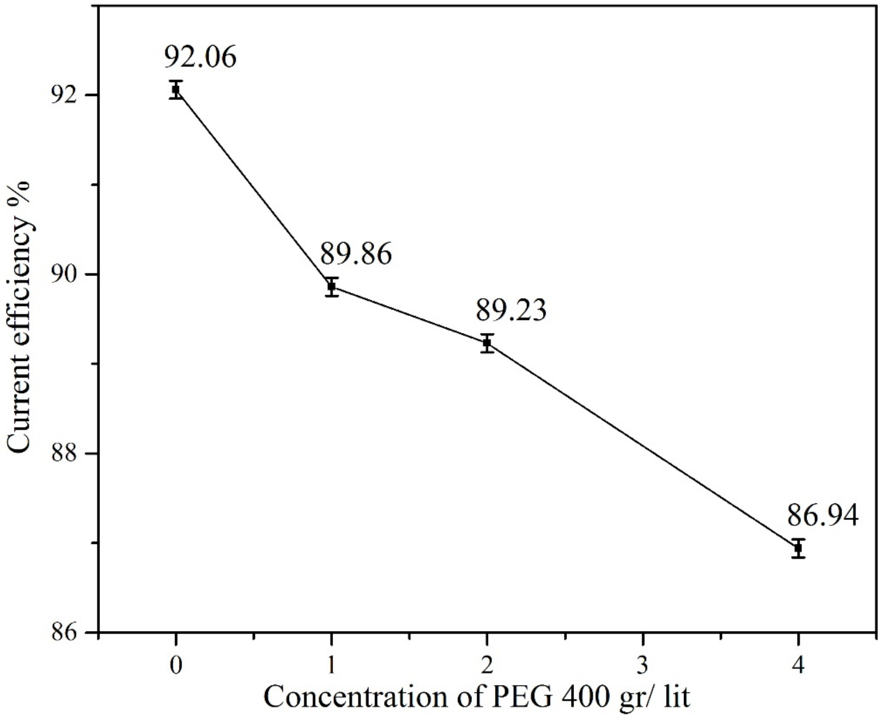

Fig. 6.20 Current efficiency of the alloy bath in the absence and presence of 1 mM CTAB at various concentrations of PEG 400 (1, 2 and 4 gr/lit).

Current efficiency of the main bath decreased with the addition of additives. The increase in PEG 400 concentration to its largest amount in this study (4gr/lit) reduced its current efficiency by 5.57%. Based on the electrochemical response of the base solution in the absence of any metallic ions or additives, hydrogen evolution started at around -1.8 V on glassy carbon electrode (Fig. 6.7 (b)). On the other hand, alloy deposition from

PEG 400 containing electrolytes occurred at potentials more positive than -1.8 (Fig 6.19). Therefore, the decline in current efficiency from the bath containing PEG 400 was only due to the blocking effects of the additive which suppressed the alloy deposition.

6.3.4.2.5.2 Surface morphology

Surface morphology of the Zn-Sn alloy deposits in the presence of CTAB and various concentrations of PEG 400 is presented in Fig. 6.21.

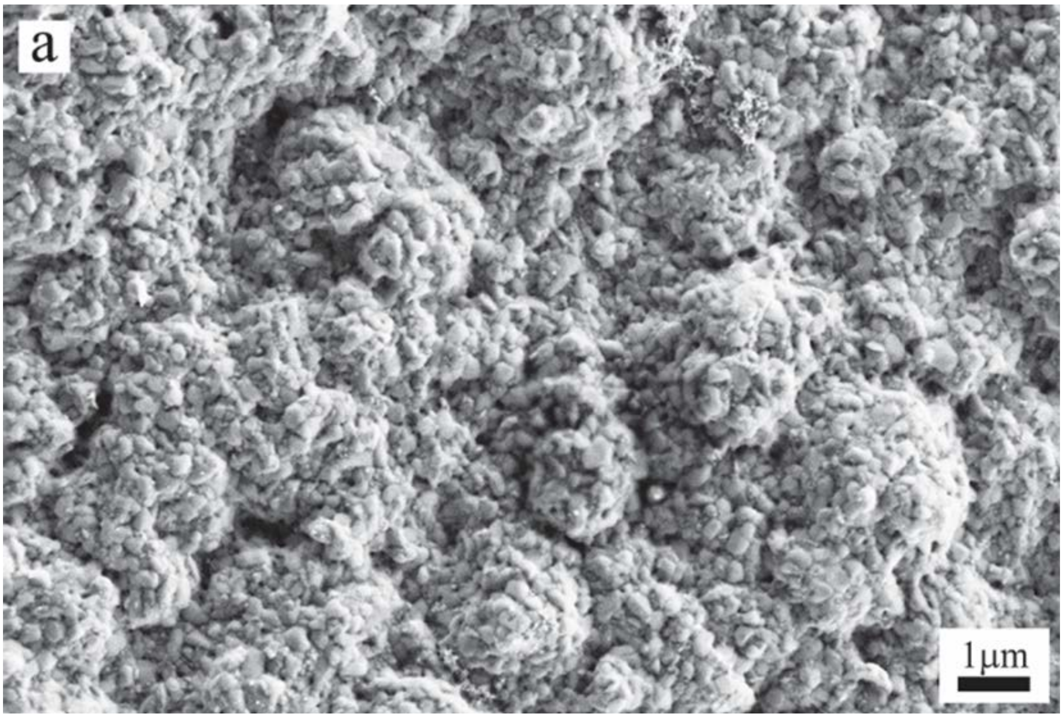

Fig. 6.21 (a) 1 gr/l PEG 400 and 1mM CTAB (T_{ON} = 5 ms, T_{OFF} = 7 ms and j = 0.047 A/cm^2)

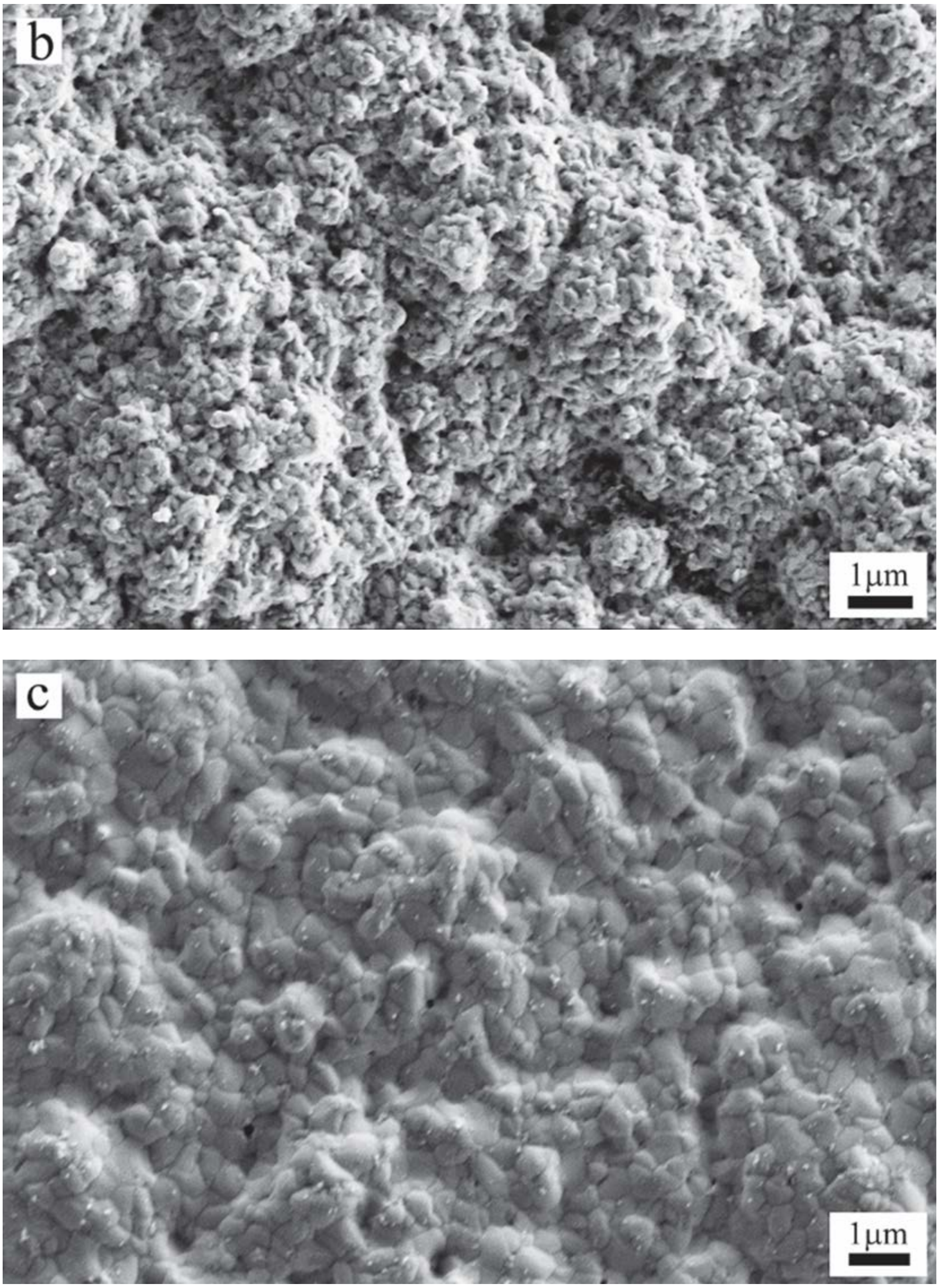

Fig. 6.21 (b) and (c) SEM micrographs of the surface morphology of the Zn-Sn alloy deposits prepared at (T_{ON} = 5 ms, T_{OFF} = 7 ms and j = 0.047 A/cm^2) at different concentration of PEG 400 (b) 2 gr/lit and (c) 4 gr/lit all the solutions contained 1mM CTAB.

Surface morphology of the Zn-Sn alloy deposit from solution with only 1 gr/lit PEG 400 consisted of grains with average size of less than 250 nm. Increase in PEG 400 concentration to 2 gr/lit did not vary the grain size and surface morphology significantly. However, grain size increased considerably with inclusion of 4 gr/lit of PEG 400 to the plating bath (Fig. 6.21 (c)).

It was observed that surface morphology of the deposits changed from a small grain size to large grain size with increase in PEG concentration. Surface morphology and structure of deposit depends on many factors such as applied current density, temperature, metal ion concentration, electrolyte convection and additives. Inclusion of organic additives into the plating bath is the most common method to control plating process and enhance quality of the coating. In the presence of additive nucleation and growth does not occur on natural centres such as the grain boundaries or defects as it occurs in the absence of additives. In this case the electrocrystallization process could be controlled. Interface inhibitors block the growth site mostly kink, and encourage frequency of nucleation and lead to grain refinement [228]. On the other hand, under very strong blocking effects active sites would be blocked and the number of formed nuclei would decrease which consequently lead to the production of coarse structure [129].

6.3.4.2.5.3 XRD and EDS analysis

Zinc and tin exhibit very small mutual solubility based on their phase diagram [101]. Therefore, Zn-Sn is considered as a mechanical type of alloy in which zinc and tin do not show a solid-solution or an intermetallic compound. The X-ray diffraction patterns of the deposits from all electrolytes revealed a mixture of hexagonal zinc and tetragonal β-Sn phases (Fig. 6.22).

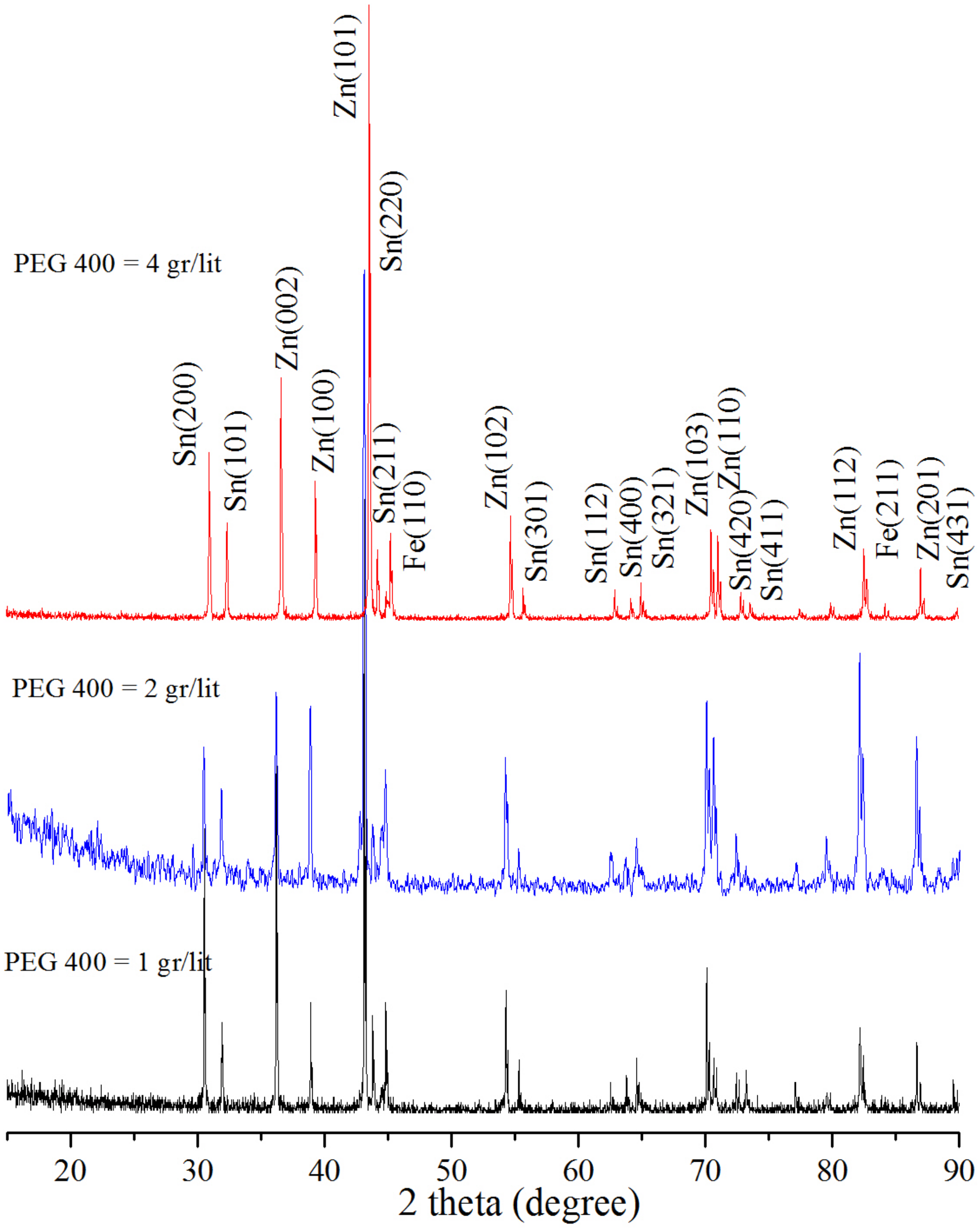

Fig. 6.22 XRD pattern of the alloy deposit in presence of 1 mM CTAB at various concentration of PEG 400.

Composition of the deposits revealed by EDS are presented in Table. 6.4. All of the deposits exhibited a combination of zinc with less than 31 wt. % of tin. Peaks of oxygen and iron were also observed in the EDS spectra of some of the samples. Oxygen may result from the oxidation of deposit due to the exposure to the environment and iron represented the steel substrates.

Table 6.4 Composition of electrodeposited coatings

Solution	Zn Wt%	Sn Wt%	Fe Wt%	Others
$S_1(400) = S_{Zn+Sn}$ + 1 mM CTAB + 1 gr/lit PEG 400	75.25 ± 0.33	23.49 ± 0.49	1.27 ± 0.4	NA
$S_2(400) = S_{Zn+Sn}$ + 1 mM CTAB + 2 gr/lit PEG 400	75.01 ± 0.97	23.97 ± 0.9	1.03 ± 0.07	NA
$S_4(400) = S_{Zn+Sn}$ + 1 mM CTAB + 4 gr/lit PEG 400	73.38 ± 1.08	24.53 ± 1.19	1.15 ± 0.12	≤0.94

6.3.4.2.6 Combination of CTAB and various concentration of PEG 2050

6.3.4.2.6.1 Cyclic voltammetry

Effects of various concentration of PEG 2050 (1, 2 and 4 gr/lit) and CTAB 1mM on the cyclic voltammetry of the alloy bath is presented in Fig. 6.23.

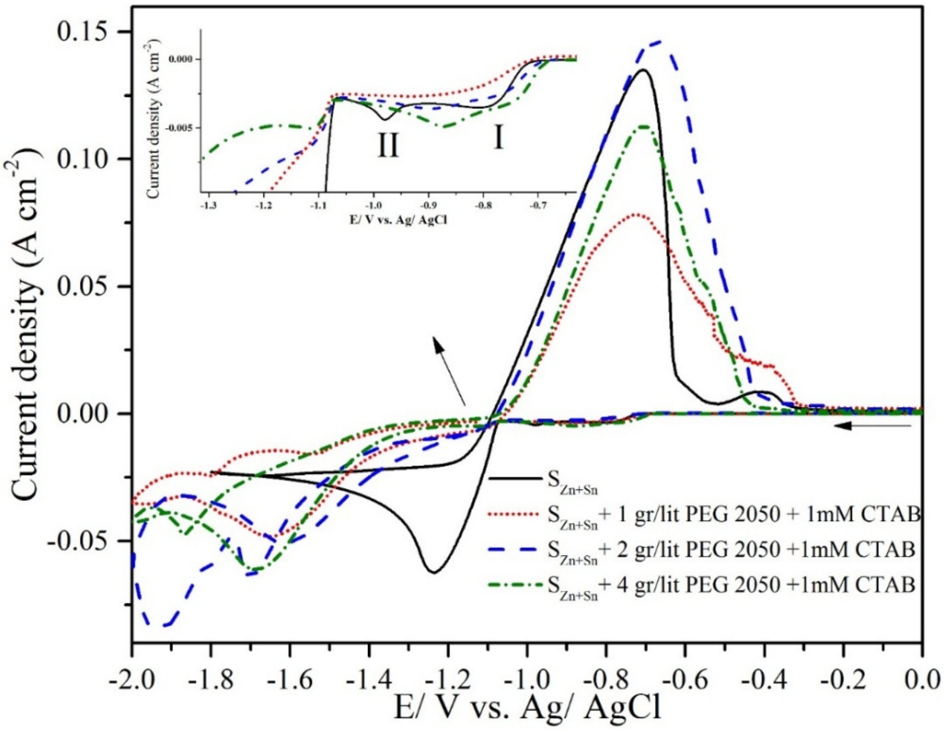

Fig. 6.23 Cyclic voltammetry of the alloy bath in the absence and presence of 1mM CTAB at various concentrations of PEG 2050 (1, 2 and 4 gr/lit).

Tin reduction moved to negative values in the presence of PEG 2050 and reduction from gluconate complex occurred as a sharp shoulder at -1.1 V to -1.2 V.

Absorption of PEG to the surface of electrode occurs through its oxygen atoms. Increase in molecular weight of PEG leads to the increase in number of oxygen atoms and consequently increase in absorption phenomena. Therefore, deposition of zinc is shifted to more negative values in the presence of PEG 2050 than PEG 400.

Two cathodic peaks observed at the anodic sweep of cyclic voltammetry in the presence of 1gr/lit PEG 2050 at -1.7 V and -1.9 V, respectively. These peaks show desorption of additive and deposition of zinc on the vacated site which was previously blocked by additives and implies that adsorption and desorption of additives was potential dependent process [131]. In contrary, no cathodic peak was observed at the anodic sweep at high concentration of PEG 2050. This indicated that high concentration of PEG 2050 could provide a stronger absorbed layer on the surface of glassy carbon electrode which its detachment requires more activation energy.

Current efficiency of the alloy bath with the inclusion of CTAB and PEG 2050 is presented in Fig. 6.24.

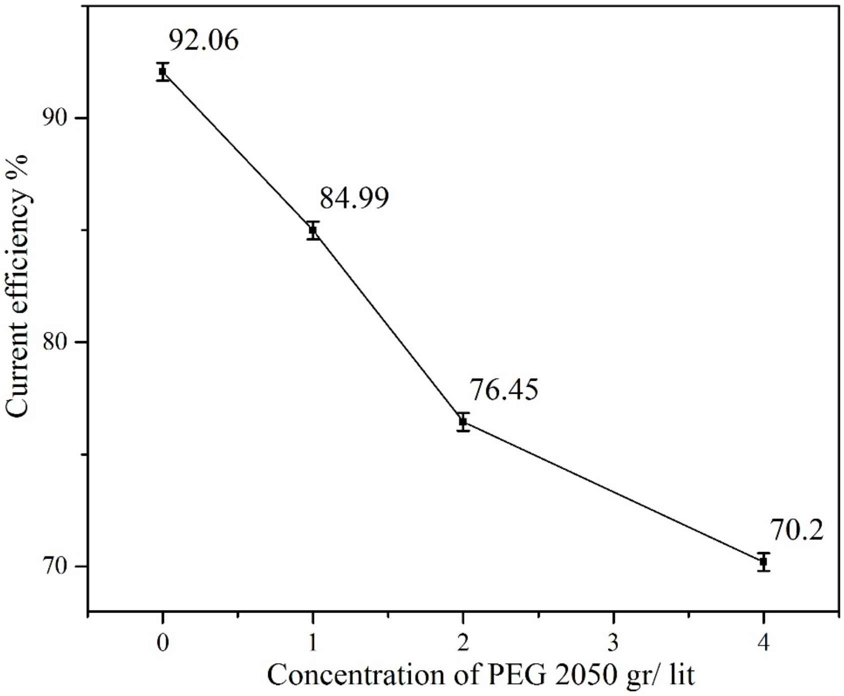

Fig. 6.24 Current efficiency of the alloy bath in the absence and presence of 1 mM CTAB at various concentrations of PEG 2050 (1, 2 and 4 gr/lit).

Current efficiency of the main bath decreased with the addition of additives. The increase in PEG 2050 concentration to its largest amount in this study (4gr/lit) reduced its current efficiency by 23.74%. Based on the electrochemical response of the base solution in the absence of any metallic ions or additives, hydrogen evolution started at around -1.8 V on glassy carbon electrode (Fig. 6.6 (b)). In the presence of PEG 2050 zinc deposition occurred simultaneously at potential more negative than -1.8. Therefore, apart from the stronger inhibitive effects of PEG 2050 than PEG 400, effects of hydrogen reduction led to the decrease of current efficiently rigorously.

6.3.4.2.6.2 Surface morphology

Surface morphology of the deposits in the presence of CTAB and various concentration of PEG 2050 is presented in Fig. 6.25. Deposition from the alloy solution containing 1gr/lit PEG 2050 and 1 mM CTAB produced compact nanocrystalline zinc-tin coating with average grain size less than 100 nm. It has been reported [228] that high concentration of additives lead to production of a deposit with an unoriented dispersion texture. In such a structure grains were extremely fine and structural element of the deposits were polygonal particle arising from three dimensional nucleation. Surface morphology of the deposit from this bath apparently resembled an unoriented dispersion deposit. Increase in PEG concentration to 2 gr/lit led to an slight increase in grain size and coating with average grain size of about 150 nm produced. Upon further addition of PEG 2050 to 4 gr/lit grain size increased significantly to 262 ± 51 nm.

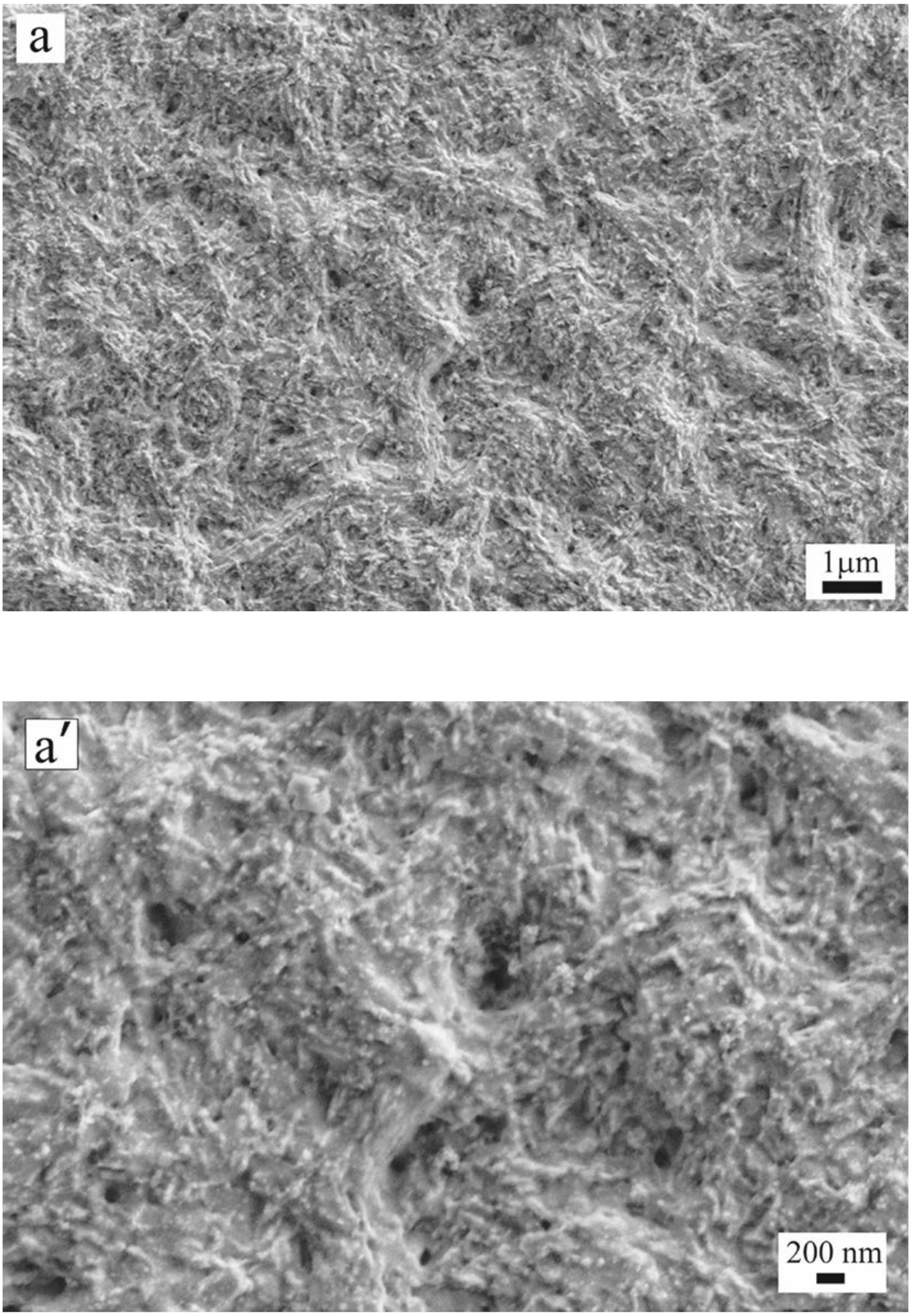

Fig. 6.25 (a) and (a′) 1 gr/lit PEG 2050 and 1mM CTAB

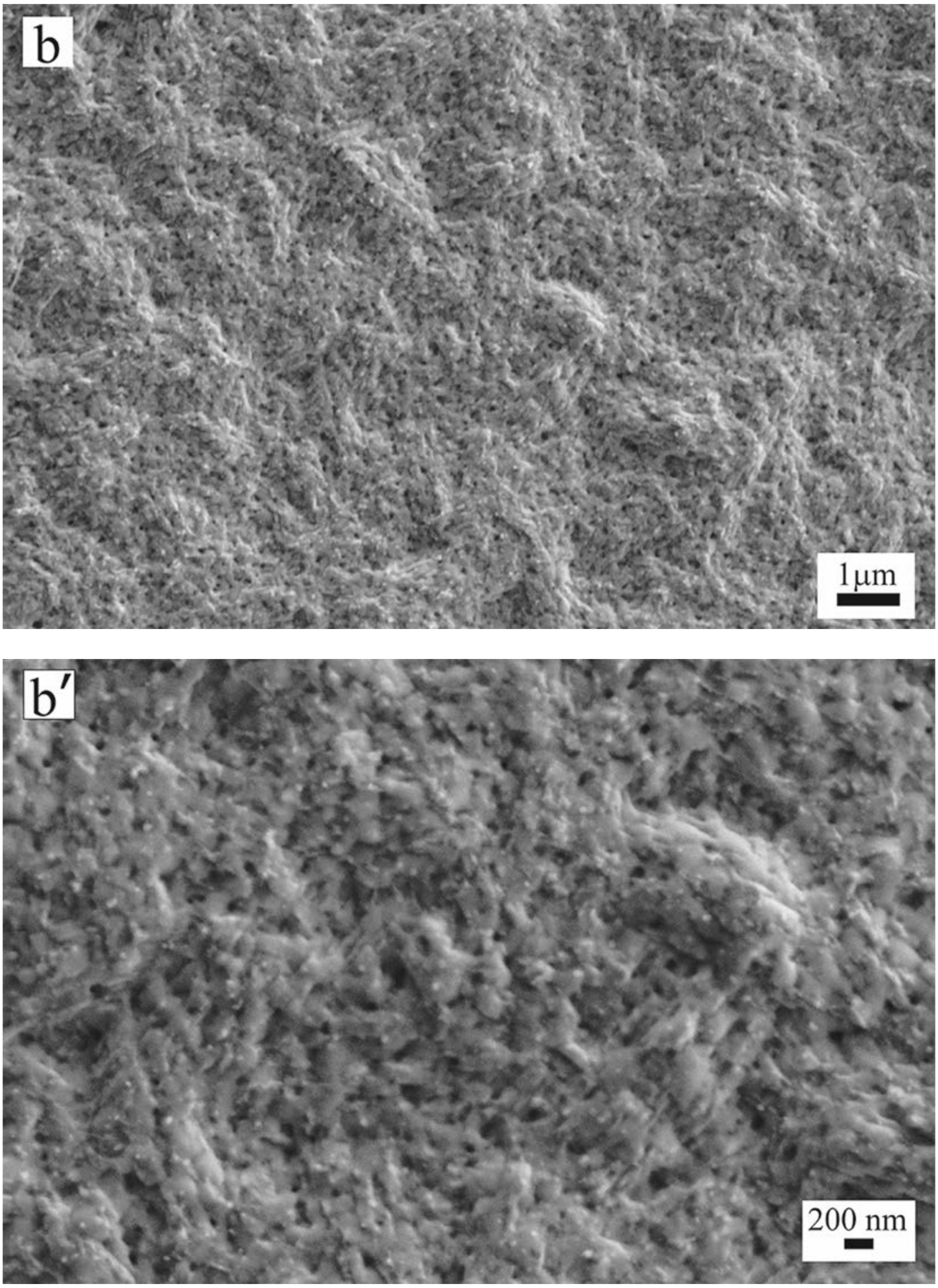

Fig. 6.25 (b) and (b′) 2 gr/lit PEG 2050 and 1mM CTAB

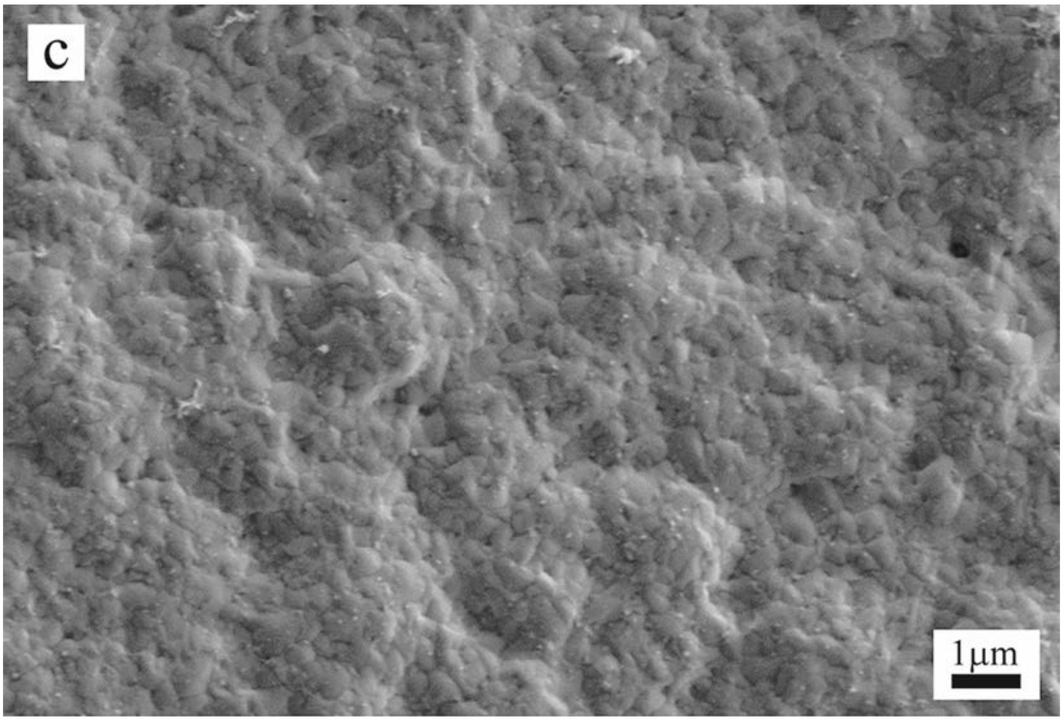

Fig. 6.25 (c) SEM micrographs of the surface morphology of the Zn-Sn alloy deposits containing 4 gr/lit PEG 2050 and 1mM CTAB prepared at T_{ON} = 5 ms, T_{OFF} = 7 ms and j = 0.047 A/cm^2.

Comparison of the surface morphology of the deposits from electrolytes of PEG 2050 with that of PEG 400 (see Fig. 6.21) shows that a more uniform and refined structure is gained with the increase in PEG molecular weight. Blocking effects and surface coverage increases with the increase in molecular weight of PEG. Therefore, the distance between blocking centre decreased and as the blocking centres got closer, the critical length of nuclei, which nucleated between them decreased [228] and finally led to the production of smaller grains in the presence of PEG 2050.

On the other hand the density of surface porosities which have mostly composed due to hydrogen evolution decreased in the presence of high concentration of PEG 400 and PEG 2050. One of the aspects of adding a surfactant to the plating electrolyte was to reduce the surface energy of the electrode and aid with the detachment of the hydrogen bubbles from the surface. The strong absorbed layer produced in the presence of high concentration of PEG 2050 and PEG 400 encourage the recombination of H atoms and release of H_2 and decrease the absorption of H_{ads} to the surface of electrode as it was reported [102] for deposition of zinc in the presence of PEG 6000 .

6.3.4.2.6.3 XRD and EDS evaluation

The X-ray diffraction patterns of the deposits from all electrolytes, which revealed a mixture of hexagonal zinc and tetragonal β-Sn phases is prersented in Fig. 6.26 .

Composition of the deposits revealed by EDS are presented in Table. 6.5. All of the deposits exhibited a combination of zinc with less than 31 wt. % of tin. Peaks of oxygen and iron were also observed in the EDS spectra of some of the samples. Oxygen may result from the oxidation of deposit due to the exposure to the environment and iron peaks represented the steel substrates.

Table 6.5 Composition of electrodeposited coatings.

Solution	Zn wt.%	Sn wt%	Fe wt.%	O and N wt.%
S_1(2050) = S_{Zn+Sn} + 1 mM CTAB + 1 gr/lit PEG 2050	72.87± 0.37	23.07 ± 0.48	0.71 ± 0.09	3.47± 0.22
S_2(2050) = S_{Zn+Sn} + 1 mM CTAB + 2 gr/lit PEG 2050	70.03 ± 0.42	22.17 ± 0.38	0.85 ± 0.33	7.95± 0.27
S_4(2050) = S_{Zn+Sn} + 1 mM CTAB + 4 gr/lit PEG 2050	79.77 ± 0.85	30.33 ± 0.85	NA	NA

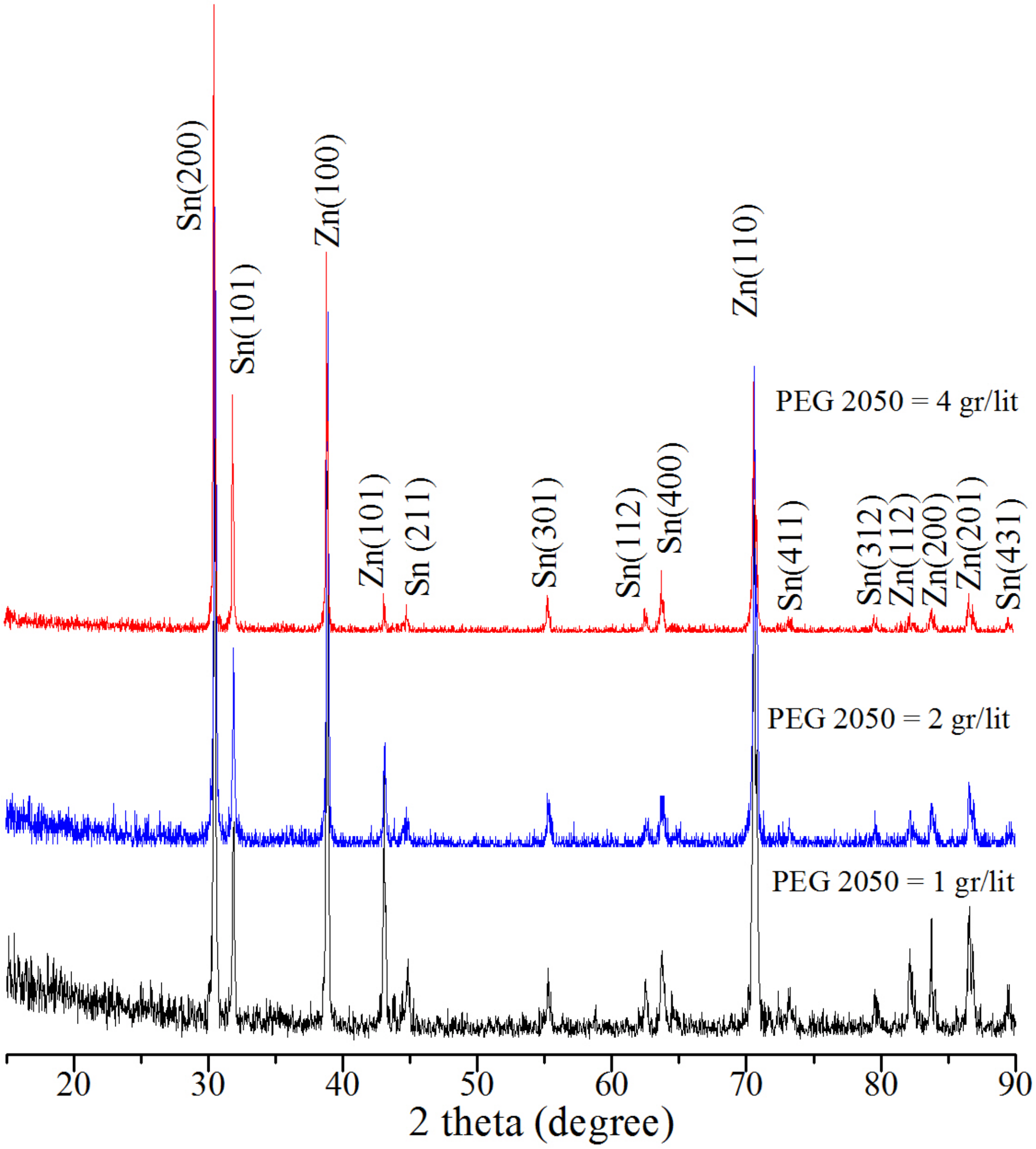

Fig. 6.26 XRD patterns of the alloy deposit in presence of 1mM CTAB at various concentration of PEG 2050.

6.4 Summary

Electrodeposition of zinc-low content tin alloy from sulfate-gluconate electrolytes with additives was investigated. Analysis of distribution of tin (II) species in the absence of gluconate showed that $SnCl_2$ and $Sn(OH)_2$ are the predominant species at the pH range of this study (4.3-4.7). In the presence of gluconate, $Sn(GH)_4^+$ was the main species in the alloy electrolyte. Distribution of zinc (II) species in the absence of gluconate showed that $ZnSO_4$ was the predominant species at the pH range of this study (4.3-4.7). In the presence of gluconate $ZnSO_4$ was the main species in the alloy electrolyte.

Cyclic voltammetry of the single metal bath of zinc and tin in the absence and presence of gluconate showed that gluconate moved the deposition potential of tin to more negative values and deposition potential of zinc to more positive values and thereby facilitate deposition of the zinc-tin alloy.

Effects of various current on-time and current off-time on the surface morphology and composition of the deposit was investigated and T_{ON} = 5 ms and To_{FF} = 7 ms was chosen for the deposition of alloy in the presence of additives.

Cyclic voltammetry of the alloy bath in the presence of additives such as thiourea, PEG and CTAB showed that adsorption of additive to the surface of electrode shifts the deposition potential to more negative values due to the blocking of the surface of glassy carbon electrode. Inhibitive effects of the additives increased with either the increase in their concentration or due to their synergic effects in the case of their combination.

Comparison of the cyclic voltammetry of the alloy bath containing CTAB and various concentration of PEG (400) with PEG (2050) suggested that inhibitive effects of CTAB and PEG on alloy deposition increase with increasing molecular weight of PEG and/or its concentration. Surface morphology of deposits exhibited a fine and more uniform structure in the presence of PEG 2050 than PEG 400. Nanocrystalline Zn-Sn alloy coating was produced from the bath containing 1 mM of CTAB and 1gr/lit PEG 2050. X-ray diffraction pattern showed peaks of hexagonal zinc and tetragonal tin and confirmed production of a mechanical type of zinc-tin alloy.

Chapter 7

Mechanical properties of nanocrystalline and ultra-fine-grained Zn-Sn coatings

7.1. Introduction

Mechanical properties of materials are affected by grain size. Most of the mechanical properties are enhanced with grain refinement, especially when the grains are at nano range (see sub-chapter 2.7.2). In order to evaluate the effects of grain size on the mechanical properties of the coatings, two types of coatings with ultra-fine grain (UFG) size and nanocrystalline (NC) grain size were selected and compared to evaluate the critical effect of grain refinement down to nano size level. The nanocrystalline zinc-tin coating (S_1 (2050) (see Table 6.5), presented in sub-chapter 6.3.4.2.6) with the average grain size of 79.99 ± 18.7 nm is presented and compared with the ultra-fine-grained zinc-tin coating (S_4 (400) (see Table 6.4), presented in sub-chapter 6.3.4.2.5) with the average grain size of 423.35 ± 46.88 nm. Initially the characteristics of each coating such as surface morphology, grain size and chemical composition are discussed. In the next stage surface profile and mechanical properties of both coatings are presented and discussed in terms of the effects of grain size. From this chapter onwards, S_1(2050) coatings will be referred to as nanocrystalline coating (NC), and S_4 (400) as ultra-fine-grained coatings (UFG).

7.2 Nanocrystalline coating characterization

7.2.1 Microstructure and grain size

Nanocrystalline zinc-tin coatings (S_1(2050)) were produced under pulse-current deposition (T_{ON}= 5 ms, T_{OFF}= 7 ms, j= 0.047 A/cm^2 and deposition time = 1200 seconds) from the alloy solution (see Table 6.1) containing 1gr/lit PEG 2050 and 1mM CTAB (see sub-chapter 6.3.4.2.6). The surface morphology, cross section and EDS spectrum of this alloy are shown respectively in Fig. 7.1 (a), (b) and (c). More images of the surface morphology of this deposit were presented in the Chapter 6 in Fig. 6.25 (a) and (a′). The nanocrystalline zinc-low content tin alloy described in sub-chapter 6.3.4.2.6.3 is composed of a mixture of hexagonal zinc and tetragonal β-Sn phases. The average zinc and tin content of this alloy is 72.87± 0.37 wt.% and 23.07± 0.48 wt. % respectively (Table 6.5).

It has to be noted that cross section image in Fig. 7.1 (b) is not provided by cutting and polishing. Small region on the surface of steel substrate was covered with epoxy before electrodeposition and after deposition the epoxy was dissolved in acetone. This process provided the access to the cross section of coating without cutting and polishing.

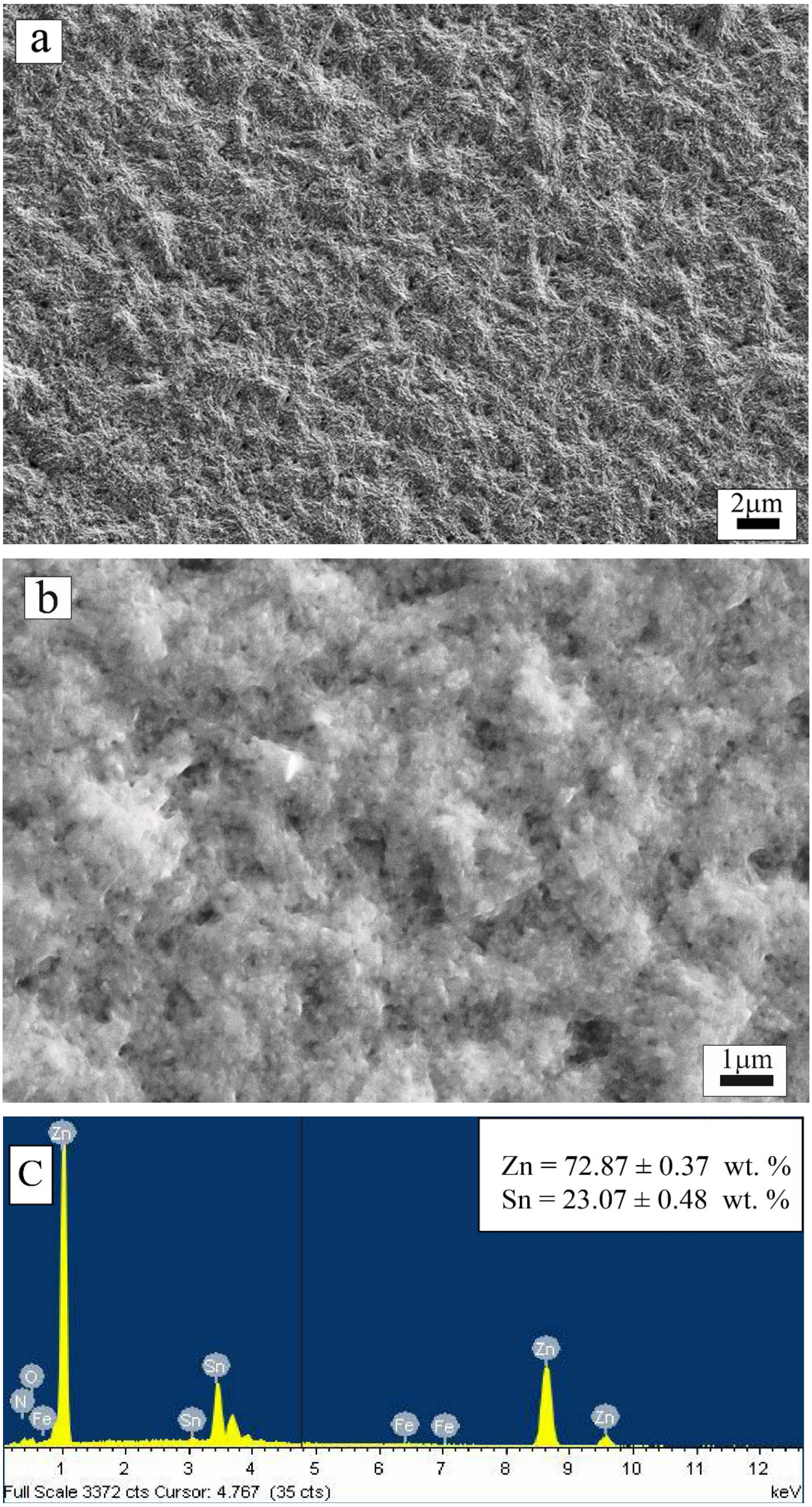

Fig. 7.1 Characteristics of nanocrystalline zinc-tin coating (a) SEM image of the surface morphology, (b) SEM image of the cross-section and (c) EDS spectrum.

The average grain size of the deposit was measured using image J software from the cross section image of the deposit. Fig. 7.2 illustrates the distribution of the grain size and shows that majority of grains are smaller than 100 nm in size which indicates the nanocrystalline structure of the deposit.

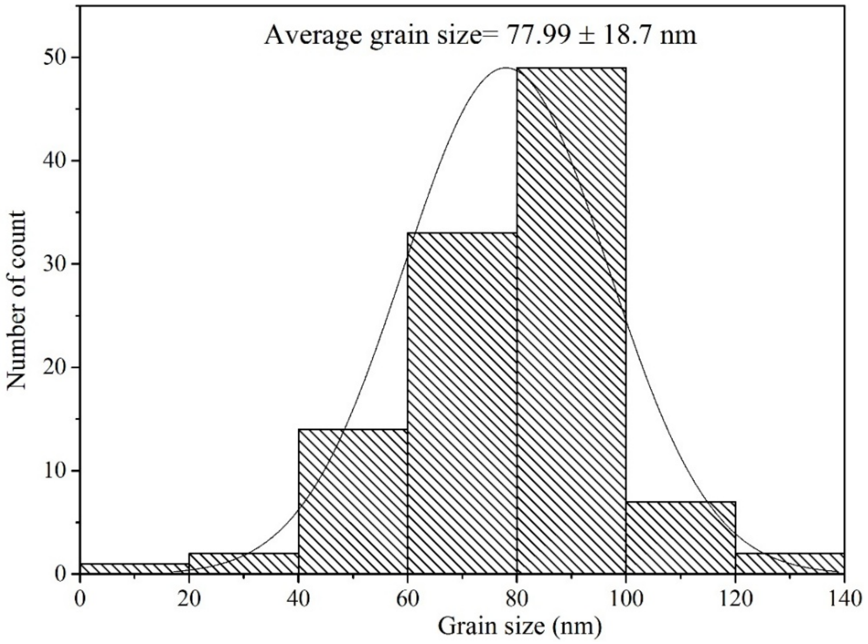

Fig. 7.2 Distribution of the grain sizes of nanocrystalline zinc-tin deposit.

Elemental mapping of the surface of nanocrystalline coating is presented in Fig. 7.3. It is observed that both Zn and Sn are present across the surface. However, some regions are richer in tin and slightly depleted of zinc. As presented previously in sub-chapter 2.6.4.1.3, zinc and tin have very low solubility in each other and tend to form separate phases of zinc and tin deposit during the electroplating condition.

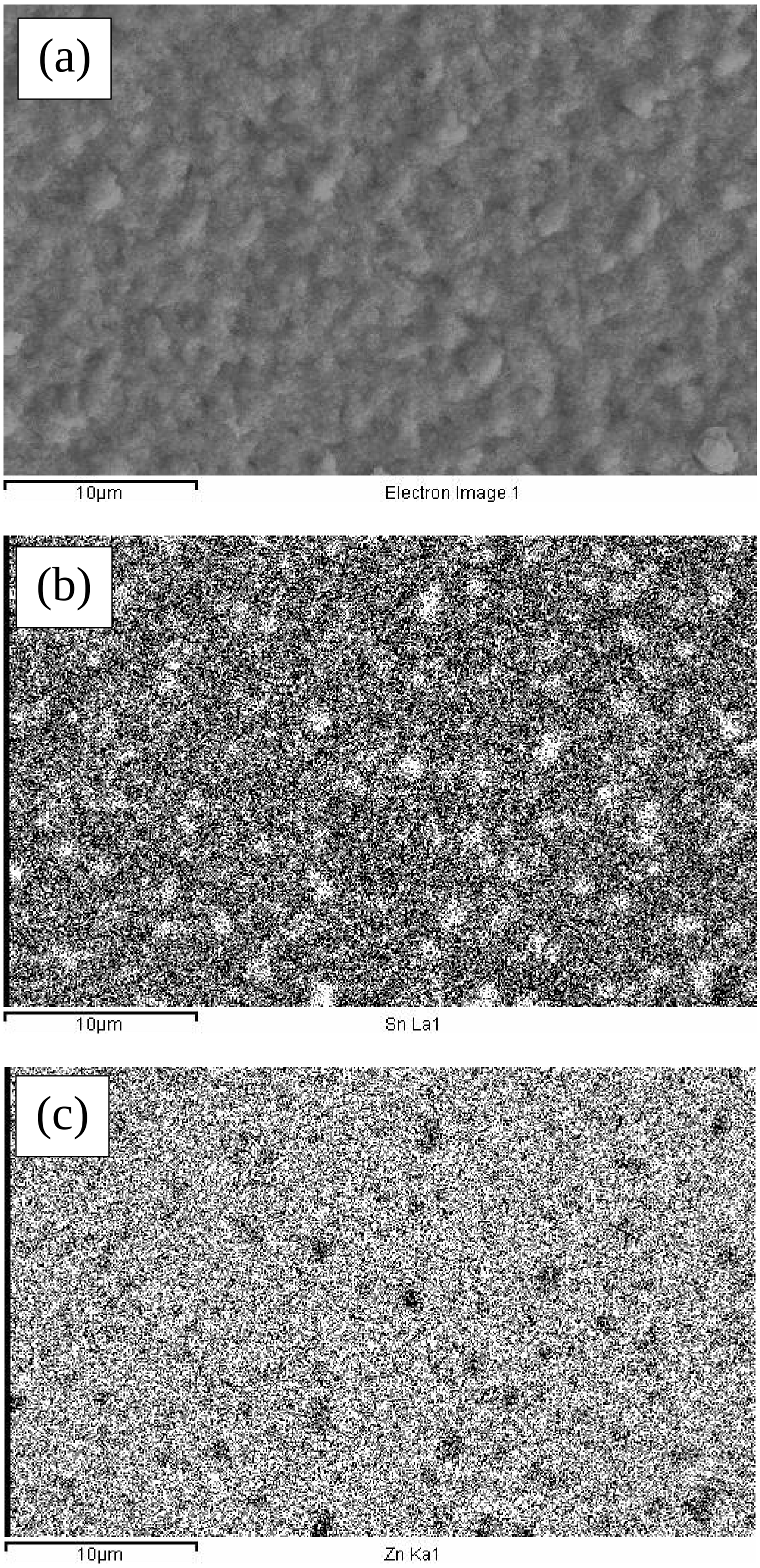

Fig. 7.3 SEM images showing (a) surface backscattered electron image of nanocrystalline coating and corresponding elemental X-ray analysis of (b) tin and (c) zinc.

7.2.2 Cross section microscopy

Optical microscopy examination of the cross section of the coating is presented in Fig. 7.4. It shows that the coating is uniformly deposited across the surface of steel electrode. Average thickness of the coating is 10± 1.07 µm.

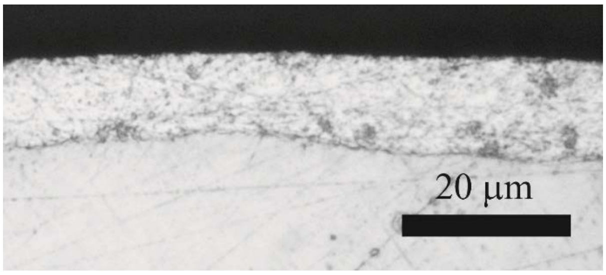

Fig. 7.4 Optical microscopy image showing a cross section of NC coating.

The edge coverage of nanocrystalline zinc-tin coating was also examined at the edge of the steel disc. A high degree of coverage was observed as is presented in Fig. 7.5.

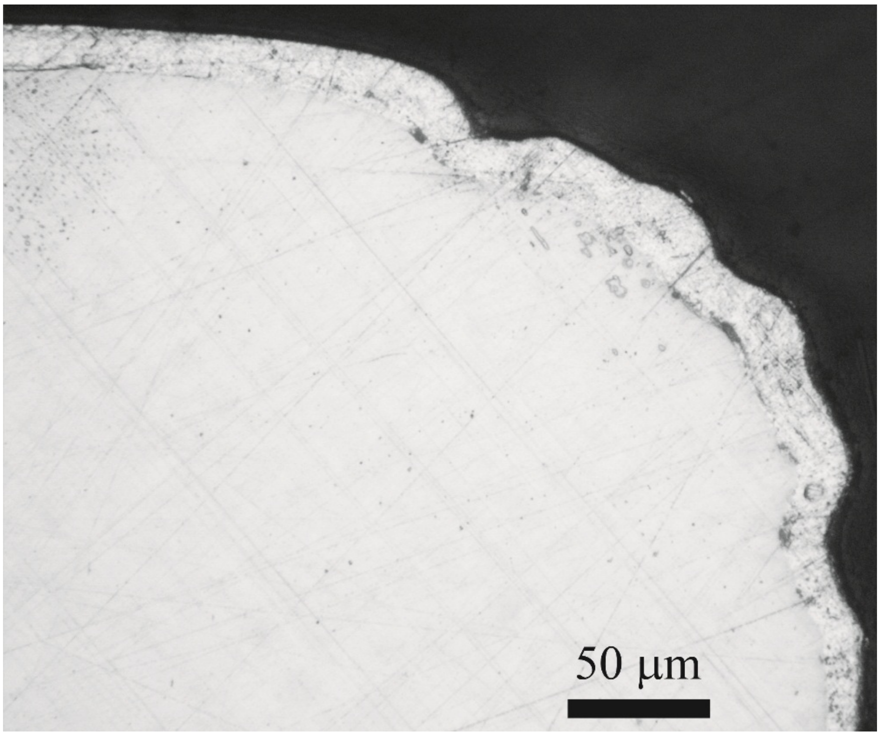

Fig. 7.5 Optical microscopy of the cross section of the nanocrystalline coating around the edge of steel disc substrate.

7.3 Ultra-fine-grained coating characterization

7.3.1 Microstructure and grain size

Ultra-fine-grained (UFG) zinc-tin coatings (S_4 (400)) were produced under pulse-current deposition (T_{ON}= 5 ms, T_{OFF}= 7 ms, i= 0.047 A/cm^2 and deposition time = 1200 seconds) from the alloy solution (see Table 6.1) containing 4gr/lit PEG 400 and 1mM CTAB (see sub-chapter 6.3.4.2.5). The surface morphology, cross section and EDS spectrum of this alloy are shown in Fig. 7.6 (a), (b) and (c) respectively. More images of the surface morphology of this deposit were presented previously in Fig. 6.25 (a) and (a′). The ultra-fine-grained zinc-low content tin alloy as presented in sub-chapter 6.3.4.2.5.3 was composed of a mixture of hexagonal zinc and tetragonal β-Sn phases. The average zinc and tin content of this alloy is 73.38± 1.08 wt.% and 24.53 ± 1.19 wt. % respectively (Table 6.4).

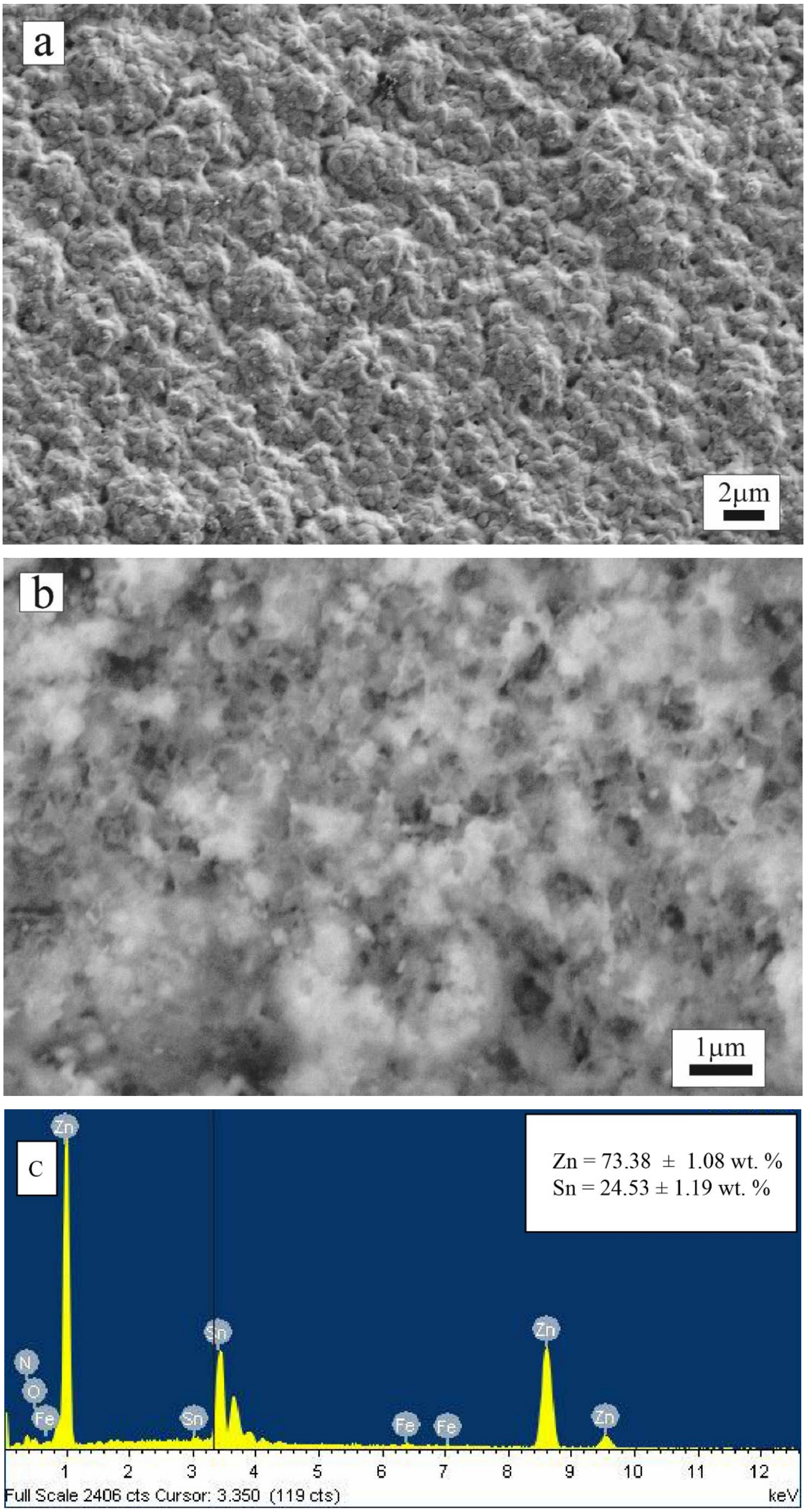

Fig. 7.6 Characteristics of ultra-fine-grained zinc-tin coating: (a) SEM image of the surface morphology, (b) SEM image of the cross-section and (c) EDS spectrum.

The average grain size of the deposit was measured using image J software from the cross section image of the deposit. Fig. 7.7 illustrates the grain size distribution and clearly shows that the majority of the grains are smaller than 500 nm in size which indicates the ultra-fine-grained structure of the deposit.

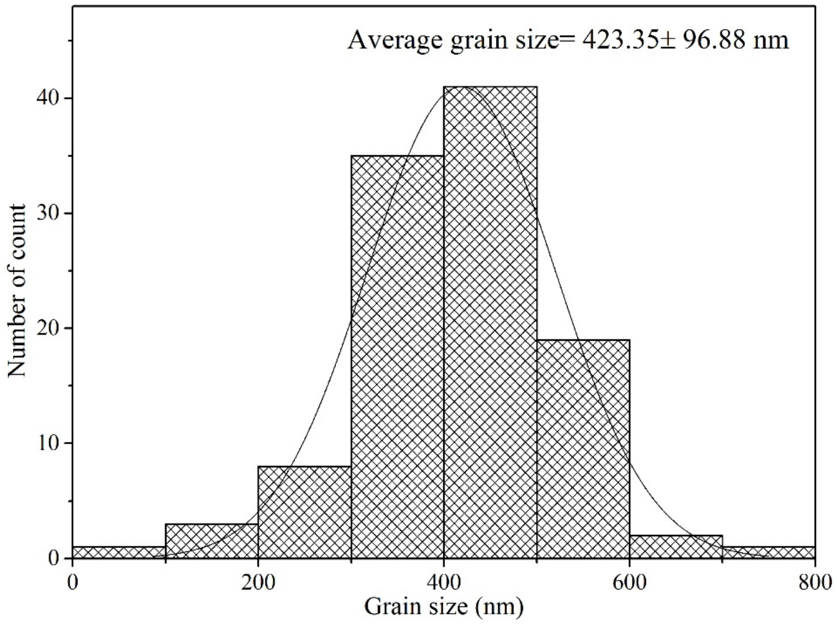

Fig. 7.7 Distribution of the grain sizes of ultra-fine-grained zinc-tin deposit.

Elemental mapping analysis of the surface of UFG coating is presented in Fig. 7.8. UFG coating showed zinc and tin distributed across the surface with some areas richer in tin, as observed for the NC coating.

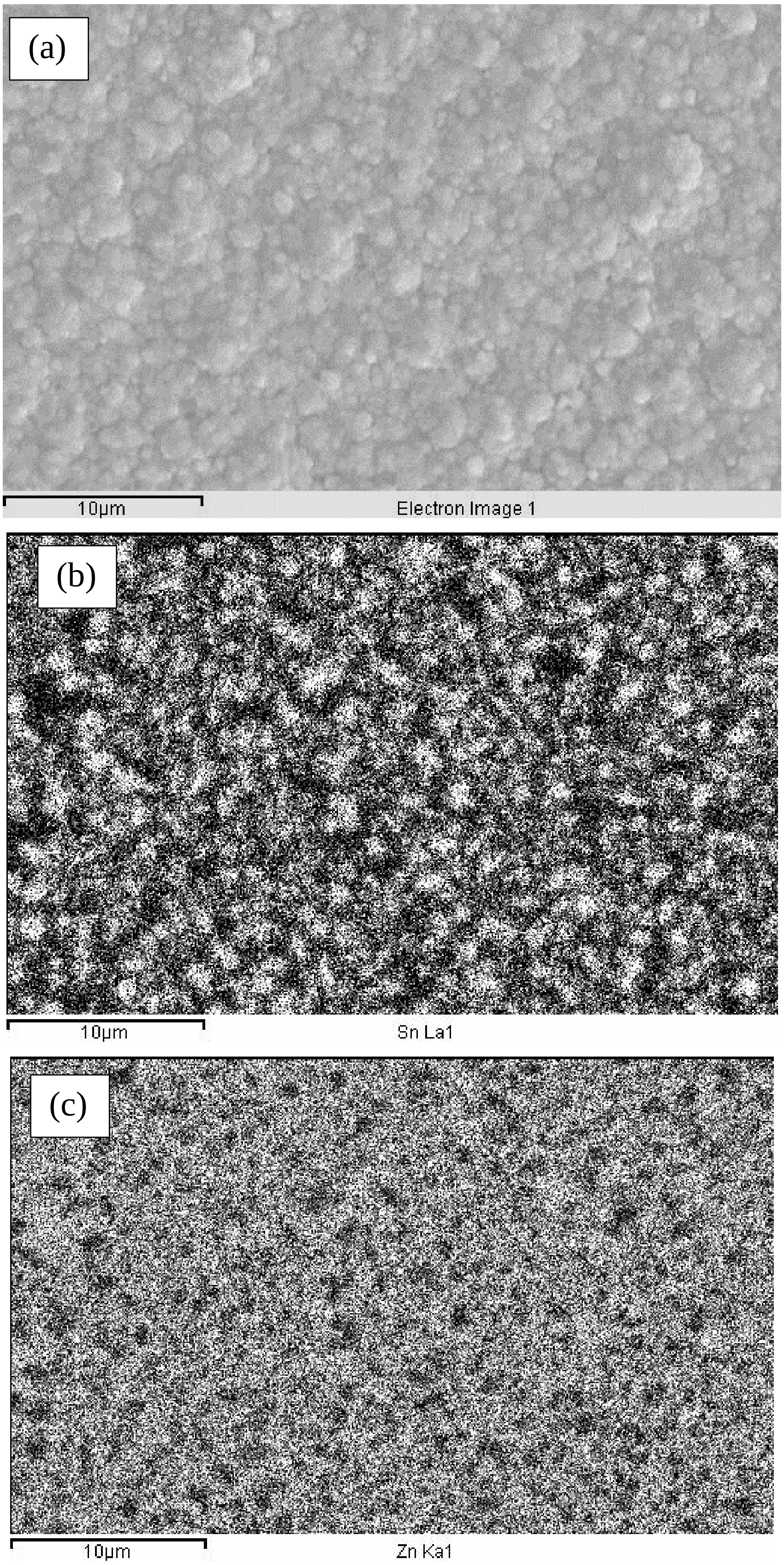

Fig. 7.8 SEM images showing (a) surface backscattered electron image of ultra-fine-grained coating and corresponding elemental X-ray analysis of (b) tin and (c) zinc.

7.3.2 Cross section microscopy

Optical microscopy examination of the cross section of the ultra-fine-grained coating is presented at Fig. 7.9. It shows that the UFG coating is uniformly deposited across the surface of steel electrode. Average thickness of the coating is 13± 0.53 µm.

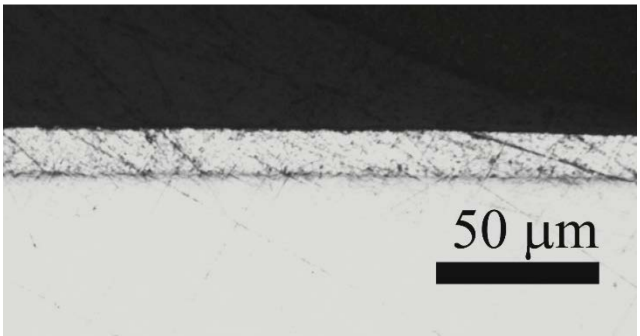

Fig. 7.9 Optical microscopy image showing cross section of the nanocrystalline zinc-tin coating.

The edge coverage of UFG coating was also examined at the edge of the steel disc. A high degree of coverage was observed as it is presented in Fig. 7.10.

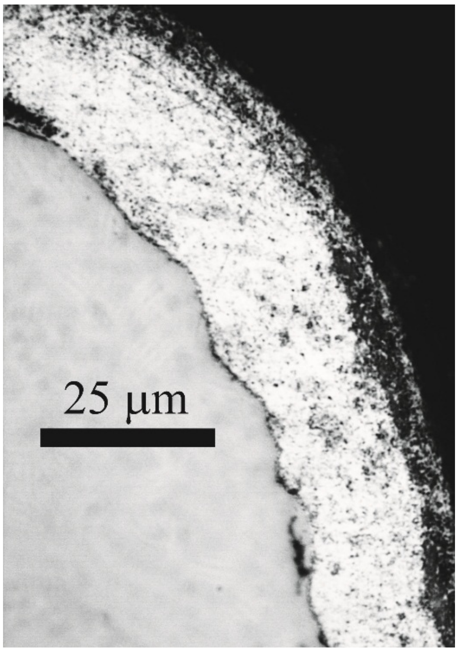

Fig. 7.10 Optical microscopy of the cross section of the ultra-fine-grained coating around the edge of steel disc substrate.

7.4 3-Dimentional Optical Profilometry

3D profilometry images of the nanocrystalline and ultra-fine-grained zinc-tin alloy coating are presented in Fig. 7.11 (a) and (b).

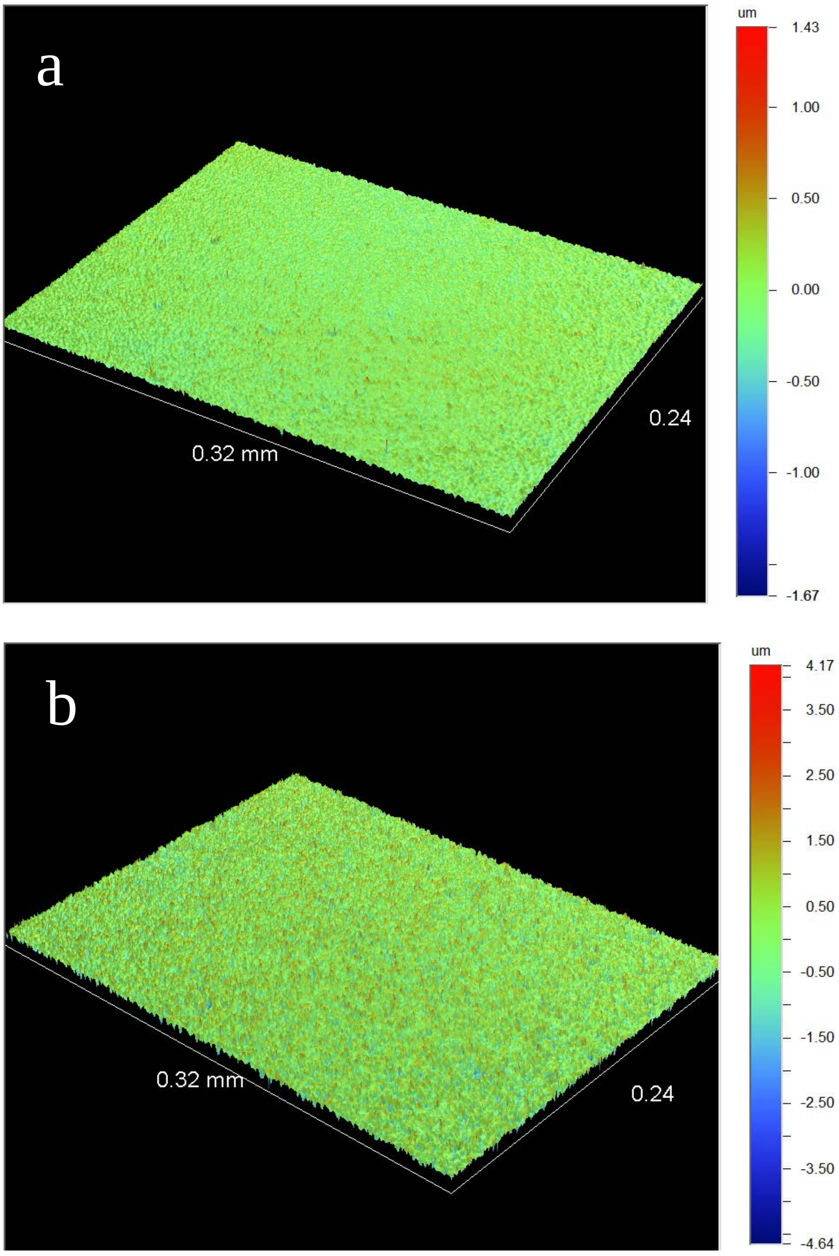

Fig. 7.11 3D profilometry images of (a) nanocrystalline (b) ultra-fine-grained zinc-tin alloy deposit. Vertical bar shows the amplitude range per image (20 K X magnification, 0.32 × 0.24 mm imaged area)

The average surface amplitude parameters such as mean roughness (S_a), root mean square roughness (S_q), skewness (S_{sk}) and kurtosis (S_{ku}) are presented in Fig. 7.12.

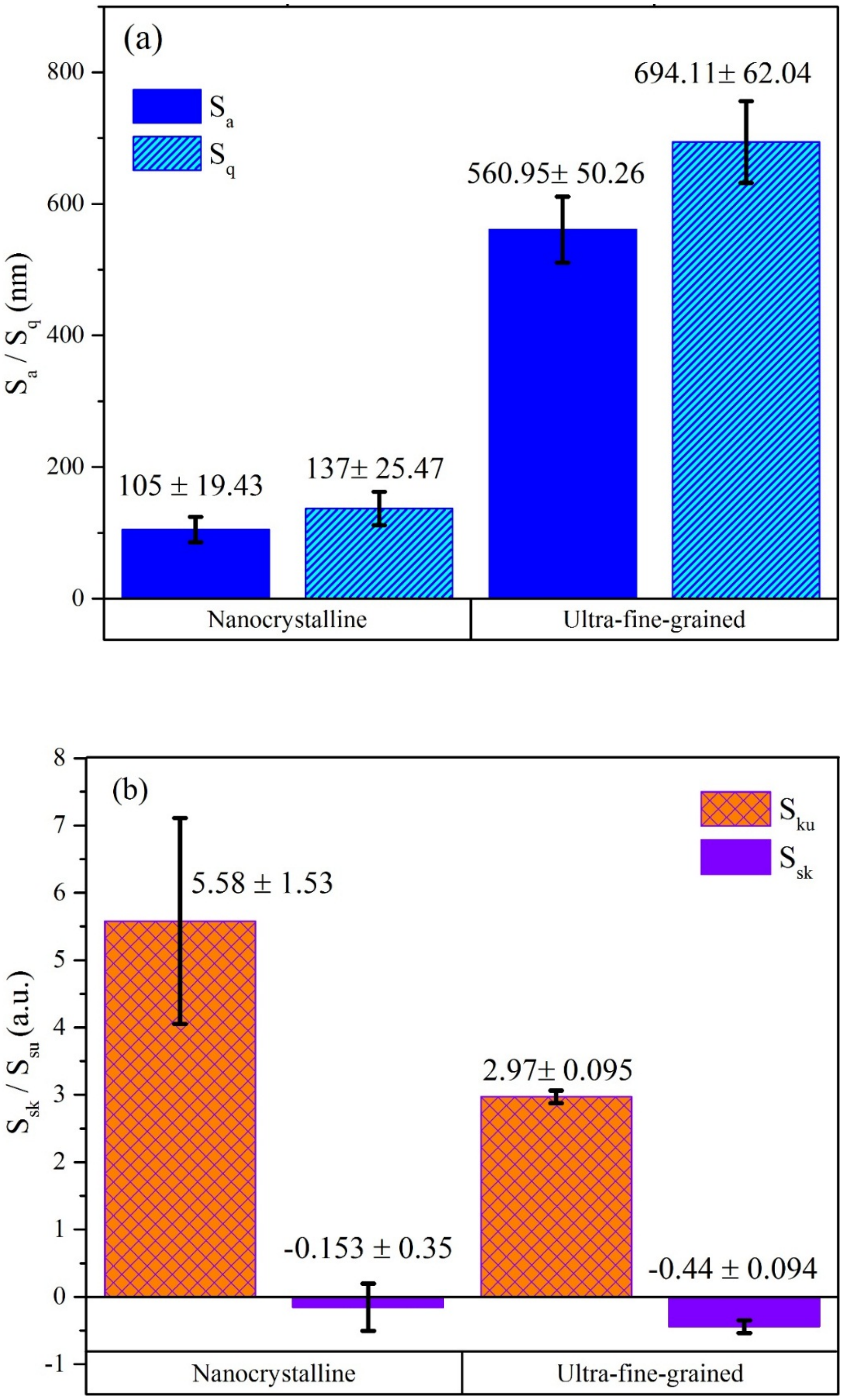

Fig. 7.12 Surface amplitude parameters of nanocrystalline and ultra-fine-grained Zn-Sn deposits.

Evaluation of the surface profile of a deposit is important due to its effects on the wear properties and friction coefficient of the deposit. Normally, rough surfaces have higher coefficient of friction and wear quickly. Therefore, measurement of the surface roughness can help with the prediction of mechanical properties of the coating.

The arithmetic average height parameter (S_a) denotes the average absolute value of the height (roughness irregularities) within a sampling area. S_q, denotes the root mean square value of the surface departures, within the sampling area.

S_a values increased from 105± 19.43 nm in NC to 560.95± 50.26 nm in UFG. S_q values increased from 137± 25.47 nm in NC to 694.11± 62.04 nm in UFG (Fig. 7.12). These results show that S_a and S_q are consistent with the surface morphology of deposits shown in Fig. 7.1 (a) and 7.6 (a) for nanocrystalline and ultra-fine-grained deposits respectively. In other words, the deposit surface roughness can be traced to the grain size. Reduction in grain size has led to the reduction in S_a and S_q.

The skewness (S_{sk}) indicates the degree of symmetry of the surface deviation about the mean reference plane. The negative sign of the skewness shows that the surface has more pores than peaks, and positive sign shows vice versa. The value of the skewness of both deposits was negative (-0.153 ± 0.35 in NC and -0.44 ± 0.094 in UFG). However, both coatings showed very small deviation from zero plane which indicated that pores exist on the surface. In electroplating, pores form during the process of hydrogen evolution and their existence is inevitable. Comparison of the skewness of nanocrystalline with ultra-fine-grained Zn-Sn deposits shows that more pores are exciting in the ultra-fine-grain structure. This is due to the different molecular weights of PEG which used for synthetize of nanocrystalline and ultra-fine-grain Zn-Sn deposits (PEG 400 and PEG 2050 were used for nanocrystalline and ultra-fine-grained deposit respectively). One of the aspects of adding a surfactant to the plating electrolyte is to reduce the surface energy of the electrode and aid with the detachment of the hydrogen bubbles from the surface. As discussed previously in sub-chapter 6.3.4.2.6.2, the strength of the absorbed layer on the surface of steel electrode produced in the presence of PEG 2050 is higher than that of PEG 400. As a result, recombination of H atoms and release of H_2 occurred in the presence of PEG 2050 and led to the decrease of the absorption of H_{ads} to the surface of electrode. Consequently less pores were produced in nanocrystalline Zn-Sn than ultra-fine-grained coatings [102].

Kurtosis (S_{ku}) shows the nature of the height distribution. If the surface heights are normally distributed (bell curve) then S_{ku} is 3.00. Surfaces composed of inordinately high peaks or deep valleys have S_{ku}>3.00 and distribution curve is leptokurtic. S_{ku}<3.00 indicates gradually varying surfaces and indicating platykurtoicat distribution curve.

S_{ku} was > 3 (5.58± 1.53) for nanocrystalline Zn-Sn and was 2.97± 0.095 for ultra-fine-grained Zn-Sn deposit which showed with the increase in grain size the distribution of the height/ valleys was gradually changing over the surface with almost normal distribution curve. However, in the nanocrystalline deposit, peaks or valleys were not normally distributed across the surface and were present as an abnormality on the surface with a leptokurtic distribution curve. Fig. 7.13 shows two of these abnormalities on the surface of nanocrystalline Zn-Sn. These valleys are mainly due to the hydrogen evolution which was previously discussed.

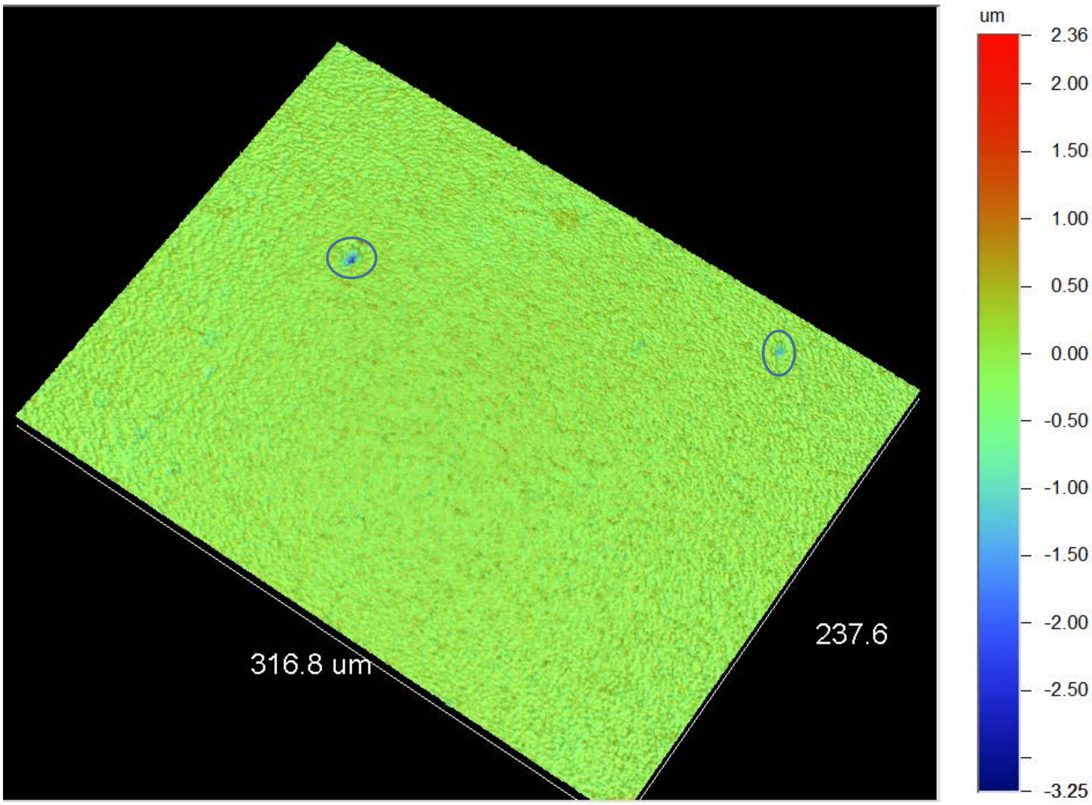

Fig. 7.13 3D optical profilometry shows abnormalities (circled in the image) on the surface of nanocrystalline Zn-Sn.

7.5. Mechanical properties of NC and UFG Zn-Sn coatings

7.5.1. Hardness and Elastic modulus

Nanoindentation was conducted to measure hardness and elastic modulus of the nanocrystalline and ultra-fine-grained Zn-Sn coatings. Fig. 7.14 (a) and (b) shows typical nanoindentation load-displacement curves of the nanocrystalline and ultra-fine-grained Zn-Sn coatings.

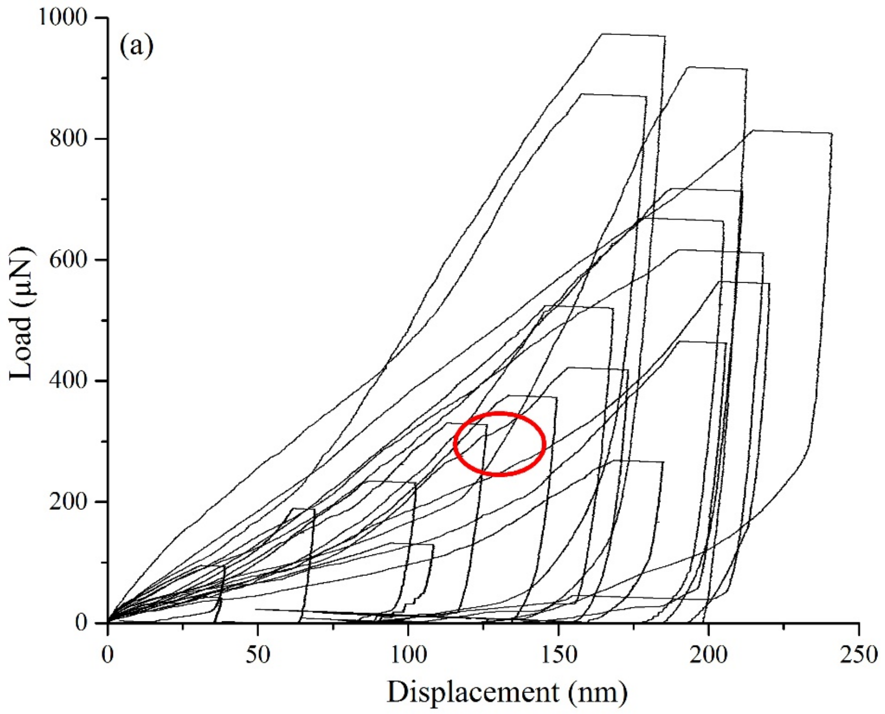

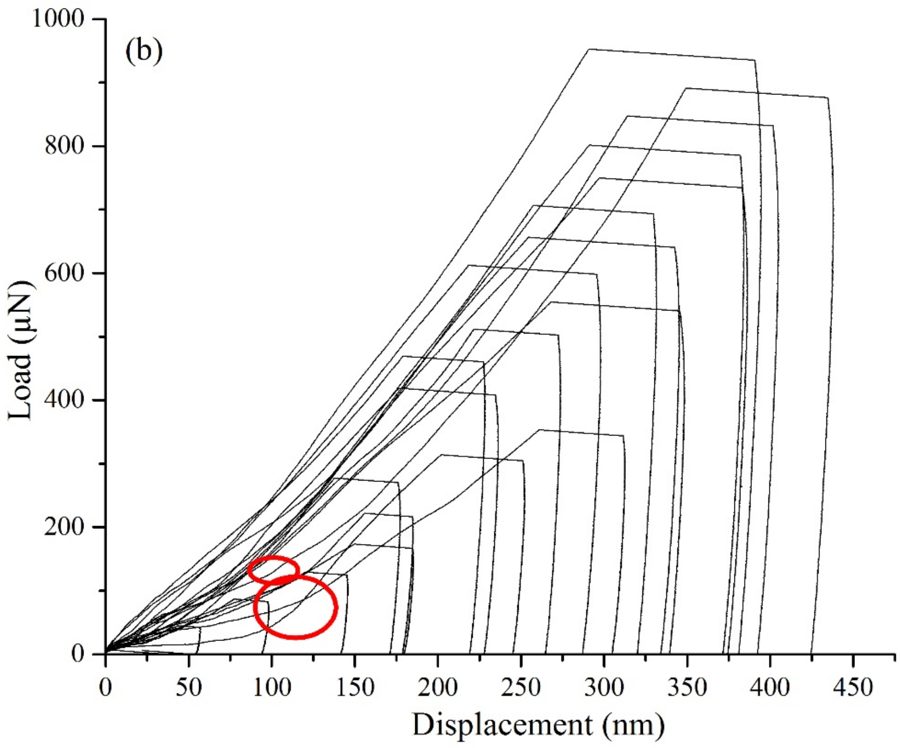

Fig. 7.14 Typical load-displacement curves for nanoindentation of: (a) nanocrystalline and (b) ultra- fine-grained Zn-Sn coatings.

Load-displacement curves of nanocrystalline and ultra-fine-grained Zn-Sn coatings show that displacement was not uniformly increasing with the increase of load. This phenomenon was mainly due to non-homogeneous distribution of zinc and tin. As it was shown by elemental mapping of both NC and UFG coatings, although zinc and tin were dispersed across the surface there were areas which were rich in tin. This difference in the concentration of tin across the surface led to variation in nano-indenting behavior as measured by force-displacement across the surface. On the other hand it has been reported [229] that under constant load, the load-displacement curve for two different grains of tin with various orientation showed significantly larger displacement for the (100) plane than the (110) due to the higher elastic modulus of (100) plane (58 GPa) than (110) plane (50 GPa). Therefore, the observed anomalous decrease in the displacement with the increased load indicates that tin grains in the alloy under the indentation area were mainly orientated along (110) planes.

Some of the load-displacement curves show traces of pop-in events (red circles in Fig. 7.14 show an example of these pop-in events). Pop-in events are plasticity initiation behavior that appears on a loading process during indentation [230]. The pop-in phenomena is interpreted as the nucleation of dislocation. Pop-in occurs if the maximum shear strength produced under the indenter is of the same magnitude as the theoretical shear strength. Then this localized high shear strength leads to nucleation of dislocations and produces a displacement discontinuity in the load-displacement curve [231].

Another reason explaining the observed decrease in penetration depth in contrast to increasing the load could be due to effects of pile-up. As the plastic deformation occurs during the loading process surface may raise up at the edge of indentation, the raised material act as a support during the indentation and leads to the decrease in the penetration depth.

The average hardness and elastic modulus of nanocrystalline and ultra-fine-grained Zn-Sn deposits are presented in Fig. 7.15 (a) and (b) respectively. Hardness of NC and UFG are 532.3 ± 140 MPa and 209.4 ± 65.8 MPa respectively. Modulus of elasticity of NC and UFG are 59.11± 15.62 GPa and 59.87 ± 11.12 GPa, respectively.

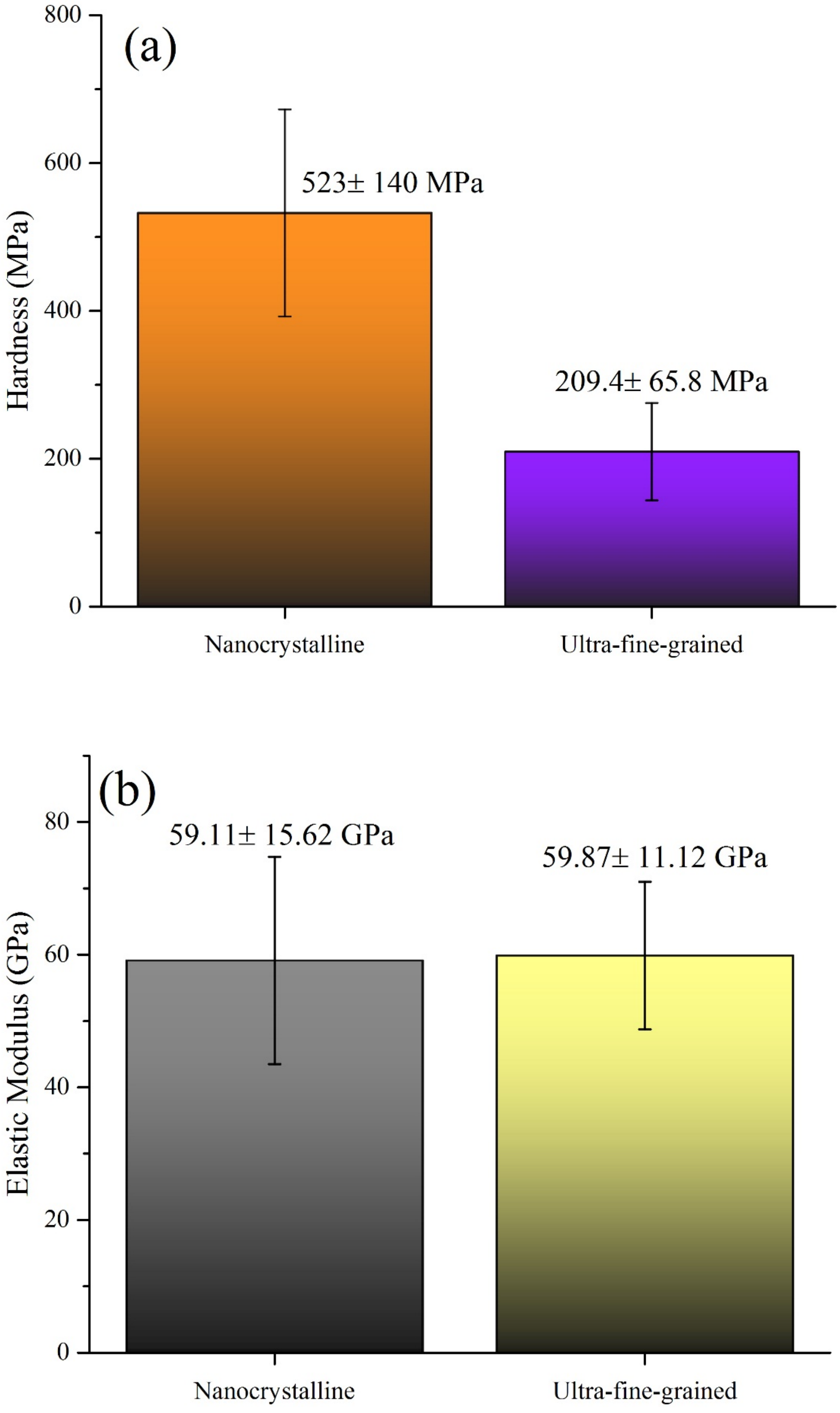

Fig. 7.15 (a) Nanohardness and (b) elastic modulus of nanocrystalline and ultra-fine-grained Zn-Sn coatings.

Hardness of material is a function of the grain size according to Hall-Petch equation. Hardness increases with decreasing grain size down to certain values of grain size (15nm), after which the reverse of the Hall-petch effects emerge. Equation 7.1 shows the Hall- Petch equation [232].

$$H = H_i + K_{H-P}\, d^{\frac{-1}{2}} \qquad (7.1)$$

Where H is the hardness, H_i is the lattice friction stress, K_{H-P} is the Hall-Petch constant and d is the grain size. Increase in hardness values with the decrease of grain size has been reported [233-237] in literature and it has mainly been explained based on the relation of grain size and grain boundaries. Generally, decrease in grain size leads to the increase in grain boundaries. These grain boundaries act as a barrier and prevent the movements of dislocations and thereby increase the hardness.

In this study decrease in grain size from 423.35± 96.88 nm to 77.99 ± 18.7 nm led to increase of hardness in accordance to Hall-Petch equation and no reverse effects of Hall-petch equation was observed.

Elastic modulus stayed almost constant with the change of the grain size. Slight decrease of elastic modulus is only reported at grain size less than 20 nm, above this threshold no significant change in elastic modulus has been observed with the change of the grain size [238].

Hardness map of the NC and UFG coatings is presented in Fig 7.16. Hardness map is a plot that describes the hardness as a function of the X and Y position on a sample.

The hardness map of NC and UFG coatings shows that hardness is changing as a function of position. This is mainly due to nonhomogeneous distribution of zinc and tin across the surface (see Fig. 7.2 and Fig. 7.7), there were some areas rich in tin and depleted from zinc. Modulus of elasticity of zinc (104.5 GPa for commercially pure zinc [239]) is higher than tin (44.3 GPa for commercially pure tin [239]), therefore zinc is harder than tin. As a result, red points with high hardness in Fig. 7.16 are attributed to zinc rich areas and purple and blue points are attributed to tin rich areas.

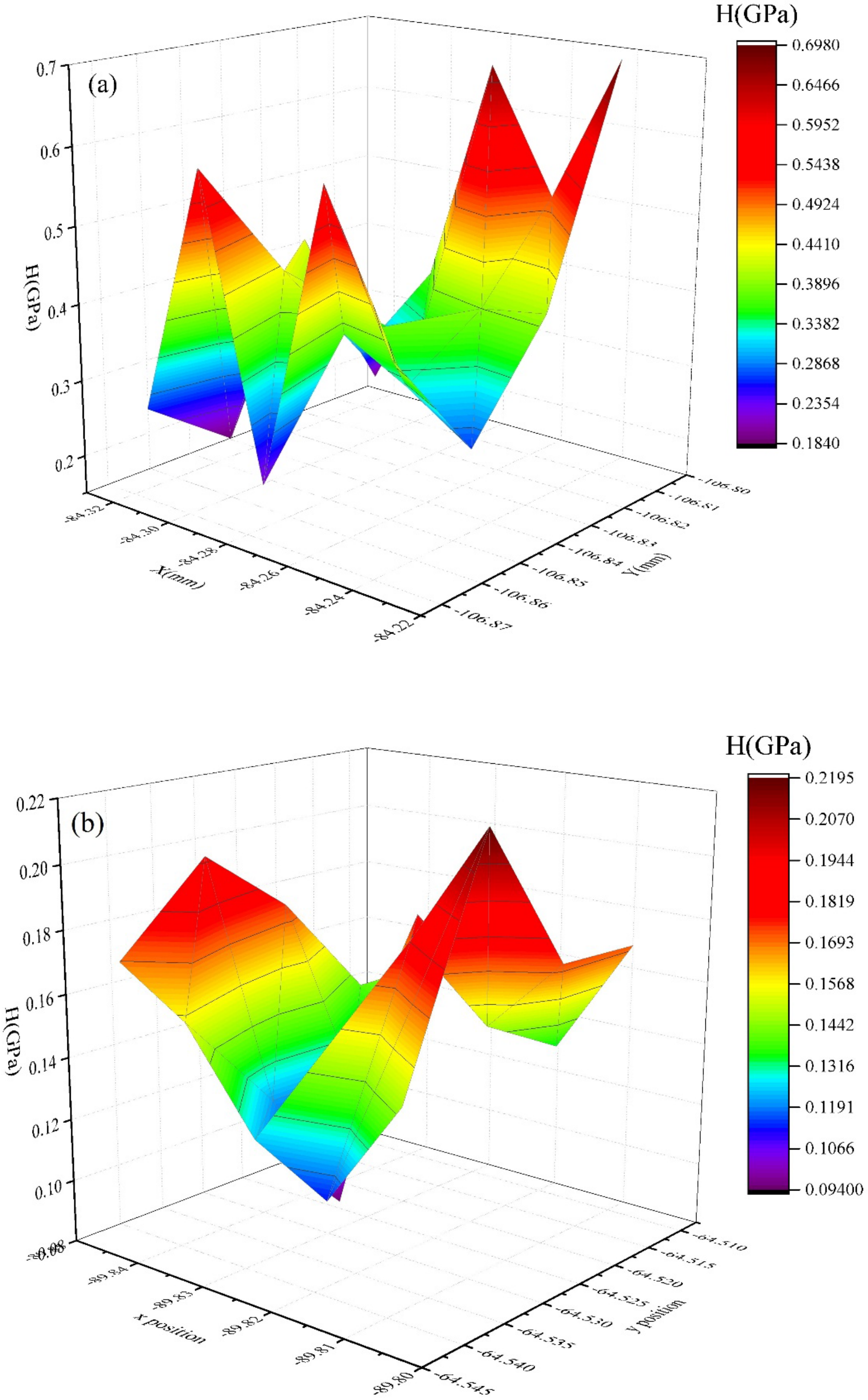

Fig. 7.16 Hardness map of (a) nanocrystalline and (b) ultra-fine-grained Zn-Sn coatings.

7.5.2 Nanoscratch

The main purpose of performing nanoscratch test was to determine coefficient of friction of the coatings. Three specimens of each coating were examined for this purpose. Fig. 7.17 (a) and (b) are nanoscratch plots showing normal displacement and coefficient of friction as a function of time respectively.

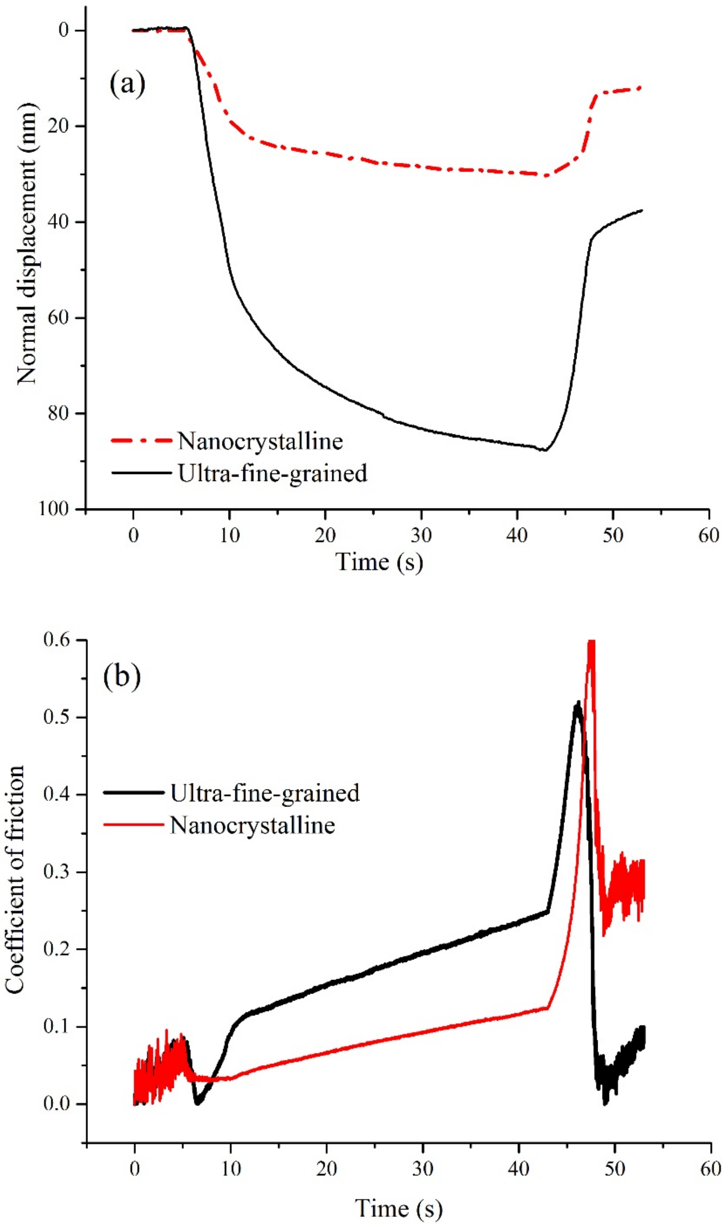

Fig. 7.17 (a) Normal displacement and (b) coefficient of friction as a function of time for nanocrystalline and ultra-fine grained Zn-Sn coatings.

Curve of the normal displacement versus time (Fig. 7.17 b) showed that for the equal amount of load which was applied during the friction test (100 µN) on both NC and UFG, a deeper groove was formed on the surface of UFG coatings. This result was in accordance with the hardness result. The lower hardness of the UFG coatings (209.4 ± 65.8) compared to the nanocrystalline coatings (532 ± 140) allows a deeper groove to be produced for the same values of force on the surface of UFG coating.

Nanocrystalline coatings exhibited a lower coefficient of friction than the UFG coatings (Fig. 7.17 (b)). For both coatings, the coefficient of friction increased with time. However, the coefficient of friction of the UFG coating increased with higher rate than the NC coating. It has been considered that the relevant part of the friction test is from 10 s to 42 s, as before 10 s the load was ramping from 0 to 100 µN, and after 42 s the load was decreasing to zero. The increase in friction coefficient with time was the effect of piling up of debris formed at the time of sliding in front of the scratching tip. Basically the lower gradient (slope) of the friction curve of NC than UFG showed that less coating was detached from the sample during the scratching process. These results showed that NC coating have a higher cohesion bonding than UFG coating. Fig 7.18 shows the SEM and 3D surface profilometer images of the surface scratch formed on the surface of NC coating.

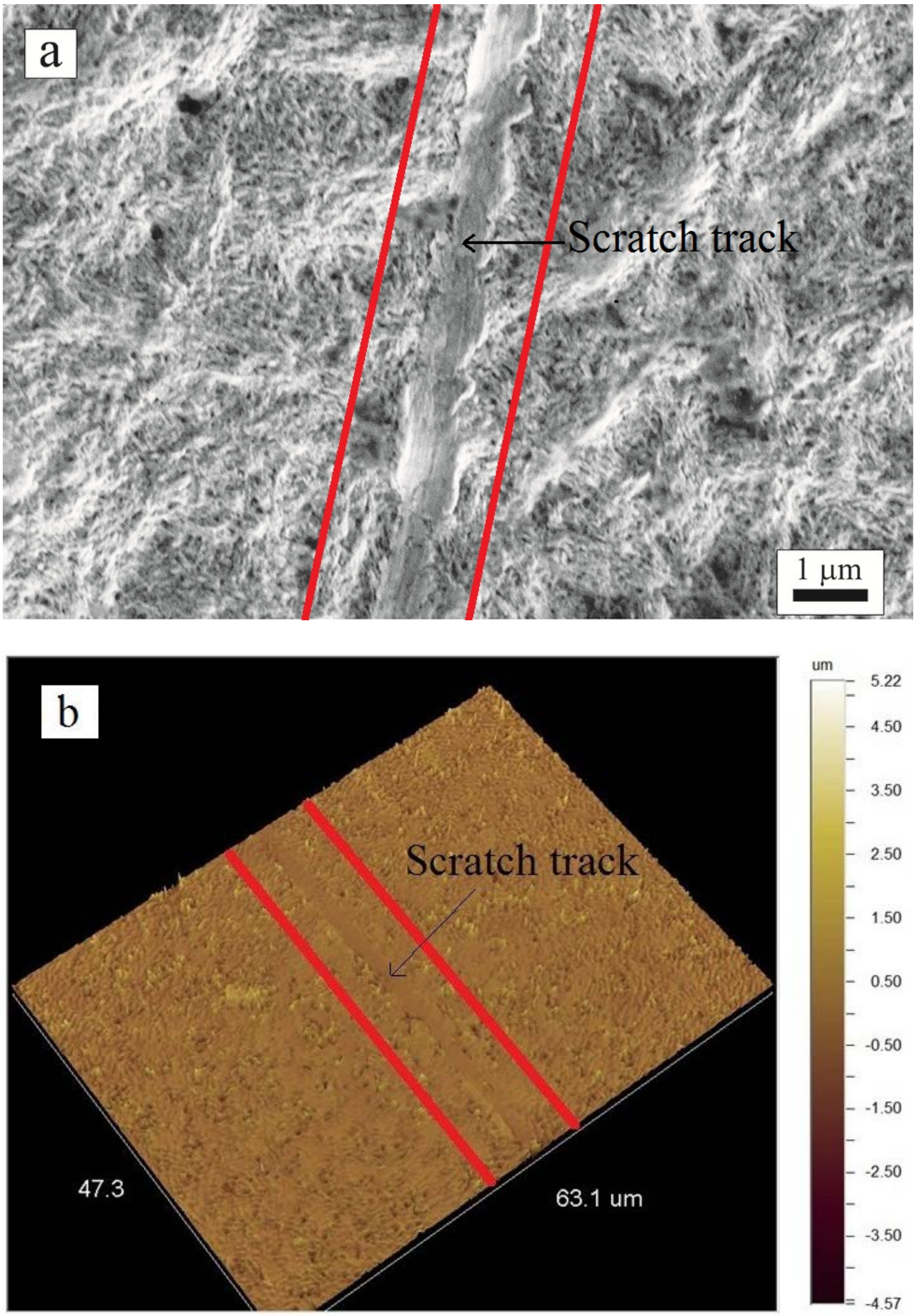

Fig. 7.18 (a) Surface appearance of NC coating after scratch test: (a) SEM image and (b) 3D surface profile.

Surface examination of the scratch did not show any pile up of the NC coating. The scratch track was relatively smooth and no accumulation of coating debris was observed on the surface.

SEM and 3D surface profilometer images of the surface scratch formed on the surface of UFG coating are presented in Fig. 7.19.

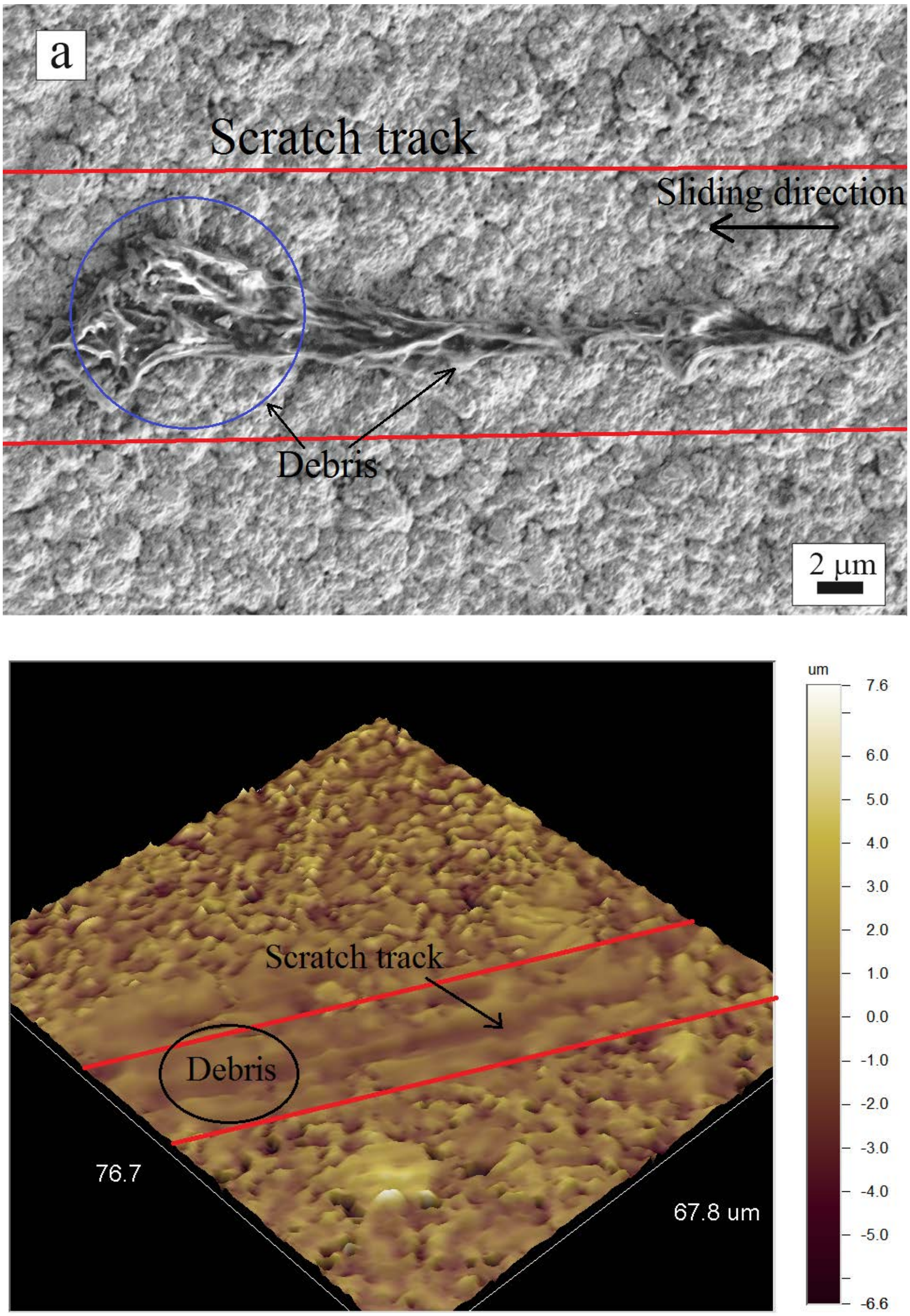

Fig. 7.19 Surface appearance of UFG coating after scratch test: (a) SEM and (b) 3D surface profile.

Unlike tracks observed on the NC coating (Fig. 7.18), scratch trail on the UFG coatings (Fig. 7.19) did not display a smooth and uniform morphology. Coating was removed during the sliding of the indenter and some of debris were piled up along the sliding direction and some accumulated at the end of the scratch line (blue circle in Fig. 7.19 (a)).

Microscopy analysis of the coatings after scratch test in conjunction with analytical analysis of coefficient of friction and scratch depth showed that NC coatings exhibited better scratch resistance properties that UFG coating and have a better cohesion bonding.

7.5.3 Wear properties

Fig 7.20 shows worn area of the NC and UFG Zn-Sn coatings which were prepared by in situ SPM system of the nanoindenter instrument.

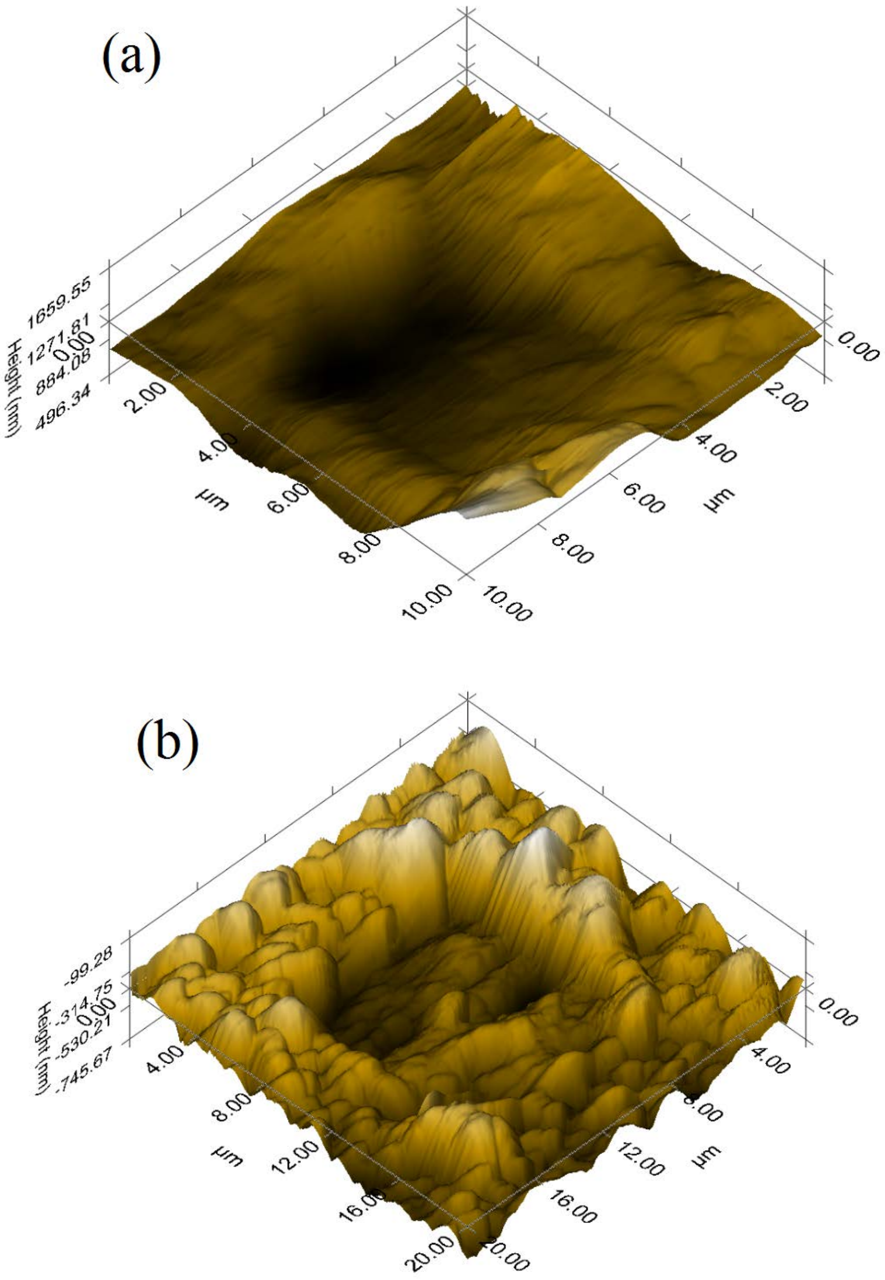

Fig. 7.20 Surface profile of the worn area of (a) nanocrystalline and (b) ultra-fine-grained Zn-Sn coatings after 10 passes under 100 µN load

The wear volume was calculated by the method explained in sub-chapter 3.5.4.3 and results are presented in Fig. 7.21.

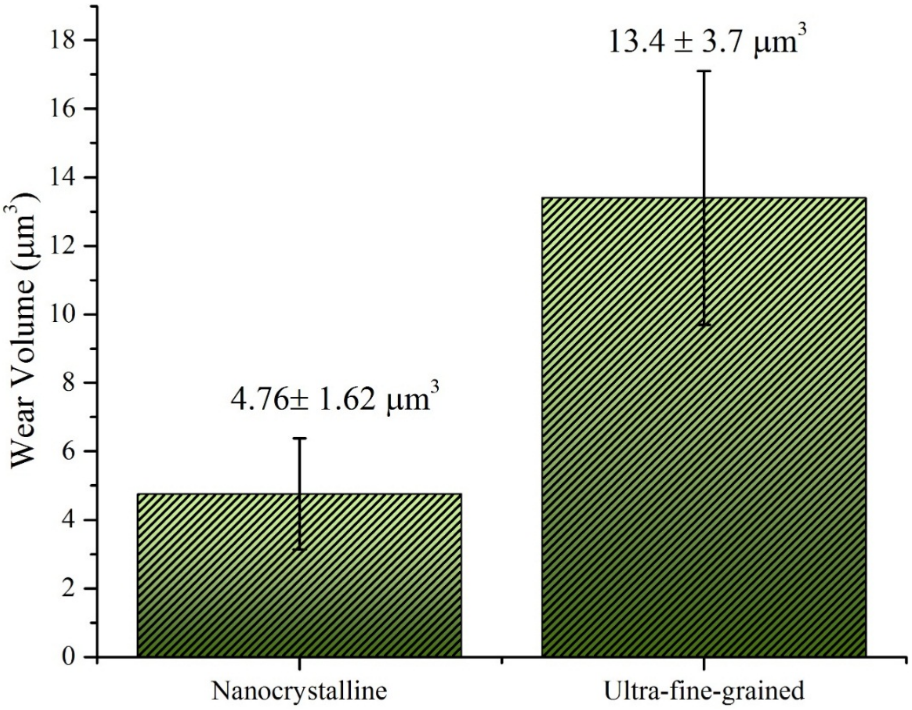

Fig. 7. 21 Wear volume of nanocrystalline and ultra-fine-grained Zn-Sn coatings under 100 µN load and 10 passes for a 5 µm ×5 µm wear area.

SEM images of the nanocrystalline and ultra-fine-grained Zn-Sn coating is presented in Fig. 7.22.

Large platelets and pile-up of wear debris were evident due to the softness of the surface plowed by the diamond indenter.

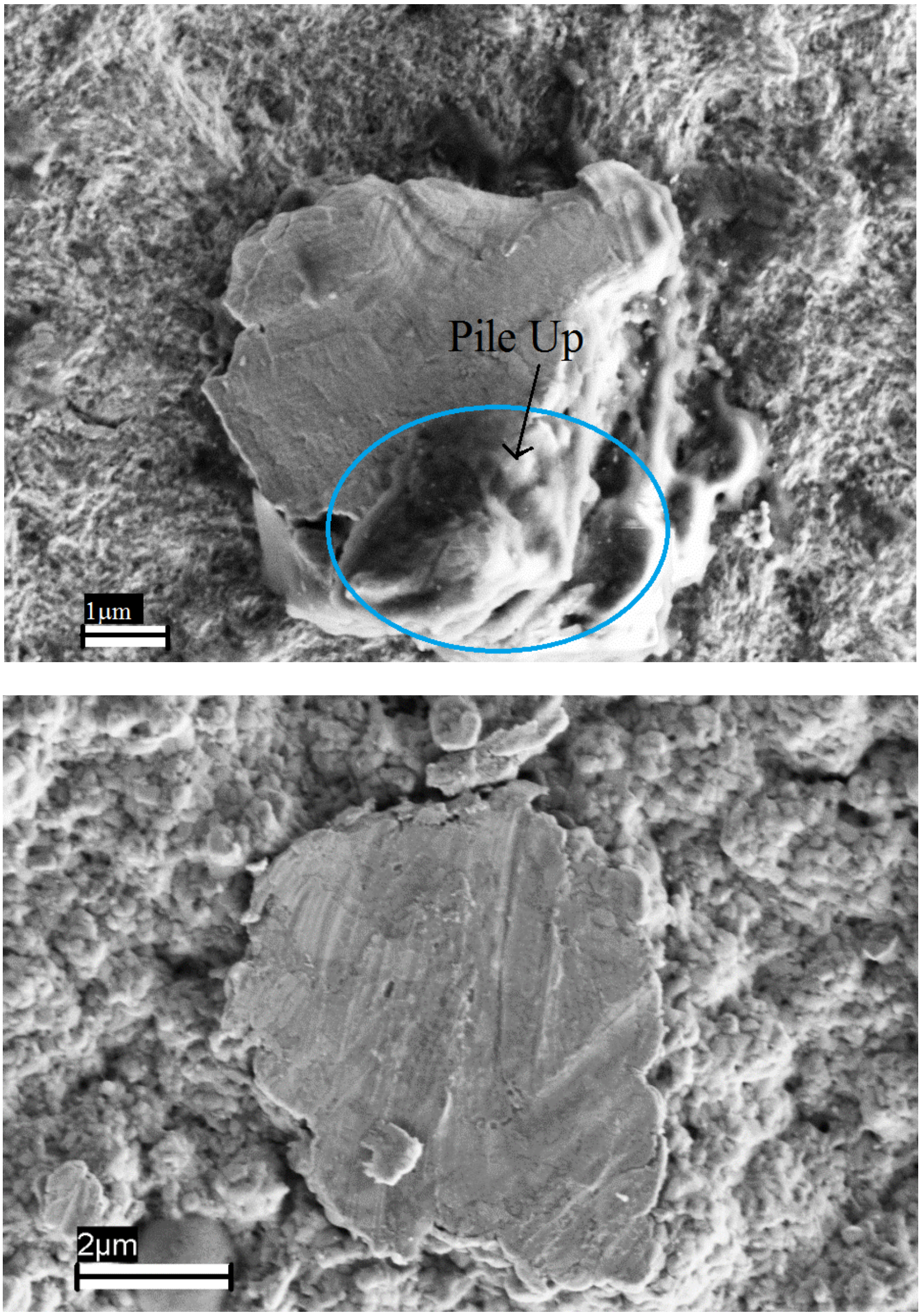

Fig. 7.22 SEM images of (a) nanocrystalline and (b) ultra-fine-grained Zn-Sn coating after 10 passes sliding wear under 100µN load and a 5µm × 5µm scan area.

Based on Archard's Law of Wear (equation 7.2), refinement of the structure leads to the improvement of wear properties of material.

$$W = K\frac{L}{H} \qquad (7\text{-}2)$$

Where W is volume worn per unit sliding distance; L is the applied load; H is the hardness of the softer of the materials in contact (Zn-Sn coating in this study), and K is a dimensionless constant. Based on this law, an increase in hardness would result in a decrease of wear volume. The decrease in wear volume from 13.4 ± 3.7 μm^3 in UFG to 4.6 ± 1.62 μm^3 in NC are well in agreement with Archard's law. The hardness of NC coating (532.3 ± 140 MPa) increased in comparison to UFG (209.4 ± 65.8 MPa) due to increase in the volume fraction of grain boundaries and triple junctions. This phenomenon also led to the decrease of the wear volume.

Generally surface deformation of the coating starts as the sliding process starts. Farhat et al. [240] showed that with the reduction of aluminum grain sizes from conventional micrometer scale down to nanocrystalline size, the damage caused by sliding was reduced and micro-plowing did not occur as fast as it occurred at the microcrystalline surface. They observed that hardness of the subsurface region increased during the sliding process and as a result the deformation process continues with more difficulty. Thus at later stages of sliding, the deformation process depends mainly on the properties of the deformed material within the subsurface region which was under sliding force, rather than on the initial properties of the starting material.

SEM image of NC and UFG (Fig. 7.22) structure coatings after the wear test shows that materials are piled up during the sliding process for NC coatings however, UFG coatings did not show any effects of pile up.

7.6 Summary

Physical and mechanical properties of nanocrystalline and ultra-fine-grained Zn-Sn coatings were evaluated in this chapter. Both NC and UFG have rich tin areas on their structure. Surface profile parameters such as mean roughness improved by grain refinement down to nano level. NC coatings exhibited superior mechanical properties such as hardness than UFG coatings. Hardness of the Zn-Sn coatings improved due to the grain refinement from 532.3± 140 MPa in NC to 209.4± 65.8 MPa in UFG.

Coefficient of friction reduced as the result of grain refinement from UFG to NC. Wear volume decreased from 13.4± 3.7 μm^3 in UFG to 4.6± 1.62 μm^3 in NC due to effects of grain refinement based on Archard's law.

Neither of NC and UFG coatings was not detached from the steel substrate during the wear and scratch tests which showed that both coatings were fully adhered to the substrate.

Chapter 8

Corrosion properties of nanocrystalline and ultra-fine-grained Zn-Sn coatings

8.1 Background

Nanocrystalline materials have small grain size (less than 100 nm) and have high volume fraction of grain boundaries in comparison to macrocrystalline and ultra-fine-grained materials. Grain boundaries which are high energy areas with high degree of disorder are considered as potential sites of corrosion initiation. Therefore, in a general view, deterioration of corrosion properties of materials with grain refinements down to nano level are expected. However, improvements of corrosion properties of nanocrystalline materials in comparison with their microcrystalline counterpart have been reported [8-10, 12-14].

In this chapter, corrosion properties of nanocrystalline (NC) and ultra-fine-grained (UFG) Zn-Sn coatings have been evaluated by electrochemical corrosion analysis. NC and UFG, Zn-Sn coatings (12 µm thickness) were prepared as detailed in Chapter 5. Open circuit potential, polarization resistance, potentiodynamic polarization tests were performed as described in Chapter 4.

8.2 Corrosion potential (E_{Corr}) measurements

Corrosion potential (Open Circuit Potential (OCP)) of nanocrystalline (NC) and ultra-fine-grained (UFG) Zn-Sn coatings in 0.63 M NaCl was measured for 12 hours and results are presented in Fig. 8.1. The average corrosion potential of UFG and NC over 12 hours at 21 ± 1°C is presented in Table 8.1.

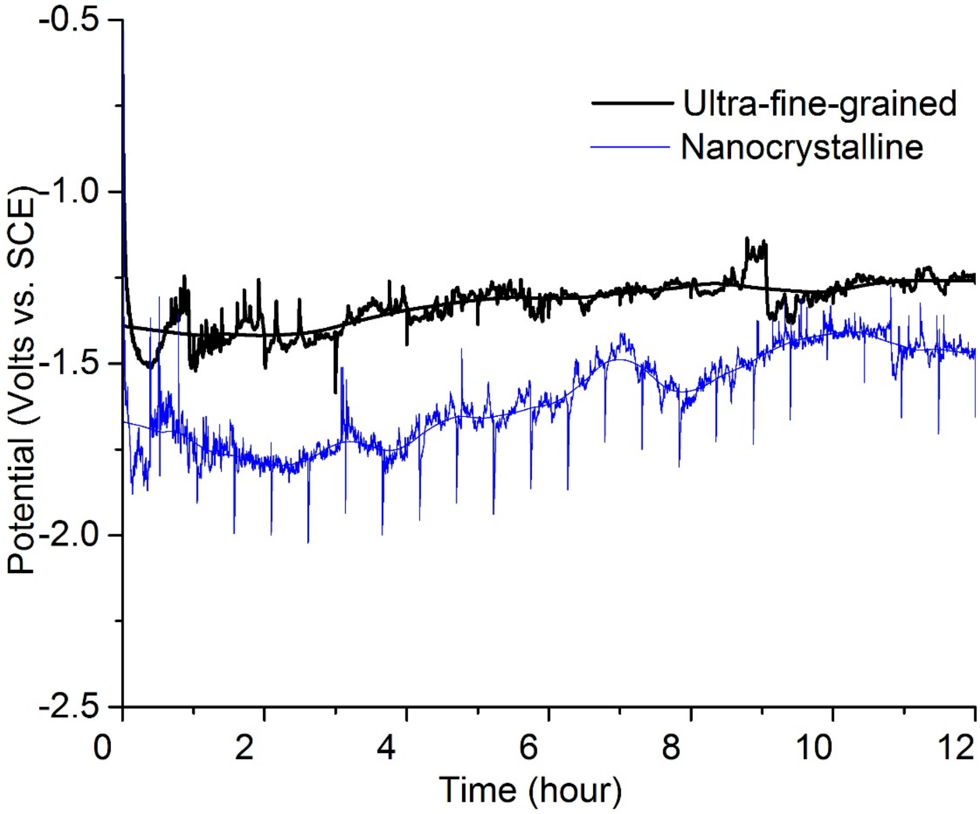

Fig. 8.1 OCP measurements of nanocrystalline and ultra-fine-grained Zn-Sn coatings in 0.63 M NaCl for 12 hours.

Table 8.1 Corrosion current of nanocrystalline and ultra-fine-grained Zn-Sn coatings.

Type of coating	OCP (Volts vs, SCE)
Nanocrystalline	-1.59 ± 0.14
Ultra-fine-grained	-1.38 ± 0.16

UFG showed a more positive corrosion potential than NC counterpart. NC coatings have higher volume fraction of grain boundaries than UFG coatings, therefore higher Gibbs free energy of the surface is expected for NC coatings. Gibbs free energy is directly related to the standard electrochemical potential of the surface [48].

$$\Delta G = -nFE \qquad (8\text{-}1)$$

Any increase in Gibbs free energy will lead to a more negative shift of the potential. This phenomenon explains the more negative values of the corrosion potential of NC coating than UFG.

8.2 Polarization resistance

Fig. 8.2 shows polarization measurements of NC and UFG coatings over 12 hours of immersion to the corrosive environment (0.63 M NaCl).

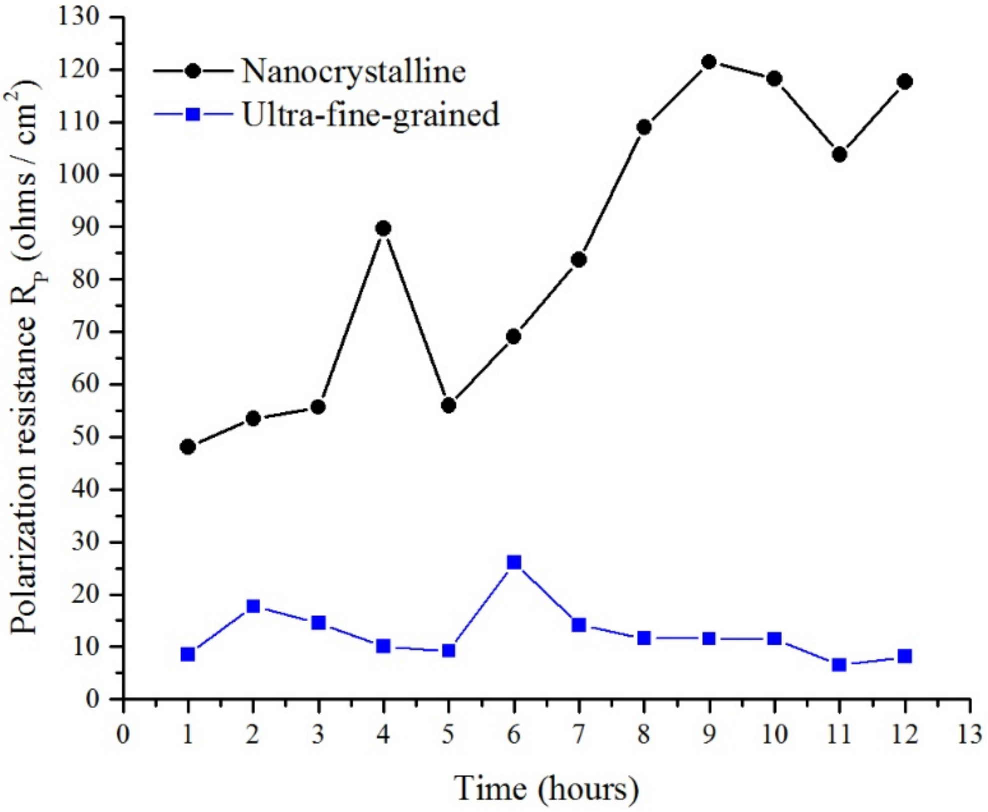

Fig. 8.2 Variation of Polarization resistance of nanocrystalline and ultra-fine-grained Zn-Sn coatings versus time in 0.63 M sodium chloride solution.

The polarization resistance of the coatings is inversely related to their corrosion rate. NC coatings showed higher polarization resistance than UFG coatings, which indicated better corrosion protection of the NC than UFG coatings. Polarization resistance of the NC coating increased with time which indicated that the corrosion properties of the NC coating were enhanced during the time. However, the polarization resistance of the UFG coatings remained almost constant with the time. The increase in polarization resistance of NC coating with time showed that a protective layer of corrosion products formed progressively on the surface which limited the dissolution of the coating. However, the corrosion continuously progressed for the UFG coating.

8.3 Potentiodynamic polarization test

Potentiodynamic polarization measurements were performed on NC and UFG coatings after 1 hour of immersion in the corrosive environment (0.63 M NaCl). Fig. 8.3 shows potentiodynamic polarization curves of NC and UFG coatings.

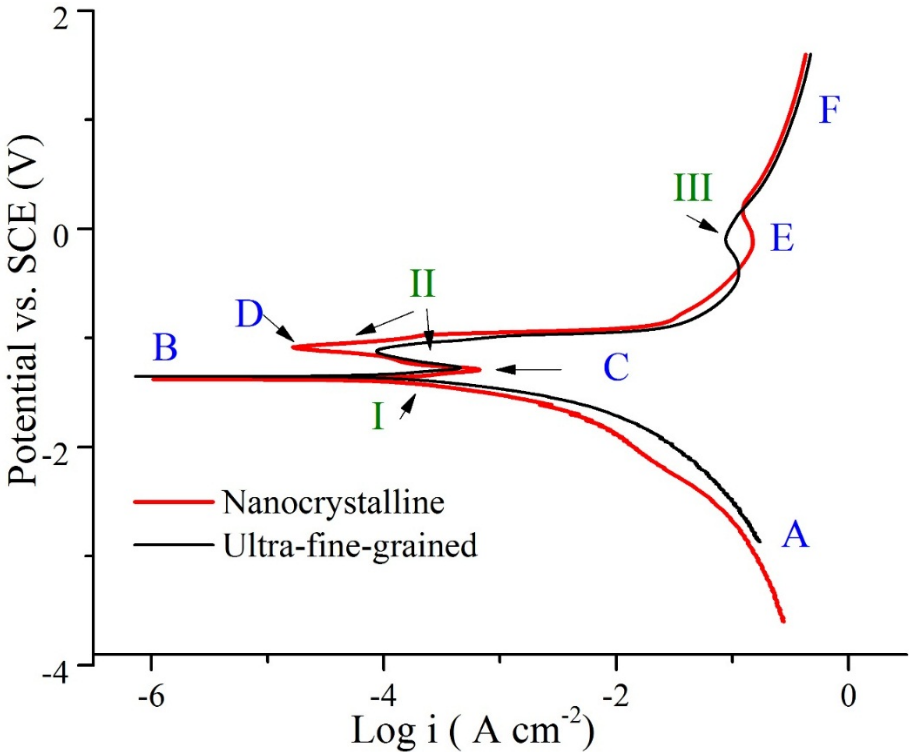

Fig. 8.3 Potentiodynamic polarization curves of NC and UFG Zn-Sn coatings in 0.63 M NaCl at 21 ± 1°C.

A significant difference between the behavior of NC and UFG coatings was the shift of NC curve to the left hand side of current density almost over the entire range of potential (except for peak III in Fig. 8.3), which indicated that NC coating had smaller anodic and cathodic reaction rates than the UFG coating during the corrosion process. Electrochemical parameters of nanocrystalline and ultra-fine grained coatings are listed in Table 8.2. The corrosion current densities (i_{corr}) were evaluated from the extrapolation of the cathodic Tafel lines to the OCP.

Table 8.2 Electrochemical parameters of nanocrystalline and ultra-fine-grained Zn-Sn coatings in 0.63 M NaCl at 21 ± 1°C after 1 hour of immersion.

Type of coating	E_{corr} (V)	i_{corr} (μA cm^{-2})
Nanocrystalline	-1.374 ± 0.0057	75.69 ± 32
Ultra-fine-grained	-1.341 ± 0.0096	84.93 ± 9.5

Based on electrochemical parameters, specifically (i_{Corr}), it is noted that although corrosion potential of NC coating was slightly more negative than UFG, the NC coating showed better protective properties than the UFG coating. These results are in agreement with the literature available on the effects of grain size on the corrosion properties of zinc coatings in 3.5 wt% in NaCl solution [241].

Two major (I and II) and one minor (III) peaks were observed at the polarization curves of NC and UFG coatings (Fig. 8.3). Based on table of electromotive force of metals (EMF series) versus standard hydrogen electrode [48], zinc is more active than tin and starts oxidation at more negative values. Hence, the first peak (I in Fig. 8.3) was attributed to zinc oxidation, and the second peak (II in Fig. 8.3) to tin (II) oxidation. The third peak (III in Fig. 8.3) was attributed to Sn^{4+} oxidation. According to the EMF series, Sn^{4+} oxidation occurs at more noble potential than Sn^{2+} and normally at positive potential versus standard hydrogen electrode [48].

Separate oxidation peaks of zinc and tin during the potentiodynamic polarization have also been reported in literature [242, 243].

Before discussing the reaction which occurred through polarization measurements from point A to F in Fig 8.3 sequentially, it should be reminded that Zn and Sn have very low solubility in each other (Fig. 2.16). Elemental mapping of the Zn and Sn in NC and UFG coatings showed that they were dispersed across the surface of the coatings with some areas richer in Sn (discussed in Chapter 7).

From point A to B in Fig. 8.3, water and oxygen molecules react with electrons and release hydroxyl. This is basically the cathodic reaction and leads to the increase of pH. For the equal values of potential, cathodic reaction of NC coating occurred at lower current densities than UFG, which indicated smaller cathodic reaction rate occurring for NC than UFC.

$$\frac{1}{2}\,O_2 + H_2O + 2e^- \rightarrow 2\,OH^- \qquad (8\text{-}2)$$

Based on the galvanic series of metals in seawater [48], zinc and tin form a galvanic couple in corrosive environment which lead to selective dissolution of the active metal (zinc in Zn-Sn alloy) in corrosive condition. Therefore, based on literatures [244-246] corrosion of the Zn-Sn alloy starts preferably in anodic areas (close vicinity to Sn rich areas) by dissolution of zinc through the following equation;

$$Zn \rightarrow \ Zn^{2+} + 2\ e^{-} \tag{8-1}$$

This is the anodic reaction occurring in the active zone of B to C of the curve (Fig. 8.3) and leads to the weight loss.

Apart from zinc oxidation, some other reaction can also occur and different types of corrosion products may form. Zinc cations (Zn^{2+}) can react with hydroxyl anion due to increase of pH and produce zinc hydroxide.

$$Zn^{2+}\ + 2\ (OH^{-}) \rightarrow Zn\ (OH)_2 \tag{8-3}$$

If dehydration occurs for this product zinc oxide can also precipitate.

$$Zn\ (OH)_2 \rightarrow ZnO + H_2O \tag{8-4}$$

It is also possible that Cl^- from the corrosive environment moves towards zinc dissolution sites and lead to the formation of zinc hydroxychloride (simonkolleite).

$$4\ ZnO\ (S) + Zn^{2+}(aq) + 5\ H_2O + 2\ Cl^{-}\ (aq) \rightarrow \ Zn_5(OH)_8Cl_2.H_2O\ (S) \tag{8-5}$$

EDS evaluation of the corrosion products after OCP measurments in 0.63 M NaCl solution showed only a few percentages of Cl^- in the corrosion products (0.07 wt%) which indicated that no simonkolleite was excited in the product. The small percentage of Cl^- in the product was due to anodic dissolution of zinc which imposed a positive charge to the surface and lead to the attraction of Cl^- anion to the surface of the products. The high concentration of oxygen detected by EDS evaluation showed that products were mainly ZnO.

Oxidation of tin at peak II (point C) occurs through the following equations:

$$Sn + 2OH^{-} \rightarrow Sn(OH)_2\ \ + 2\ e^{-} \tag{8-6}$$

$$Sn(OH)_2 \rightarrow SnO + H_2O \tag{8-7}$$

With the continuation of corrosion (point D to E) the following reaction occurred at peak (III) [242].

$$Sn(OH)_2 + 2\ OH^{-} \rightarrow Sn(OH)_4 + 2e^{-} \tag{8-8}$$

$$SnO +\ H_2O + 2\ OH^{-} \rightarrow Sn\ (OH)_4\ + 2e^{-} \tag{8-9}$$

SnO_2 will form as result of the dehydration of this product by the following equation:

$$Sn(OH)_4 \rightarrow SnO_2 + 2\ H_2O \tag{8-10}$$

Comparison of the potential of peak (II) in NC (-1.103 ± 0.015 V) and UFG (-1.156 ± 0.06 V), and peak (III) in NC (0.127 ± 0.085 V) and UFG (-0.095 ± 0.22 V) shows that corrosion products on the surface of NC coating form a more effective barrier which shifts this oxidation reaction to more positive potentials.

The above results showed that corrosion properties of NC were improved in comparison with UFG coatings.

8.4 Surface characterization of the corroded coatings

In order to investigate the corrosion process of NC and UFG coatings in 0.63 M NaCl solution at 21 ± 1°C, fresh samples of each coating were prepared and the potentiodynamic polarization were conducted following the same routine described in sub-chapter 3.4.3.3. However, the experiments were terminated at each of points 1, 2 and 3 (see Fig. 8.4). Then retrieved samples were taken out from the corrosion cell and slightly washed to prevent crystallization of NaCl on the surface of the working electrode and then analyzed by SEM. Fig. 8.4 shows the points on the complete polarization curves where the experiments were terminated to give an idea of the progression of corrosion.

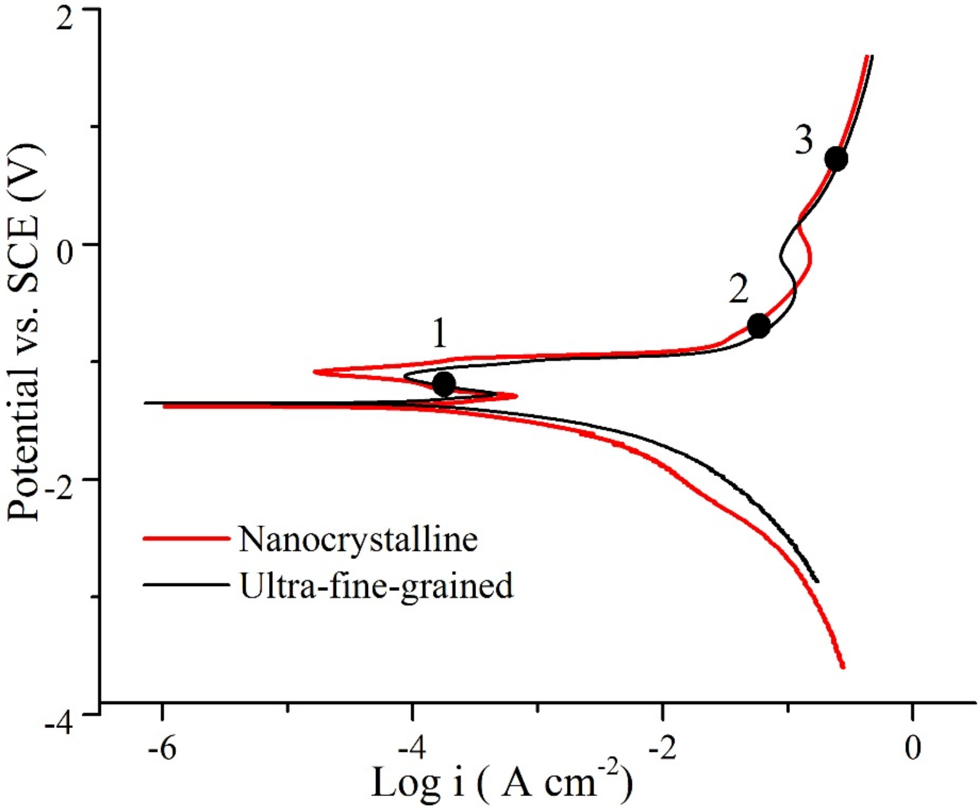

Fig. 8.4 Polarization curves of nanocrystalline and ultra-fine-grained Zn-Sn coatings showing the terminated points.

The surface morphology of NC and UFG coatings after termination of experiment at point 1 in Fig. 8.4 is presented in Fig. 8.5.

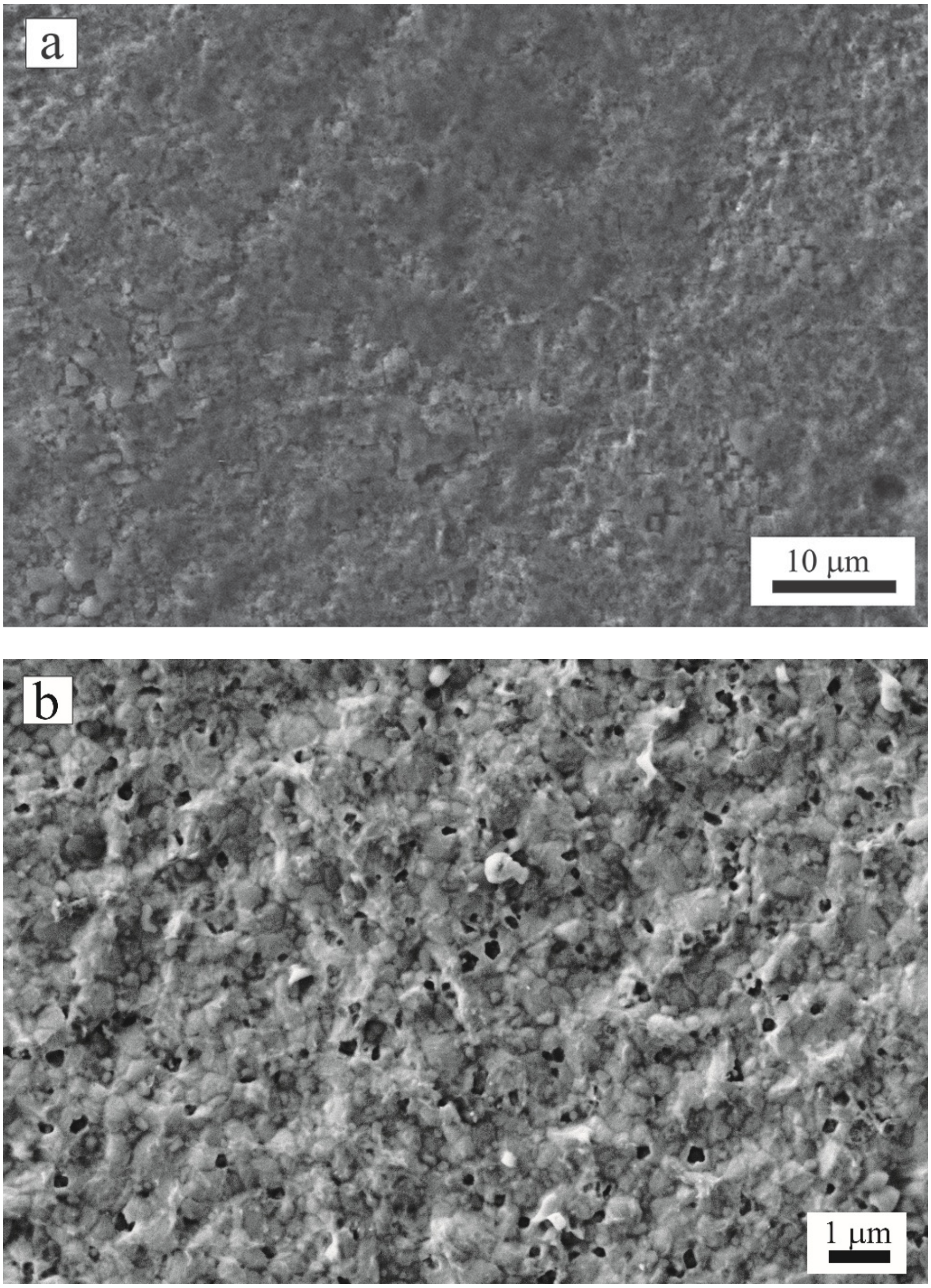

Fig. 8.5 SEM images of (a) nanocrystalline (b) ultra-fine-grained Zn-Sn coating after termination of experiment at point 1 in Fig. 8.4.

After termination of experiments at point 1, the surface of NC coating (Fig. 8.5 (a)) was covered with a thin layer of corrosion product and had a few pin holes on it. While the surface of the UFG (Fig. 8.5 (b)) was partially covered with corrosion products and had small holes which were distributed across the surface of the coating. At point 1 in Fig 8.4, both NC and UFG coatings have undergone dezincification (see sub-chapter 8.3). Selective dissolution of zinc occurred due to galvanic couple of zinc and tin and started at areas which were richer in tin. Therefore, pin holes were expected for both coatings. However, due to the higher volume fraction of grain boundaries in NC coating, zinc corrodes evenly across the surface in comparison with UFG coating, and this leads to the formation of a passivation layer (Fig. 8.3 (b)). In UFG coating, selective dissolution of zinc was more localized and resulted in the formation of small holes.

The surface morphology of the coatings after termination of experiments at point 2 of Fig. 8.4 is presented in Fig. 8.6.

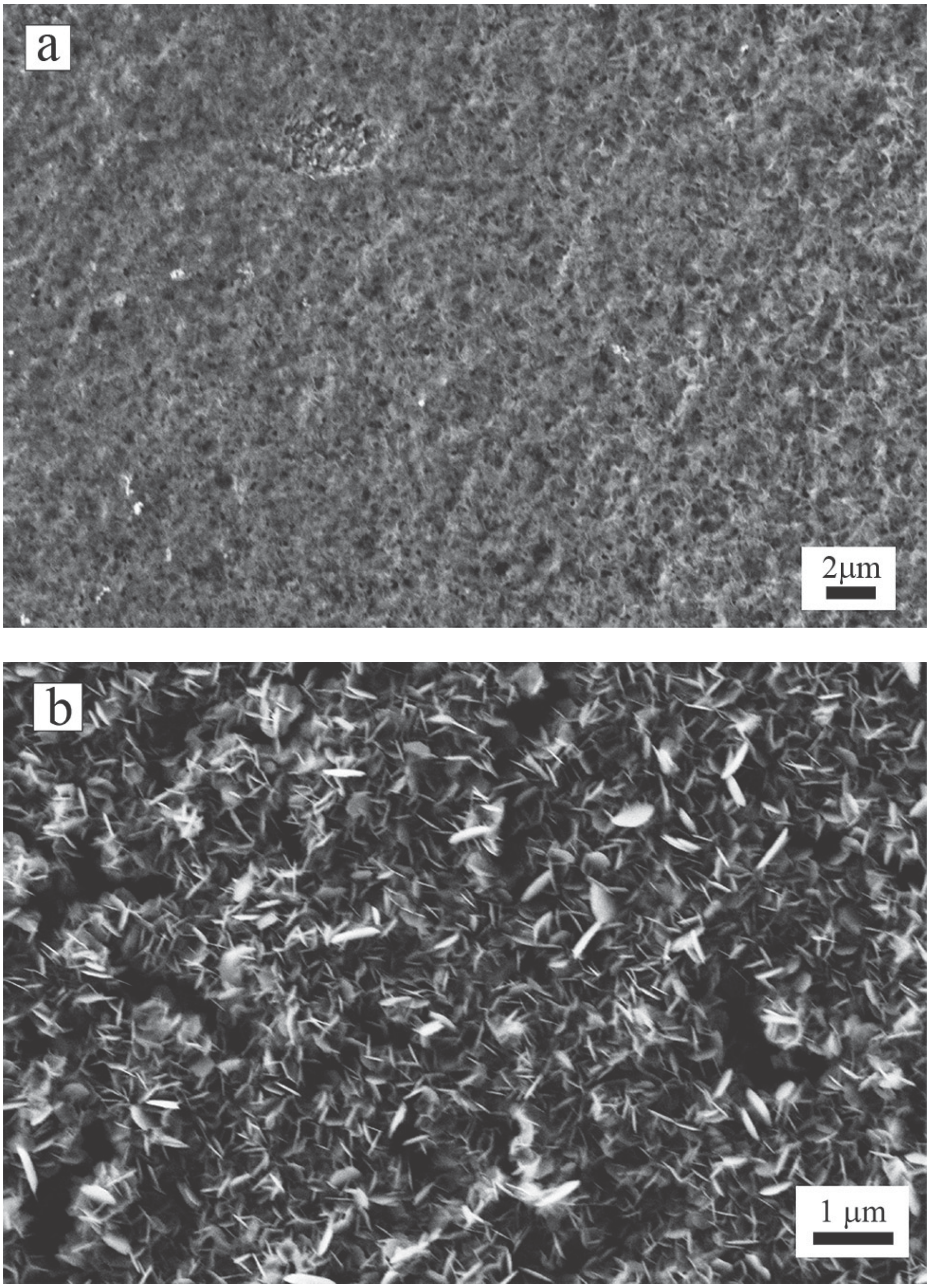

Fig. 8.6 SEM images of (a) nanocrystalline and (b) ultra-fine-grained coatings after polarization test was terminated at point 2 of Fig. 8.4.

At point 2 in Fig. 8.4, both zinc and tin have been corroded, but the surface of NC coating is covered with a fine and uniform layer of corrosion products, whereas corrosion products of the UFG coatings consisted of hexagonal platelets which were orientated perpendicularly to the surface of electrode. The high volume fraction of grain boundaries in NC coatings lead to the formation of a fine and uniform corrosion microstructure as each boundary act as a high energy area for the initiation of corrosion. However, in UFG coatings, micro-galvanic cell between zinc and tin phases, as well as surface defects act as high energy areas for the initiation of corrosion. As none of the surface defects, nor of the tin rich areas were uniformly dispersed across the surface, the corrosion products were also not uniformly dispersed across the surface in comparison with the NC coatings.

The surface morphology of the coatings after termination of experiments at point 3 is presented in Fig 8.7.

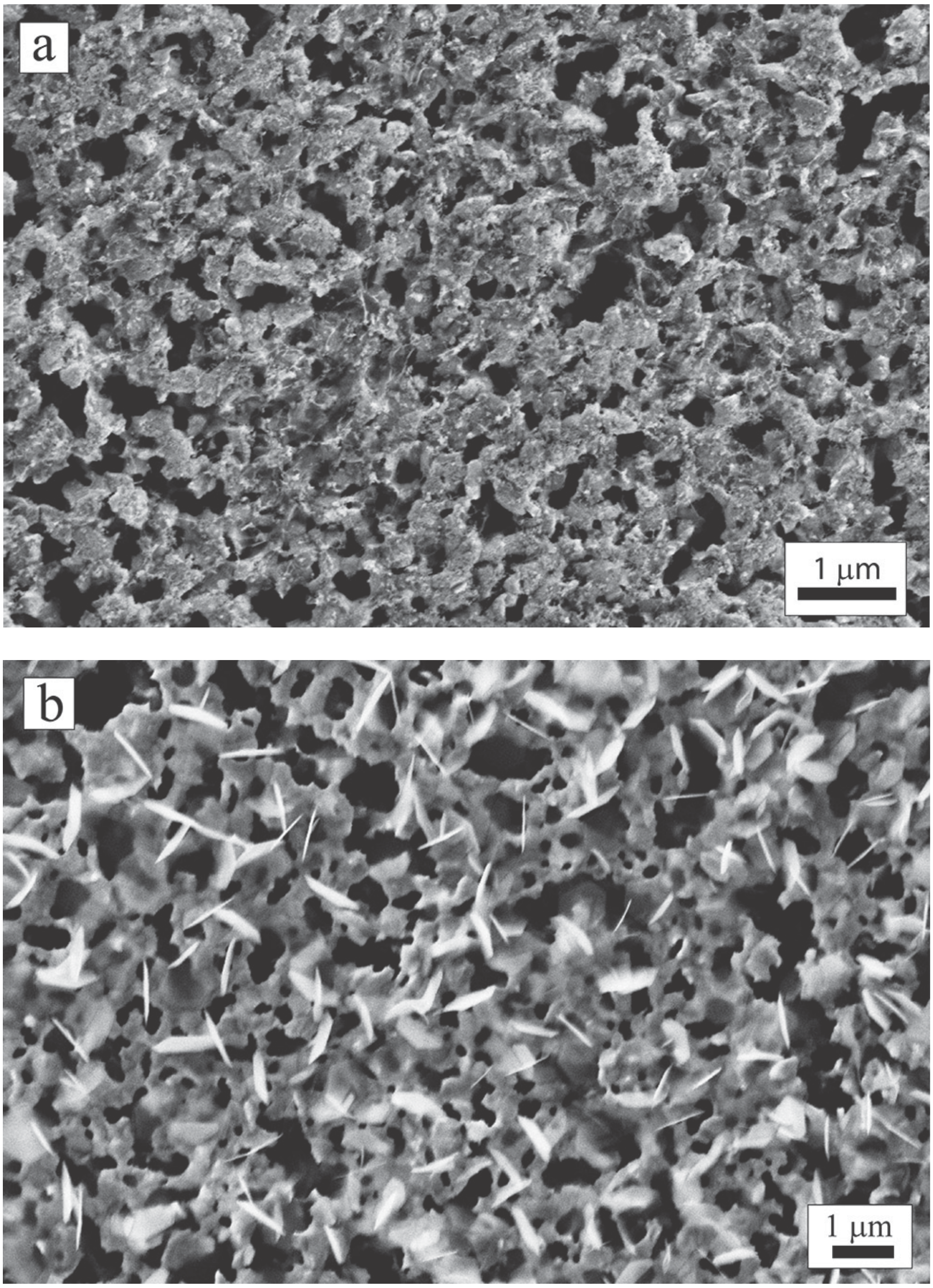

Fig. 8.7 SEM images of (a) nanocrystalline and (b) ultra-fine-grained coatings after polarization test was terminated at point 3 of Fig. 8.4.

Both NC and UFG coatings showed a porous structure after terminating polarization test at point 3. However, the UFG coating was more porous. The interesting point is that grains of NC coating are covered with corrosion products but the UFG grains just have small amount of corrosion products attached to them.

The formation of holes or pinholes is not only due to the selective dissolution of zinc at the anodic region of the surface (close vicinity to tin rich area) (Fig. 8.5), but also to the orientation of corrosion products in relation to the coatings. Perpendicular direction of corrosion products in relation to the surface leads to only small coverage of the non-corroded surface by the corrosion product and therefore leads to the easier access of corrosive media down to the sub-layers and substrate.

On the other hand, holes on the surface and inside the coatings can also form due to the type of corrosive environment (3.5 wt% of NaCl). It has been reported [247-249] that anions of Cl^- can absorb and penetrate towards the inside of metal/ oxide interface via grain boundaries of the oxide layer, and will locally breakdown the coating or passivated layer, leading to pitting or re-passivation .

Fig. 8.8 shows a lower magnification image of the surface of UFG coating after the experiment was terminated at point 3. Multiple cracks were produced and propagated across the surface (the circled area shows the cracks).

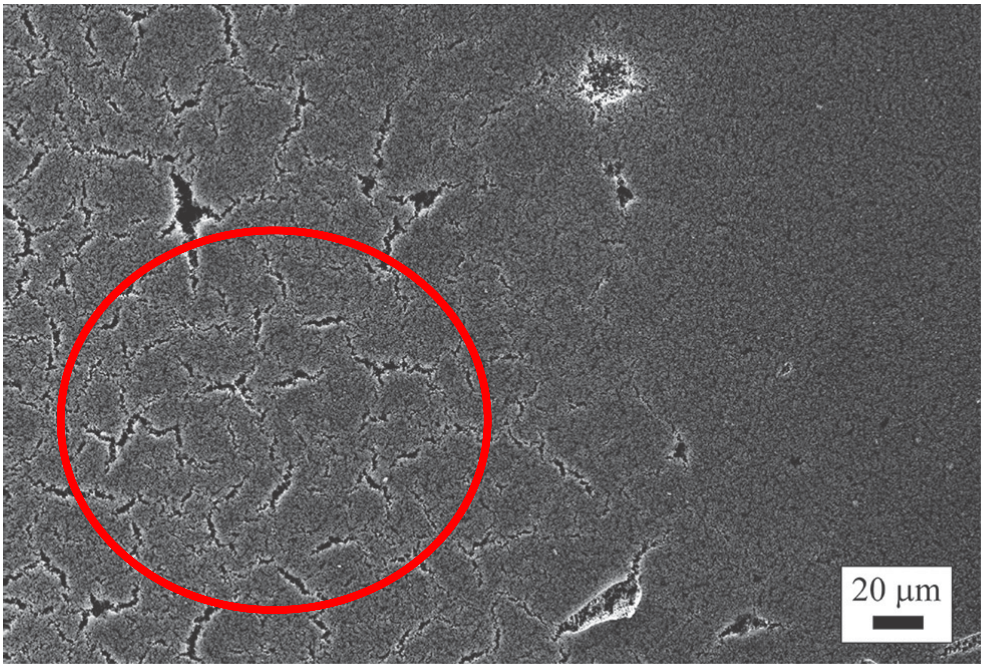

Fig. 8.8 SEM image of the ultra-fine-grained Zn-Sn coating after polarization test was terminated at point 3 of Fig. 8.4. Red circle shows an area with multiple cracks.

Tin and zinc oxide can behave like n-type semiconductors and induce a positive charge at the interface between the substrate and the oxide layer, thus enhancing the absorption of chloride and hydroxide anions to the coating. On the other hand, Cl^- and cations of zinc (Zn^{2+}) and tin (Sn^{2+}) combine together to form zinc and tin chloride complexes respectively. Such a mechanism leads to the formation of cracks. Increase in complex formation increases the internal stresses and promotes the localized breakdown and initiation of pits.

The surface morphology of the coatings after performing a complete polarization test is presented in Fig. 8.8.

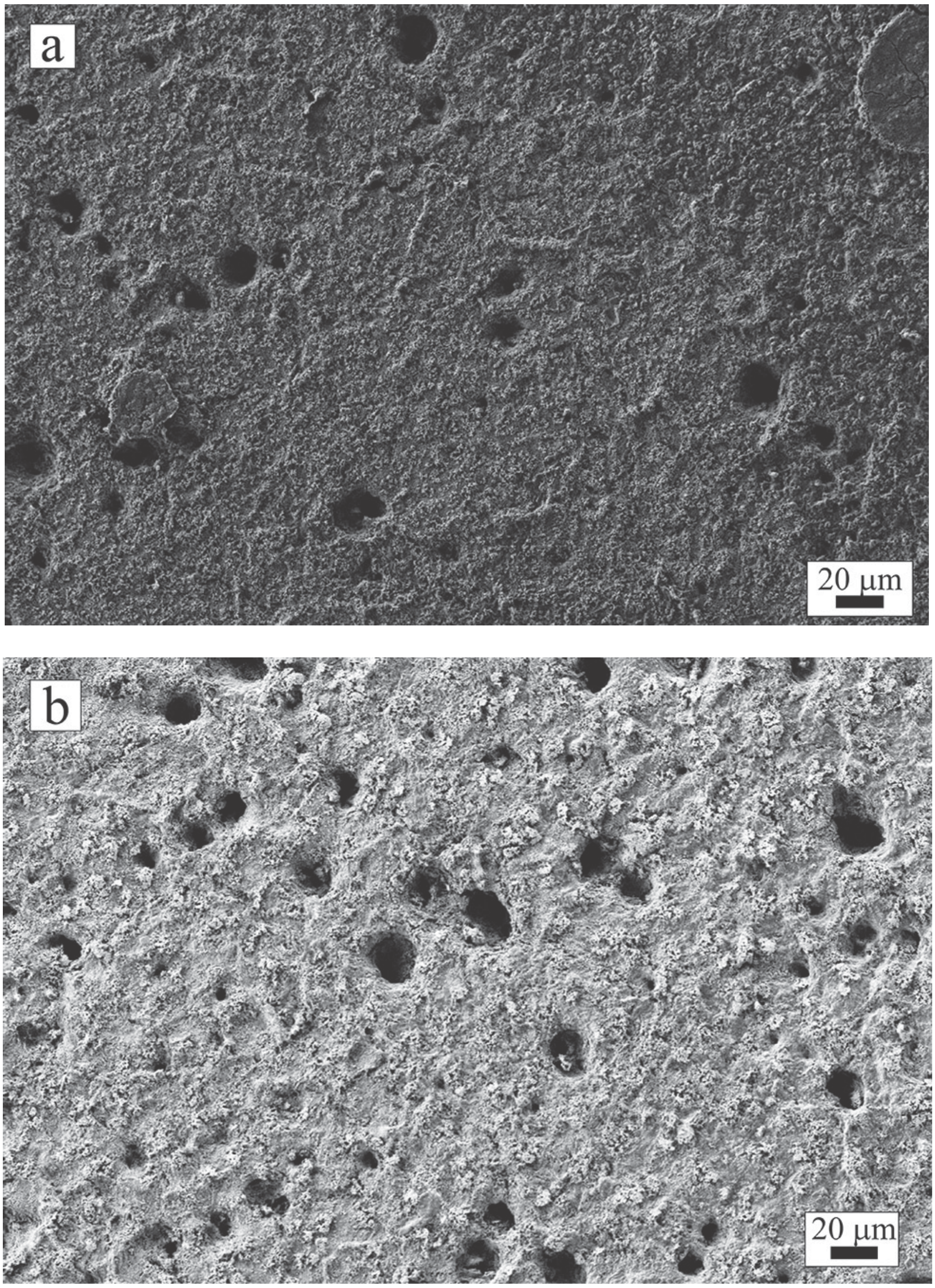

Fig. 8.9 SEM images of (a) nanocrystalline and (b) ultra-fine-grained Zn-Sn coatings after a completed polarization test.

Comparison of the SEM images in Fig. 8.9 (a) and (b) shows that the number of pits is greater for the UFG coating than the NC one. This results clearly shows improved corrosion resistance of Nanocrystalline Zn-Sn in comparison to UFG structure.

8.5 Summary

Corrosion properties of nanocrystalline and ultra-fine-grained coatings were studied and compared in this chapter.

Although, nanocrystalline coating exhibited lower corrosion potential than ultra-fine coatings, they corrode at a lower rate than ultra-fine-grained coatings.

Corrosion of Zn-Sn alloys starts with the selective dissolution of zinc in the alloy.

Corrosion products of NC coatings have better barrier properties than UFG coatings as they are more compact and can prevent corrosion better.

Chapter 9

Conclusions and Future work

9.1 Conclusions

This thesis started with a benchmarking of commercial coatings of self-piercing rivet which are currently in use by automotive industry. Zinc-low content tin alloy are amongst the promising coatings for self-piercing rivets. Due to specific characteristics of nanocrystalline material and the fact that corrosion properties of this nano grain material is a controversial issue, fabrication of nanocrystalline zinc-tin alloy was selected as a plausible way of eliminating defects such as fretting and corrosion involved with SPR. Fabrication of nanocrystalline zinc-low content tin was conducted by exploring various environmental friendly electrolytes and gluconate electrolyte were selected amongst them. However, fabrication of nanocrystalline structure was not possible without using various additives. A systematic study on the effects of organic additives led to fabrication of nanocrystalline zinc-tin in the presence of PEG and CTAB. To provide a clear idea of the effects of microstructure and grain refinement down to nano levels mechanical and corrosion properties of nanocrystalline and ultra-fine-grained zinc-tin coatings were evaluated and studied. These studies were concluded as follows:

9.1.1 Benchmarking of SPR rivets

Rivets with Zn-Sn, Almac and aluminum coatings have been used to join magnesium sheets by laser assisted self-pierce riveting (LSPR). Possible effects of laser assisted self-pierce riveting on the rivet’s coating were examined by characterizing the rivets coating before and after joining of Mg sheets. It was found that, failure such as peeling was not observed for Zn-Sn and aluminum coatings of the self- piercing rivets during the laser assisted self-pierce riveting. However, thickness of the mechanically plated Zn-Sn coatings increased at the top sheet (25%-30% of the original thickness (20 μm)) and decreased at the bottom sheet (up to 75% reduction to the original thickness) due to the joining force. In contrast, electroplated aluminum coating appeared not to be affected by the joining process and thickness of the coating remained unchanged (20-25 μm) during the riveting process.

9.1.2 Electrodeposition of nanocrystalline zinc from sulfate-gluconate bath

Electrodeposition of zinc from sulfate and sulfate-gluconate electrolytes in the presence and absence of additives such as Polyethylene glycol (PEG), hexadecyltrimethylammonium bromide (CTAB) and thiourea has been investigated. The analysis of the distribution of zinc (II) species showed that $ZnSO_4$ was the main species in both sulfate and sulfate-gluconate electrolytes. Cyclic voltammetry and chronoamperometry, along with surface morphology and XRD analyses confirmed that gluconate complex agent played a predominant role on the electrodeposition of zinc from sulfate-gluconate baths. Additives changed the electrochemical responses of the electrolytes and the preferred orientation of the grains. Their synergistic effects produced nanocrystalline zinc plated structure from both sulfate and sulfate-gluconate electrolyte systems. However, the role of depositing ligand on the surface morphology and preferred orientation became negligible as the number of additives increased in the plating bath.

9.1.3 Electrodeposition of nanocrystalline zinc-tin alloy

Electrodeposition of zinc-low content tin alloy from sulfate-gluconate electrolytes with additives was investigated. Analysis of distribution of tin (II) species in the absence of gluconate showed that $SnCl_2$ and $Sn(OH)_2$ are the predominant species at the pH range of this study (4.3-4.7). In the presence of gluconate, $Sn(GH)_4^+$ was the main species in the alloy electrolyte. Distribution of zinc (II) species in the absence of gluconate showed that $ZnSO_4$ was the predominant species at the pH range of this study (4.3-4.7). In the presence of gluconate $ZnSO_4$ was the main species in the alloy electrolyte.

Cyclic voltammetry of the single metal bath of zinc and tin in the absence and presence of gluconate showed that gluconate moved the deposition potential of tin to more negative values and deposition potential of zinc to more positive values and thereby facilitate deposition of the zinc-tin alloy.

Effects of various current on-time and current off-time on the surface morphology and composition of the deposit was investigated and T_{ON} = 5 ms and To_{FF} = 7 ms was chosen for the deposition of alloy in the presence of additives.

Cyclic voltammetry of the alloy bath in the presence of additives such as thiourea, PEG and CTAB showed that adsorption of additive to the surface of electrode shifts the deposition potential to more negative values due to the blocking of the surface of glassy carbon electrode. Inhibitive effects of the additives increased with either the increase in their concentration or due to their synergic effects in the case of their combination.

Comparison of the cyclic voltammetry of the alloy bath containing CTAB and various concentration of PEG (400) with PEG (2050) suggested that inhibitive effects of CTAB and PEG on alloy deposition increase with increasing molecular weight of PEG and/or its concentration. Surface morphology of deposits exhibited a fine and more uniform structure in the presence of PEG 2050 than PEG 400. Nanocrystalline Zn-Sn alloy coating was produced from the bath containing 1 mM of CTAB and 1gr/lit PEG 2050. X-ray diffraction pattern showed peaks of hexagonal zinc and tetragonal tin and confirmed production of a mechanical type of zinc-tin alloy.

9.1.4 Mechanical properties of nanocrystalline zinc-tin alloys

Physical and mechanical properties of nanocrystalline (NC) and ultra-fine-grained (UFG) Zn-Sn coatings were evaluated and results exhibited superior mechanical properties of nanocrystalline structure than ultra-fine-grained coatings. Hardness of the Zn-Sn coatings improved from 209.4 ± 65.8 MPa at ultra-fine-grained coatings to 532.3 ± 140 MP at nanocrystalline coating due to the grain refinement, while the modulus of elasticity remained unchanged. Grain refinement also had also effect on the coefficient of friction and has a lower value for a nanocrystalline structure compared with an ultra-fine-grain structure. Wear volume decreased with grain refinement from 13.4 ± 3.7 μm^3 in UFG to 4.76 ± 1.62 μm^3 in NC based on the Archard's law.

9.1.5 Corrosion properties of nanocrystalline zinc-tin alloys

Corrosion properties of nanocrystalline and ultra-fine-grained coatings were studied. Corrosion of Zn-Sn alloys in this study started with the selective dissolution of zinc in the alloy. Although, nanocrystalline coating exhibited lower corrosion potential than ultra-fine coatings they corroded with a smaller rate than ultra-fine-grained coatings.

Corrosion products of NC coatings have better barrier properties than UFG coatings as they are more compact and can reduce corrosion better.

9.2 Future Work

Several methods applied for the characterization of the fabricated nanocrystalline zinc-tin alloys. However, the following efforts would provide a better understanding of how these coatings work in real industry.

a) To perform salt-spray test and examine corrosion properties of these coatings under various corrosive media.

b) To apply these coatings to a bare steel rivet and use it for joining Al sheet. Then perform a full examination of the coating after joining process.

c) To perform an immersion corrosion for the joints which are coated by nanocrystalline zinc-tin coatings.

d) To add TiO_2 or Al_2O_3 nano powder to the plating bath and produce nanocomposite TiO_2-Zn-Sn or Al_2O_3-Zn-Sn coating and to evaluate the properties of the coating. Fig. 9.1 shows the SEM image of the initial stages of this study, conducted for the fabrication of TiO_2-Zn-Sn nanocomposite coatings. TiO_2 nanoparticles were deposited at grain boundaries of Zn-Sn coating. However, the grain size was larger than our expectation. Therefore further studies on the evaluation of the plating parameter is essential.

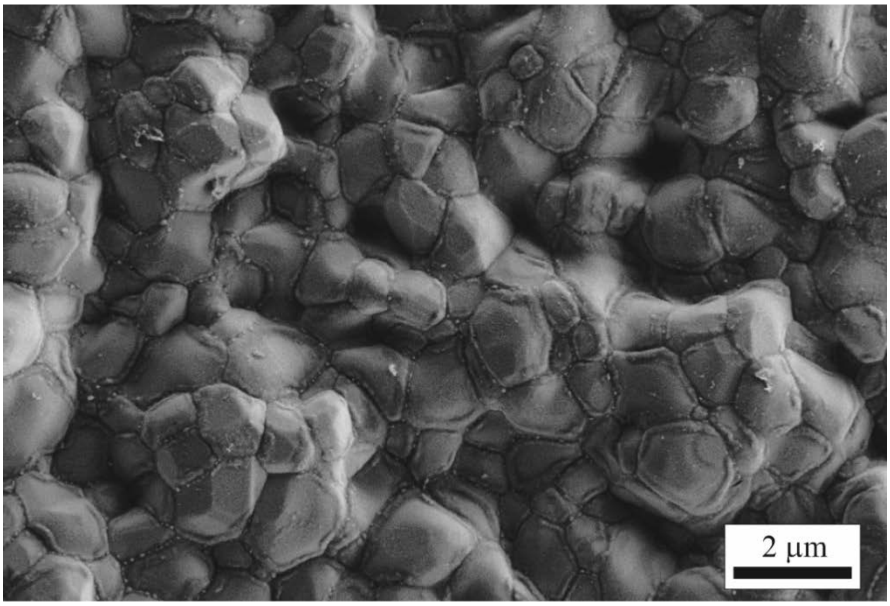

Fig. 9.1 SEM image showing deposited TiO_2 at grain boundaries of Sn-Zn alloy.

e) To evaluate fabrication of nanocrystalline zinc-tin coatings form organic electrolytes instead of aqueous electrolytes to eliminate the effects of hydrogen evolution and diminish the surface porosities which are inevitable for the deposition of metallic alloys from aqueous electrolytes.

List of References

[1] F. a. Drake, "Global Warming,": Hoboken : Taylor and Francis, 2014.

[2] A. Mayyas, A. Qattawi, M. Omar, and D. Shan, "Design for sustainability in automotive industry: A comprehensive review,"Renewable and Sustainable Energy Reviews, vol. 16, pp. 1845-1862, 2012.

[3] A. Chrysanthou and X. Sun, "Self-Piercing Riveting: Properties, Processes and Applications", in Self-Piercing Riveting: Properties, Processes and Applications, pp. 1-214. 2014.

[4] C. B. Elliott Iii and D. W. Hoeppner, "The importance of wear and corrosion on the fretting fatigue behavior of two aluminum alloys," Wear, vol. 236, pp. 128-133, 1999.

[5] L. Huang, J. Bonnen, J. Lasecki, H. Guo, and X. Su, "Fatigue and fretting of mixed metal self-piercing riveted joint," International Journal of Fatigue, vol. 83, pp. 230-239, 2016.

[6] S. C. Tjong and H. Chen, "Nanocrystalline materials and coatings," Materials Science and Engineering R: Reports, vol. 45, pp. 1-88, 2004.

[7] K. S. Kumar, H. Van Swygenhoven, and S. Suresh, "Mechanical behavior of nanocrystalline metals and alloys," Acta Materialia, vol. 51, pp. 5743-5774, 2003.

[8] V. Afshari and C. Dehghanian, "Effects of grain size on the electrochemical corrosion behaviour of electrodeposited nanocrystalline Fe coatings in alkaline solution," Corrosion Science, vol. 51, pp. 1844-1849, 2009.

[9] S. K. Ghosh, G. K. Dey, R. O. Dusane, and A. K. Grover, "Improved pitting corrosion behaviour of electrodeposited nanocrystalline Ni-Cu alloys in 3.0 wt.% NaCl solution," Journal of Alloys and Compounds, vol. 426, pp. 235-243, 2006.

[10] R. K. Gupta and N. Birbilis, "The influence of nanocrystalline structure and processing route on corrosion of stainless steel: A review," Corrosion Science, vol. 92, pp. 1-15, 2015.

[11] D. H. Jeong, F. Gonzalez, G. Palumbo, K. T. Aust, and U. Erb, "The effect of grain size on the wear properties of electrodeposited nanocrystalline nickel coatings," Scripta Materialia, vol. 44, pp. 493-499, 2001.

[12] Q. Li, Z. Feng, J. Zhang, P. Yang, F. Li, and M. An, "Pulse reverse electrodeposition and characterization of nanocrystalline zinc coatings," RSC Advances, vol. 4, pp. 52562-52570, 2014.

[13] L. Liu, Y. Li, and F. Wang, "Electrochemical Corrosion Behavior of Nanocrystalline Materials; a Review," Journal of Materials Science & Technology, vol. 26, pp. 1-14, 2010.

[14] K. M. S. Youssef, C. C. Koch, and P. S. Fedkiw, "Improved corrosion behavior of nanocrystalline zinc produced by pulse-current electrodeposition," Corrosion Science, vol. 46, pp. 51-64, 2004.

[15] U. Erb, "Electrodeposited nanocrystals: Synthesis, properties and industrial applications," Nanostructured Materials, vol. 6, pp. 533-538, 1995.

[16] M. Bhardwaj, K. Balani, R. Balasubramaniam, S. Pandey, and A. Agarwal, "Effect of current density and grain refining agents on pulsed electrodeposition of nanocrystalline nickel," Surface Engineering, vol. 27, pp. 642-648, 2011.

[17] M. S. Chandrasekar, Shanmugasigamani, and P. Malathy, "Synergetic effects of pulse constraints and additives in electrodeposition of nanocrystalline zinc: Corrosion, structural and textural characterization," Materials Chemistry and Physics, vol. 124, pp. 516-528, 2010.

[18] S. M. Chavan, M. K. Babrekar, S. S. More, and K. M. Jadhav, "Structural and optical properties of nanocrystalline Ni-Zn ferrite thin films," Journal of Alloys and Compounds, vol. 507, pp. 21-25, 2010.

[19] I. Gurrappa and L. Binder, "Electrodeposition of nanostructured coatings and their characterization - A review," Science and Technology of Advanced Materials, vol. 9, 2008.

[20] M. Li, S. Luo, Y. Qian, W. Zhang, L. Jiang, and J. Shen, "Effect of additives on electrodeposition of nanocrystalline zinc from acidic sulfate solutions," Journal of the Electrochemical Society, vol. 154, pp. D567-D571, 2007.

[21] M. C. Li, L. L. Jiang, W. Q. Zhang, Y. H. Qian, S. Z. Luo, and J. N. Shen, "Electrodeposition of nanocrystalline zinc from acidic sulfate solutions containing thiourea and benzalacetone as additives," Journal of Solid State Electrochemistry, vol. 11, pp. 549-553, 2007.

[22] C. Ma, S. Wang, and F. C. Walsh, "The electrodeposition of nanocrystalline Cobalt-Nickel-Phosphorus alloy coatings: A review," Transactions of the Institute of Metal Finishing, vol. 93, pp. 275-280, 2015.

[23] C. Ma, S. C. Wang, and F. C. Walsh, "Electrodeposition of nanocrystalline nickel-cobalt binary alloy coatings: A review," Transactions of the Institute of Metal Finishing, vol. 93, pp. 104-112, 2015.

[24] H. B. Muralidhara and Y. Arthoba Naik, "Electrochemical deposition of nanocrystalline zinc on steel substrate from acid zincate bath," Surface and Coatings Technology, vol. 202, pp. 3403-3412, 2008.

[25] J. W. McAuley, "Global Sustainability and Key Needs in Future Automotive Design," Environmental Science and Technology, vol. 37, pp. 5414-5416, 2003.

[26] M. A. Omar, The Automotive Body Manufacturing Systems and Processes, 2011.

[27] A. Mayyas, Q. Shen, A. Mayyas, M. abdelhamid, D. Shan, A. Qattawi, et al., "Using Quality Function Deployment and Analytical Hierarchy Process for material selection of Body-In-White," Materials and Design, vol. 32, pp. 2771-2782, 2011.

[28] K. Mori, T. Kato, Y. Abe, and Y. Ravshanbek, "Plastic joining of ultra high strength steel and aluminium alloy sheets by self piercing rivet," CIRP Annals - Manufacturing Technology, vol. 55, pp. 283-286, 2006.

[29] M. Fu and P. K. Mallick, "Fatigue of self-piercing riveted joints in aluminum alloy 6111," International Journal of Fatigue, vol. 25, pp. 183-189, 2003.

[30] E. Atzeni, R. Ippolito, and L. Settineri, "Experimental and numerical appraisal of self-piercing riveting," CIRP Annals - Manufacturing Technology, vol. 58, pp. 17-20, 2009.

[31] T. A. Barnes and I. R. Pashby, "Joining techniques for aluminum spaceframes used in automobiles. Part II - adhesive bonding and mechanical fasteners," Journal of Materials Processing Technology, vol. 99, pp. 72-79, 2000.

[32] J. Varis, "Economics of clinched joint compared to riveted joint and example of applying calculations to a volume product," Journal of Materials Processing Technology, vol. 172, pp. 130-138, 2006.

[33] N. Bonde and S. Grange-Jansson, "Self-piercing riveting in high strength steel-a way to increase fatigue life," Advanced Technologies & Process, 1996.

[34] L. Han, Y. K. Chen, A. Chrysanthou, and J. M. O'Sullivan, "Self-Pierce Riveting: A New Way for Joining Structures," ASME Conference Proceedings, vol. 2002, pp. 123-127, 2002.

[35] X. He, I. Pearson, and K. Young, "Self-pierce riveting for sheet materials: State of the art," Journal of Materials Processing Technology, vol. 199, pp. 27-36, 2008.

[36] W. S. Miller, L. Zhuang, J. Bottema, A. J. Wittebrood, P. De Smet, A. Haszler, et al., "Recent development in aluminium alloys for the automotive industry," Materials Science and Engineering A, vol. 280, pp. 37-49, 2000.

[37] L. Han, A. Chrysanthou, and J. M. O'Sullivan, "Fretting behaviour of self-piercing riveted aluminium alloy joints under different interfacial conditions," Materials & Design, vol. 27, pp. 200-208, 2006.

[38] L. Han, A. Chrysanthou, and K. W. Young, "Mechanical behaviour of self-piercing riveted multi-layer joints under different specimen configurations," Materials & Design, vol. 28, pp. 2024-2033, 2007.

[39] Y. Xu, "Effects of factors on physical attributes of self-piercing riveted joints," Science and Technology of Welding and Joining, vol. 11, pp. 666-671, 2006.

[40] R. Porcaro, M. Langseth, S. Weyer, and H. Hooputra, "An experimental and numerical investigation on self-piercing riveting," International Journal of Material Forming, vol. 1, pp. 1307-1310, 2008.

[41] C. G. Pickin, K. Young, and I. Tuersley, "Joining of lightweight sandwich sheets to aluminium using self-pierce riveting," Materials and Design, vol. 28, pp. 2361-2365, 2007.

[42] Y. Durandet, R. Deam, A. Beer, W. Song, and S. Blacket, "Laser assisted self-pierce riveting of AZ31 magnesium alloy strips," Materials & Design, vol. 31, Supplement 1, pp. S13-S16, 2010.

[43] M. M. Abou-Krisha, "Electrochemical studies of zinc-nickel codeposition in sulphate bath," Applied Surface Science, vol. 252, pp. 1035-1048, 2005.

[44] A. Chrysanthou, "Fatigue behaviour of self-piercing riveted joints," in Self-Piercing Riveting: Properties, Processes and Applications, ed, 2014, pp. 33-40.

[45] F. J. Fabri Miranda, O. E. Barcia, O. R. Mattos, and R. Wiart, "Electrodeposition of Zn-Ni alloys in sulfate electrolytes: I. Experimental approach," Journal of the Electrochemical Society, vol. 144, pp. 3441-3449, 1997.

[46] P. K. Mallick and M. Fu, "Effect of process variables on the static and fatigue properties of self-piercing riveted joints in aluminum alloy 5754," Society of Automotive Engineers, SAE vol. 2001-01-0825, 2001.

[47] X. Sun, E. V. Stephens, and M. A. Khaleel, "Fatigue behaviors of self-piercing rivets joining similar and dissimilar sheet metals," International Journal of Fatigue, vol. 29, pp. 370-386, 2007.

[48] M. G. Fontana and N. D. Greene, Corrosion Engineering 3ed. New York: McGraw-Hill, 1986.

[49] A. Zaki, "Principles of Corrosion Engineering and Corrosion Control," ed: Butterworth-Heinemann, 2006, p. 673.

[50] J. I. Skar, "Corrosion and corrosion prevention of magnesium alloys," Materials and Corrosion, vol. 50, pp. 2-6, 1999.

[51] G. Song, B. Johannesson, S. Hapugoda, and D. StJohn, "Galvanic corrosion of magnesium alloy AZ91D in contact with an aluminium alloy, steel and zinc," Corrosion Science, vol. 46, pp. 955-977, 2004.

[52] R. P. Schlitt and R. K. Eschebach, "Material selection and corrosion protection for bi-metallic systems in automotive environments," in Proceedings of the 2nd Automotive Corrosion Prevention Conference., Dearborn, MI, USA, 1983, pp. 199-214.

[53] R. M. Howard and S. P. Sunday, "Corrosion performance of steel self-piercing rivets when used with aluminum components," Dearborn, MI, USA, 1983, pp. 73-79.

[54] A. Chrysanthou, "Corrosion behaviour of self-piercing riveted joints" in Self-Piercing Riveting: Properties, Processes and Applications, pp. 41-55, 2014

[55] L. Han, A. Chrysanthou, K. W. Young, and J. M. O'Sullivan, "Characterization of fretting fatigue in self-piercing riveted aluminium alloy sheets," Fatigue & Fracture of Engineering Materials & Structures, vol. 29, pp. 646-654, 2006.

[56] R. B. Waterhouse and A. Iwabuchi, "High temperature fretting wear of four titanium alloys," Wear, vol. 106, pp. 303-313, 1985.

[57] Y. K. Chen, L. Han, A. Chrysanthou, and J. M. O'Sullivan, "Fretting wear in self-piercing riveted aluminium alloy sheet," Wear, vol. 255, pp. 1463-1470, 2003.

[58] W. M. J. C. Verberne, "Zinc-cobalt alloy electrodeposition," in Technical Papers, Annual Technical Conference and Exhibition - Institute of Metal Finishing, 1985, pp. 49-62.

[59] J. S. F. V. Sekhon, "Fastener with protective metal-organic base coating," United States Patent 3983304, 1976.

[60] J. S. Sekhon, "Protective coating material," United States Patent 3/979/351, 1976.

[61] W. A. E. Schubert, K. Stephen , Parker, Eric G, Van Boven, Albert W., "Fastener coating and process," United States Patent, 1996.

[62] D. J. G. E. Kurr, "Corrosion resistant fasteners having an oil-free polyester top coating and method of manufacturing same," United States Patent US4206264 A , 1980.

[63] P. R. Roberge, "Handbook of Corrosion Engineering," ed: McGraw-Hill, 2000.

[64] H. ASM, Ed., ASM handbooks volume 5 :Surface Engineering online Materials Park, Ohio : ASM International, pp. 635-641, 2003.

[65] N. Zaki, "Trivalent chrome conversion coating for zinc and zinc alloys," Metal Finishing, vol. 105, pp. 425-435, 2007.

[66] B. Chatterjee, "Sherardizing," Metal Finishing, vol. 102, pp. 40-46, 2004.

[67] G. Allison, "Mechanical plating," Metal Finishing, vol. 93, 1995.

[68] G. M. Allison, "Mechanical plating," Metal Finishing, vol. 100, pp. 384-393, 2002.

[69] A. Satow, "Mechanical plating and galvanizing," Metal Finishing, vol. 105, pp. 342-349, 2007.

[70] Available:http://www.pfonline.com/articles/why-use-dip-spin-coating-technology

[71] J. G. Liu and C. W. Yan, "Electrochemical characteristics of corrosion behavior of organic/Dacromet composite systems pretreated with gamma-aminopropyltriethoxysilane," Surface and Coatings Technology, vol. 200, pp. 4976-4986, 2006.

[72] L. Jianguo, G. Gaoping, and Y. Chuanwei, "Enhancement of the erosion-corrosion resistance of Dacromet with hybrid SiO2 sol-gel," Surface and Coatings Technology, vol. 200, pp. 4967-4975, 2006.

[73] F. Gheno, "Clean processes - Alternatives to electroplating," Transactions of the Institute of Metal Finishing, vol. 74, pp. 7-10, 1996.

[74] H. Krause-Heringer, "Dacromat: A new corrosion protection for fasteners," Product Finishing (London), vol. 30, pp. 29-32, 1977.

[75] H. Hu, N. Li, and Y. Zhu, "Effect of chromate on the electrochemical behavior of sintered Zn-Al coating in seawater," Surface and Coatings Technology, vol. 202, pp. 5847-5852, 2008.

[76] D. Crotty, "Zinc alloy plating for the automotive industry," Metal Finishing, vol. 94, pp. 54-54, 1996.

[77] H. Ashassi-Sorkhabi, A. Hagrah, N. Parvini-Ahmadi, and J. Manzoori, "Zinc-nickel alloy coatings electrodeposited from a chloride bath using direct and pulse current," Surface and Coatings Technology, vol. 140, pp. 278-283, 2001.

[78] M. A. Pech-Canul, R. Ramanauskas, and L. Maldonado, "An electrochemical investigation of passive layers formed on electrodeposited Zn and Zn-alloy coatings in alkaline solutions," Electrochimica Acta, vol. 42, pp. 255-260, 1997.

[79] G. Roventi, R. Fratesi, R. A. Della Guardia, and G. Barucca, "Normal and anomalous codeposition of Zn-Ni alloys from chloride bath," Journal of Applied Electrochemistry, vol. 30, pp. 173-179, 2000.

[80] J. M. C. Mol, Z. F. Lodhi, A. Hovestad, L. t Hoen-Velterop, H. Terryn, and J. H. W. de Wit, "Electrodeposition and corrosion properties of zn-co and zn-co-fe alloy coatings," in Handbook of Material Science Research, ed, 2010, pp. 347-368.

[81] N. Boshkov, K. Petrov, S. Vitkova, S. Nemska, and G. Raichevsky, "Composition of the corrosion products of galvanic alloys Zn-Co and their influence on the protective ability," Surface and Coatings Technology, vol. 157, pp. 171-178, 2002.

[82] P. Marino, "British Patent ", 10, 133 1915.

[83] J. W. Cuthbertson and R. M. Angles, J. Electrochem. Soc., vol. 94, 1948.

[84] E. Budman and M. McCoy, "Tin-zinc plating," Metal Finishing, vol. 93, pp. 10-11,14-15, 1995.

[85] S. Dubent, M. L. A. D. Mertens, and M. Saurat, "Electrodeposition, characterization and corrosion behaviour of tin-20 wt.% zinc coatings electroplated from a non-cyanide alkaline bath," Materials Chemistry and Physics, vol. 120, pp. 371-380, 2010.

[86] C. C. Hu and C. K. Wang, "Effects of composition and reflowing on the corrosion behavior of Sn-Zn deposits in brine media," Electrochimica Acta, vol. 51, pp. 4125-4134, 2006.

[87] S. Dubent, M. De Petris-Wery, M. Saurat, and H. F. Ayedi, "Composition control of tin-zinc electrodeposits through means of experimental strategies," Materials Chemistry and Physics, vol. 104, pp. 146-152, 2007.

[88] O. A. Ashiru and J. Shirokoff, "Electrodeposition and characterization of tin-zinc alloy coatings," Applied Surface Science, vol. 103, pp. 159-169, 1996.

[89] E. Guaus and J. Torrent-Burgués, "Tin-zinc electrodeposition from sulphate-gluconate baths," Journal of Electroanalytical Chemistry, vol. 549, pp. 25-36, 2003.

[90] E. Guaus and J. Torrent-Burgués, "Tin-zinc electrodeposition from sulphate-tartrate baths," Journal of Electroanalytical Chemistry, vol. 575, pp. 301-309, 2005.

[91] K. Wang, H. W. Pickering, and K. G. Weil, "EQCM studies of the electrodeposition and corrosion of tin–zinc coatings," Electrochimica Acta, vol. 46, pp. 3835-3840, 2001.

[92] S. Vitkova, V. Ivanova, and G. Raichevsky, "Electrodeposition of low tin content zinc-tin alloys," Surface and Coatings Technology, vol. 82, pp. 226-231, 1996.

[93] M. Arici, H. Nazir, and M. L. Aksu, "Investigation of Sn-Zn electrodeposition from acidic bath on EQCM," Journal of Alloys and Compounds, vol. 509, pp. 1534-1537, 2011.

[94] H. Kazimierczak, P. Ozga, A. Jałowiec, and R. Kowalik, "Tin–zinc alloy electrodeposition from aqueous citrate baths," Surface and Coatings Technology, vol. 240, pp. 311-319, 2014.

[95] S. M. Abdel-Wahab, E. Mohamed, S. M. Rashwan, and M. M. Kamel, "Electroplating of Sn-Zn alloys from aqueous gluconate baths," Metall, vol. 54, pp. 268-272, 2000.

[96] A. P. Abbott, G. Capper, K. J. McKenzie, and K. S. Ryder, "Electrodeposition of zinc-tin alloys from deep eutectic solvents based on choline chloride," Journal of Electroanalytical Chemistry, vol. 599, pp. 288-294, 2007.

[97] G. N. Guseva and T. A. Vagramyan, "Electrodeposition of copper-zinc-tin alloy from pyrophosphate electrolytes," Protection of Metals (English translation of Zaschita Metallov), vol. 21, pp. 381-382, 1985.

[98] T. A. Vagramyan, B. Ode Osama, and E. V. Kharlamova, "Some special features of electrodeposition of a zinc-tin alloy from pyrophosfate electrolytes in the presence of surface-active compounds I," Protection of Metals (English translation of Zaschita Metallov), vol. 22, pp. 496-498, 1986.

[99] V. S. Vasantha, M. Pushpavanam, and V. S. Muralidharan, "Electrodeposition and dissolution of Sn-Zn alloy films on glassy carbon," Proceedings of the Indian Academy of Sciences - Chemical Sciences, vol. 107, pp. 581-591, 1995.

[100] E. Budman and R. R. Sizelove, "Zinc alloy plating," Metal Finishing, vol. 97, pp. 334-339, 1999.

[101] "Alloy Phase Diagram Center," in Alloy phase diagrams, A. S. M. International, Ed., ed. Materials Park, OH: Materials Park, OH : ASM International., 2006.

[102] L. Mirkova, G. Maurin, I. Krastev, and C. Tsvetkova, "Hydrogen evolution and permeation into steel during zinc electroplating; effect of organic additives," Journal of Applied Electrochemistry, vol. 31, pp. 647-654, 2001.

[103] ASTM, "Standard Test Method for Mechanical Hydrogen Embrittlement Evaluation of Plating/Coating Processes and Service Environments," in F519, ed.

[104] M. C. Chrysler, "Hydrogen embrittelment PS 9500," ed.

[105] C. M. Ford, "Hydrogen embrittlement WSS M99 A3-A," ed.

[106] J. W. Dini, "Electrodeposition - The Materials Science of Coatings and Substrates," ed: William Andrew Publishing/Noyes, pp. 141-147.

[107] V. Bostanov, E. Mladenova, and D. Kashchiev, "Nucleation rate in electrocrystallization of cadmium on the Cd(0001) crystal face," Journal of Electroanalytical Chemistry, vol. 481, pp. 7-12, 2000.

[108] D. Kashchiev and A. Milchev, "Kinetics of the initial stage of electrolytic deposition of metals I. General theory," Thin Solid Films, vol. 28, pp. 189-200, 1975.

[109] F. A. Lowenheim, Modern Electroplating, 3rd Ed.. ed. New York: New York : Wiley, 1974.

[110] Y. D. a. Gamburg, "Theory and Practice of Metal Electrodeposition," G. a. Zangari and SpringerLink, Eds., ed: Springer eBooks, 2011.

[111] S. S. Abd El Rehim, S. M. Sayyah, and M. M. El Deeb, "Electroplating of tin from acidic gluconate baths," Plating and Surface Finishing, vol. 87, pp. 93-98, 2000.

[112] E. Rudnik and G. Włoch, "Studies on the electrodeposition of tin from acidic chloride–gluconate solutions," Applied Surface Science, vol. 265, pp. 839-849, 2013.

[113] S. S. Abd El Rehim, S. M. Sayyah, and M. M. El Deeb, "Electroplating of copper films on steel substrates from acidic gluconate baths," Applied Surface Science, vol. 165, pp. 249-254, 2000.

[114] S. S. Abd El Rehim, M. A. M. Ibrahim, and M. M. Dankeria, "Electrodeposition of cobalt from gluconate electrolyte," Journal of Applied Electrochemistry, vol. 32, pp. 1019-1027, 2002.

[115] A. E. Chester, "Acid zinc electroplating and electrolyte therefor," 1951.

[116] A. E. Chester, "Acid zinc electroplating and electrolyte therefor", 1952.

[117] A. Survila, Z. Mockus, S. Kanapeckaite, and G. Stalnionis, "Kinetics of zinc and copper reduction in gluconate-sulfate solutions," Electrochimica Acta, vol. 94, pp. 307-313, 2013.

[118] A. Survila, Z. Mockus, S. Kanapeckaité, V. Jasulaitiené, and R. Jušknas, "Codeposition of copper and tin from acid sulphate solutions containing gluconic acid," Journal of Electroanalytical Chemistry, vol. 647, pp. 123-127, 2010.

[119] M. M. Kamel, "Anomalous codeposition of Co-Ni: Alloys from gluconate baths," Journal of Applied Electrochemistry, vol. 37, pp. 483-489, 2007.

[120] S. S. Abd El Rehim, M. A. M. Ibrahim, M. M. Dankeria, and M. Emad, "Electrodeposition of amorphous cobalt-manganese alloys on to steel from gluconate baths," Transactions of the Institute of Metal Finishing, vol. 80, pp. 105-109, 2002.

[121] D. T. Sawyer, "Metal-gluconate complexes," Chemical Reviews, vol. 64, pp. 633-643, 1964.

[122] Z. Zhang, P. Gibson, S. B. Clark, G. Tian, P. L. Zanonato, and L. Rao, "Lactonization and protonation of gluconic acid: A thermodynamic and kinetic study by potentiometry, NMR and ESI-MS," Journal of Solution Chemistry, vol. 36, pp. 1187-1200, 2007.

[123] V. Ravindran and V. S. Muralidharan, "Characterisation of zinc electrodeposits for corrosion resistance," Corrosion Reviews, vol. 15, pp. 523-532, 1997.

[124] A. a. Apelblat, "Citric Acid," SpringerLink, Ed., ed, 2014.

[125] C. A. Gervasi, M. V. Fiori Bimbi, and P. E. Alvarez, "Characterization of anodic tin passive films formed in citrate buffer solutions," Journal of Electroanalytical Chemistry, vol. 625, pp. 60-68, 2009.

[126] G. Meng, L. Zhang, Y. Shao, T. Zhang, and F. Wang, "Study of the electrochemical behaviour of nanocrystalline zinc by statistical methods," Corrosion Science, vol. 51, pp. 1685-1689, 2009.

[127] L. Oniciu and L. Mureşan, "Some fundamental aspects of levelling and brightening in metal electrodeposition," Journal of Applied Electrochemistry, vol. 21, pp. 565-574, 1991.

[128] S. S. Kruglikov, N. T. Kudriavtsev, G. F. Vorobiova, and A. Y. A. Antonov, "On the mechanism of levelling by addition agents in electrodeposition of metals," Electrochimica Acta, vol. 10, pp. 253-261, 1965.

[129] G. Trejo, H. Ruiz, R. O. Borges, and Y. Meas, "Influence of polyethoxylated additives on zinc electrodeposition from acidic solutions," Journal of Applied Electrochemistry, vol. 31, pp. 685-692, 2001.

[130] S. J. Banik and R. Akolkar, "Suppressing dendrite growth during zinc electrodeposition by PEG-200 additive," Journal of the Electrochemical Society, vol. 160, pp. D519-D523, 2013.

[131] J. C. Ballesteros, P. Díaz-Arista, Y. Meas, R. Ortega, and G. Trejo, "Zinc electrodeposition in the presence of polyethylene glycol 20000," Electrochimica Acta, vol. 52, pp. 3686-3696, 2007.

[132] K. D. Song, K. B. Kim, S. H. Han, and H. Lee, "Effect of Additives on Hydrogen Evolution and Absorption during Zn Electrodeposition Investigated by EQCM," Electrochemical and Solid-State Letters, vol. 7, pp. C20-C24, 2004.

[133] A. Gomes and M. I. da Silva Pereira, "Zn electrodeposition in the presence of surfactants. Part I. Voltammetric and structural studies," Electrochimica Acta, vol. 52, pp. 863-871, 2006.

[134] A. Gomes and M. I. Da Silva Pereira, "Pulsed electrodeposition of Zn in the presence of surfactants," Electrochimica Acta, vol. 51, pp. 1342-1350, 2006.

[135] K. O. Nayana, T. V. Venkatesha, B. M. Praveen, and K. Vathsala, "Synergistic effect of additives on bright nanocrystalline zinc electrodeposition," Journal of Applied Electrochemistry, vol. 41, pp. 39-49, 2011.

[136] K. O. Nayana and T. V. Venkatesha, "Bright zinc electrodeposition and study of influence of synergistic interaction of additives on coating properties," Journal of Industrial and Engineering Chemistry.

[137] K. M. S. Youssef, C. C. Koch, and P. S. Fedkiw, "Influence of Additives and Pulse Electrodeposition Parameters on Production of Nanocrystalline Zinc from Zinc Chloride Electrolytes," Journal of the Electrochemical Society, vol. 151, pp. C103-C111, 2004.

[138] M. Mouanga, L. Ricq, J. Douglade, and P. Berçot, "Effects of some additives on the corrosion behaviour and preferred orientations of zinc obtained by continuous current deposition," Journal of Applied Electrochemistry, vol. 37, pp. 283-289, 2007.

[139] H. B. Muralidhara, Y. Arthoba Naik, J. Balasubramanyam, K. Yogesh Kumar, H. Hanumanthappa, and M. S. Veena, "Nanocrystalline zinc coating on steel substrate using condensation product of glycyl-glycine (GGL) and vanillin

(VNL) and its corrosion study," International Journal of Chemical Sciences, vol. 10, pp. 524-538, 2012.

[140] K. Saber, C. C. Koch, and P. S. Fedkiw, "Pulse current electrodeposition of nanocrystalline zinc," Materials Science and Engineering A, vol. 341, pp. 174-181, 2003.

[141] M. Paunovic, M. Schlesinger, and D. D. Snyder, "Fundamental Considerations," in Modern Electroplating, ed: John Wiley & Sons, Inc., 2010, pp. 1-32.

[142] G. Devaraj, S. Guruviah, and S. K. Seshadri, "Pulse plating," Materials Chemistry and Physics, vol. 25, pp. 439-461, 1990.

[143] M. S. Chandrasekar and M. Pushpavanam, "Pulse and pulse reverse plating—Conceptual, advantages and applications," Electrochimica Acta, vol. 53, pp. 3313-3322, 2008.

[144] S. Mohan, R. M. Krishnan, N. G. Renganathan, S. Raman, B. Ganes Kesari, and H. Latha, "Corrosion studies on pulsed and direct current chromium deposits," Transactions of the Institute of Metal Finishing, vol. 81, pp. 172-175, 2003.

[145] A. Stankevičiute, K. Leinartas, G. Bikulčius, D. Virbalyte, A. Sudavičius, and E. Juzeliunas, "Deposition of Zn-Co by constant and pulsed current," Journal of Applied Electrochemistry, vol. 28, pp. 89-95, 1997.

[146] H. Gleiter, "Nanocrystalline materials," Progress in Materials Science, vol. 33, pp. 223-315, 1989.

[147] H. Gleiter, "Nanostructured materials: basic concepts and microstructure," Acta Materialia, vol. 48, pp. 1-29, 2000.

[148] H. Gleiter, "Nanostructured materials: state of the art and perspectives," Zeitschrift fuer Metallkunde/Materials Research and Advanced Techniques, vol. 86, pp. 78-83, 1995.

[149] H. Gleiter, "Nanostructured materials: state of the art and perspectives," Nanostructured Materials, vol. 6, pp. 3-14, 1995.

[150] P. G. Sanders, J. A. Eastman, and J. R. Weertman, "Elastic and tensile behavior of nanocrystalline copper and palladium," Acta Materialia, vol. 45, pp. 4019-4025, 1997.

[151] P. G. Sanders, G. E. Fougere, L. J. Thompson, J. A. Eastman, and J. R. Weertman, "Improvements in the synthesis and compaction of nanocrystalline materials," Nanostructured Materials, vol. 8, pp. 243-252, 1997.

[152] C. C. Koch, "Synthesis of nanostructured materials by mechanical milling: Problems and opportunities," Nanostructured Materials, vol. 9, pp. 13-22, 1997.

[153] V. L. Tellkamp, A. Melmed, and E. J. Lavernia, "Mechanical behavior and microstructure of a thermally stable bulk nanostructured Al alloy," Metallurgical and Materials Transactions A: Physical Metallurgy and Materials Science, vol. 32, pp. 2335-2343, 2001.

[154] X. Zhang, H. Wang, R. O. Scattergood, J. Narayan, and C. C. Koch, "Evolution of microstructure and mechanical properties of in situ consolidated bulk ultra-fine-grained and nanocrystalline Zn prepared by ball milling," Materials Science and Engineering A, vol. 344, pp. 175-181, 2003.

[155] F. Zhou, X. Z. Liao, Y. T. Zhu, S. Dallek, and E. J. Lavernia, "Microstructural evolution during recovery and recrystallization of a nanocrystalline Al-Mg alloy prepared by cryogenic ball milling," Acta Materialia, vol. 51, pp. 2777-2791, 2003.

[156] R. Z. Valiev, R. K. Islamgaliev, and I. V. Alexandrov, "Bulk nanostructured materials from severe plastic deformation," Progress in Materials Science, vol. 45, pp. 103-189, 2000.

[157] B. Ben-Nissan and A. H. Choi, "Sol-gel production of bioactive nanocoatings for medical applications. Part 1: An introduction," Nanomedicine, vol. 1, pp. 311-319, 2006.

[158] N. Pinna and M. Niederberger, "Surfactant-free nonaqueous synthesis of metal oxide nanostructures," Angewandte Chemie - International Edition, vol. 47, pp. 5292-5304, 2008.

[159] C. C. Wang and J. Y. Ying, "Sol-gel synthesis and hydrothermal processing of anatase and rutile titania nanocrystals," Chemistry of Materials, vol. 11, pp. 3113-3120, 1999.

[160] N. L. Wu, S. Y. Wang, and I. A. Rusakova, "Inhibition of crystallite growth in the sol-gel synthesis of nanocrystalline metal oxides," Science, vol. 285, pp. 1375-1377, 1999.

[161] M. A. Meyers, A. Mishra, and D. J. Benson, "Mechanical properties of nanocrystalline materials," Progress in Materials Science, vol. 51, pp. 427-556, 2006.

[162] C. C. Koch, "Ductility in nanostructured and ultra fine-grained materials: Recent evidence for optimism," Journal of Metastable and Nanocrystalline Materials, vol. 18, pp. 9-20, 2003.

[163] C. C. Koch, D. G. Morris, K. Lu, and A. Inoue, "Ductility of nanostructured materials," MRS Bulletin, vol. 24, pp. 54-58, 1999.

[164] A. K. Mukherjee, "An examination of the constitutive equation for elevated temperature plasticity," Materials Science and Engineering A, vol. 322, pp. 1-22, 2002.

[165] S. X. McFadden, "High strain rate superplasticity in microcrystalline and nanocrystalline materials," Materials Science and Technology, vol. 16, pp. 1340-1344, 2000.

[166] S. X. McFadden, R. S. Mishra, R. Z. Vallev, A. P. Zhilyaev, and A. K. Mukherjee, "Low-temperature superplasticity in nanostructured nickel and metal alloys," Nature, vol. 398, pp. 684-686, 1999.

[167] S. X. McFadden, R. Z. Valiev, and A. K. Mukherjee, "Superplasticity in nanocrystalline Ni_3Al," Materials Science and Engineering A, vol. 319-321, pp. 849-853, 2001.

[168] T. Hanlon, E. D. Tabachnikova, and S. Suresh, "Fatigue behavior of nanocrystalline metals and alloys," International Journal of Fatigue, vol. 27, pp. 1147-1158, 2005.

[169] V. Patlan, K. Higashi, K. Kitagawa, A. Vinogradov, and M. Kawazoe, "Cyclic response of fine grain 5056 Al-Mg alloy processed by equal-channel angular pressing," Materials Science and Engineering A, vol. 319-321, pp. 587-591, 2001.

[170] K. D. Ralston and N. Birbilis, "Effect of grain size on corrosion: A review," Corrosion, vol. 66, pp. 0750051-07500513, 2010.

[171] M. G. Alvarez, S. M. Vazquez, J. Moya, and H. Sirkin, "Anodic behaviour of Fe73.5Si13.5-xAlxB9 Nb3Cu1 (x = 0-2) amorphous, nanostructured and crystalline alloys," Scripta Materialia, vol. 44, pp. 507-512, 2001.

[172] O. Elkedim, H. S. Cao, and P. Fluzin, "Hardness and corrosion performance of nanocrystalline iron powder prepared by ball milling: comparison with different iron obtained by conventional methods," Materials Science Forum, vol. 312, pp. 635-640, 1999.

[173] B. Hadzima, M. Janeček, Y. Estrin, and H. S. Kim, "Microstructure and corrosion properties of ultrafine-grained interstitial free steel," Materials Science and Engineering A, vol. 462, pp. 243-247, 2007.

[174] R. B. Inturi and Z. Szklarska-Smialowska, "The pitting corrosion of sputtered Fe base alloy films," Corrosion Science, vol. 34, pp. 1973-1989, 1993.

[175] S. G. Wang, C. B. Shen, K. Long, H. Y. Yang, F. H. Wang, and Z. D. Zhang, "Preparation and electrochemical corrosion behavior of bulk nanocrystalline ingot iron in HCI acid solution," Journal of Physical Chemistry B, vol. 109, pp. 2499-2503, 2005.

[176] S. G. Wang, C. B. Shen, K. Long, T. Zhang, F. H. Wang, and Z. D. Zhang, "The electrochemical corrosion of bulk nanocrystalline ingot iron in acidic sulfate solution," Journal of Physical Chemistry B, vol. 110, pp. 377-382, 2006.

[177] W. Zeiger, M. Schneider, and H. Worch, "Passivity and pitting corrosion of a nanocrystalline FeAl8-alloy," in Materials Science Forum vol. 269-272, ed, 1998, pp. 833-836.

[178] Y. w. Hao, B. Deng, C. Zhong, Y. m. Jiang, and J. Li, "Effect of Surface Mechanical Attrition Treatment on Corrosion Behavior of 316 Stainless Steel," Journal of Iron and Steel Research International, vol. 16, pp. 68-72, 2009.

[179] Y. Li, F. Wang, and G. Liu, "Grain size effect on the electrochemical corrosion behavior of surface nanocrystallized low-carbon steel," Corrosion, vol. 60, pp. 891-896, 2004.

[180] M. Pisarek, P. Kędzierzawski, M. Janik-Czachor, and K. J. Kurzydłowski, "Effect of hydrostatic extrusion on passivity breakdown on 303 austenitic stainless steel in chloride solution," Journal of Solid State Electrochemistry, vol. 13, pp. 283-291, 2009.

[181] W. R. Osório, C. M. Freire, and A. Garcia, "The role of macrostructural morphology and grain size on the corrosion resistance of Zn and Al castings," Materials Science and Engineering A, vol. 402, pp. 22-32, 2005.

[182] "Worldwide guide to equivalent irons and steels," P. Conti, F. Cverna, and A. S. M. I. M. P. D. Committee, Eds., 5th edition.. ed. Materials Park, Ohio: Materials Park, Ohio : ASM International, 2006.

[183] M. Stern and A. L. Geary, "Electrochemical polarization I. A theoretical analysis of the shape of polarization curves," Journal of the electrochemical society, vol. 104, pp. 56-63, 1957.

[184] http://www.laserfocusworld.com.

[185] B. D. Cullity, Elements of X-ray Diffraction, 2nd ed.: Addison-wesley 1978.

[186] L. P. Berube, "Quantitative method of determining the degree of texture of zinc electrodeposits," Journal of the Electrochemical Society, vol. 136, pp. 2314-2315, 1989.

[187] "http://science.howstuffworks.com."

[188] W. C. Oliver, "An improved technique for determining hardness and elastic modulus using load and displacement sensing indentation experiments," Journal of Materials Research, vol. 7, pp. 1564-1583, 1992.

[189] Y. Bao, L. Liu, and Y. Zhou, "Assessing the elastic parameters and energy-dissipation capacity of solid materials: A residual indent may tell all," Acta Materialia, vol. 53, pp. 4857-4862, 2005.

[190] M. Sedlaček, B. Podgornik, and J. Vižintin, "Influence of surface preparation on roughness parameters, friction and wear," Wear, vol. 266, pp. 482-487, 2009.

[191] M. Golben and M. Maplewood, "Process of plating metal objects," United States Patent 3400012, 1968.

[192] A. Brooks, "Mechanical Plating," Metal Finishing, vol. 81, pp. 53-57, 1983.

[193] R. Pottberg, "Preparation of metallic surfaces for cladding with comminuted metals and the products so clad," U.S. Patent 3,164,448, 1965.

[194] E. Clayton, "Metal Plating," United State Patent 3132043, 1964.

[195] E. Clayton, "Cladding Metal," United State Patent 2640002, 1953.

[196] E. Clayton, "Metal Coating Process," United State Patent 3023127, 1962.

[197] A. K. Sinha, Physical Metallurgy Handbook. New York: McGraw-Hill, 2003.

[198] A. Survila, Electrochemistry of metal complexes : applications from electroplating to oxide layer formation, first ed.: Wiley-VCH Verlag GmbH & CO. KGaA, 2015.

[199] G. A. Eby, "Zinc lozenges: Cold cure or candy solution chemistry determinations," Bioscience Reports, vol. 24, pp. 23-39, 2004.

[200] A. E. Martell and L. G. Sillen, Stability Constants of Metal- Ion Complexes. London: London : Chemical Society, 1964.

[201] A. Survila, Z. Mockus, S. Kanapeckaitė, and G. Stalnionis, "Kinetics of zinc and copper reduction in gluconate–sulfate solutions," Electrochimica Acta, vol. 94, pp. 307-313, 2013.

[202] V. S. Vasantha and V. S. Muralidharan, "Electrochemical behaviour of zinc gluconate complexes," Proceedings of the Indian Academy of Sciences - Chemical Sciences, vol. 106, pp. 825-836, 1994.

[203] B. Bozzini, C. Mele, L. D'Urzo, G. Giovannelli, and S. Natali, "Electrodeposition of Cu from acidic sulphate solutions in the presence of PEG: An electrochemical and spectroelectrochemical investigation - Part I," Journal of Applied Electrochemistry, vol. 36, pp. 789-800, 2006.

[204] S.-L. Ko, J.-Y. Lin, Y.-Y. Wang, and C.-C. Wan, "Effect of the molecular weight of polyethylene glycol as single additive in copper deposition for interconnect metallization," Thin Solid Films, vol. 516, pp. 5046-5051, 2008.

[205] B. Scharifker and G. Hills, "Theoretical and experimental studies of multiple nucleation," Electrochimica Acta, vol. 28, pp. 879-889, 1983.

[206] G. Gunawardena, G. Hills, I. Montenegro, and B. Scharifker, "Electrochemical nucleation Part I. General considerations," Journal of Electroanalytical Chemistry and Interfacial Electrochemistry, vol. 138, pp. 225-239, 1982.

[207] C. G. Zoski, "Handbook of Electrochemistry," ed: Elsevier, 2007, pp. 839-840.

[208] H. Yan, J. Downes, P. J. Boden, and S. J. Harris, "A model for nanolaminated growth patterns in Zn and Zn-Co electrodeposits," Journal of the Electrochemical Society, vol. 143, pp. 1577-1583, 1996.

[209] R. Wang, D. Kirk, and G. Zhang, "Effects of deposition conditions on the morphology of zinc deposits from alkaline zincate solutions," J. Electrochem. Soc., vol. 153, pp. C357-C364, 2006.

[210] R. M. Bozorth, "The Orientations of Crystals in Electrodeposited Metals," Physical Review, vol. 26, pp. 390-400, 1925.

[211] N. A. Pangarov, "Preferred orientations in electro-deposited metals," Journal of Electroanalytical Chemistry, vol. 9, pp. 70-85, 1965.

[212] N. A. Pangarov, " Orientation of crystallites during electrodeposition of metals," Protection of Metals (English translation of Zashchita Metallov), vol. 5, pp. 411-423, 1969.

[213] N. A. Pangarov, "On the crystal orientation of electrodeposited metals," Electrochimica Acta, vol. 9, pp. 721-726, 1964.

[214] K. M. Youssef, C. C. Koch, and P. S. Fedkiw, "Influence of pulse plating parameters on the synthesis and preferred orientation of nanocrystalline zinc from zinc sulfate electrolytes," Electrochimica Acta, vol. 54, pp. 677-683, 2008.

[215] N. A. Pangarov, "The crystal orientation of electrodeposited metals," Electrochimica Acta, vol. 7, pp. 139-146, 1962.

[216] A. K. N. Reddy, "Preferred orientations in nickel electro-deposits. I. The mechanism of development of textures in nickel electro-deposits," Journal of Electroanalytical Chemistry, vol. 6, pp. 141-152, 1963.

[217] A. K. N. Reddy and S. K. Rajagopalan, "Preferred orientations in nickel electro-deposits. II. A consideration of the effect of deposition conditions on the

textures developed," Journal of Electroanalytical Chemistry, vol. 6, pp. 153-158, 1963.

[218] A. K. N. Reddy and S. R. Rajagopalan, "Preferred orientation of nickel electro-deposits. III. Generalization of the theory," Journal of Electroanalytical Chemistry, vol. 6, pp. 159-163, 1963.

[219] J. Torrent-Burgués, E. Guaus, and F. Sanz, "Initial stages of tin electrodeposition from sulfate baths in the presence of gluconate," Journal of Applied Electrochemistry, vol. 32, pp. 225-230, 2002.

[220] A. Survila, Z. Mockus, and S. Kanapeckaite, "Kinetics of Sn and Co codeposition in citrate solutions," Electrochimica Acta, vol. 46, pp. 571-577, 2000.

[221] A. Survila and P. V. Stasiukaitis, "Linear potential sweep voltammetry of electroreduction of labile metal complexes - I. Background model," Electrochimica Acta, vol. 42, pp. 1113-1119, 1997.

[222] B. Bozzini, L. D'Urzo, M. Re, and F. De Riccardis, "Electrodeposition of Cu from acidic sulphate solutions containing cetyltrimethylammonium bromide (CTAB)," Journal of Applied Electrochemistry, vol. 38, pp. 1561-1569, 2008.

[223] T. C. Franklin, J. Darlington, and R. Fierro, "Ion pairing as a method of controlling the composition of electrodpeposited alloys," Journal of the Electrochemical Society, vol. 133, pp. 893-896, 1986.

[224] H. Fischer, "Aspects of inhibition in electrodeposition of compact metals. 1. Effects of electrochemical inhibition," Electrodeposition and Surface Treatments, vol. 1, pp. 239-251, 1973.

[225] T. C. Franklin, T. Williams, T. S. N. Sankara Narayanan, R. Guhl, and G. Hair, "A comparison of the effects of ion pairing and blocking additives on electrodeposition of zinc and cadmium," Journal of the Electrochemical Society, vol. 144, pp. 3064-3066, 1997.

[226] H. Nakano, S. Oue, T. Miki, S. Kobayashi, and H. Fukushima, "Effect of polyethylene glycol on the morphology of Zn electrodeposited on steel sheet," ISIJ International, vol. 46, pp. 106-110, 2006.

[227] J. J. Kelly and A. C. West, "Copper deposition in the presence of polyethylene glycol: I. Quartz crystal microbalance study," Journal of the Electrochemical Society, vol. 145, pp. 3472-3476, 1998.

[228] H. Fischer, "Aspects of inhibition in electrodeposition of compact metals II. Effects of morphological interface inhibition," Electrodeposition and Surface Treatments, vol. 1, pp. 319-337, 1973.

[229] A. Campbellová, P. Klapetek, V. Buršíková, M. Valtr, and J. Buršík, "Small-load nanoindentation experiments on metals," Surface and Interface Analysis, vol. 42, pp. 766-769, 2010.

[230] T. Ohmura, L. Zhang, K. Sekido, and K. Tsuzaki, "Effects of lattice defects on indentation-induced plasticity initiation behavior in metals," Journal of Materials Research, vol. 27, pp. 1742-1749, 2012.

[231] C. A. Schuh, "Nanoindentation studies of materials," Materials Today, vol. 9, pp. 32-40, 2006.

[232] A. H. Chokshi, A. Rosen, J. Karch, and H. Gleiter, "On the validity of the hall-petch relationship in nanocrystalline materials," Scripta Metallurgica, vol. 23, pp. 1679-1683, 1989/10/01 1989.

[233] G. W. Nieman, J. R. Weertman, and R. W. Siegel, "Mechanical behavior of nanocrystalline Cu and Pd," Journal of Materials Research, vol. 6, pp. 1012-1027, 1991.

[234] J. Chen, L. Lu, and K. Lu, "Hardness and strain rate sensitivity of nanocrystalline Cu," Scripta Materialia, vol. 54, pp. 1913-1918, 2006.

[235] M. Furukawa, Z. Horita, M. Nemoto, R. Z. Valiev, and T. G. Langdon, "Microhardness measurements and the hall-petch relationship in an Al-Mg alloy with submicrometer grain size," Acta Materialia, vol. 44, pp. 4619-4629, 1996.

[236] G. D. Hughes, S. D. Smith, C. S. Pande, H. R. Johnson, and R. W. Armstrong, "Hall-petch strengthening for the microhardness of twelve nanometer grain diameter electrodeposited nickel," Scripta Metallurgica, vol. 20, pp. 93-97, 1986.

[237] C. Suryanarayana and C. C. Koch, "Nanocrystalline materials – Current research and future directions," Hyperfine Interactions, vol. 130, pp. 5-44, 2000.

[238] J. D. Giallonardo, U. Erb, K. T. Aust, and G. Palumbo, "The influence of grain size and texture on the Young's modulus of nanocrystalline nickel and nickel-iron alloys," Philosophical Magazine, vol. 91, pp. 4594-4605, 2011.

[239] W. Callister, Materials science and engineering : an introduction, 7th ed. New York, NY: John Wiley & Sons 1940.

[240] Z. N. Farhat, Y. Ding, D. O. Northwood, and A. T. Alpas, "Effect of grain size on friction and wear of nanocrystalline aluminum," Materials Science and Engineering A, vol. 206, pp. 302-313, 1996.

[241] Q. Li, Z. Feng, L. Liu, H. Xu, W. Ge, F. Li, et al., "Deciphering the formation mechanism of a protective corrosion product layer from electrochemical and natural corrosion behaviors of a nanocrystalline zinc coating," RSC Advances, vol. 5, pp. 32479-32490, 2015.

[242] M. F. M. Nazeri and A. A. Mohamad, "Corrosion measurement of Sn-Zn lead-free solders in 6 M KOH solution," Measurement: Journal of the International Measurement Confederation, vol. 47, pp. 820-826, 2014.

[243] M. F. M. Nazeri, A. B. Ismail, and A. A. Mohamad, "Effect of polarizations on Sn-Zn solders alloys in alkaline electrolyte," Journal of Alloys and Compounds, vol. 606, pp. 278-287, 2014.

[244] J. C. Liu, G. Zhang, S. Nagao, J. T. Jiu, M. Nogi, T. Sugahara, et al., "Metastable pitting and its correlation with electronic properties of passive films on Sn-xZn solder alloys," Corrosion Science, vol. 99, pp. 154-163, 2015.

[245] T. H. Muster and I. S. Cole, "The protective nature of passivation films on zinc: Surface charge," Corrosion Science, vol. 46, pp. 2319-2335, 2004.

[246] J. C. Liu, Z. H. Wang, J. Y. Xie, J. S. Ma, G. Zhang, and K. Suganuma, "Understanding corrosion mechanism of Sn-Zn alloys in NaCl solution via corrosion products characterization," Materials and Corrosion, vol. 67, pp. 522-530, 2016.

[247] P. Marcus, V. Maurice, and H. H. Strehblow, "Localized corrosion (pitting): A model of passivity breakdown including the role of the oxide layer nanostructure," Corrosion Science, vol. 50, pp. 2698-2704, 2008.

[248] Z. Szklarska-Smialowska, "Mechanism of pit nucleation by electrical breakdown of the passive film," Corrosion Science, vol. 44, pp. 1143-1149, 2002.

[249] G. S. Frankel, "Pitting corrosion of metals: A review of the critical factors," Journal of the Electrochemical Society, vol. 145, pp. 2186-2198, 1998.

Appendices

- **Reference Number 2.**

ELSEVIER LICENSE TERMS AND CONDITIONS

This Agreement between Mahsa Esfahani ("You") and Elsevier ("Elsevier") consists of your license details and the terms and conditions provided by Elsevier and Copyright Clearance Center.

License Number	3967280531620
License date	13/10/2016
Licensed Content Publisher	Elsevier
Licensed Content Publication	Renewable and Sustainable Energy Reviews
Licensed Content Title	Design for sustainability in automotive industry: A comprehensive review
Licensed Content Author	Ahmad Mayyas,Ala Qattawi,Mohammed Omar,Dongri Shan
Licensed Content Date	May 2012
Licensed Content Volume	16
Licensed Content Issue	4
Licensed Content Pages	18
Start Page	1845
End Page	1862
Type of Use	reuse in a thesis/dissertation
Portion	figures/tables/illustrations
Number of figures/tables/illustrations	1
Format	both print and electronic
Are you the author of this Elsevier article?	No
Will you be translating?	No
Original figure numbers	Fig. 9
Title of your thesis/dissertation	Surface Engineering of Hybrid Joints for Sub-Assembly
Expected completion date	Oct 2016
Estimated size (number of pages)	250
Elsevier VAT number	GB 494 6272 12
Requestor Location	Mahsa Esfahani John Street Hawthorn Melbourne, VIC 3122Australia
Total	0.00 USD

Terms and Conditions

INTRODUCTION

1. The publisher for this copyrighted material is Elsevier. By clicking "accept" in connection with completing this licensing transaction, you agree that the following terms and conditions apply to this transaction (along with the Billing and Payment terms and conditions established by Copyright Clearance Center, Inc. ("CCC"), at the time that you opened your Rightslink account and that are available at any time at http://myaccount.copyright.com).

GENERAL TERMS

2. Elsevier hereby grants you permission to reproduce the aforementioned material subject to the terms and conditions indicated.

3. Acknowledgement: If any part of the material to be used (for example, figures) has appeared in our publication with credit or acknowledgement to another source, permission must also be sought from that source. If such permission is not obtained then that material may not be included in your publication/copies. Suitable acknowledgement to the source must be made, either as a footnote or in a reference list at the end of your publication, as follows:

"Reprinted from Publication title, Vol /edition number, Author(s), Title of article / title of chapter, Pages No., Copyright (Year), with permission from Elsevier [OR APPLICABLE SOCIETY COPYRIGHT OWNER]." Also Lancet special credit - "Reprinted from The Lancet, Vol. number, Author(s), Title of article, Pages No., Copyright (Year), with permission from Elsevier."
4. Reproduction of this material is confined to the purpose and/or media for which permission is hereby given.
5. Altering/Modifying Material: Not Permitted. However figures and illustrations may be altered/adapted minimally to serve your work. Any other abbreviations, additions, deletions and/or any other alterations shall be made only with prior written authorization of Elsevier Ltd. (Please contact Elsevier at permissions@elsevier.com)
6. If the permission fee for the requested use of our material is waived in this instance, please be advised that your future requests for Elsevier materials may attract a fee.
7. Reservation of Rights: Publisher reserves all rights not specifically granted in the combination of (i) the license details provided by you and accepted in the course of this licensing transaction, (ii) these terms and conditions and (iii) CCC's Billing and Payment terms and conditions.
8. License Contingent Upon Payment: While you may exercise the rights licensed immediately upon issuance of the license at the end of the licensing process for the transaction, provided that you have disclosed complete and accurate details of your proposed use, no license is finally effective unless and until full payment is received from you (either by publisher or by CCC) as provided in CCC's Billing and Payment terms and conditions. If full payment is not received on a timely basis, then any license preliminarily granted shall be deemed automatically revoked and shall be void as if never granted. Further, in the event that you breach any of these terms and conditions or any of CCC's Billing and Payment terms and conditions, the license is automatically revoked and shall be void as if never granted. Use of materials as described in a revoked license, as well as any use of the materials beyond the scope of an unrevoked license, may constitute copyright infringement and publisher reserves the right to take any and all action to protect its copyright in the materials.
9. Warranties: Publisher makes no representations or warranties with respect to the licensed material.
10. Indemnity: You hereby indemnify and agree to hold harmless publisher and CCC, and their respective officers, directors, employees and agents, from and against any and all claims arising out of your use of the licensed material other than as specifically authorized pursuant to this license.
11. No Transfer of License: This license is personal to you and may not be sublicensed, assigned, or transferred by you to any other person without publisher's written permission.
12. No Amendment Except in Writing: This license may not be amended except in a writing signed by both parties (or, in the case of publisher, by CCC on publisher's behalf).
13. Objection to Contrary Terms: Publisher hereby objects to any terms contained in any purchase order, acknowledgment, check endorsement or other writing prepared by you, which terms are inconsistent with these terms and conditions or CCC's Billing and Payment terms and conditions. These terms and conditions, together with CCC's Billing and Payment terms and conditions (which are incorporated herein), comprise the entire agreement between you and publisher (and CCC) concerning this licensing transaction. In the event of any conflict between your obligations established by these terms and conditions and those established by CCC's Billing and Payment terms and conditions, these terms and conditions shall control.
14. Revocation: Elsevier or Copyright Clearance Center may deny the permissions described in this License at their sole discretion, for any reason or no reason, with a full refund payable to you. Notice of such denial will be made using the contact information provided by you. Failure to receive such notice will not alter or invalidate the denial. In no event will Elsevier or Copyright Clearance Center be responsible or liable for any costs, expenses or damage incurred by you as a result of a denial of your permission request, other than a refund of the amount(s) paid by you to Elsevier and/or Copyright Clearance Center for denied permissions.

LIMITED LICENSE

The following terms and conditions apply only to specific license types:

15. **Translation**: This permission is granted for non-exclusive world **English** rights only unless your license was granted for translation rights. If you licensed translation rights you may only translate this content into the languages you requested. A professional translator must perform all translations and reproduce the content word for word preserving the integrity of the article.

16. **Posting licensed content on any Website**: The following terms and conditions apply as follows: Licensing material from an Elsevier journal: All content posted to the web site must maintain the copyright information line on the bottom of each image; A hyper-text must be included to the Homepage of the journal from which you are licensing at http://www.sciencedirect.com/science/journal/xxxxx or the Elsevier homepage for books at http://www.elsevier.com; Central Storage: This license does not include permission for a scanned version of the material to be stored in a central repository such as that provided by Heron/XanEdu.

Licensing material from an Elsevier book: A hyper-text link must be included to the Elsevier homepage at http://www.elsevier.com . All content posted to the web site must maintain the copyright information line on the bottom of each image.

Posting licensed content on Electronic reserve: In addition to the above the following clauses are applicable: The web site must be password-protected and made available only to bona fide students registered on a relevant course. This permission is granted for 1 year only. You may obtain a new license for future website posting.

17. **For journal authors:** the following clauses are applicable in addition to the above:

Preprints:

A preprint is an author's own write-up of research results and analysis, it has not been peer-reviewed, nor has it had any other value added to it by a publisher (such as formatting, copyright, technical enhancement etc.).

Authors can share their preprints anywhere at any time. Preprints should not be added to or enhanced in any way in order to appear more like, or to substitute for, the final versions of articles however authors can update their preprints on arXiv or RePEc with their Accepted Author Manuscript (see below).

If accepted for publication, we encourage authors to link from the preprint to their formal publication via its DOI. Millions of researchers have access to the formal publications on ScienceDirect, and so links will help users to find, access, cite and use the best available version. Please note that Cell Press, The Lancet and some society-owned have different preprint policies. Information on these policies is available on the journal homepage.

Accepted Author Manuscripts: An accepted author manuscript is the manuscript of an article that has been accepted for publication and which typically includes author-incorporated changes suggested during submission, peer review and editor-author communications.

Authors can share their accepted author manuscript:

- immediately

via their non-commercial person homepage or blog

by updating a preprint in arXiv or RePEc with the accepted manuscript

via their research institute or institutional repository for internal institutional uses or as part of an invitation-only research collaboration work-group

directly by providing copies to their students or to research collaborators for their personal use

for private scholarly sharing as part of an invitation-only work group on commercial sites with which Elsevier has an agreement

- after the embargo period

via non-commercial hosting platforms such as their institutional repository

via commercial sites with which Elsevier has an agreement

In all cases accepted manuscripts should:

- link to the formal publication via its DOI
- bear a CC-BY-NC-ND license - this is easy to do
- if aggregated with other manuscripts, for example in a repository or other site, be shared in alignment with our hosting policy not be added to or enhanced in any way to appear more like, or to substitute for, the published journal article.

Published journal article (JPA): A published journal article (PJA) is the definitive final record of published research that appears or will appear in the journal and embodies all value-adding publishing activities including peer review co-ordination, copy-editing, formatting, (if relevant) pagination and online enrichment.

Policies for sharing publishing journal articles differ for subscription and gold open access articles:

Subscription Articles: If you are an author, please share a link to your article rather than the full-text. Millions of researchers have access to the formal publications on ScienceDirect, and so links will help your users to find, access, cite, and use the best available version.

Theses and dissertations which contain embedded PJAs as part of the formal submission can be posted publicly by the awarding institution with DOI links back to the formal publications on ScienceDirect.

If you are affiliated with a library that subscribes to ScienceDirect you have additional private sharing rights for others' research accessed under that agreement. This includes use for classroom teaching and internal training at the institution (including use in course packs and courseware programs), and inclusion of the article for grant funding purposes.

Gold Open Access Articles: May be shared according to the author-selected end-user license and should contain a CrossMark logo, the end user license, and a DOI link to the formal publication on ScienceDirect.

Please refer to Elsevier's posting policy for further information.

18. **For book authors** the following clauses are applicable in addition to the above: Authors are permitted to place a brief summary of their work online only. You are not allowed to download and post the published electronic version of your chapter, nor may you scan the printed edition to create an electronic version. **Posting to a repository:** Authors are permitted to post a summary of their chapter only in their institution's repository.

19. **Thesis/Dissertation**: If your license is for use in a thesis/dissertation your thesis may be submitted to your institution in either print or electronic form. Should your thesis be published commercially, please reapply for permission. These requirements include permission for the Library and Archives of Canada to supply single copies, on demand, of the complete thesis and include permission for Proquest/UMI to supply single copies, on demand, of the complete thesis. Should your thesis be published commercially, please reapply for permission. Theses and dissertations which contain embedded PJAs as part of the formal submission can be posted publicly by the awarding institution with DOI links back to the formal publications on ScienceDirect.

Elsevier Open Access Terms and Conditions

You can publish open access with Elsevier in hundreds of open access journals or in nearly 2000 established subscription journals that support open access publishing. Permitted third party re-use of these open access articles is defined by the author's choice of Creative Commons user license. See our open access license policy for more information.

Terms & Conditions applicable to all Open Access articles published with Elsevier:

Any reuse of the article must not represent the author as endorsing the adaptation of the article nor should the article be modified in such a way as to damage the author's honour or reputation. If any changes have been made, such changes must be clearly indicated.

The author(s) must be appropriately credited and we ask that you include the end user license and a DOI link to the formal publication on ScienceDirect.

If any part of the material to be used (for example, figures) has appeared in our publication with credit or acknowledgement to another source it is the responsibility of the user to ensure their reuse complies with the terms and conditions determined by the rights holder.

Additional Terms & Conditions applicable to each Creative Commons user license:

CC BY: The CC-BY license allows users to copy, to create extracts, abstracts and new works from the Article, to alter and revise the Article and to make commercial use of the Article (including reuse and/or resale of the Article by commercial entities), provided the user gives appropriate credit (with a link to the formal publication through the relevant DOI), provides a link to the license, indicates if changes were made and the licensor is not represented as endorsing the use made of the work. The full details of the license are available at http://creativecommons.org/licenses/by/4.0.

CC BY NC SA: The CC BY-NC-SA license allows users to copy, to create extracts, abstracts and new works from the Article, to alter and revise the Article, provided this is not done for commercial purposes, and that the user gives appropriate credit (with a link to the formal publication through the relevant DOI), provides a link to the license, indicates if changes were made and the licensor is not represented as endorsing the use made of the work. Further, any new works must be made available on the same conditions. The full details of the license are available at http://creativecommons.org/licenses/by-nc-sa/4.0.

CC BY NC ND: The CC BY-NC-ND license allows users to copy and distribute the Article, provided this is not done for commercial purposes and further does not permit distribution of the Article if it is changed or edited in any way, and provided the user gives appropriate credit (with a link to the formal publication through the relevant DOI), provides a link to the license, and that the licensor is not represented as endorsing the use made of the work. The full details of the license are available at http://creativecommons.org/licenses/by-nc-nd/4.0. Any commercial reuse of Open Access articles published with a CC BY NC SA or CC BY NC ND license requires permission from Elsevier and will be subject to a fee.

Commercial reuse includes:

- Associating advertising with the full text of the Article
- Charging fees for document delivery or access
- Article aggregation
- Systematic distribution via e-mail lists or share buttons

Posting or linking by commercial companies for use by customers of those companies.

20. **Other Conditions**: v1.8

- **Reference number 4.**

ELSEVIER LICENSE TERMS AND CONDITIONS

This Agreement between Mahsa Esfahani ("You") and Elsevier ("Elsevier") consists of your license details and the terms and conditions provided by Elsevier and Copyright Clearance Center.

License Number	3967900154181
License date	14/10/2016
Licensed Content Publisher	Elsevier
Licensed Content Publication	Acta Materialia
Licensed Content Title	Mechanical behavior of nanocrystalline metals and alloys11The Golden Jubilee Issue—Selected topics in Materials Science and Engineering: Past, Present and Future, edited by S. Suresh
Licensed Content Author	K.S Kumar,H Van Swygenhoven,S Suresh
Licensed Content Date	25 November 2003
Licensed Content Volume	51
Licensed Content Issue	19
Licensed Content Pages	32
Start Page	5743
End Page	5774
Type of Use	reuse in a thesis/dissertation
Intended publisher of new work	other
Portion	figures/tables/illustrations
Number of figures/tables/illustrations	1
Format	both print and electronic
Are you the author of this Elsevier article?	No
Will you be translating?	No
Original figure numbers	Fig. 1
Title of your thesis/dissertation	Surface Engineering of Hybrid Joints for sub-assembly
Expected completion date	Oct 2016
Estimated size (number of pages)	250
Elsevier VAT number	GB 494 6272 12
Requestor Location	Mahsa Esfahani John Street Hawthorn Melbourne, VIC 3122Australia
Total	0.00 AUD
Terms and Conditions	

INTRODUCTION

1. The publisher for this copyrighted material is Elsevier. By clicking "accept" in connection with completing this licensing transaction, you agree that the following terms and conditions apply to this transaction (along with the Billing and Payment terms and conditions established by Copyright Clearance Center, Inc. ("CCC"), at the time that you opened your Rightslink account and that are available at any time at http://myaccount.copyright.com).

GENERAL TERMS

2. Elsevier hereby grants you permission to reproduce the aforementioned material subject to the terms and conditions indicated.
3. Acknowledgement: If any part of the material to be used (for example, figures) has appeared in our publication with credit or acknowledgement to another source, permission must also be sought from that source. If such permission is not obtained then that material may not be included in your publication/copies. Suitable acknowledgement to the source must be made, either as a footnote or in a reference list at the end of your publication, as follows:
"Reprinted from Publication title, Vol /edition number, Author(s), Title of article / title of chapter, Pages No., Copyright (Year), with permission from Elsevier [OR APPLICABLE SOCIETY COPYRIGHT OWNER]." Also Lancet special credit - "Reprinted from The Lancet, Vol. number, Author(s), Title of article, Pages No., Copyright (Year), with permission from Elsevier."
4. Reproduction of this material is confined to the purpose and/or media for which permission is hereby given.
5. Altering/Modifying Material: Not Permitted. However figures and illustrations may be altered/adapted minimally to serve your work. Any other abbreviations, additions, deletions and/or any other alterations shall be made only with prior written authorization of Elsevier Ltd. (Please contact Elsevier at permissions@elsevier.com)
6. If the permission fee for the requested use of our material is waived in this instance, please be advised that your future requests for Elsevier materials may attract a fee.
7. Reservation of Rights: Publisher reserves all rights not specifically granted in the combination of (i) the license details provided by you and accepted in the course of this licensing transaction, (ii) these terms and conditions and (iii) CCC's Billing and Payment terms and conditions.
8. License Contingent Upon Payment: While you may exercise the rights licensed immediately upon issuance of the license at the end of the licensing process for the transaction, provided that you have disclosed complete and accurate details of your proposed use, no license is finally effective unless and until full payment is received from you (either by publisher or by CCC) as provided in CCC's Billing and Payment terms and conditions. If full payment is not received on a timely basis, then any license preliminarily granted shall be deemed automatically revoked and shall be void as if never granted. Further, in the event that you breach any of these terms and conditions or any of CCC's Billing and Payment terms and conditions, the license is automatically revoked and shall be void as if never granted. Use of materials as described in a revoked license, as well as any use of the materials beyond the scope of an unrevoked license, may constitute copyright infringement and publisher reserves the right to take any and all action to protect its copyright in the materials.
9. Warranties: Publisher makes no representations or warranties with respect to the licensed material.
10. Indemnity: You hereby indemnify and agree to hold harmless publisher and CCC, and their respective officers, directors, employees and agents, from and against any and all claims arising out of your use of the licensed material other than as specifically authorized pursuant to this license.
11. No Transfer of License: This license is personal to you and may not be sublicensed, assigned, or transferred by you to any other person without publisher's written permission.
12. No Amendment Except in Writing: This license may not be amended except in a writing signed by both parties (or, in the case of publisher, by CCC on publisher's behalf).
13. Objection to Contrary Terms: Publisher hereby objects to any terms contained in any purchase order, acknowledgment, check endorsement or other writing prepared by you, which terms are inconsistent with these terms and conditions or CCC's Billing and Payment terms and conditions. These terms and conditions, together with CCC's Billing and Payment terms and conditions (which are incorporated herein), comprise the entire agreement between you and publisher (and CCC) concerning this licensing transaction. In the event of any conflict between your obligations established by these terms and conditions and those established by CCC's Billing and Payment terms and conditions, these terms and conditions shall control.
14. Revocation: Elsevier or Copyright Clearance Center may deny the permissions described in this License at their sole discretion, for any reason or no reason, with a full refund payable to you. Notice of such denial will be made using the contact information provided by you. Failure to receive such notice

will not alter or invalidate the denial. In no event will Elsevier or Copyright Clearance Center be responsible or liable for any costs, expenses or damage incurred by you as a result of a denial of your permission request, other than a refund of the amount(s) paid by you to Elsevier and/or Copyright Clearance Center for denied permissions.

LIMITED LICENSE

The following terms and conditions apply only to specific license types:

15. **Translation**: This permission is granted for non-exclusive world **English** rights only unless your license was granted for translation rights. If you licensed translation rights you may only translate this content into the languages you requested. A professional translator must perform all translations and reproduce the content word for word preserving the integrity of the article.

16. **Posting licensed content on any Website**: The following terms and conditions apply as follows: Licensing material from an Elsevier journal: All content posted to the web site must maintain the copyright information line on the bottom of each image; A hyper-text must be included to the Homepage of the journal from which you are licensing at http://www.sciencedirect.com/science/journal/xxxxx or the Elsevier homepage for books at http://www.elsevier.com; Central Storage: This license does not include permission for a scanned version of the material to be stored in a central repository such as that provided by Heron/XanEdu.

Licensing material from an Elsevier book: A hyper-text link must be included to the Elsevier homepage at http://www.elsevier.com . All content posted to the web site must maintain the copyright information line on the bottom of each image.

Posting licensed content on Electronic reserve: In addition to the above the following clauses are applicable: The web site must be password-protected and made available only to bona fide students registered on a relevant course. This permission is granted for 1 year only. You may obtain a new license for future website posting.

17. **For journal authors:** the following clauses are applicable in addition to the above:

Preprints:

A preprint is an author's own write-up of research results and analysis, it has not been peer-reviewed, nor has it had any other value added to it by a publisher (such as formatting, copyright, technical enhancement etc.).

Authors can share their preprints anywhere at any time. Preprints should not be added to or enhanced in any way in order to appear more like, or to substitute for, the final versions of articles however authors can update their preprints on arXiv or RePEc with their Accepted Author Manuscript (see below).

If accepted for publication, we encourage authors to link from the preprint to their formal publication via its DOI. Millions of researchers have access to the formal publications on ScienceDirect, and so links will help users to find, access, cite and use the best available version. Please note that Cell Press, The Lancet and some society-owned have different preprint policies. Information on these policies is available on the journal homepage.

Accepted Author Manuscripts: An accepted author manuscript is the manuscript of an article that has been accepted for publication and which typically includes author-incorporated changes suggested during submission, peer review and editor-author communications.

Authors can share their accepted author manuscript:

- immediately

via their non-commercial person homepage or blog

by updating a preprint in arXiv or RePEc with the accepted manuscript

via their research institute or institutional repository for internal institutional uses or as part of an invitation-only research collaboration work-group

directly by providing copies to their students or to research collaborators for their personal use

for private scholarly sharing as part of an invitation-only work group on commercial sites with which Elsevier has an agreement

- after the embargo period

via non-commercial hosting platforms such as their institutional repository

via commercial sites with which Elsevier has an agreement

In all cases accepted manuscripts should:

- link to the formal publication via its DOI
- bear a CC-BY-NC-ND license - this is easy to do

- if aggregated with other manuscripts, for example in a repository or other site, be shared in alignment with our hosting policy not be added to or enhanced in any way to appear more like, or to substitute for, the published journal article.

Published journal article (JPA): A published journal article (PJA) is the definitive final record of published research that appears or will appear in the journal and embodies all value-adding publishing activities including peer review co-ordination, copy-editing, formatting, (if relevant) pagination and online enrichment.

Policies for sharing publishing journal articles differ for subscription and gold open access articles:

Subscription Articles: If you are an author, please share a link to your article rather than the full-text. Millions of researchers have access to the formal publications on ScienceDirect, and so links will help your users to find, access, cite, and use the best available version.

Theses and dissertations which contain embedded PJAs as part of the formal submission can be posted publicly by the awarding institution with DOI links back to the formal publications on ScienceDirect.

If you are affiliated with a library that subscribes to ScienceDirect you have additional private sharing rights for others' research accessed under that agreement. This includes use for classroom teaching and internal training at the institution (including use in course packs and courseware programs), and inclusion of the article for grant funding purposes.

Gold Open Access Articles: May be shared according to the author-selected end-user license and should contain a CrossMark logo, the end user license, and a DOI link to the formal publication on ScienceDirect.

Please refer to Elsevier's posting policy for further information.

18. **For book authors** the following clauses are applicable in addition to the above: Authors are permitted to place a brief summary of their work online only. You are not allowed to download and post the published electronic version of your chapter, nor may you scan the printed edition to create an electronic version. **Posting to a repository:** Authors are permitted to post a summary of their chapter only in their institution's repository.

19. **Thesis/Dissertation**: If your license is for use in a thesis/dissertation your thesis may be submitted to your institution in either print or electronic form. Should your thesis be published commercially, please reapply for permission. These requirements include permission for the Library and Archives of Canada to supply single copies, on demand, of the complete thesis and include permission for Proquest/UMI to supply single copies, on demand, of the complete thesis. Should your thesis be published commercially, please reapply for permission. Theses and dissertations which contain embedded PJAs as part of the formal submission can be posted publicly by the awarding institution with DOI links back to the formal publications on ScienceDirect.

Elsevier Open Access Terms and Conditions

You can publish open access with Elsevier in hundreds of open access journals or in nearly 2000 established subscription journals that support open access publishing. Permitted third party re-use of these open access articles is defined by the author's choice of Creative Commons user license. See our open access license policy for more information.

Terms & Conditions applicable to all Open Access articles published with Elsevier:

Any reuse of the article must not represent the author as endorsing the adaptation of the article nor should the article be modified in such a way as to damage the author's honour or reputation. If any changes have been made, such changes must be clearly indicated.

The author(s) must be appropriately credited and we ask that you include the end user license and a DOI link to the formal publication on ScienceDirect.

If any part of the material to be used (for example, figures) has appeared in our publication with credit or acknowledgement to another source it is the responsibility of the user to ensure their reuse complies with the terms and conditions determined by the rights holder.

Additional Terms & Conditions applicable to each Creative Commons user license:

CC BY: The CC-BY license allows users to copy, to create extracts, abstracts and new works from the Article, to alter and revise the Article and to make commercial use of the Article (including reuse and/or resale of the Article by commercial entities), provided the user gives appropriate credit (with a link to the formal publication through the relevant DOI), provides a link to the license, indicates if changes were made and the licensor is not represented as endorsing the use made of the work. The full details of the license are available at http://creativecommons.org/licenses/by/4.0.

CC BY NC SA: The CC BY-NC-SA license allows users to copy, to create extracts, abstracts and new works from the Article, to alter and revise the Article, provided this is not done for commercial purposes, and that the user gives appropriate credit (with a link to the formal publication through the relevant DOI), provides a link to the license, indicates if changes were made and the licensor is not represented as endorsing the use made of the work. Further, any new works must be made available on the same conditions. The full details of the license are available at http://creativecommons.org/licenses/by-nc-sa/4.0.

CC BY NC ND: The CC BY-NC-ND license allows users to copy and distribute the Article, provided this is not done for commercial purposes and further does not permit distribution of the Article if it is changed or edited in any way, and provided the user gives appropriate credit (with a link to the formal publication through the relevant DOI), provides a link to the license, and that the licensor is not represented as endorsing the use made of the work. The full details of the license are available at http://creativecommons.org/licenses/by-nc-nd/4.0. Any commercial reuse of Open Access articles published with a CC BY NC SA or CC BY NC ND license requires permission from Elsevier and will be subject to a fee.

Commercial reuse includes:

- Associating advertising with the full text of the Article
- Charging fees for document delivery or access
- Article aggregation
- Systematic distribution via e-mail lists or share buttons

Posting or linking by commercial companies for use by customers of those companies.

- **Reference number 11.**

Title: Effects of factors on physical attributes of self-piercing riveted joints
Author: Y. Xu
Publication: Science and Technology of Welding and Joining Online
Publisher: Taylor & Francis
Date: Nov 1, 2006
Copyright © 2006 Taylor & Francis

Logged in as:
Mahsa Esfahani
Account #:
3001072438

Thesis/Dissertation Reuse Request

Taylor & Francis is pleased to offer reuses of its content for a thesis or dissertation free of charge contingent on resubmission of permission request if work is published.

Copyright © 2017 Copyright Clearance Center, Inc. All Rights Reserved. Privacy statement. Terms and Conditions.
Comments? We would like to hear from you. E-mail us at customercare@copyright.com

- **Reference number 53.**

SAE International / Permission to reuse Figures

From: copyright [mailto:copyright@sae.org]
Sent: Tuesday, 25 October 2016 5:22 AM
To: Mahsa Esfahani <mesfahani@swin.edu.au>
Subject: SAE International / Permission to reuse Figures

Dear Mahsa,

Thank you for your patience during review and processing of your request.

Please be advised, reproduction use of Figures 6 and 9 of SAE Paper: Howard, R. and Sunday, S., "The Corrosion Performance of Steel Self-Piercing Rivets When Used with Aluminum Components," 831816, 1983, doi:10.4271/831816, is hereby granted, and subject to the following terms and conditions:

-Permission is granted for non-exclusive English language rights, and for the specific use as indicated in your email;

-Permission is required for new requests, or for further use of the material;

-The SAE material must be clearly identified and include the following statement “Reprinted with Permission from SAE International”;

-We also request that you include a complete reference to the SAE document in the reference section for each figure used;

-This permission does not cover any third-party copyrighted work which may appear in the material requested;

-Licensor’s use of this material, in whole or in part, is entirely its responsibility, and SAE International does not warrant or is not responsible for any use of the material.

Thank you.

- **Reference number 54.**

ELSEVIER LICENSE TERMS AND CONDITIONS

This Agreement between Mahsa Esfahani ("You") and Elsevier ("Elsevier") consists of your license details and the terms and conditions provided by Elsevier and Copyright Clearance Center.

License Number	3972440542492
License date	
Licensed Content Publisher	Elsevier
Licensed Content Publication	Elsevier Books
Licensed Content Title	Self-Piercing Riveting
Licensed Content Author	A. Chrysanthou
Licensed Content Date	2014
Licensed Content Volume	n/a
Licensed Content Issue	n/a
Licensed Content Pages	15
Start Page	41
End Page	55
Type of Use	reuse in a thesis/dissertation
Portion	figures/tables/illustrations
Number of figures/tables/illustrations	1
Format	both print and electronic
Are you the author of this Elsevier chapter?	No
Will you be translating?	No
Order reference number	
Original figure numbers	Fig. 4.6
Title of your thesis/dissertation	Surface Engineering of Hybrid Joints for sub-assembly
Expected completion date	Oct 2016
Estimated size (number of pages)	250
Elsevier VAT number	GB 494 6272 12
Total	0.00 AUD

Terms and Conditions

INTRODUCTION

1. The publisher for this copyrighted material is Elsevier. By clicking "accept" in connection with completing this licensing transaction, you agree that the following terms and conditions apply to this transaction (along with the Billing and Payment terms and conditions established by Copyright Clearance Center, Inc. ("CCC"), at the time that you opened your Rightslink account and that are available at any time at http://myaccount.copyright.com).

GENERAL TERMS

2. Elsevier hereby grants you permission to reproduce the aforementioned material subject to the terms and conditions indicated.

3. Acknowledgement: If any part of the material to be used (for example, figures) has appeared in our publication with credit or acknowledgement to another source, permission must also be sought from that source. If such permission is not obtained then that material may not be included in your publication/copies. Suitable acknowledgement to the source must be made, either as a footnote or in a reference list at the end of your publication, as follows:
"Reprinted from Publication title, Vol /edition number, Author(s), Title of article / title of chapter, Pages No., Copyright (Year), with permission from Elsevier [OR APPLICABLE SOCIETY COPYRIGHT OWNER]." Also Lancet special credit - "Reprinted from The Lancet, Vol. number, Author(s), Title of article, Pages No., Copyright (Year), with permission from Elsevier."
4. Reproduction of this material is confined to the purpose and/or media for which permission is hereby given.
5. Altering/Modifying Material: Not Permitted. However figures and illustrations may be altered/adapted minimally to serve your work. Any other abbreviations, additions, deletions and/or any other alterations shall be made only with prior written authorization of Elsevier Ltd. (Please contact Elsevier at permissions@elsevier.com)
6. If the permission fee for the requested use of our material is waived in this instance, please be advised that your future requests for Elsevier materials may attract a fee.
7. Reservation of Rights: Publisher reserves all rights not specifically granted in the combination of (i) the license details provided by you and accepted in the course of this licensing transaction, (ii) these terms and conditions and (iii) CCC's Billing and Payment terms and conditions.
8. License Contingent Upon Payment: While you may exercise the rights licensed immediately upon issuance of the license at the end of the licensing process for the transaction, provided that you have disclosed complete and accurate details of your proposed use, no license is finally effective unless and until full payment is received from you (either by publisher or by CCC) as provided in CCC's Billing and Payment terms and conditions. If full payment is not received on a timely basis, then any license preliminarily granted shall be deemed automatically revoked and shall be void as if never granted. Further, in the event that you breach any of these terms and conditions or any of CCC's Billing and Payment terms and conditions, the license is automatically revoked and shall be void as if never granted. Use of materials as described in a revoked license, as well as any use of the materials beyond the scope of an unrevoked license, may constitute copyright infringement and publisher reserves the right to take any and all action to protect its copyright in the materials.
9. Warranties: Publisher makes no representations or warranties with respect to the licensed material.
10. Indemnity: You hereby indemnify and agree to hold harmless publisher and CCC, and their respective officers, directors, employees and agents, from and against any and all claims arising out of your use of the licensed material other than as specifically authorized pursuant to this license.
11. No Transfer of License: This license is personal to you and may not be sublicensed, assigned, or transferred by you to any other person without publisher's written permission.
12. No Amendment Except in Writing: This license may not be amended except in a writing signed by both parties (or, in the case of publisher, by CCC on publisher's behalf).
13. Objection to Contrary Terms: Publisher hereby objects to any terms contained in any purchase order, acknowledgment, check endorsement or other writing prepared by you, which terms are inconsistent with these terms and conditions or CCC's Billing and Payment terms and conditions. These terms and conditions, together with CCC's Billing and Payment terms and conditions (which are incorporated herein), comprise the entire agreement between you and publisher (and CCC) concerning this licensing transaction. In the event of any conflict between your obligations established by these terms and conditions and those established by CCC's Billing and Payment terms and conditions, these terms and conditions shall control.
14. Revocation: Elsevier or Copyright Clearance Center may deny the permissions described in this License at their sole discretion, for any reason or no reason, with a full refund payable to you. Notice of such denial will be made using the contact information provided by you. Failure to receive such notice will not alter or invalidate the denial. In no event will Elsevier or Copyright Clearance Center be responsible or liable for any costs, expenses or damage incurred by you as a result of a denial of your permission request, other than a refund of the amount(s) paid by you to Elsevier and/or Copyright Clearance Center for denied permissions.

LIMITED LICENSE
The following terms and conditions apply only to specific license types:
15. **Translation**: This permission is granted for non-exclusive world **English** rights only unless your license was granted for translation rights. If you licensed translation rights you may only translate this

content into the languages you requested. A professional translator must perform all translations and reproduce the content word for word preserving the integrity of the article.

16. **Posting licensed content on any Website**: The following terms and conditions apply as follows: Licensing material from an Elsevier journal: All content posted to the web site must maintain the copyright information line on the bottom of each image; A hyper-text must be included to the Homepage of the journal from which you are licensing at http://www.sciencedirect.com/science/journal/xxxxx or the Elsevier homepage for books at http://www.elsevier.com; Central Storage: This license does not include permission for a scanned version of the material to be stored in a central repository such as that provided by Heron/XanEdu.

Licensing material from an Elsevier book: A hyper-text link must be included to the Elsevier homepage at http://www.elsevier.com . All content posted to the web site must maintain the copyright information line on the bottom of each image.

Posting licensed content on Electronic reserve: In addition to the above the following clauses are applicable: The web site must be password-protected and made available only to bona fide students registered on a relevant course. This permission is granted for 1 year only. You may obtain a new license for future website posting.

17. **For journal authors:** the following clauses are applicable in addition to the above:

Preprints:

A preprint is an author's own write-up of research results and analysis, it has not been peer-reviewed, nor has it had any other value added to it by a publisher (such as formatting, copyright, technical enhancement etc.).

Authors can share their preprints anywhere at any time. Preprints should not be added to or enhanced in any way in order to appear more like, or to substitute for, the final versions of articles however authors can update their preprints on arXiv or RePEc with their Accepted Author Manuscript (see below).

If accepted for publication, we encourage authors to link from the preprint to their formal publication via its DOI. Millions of researchers have access to the formal publications on ScienceDirect, and so links will help users to find, access, cite and use the best available version. Please note that Cell Press, The Lancet and some society-owned have different preprint policies. Information on these policies is available on the journal homepage.

Accepted Author Manuscripts: An accepted author manuscript is the manuscript of an article that has been accepted for publication and which typically includes author-incorporated changes suggested during submission, peer review and editor-author communications.

Authors can share their accepted author manuscript:

- - immediately
    - via their non-commercial person homepage or blog
    - by updating a preprint in arXiv or RePEc with the accepted manuscript
    - via their research institute or institutional repository for internal institutional uses or as part of an invitation-only research collaboration work-group
    - directly by providing copies to their students or to research collaborators for their personal use
    - for private scholarly sharing as part of an invitation-only work group on commercial sites with which Elsevier has an agreement
- - after the embargo period
    - via non-commercial hosting platforms such as their institutional repository
    - via commercial sites with which Elsevier has an agreement

In all cases accepted manuscripts should:

- - link to the formal publication via its DOI
- - bear a CC-BY-NC-ND license - this is easy to do
- - if aggregated with other manuscripts, for example in a repository or other site, be shared in alignment with our hosting policy not be added to or enhanced in any way to appear more like, or to substitute for, the published journal article.

Published journal article (JPA): A published journal article (PJA) is the definitive final record of published research that appears or will appear in the journal and embodies all value-adding publishing activities including peer review co-ordination, copy-editing, formatting, (if relevant) pagination and online enrichment.

Policies for sharing publishing journal articles differ for subscription and gold open access articles:

Subscription Articles: If you are an author, please share a link to your article rather than the full-text. Millions of researchers have access to the formal publications on ScienceDirect, and so links will help your users to find, access, cite, and use the best available version.
Theses and dissertations which contain embedded PJAs as part of the formal submission can be posted publicly by the awarding institution with DOI links back to the formal publications on ScienceDirect.
If you are affiliated with a library that subscribes to ScienceDirect you have additional private sharing rights for others' research accessed under that agreement. This includes use for classroom teaching and internal training at the institution (including use in course packs and courseware programs), and inclusion of the article for grant funding purposes.
Gold Open Access Articles: May be shared according to the author-selected end-user license and should contain a CrossMark logo, the end user license, and a DOI link to the formal publication on ScienceDirect.
Please refer to Elsevier's posting policy for further information.
18. **For book authors** the following clauses are applicable in addition to the above: Authors are permitted to place a brief summary of their work online only. You are not allowed to download and post the published electronic version of your chapter, nor may you scan the printed edition to create an electronic version. **Posting to a repository:** Authors are permitted to post a summary of their chapter only in their institution's repository.
19. **Thesis/Dissertation**: If your license is for use in a thesis/dissertation your thesis may be submitted to your institution in either print or electronic form. Should your thesis be published commercially, please reapply for permission. These requirements include permission for the Library and Archives of Canada to supply single copies, on demand, of the complete thesis and include permission for Proquest/UMI to supply single copies, on demand, of the complete thesis. Should your thesis be published commercially, please reapply for permission. Theses and dissertations which contain embedded PJAs as part of the formal submission can be posted publicly by the awarding institution with DOI links back to the formal publications on ScienceDirect.

Elsevier Open Access Terms and Conditions
You can publish open access with Elsevier in hundreds of open access journals or in nearly 2000 established subscription journals that support open access publishing. Permitted third party re-use of these open access articles is defined by the author's choice of Creative Commons user license. See our open access license policy for more information.
Terms & Conditions applicable to all Open Access articles published with Elsevier:
Any reuse of the article must not represent the author as endorsing the adaptation of the article nor should the article be modified in such a way as to damage the author's honour or reputation. If any changes have been made, such changes must be clearly indicated.
The author(s) must be appropriately credited and we ask that you include the end user license and a DOI link to the formal publication on ScienceDirect.
If any part of the material to be used (for example, figures) has appeared in our publication with credit or acknowledgement to another source it is the responsibility of the user to ensure their reuse complies with the terms and conditions determined by the rights holder.
Additional Terms & Conditions applicable to each Creative Commons user license:
CC BY: The CC-BY license allows users to copy, to create extracts, abstracts and new works from the Article, to alter and revise the Article and to make commercial use of the Article (including reuse and/or resale of the Article by commercial entities), provided the user gives appropriate credit (with a link to the formal publication through the relevant DOI), provides a link to the license, indicates if changes were made and the licensor is not represented as endorsing the use made of the work. The full details of the license are available at http://creativecommons.org/licenses/by/4.0.
CC BY NC SA: The CC BY-NC-SA license allows users to copy, to create extracts, abstracts and new works from the Article, to alter and revise the Article, provided this is not done for commercial purposes, and that the user gives appropriate credit (with a link to the formal publication through the relevant DOI), provides a link to the license, indicates if changes were made and the licensor is not represented as endorsing the use made of the work. Further, any new works must be made available on the same conditions. The full details of the license are available at http://creativecommons.org/licenses/by-nc-sa/4.0.
CC BY NC ND: The CC BY-NC-ND license allows users to copy and distribute the Article, provided this is not done for commercial purposes and further does not permit distribution of the Article if it is changed or edited in any way, and provided the user gives appropriate credit (with a link to the formal publication through the relevant DOI), provides a link to the license, and that the licensor is not represented as endorsing the use made of the work. The full details of the license are available at http://creativecommons.org/licenses/by-nc-nd/4.0. Any commercial reuse of Open Access articles

published with a CC BY NC SA or CC BY NC ND license requires permission from Elsevier and will be subject to a fee.

Commercial reuse includes:

- Associating advertising with the full text of the Article
- Charging fees for document delivery or access
- Article aggregation
- Systematic distribution via e-mail lists or share buttons

Posting or linking by commercial companies for use by customers of those companies.
20. **Other Conditions**: V1.8

- **Reference number 55.**

JOHN WILEY AND SONS LICENSE TERMS AND CONDITIONS

This Agreement between Mahsa Esfahani ("You") and John Wiley and Sons ("John Wiley and Sons") consists of your license details and the terms and conditions provided by John Wiley and Sons and Copyright Clearance Center.

License Number	3967440213220
License date	
Licensed Content Publisher	John Wiley and Sons
Licensed Content Publication	Fatigue & Fracture of Engineering Materials & Structures
Licensed Content Title	Characterization of fretting fatigue in self-piercing riveted aluminium alloy sheets
Licensed Content Author	L. HAN,A. CHRYSANTHOU,K. W. YOUNG,J. M. O\'SULLIVAN
Licensed Content Date	Jul 12, 2006
Licensed Content Pages	9
Type of use	Dissertation/Thesis
Requestor type	University/Academic
Format	Print and electronic
Portion	Figure/table
Number of figures/tables	3
Original Wiley figure/table number(s)	Fig. 2, 6 (a), 8(a)
Will you be translating?	No
Title of your thesis / dissertation	Surface Engineering of Hybrid Joints for sub-assembly
Expected completion date	Oct 2016
Expected size (number of pages)	250
Requestor Location	Mahsa Esfahani John Street Hawthorn Melbourne, VIC 3122 Australia
Publisher Tax ID	EU826007151
Total	0.0 AUD

TERMS AND CONDITIONS

This copyrighted material is owned by or exclusively licensed to John Wiley & Sons, Inc. or one of its group companies (each a"Wiley Company") or handled on behalf of a society with which a Wiley Company has exclusive publishing rights in relation to a particular work (collectively "WILEY"). By clicking "accept" in connection with completing this licensing transaction, you agree that the following terms and conditions apply to this transaction (along with the billing and payment terms and conditions established by the Copyright Clearance Center Inc., ("CCC's Billing and Payment terms and conditions"), at the time that you opened your RightsLink account (these are available at any time at http://myaccount.copyright.com).

Terms and Conditions

The materials you have requested permission to reproduce or reuse (the "Wiley Materials") are protected by copyright.

You are hereby granted a personal, non-exclusive, non-sub licensable (on a stand-alone basis), non-transferable, worldwide, limited license to reproduce the Wiley Materials for the purpose specified in the licensing process. This license, **and any CONTENT (PDF or image file) purchased as part of your order,** is for a one-time use only and limited to any maximum distribution number specified in the license. The first instance of republication or reuse granted by this license must be completed within two years of the date of the grant of this license (although copies prepared before the end date may be distributed thereafter). The Wiley Materials shall not be used in any other manner or for any other purpose, beyond what is granted in the license. Permission is granted subject to an appropriate acknowledgement given to the author, title of the material/book/journal and the publisher. You shall also duplicate the copyright notice that appears in the Wiley publication in your use of the Wiley Material. Permission is also granted on the understanding that nowhere in the text is a previously published source acknowledged for all or part of this Wiley Material. Any third party content is expressly excluded from this permission.

With respect to the Wiley Materials, all rights are reserved. Except as expressly granted by the terms of the license, no part of the Wiley Materials may be copied, modified, adapted (except for minor reformatting required by the new Publication), translated, reproduced, transferred or distributed, in any form or by any means, and no derivative works may be made based on the Wiley Materials without the prior permission of the respective copyright owner.**For STM Signatory Publishers clearing permission under the terms of the STM Permissions Guidelines only, the terms of the license are extended to include subsequent editions and for editions in other languages, provided such editions are for the work as a whole in situ and does not involve the separate exploitation of the permitted figures or extracts,** You may not alter, remove or suppress in any manner any copyright, trademark or other notices displayed by the Wiley Materials. You may not license, rent, sell, loan, lease, pledge, offer as security, transfer or assign the Wiley Materials on a stand-alone basis, or any of the rights granted to you hereunder to any other person.

The Wiley Materials and all of the intellectual property rights therein shall at all times remain the exclusive property of John Wiley & Sons Inc, the Wiley Companies, or their respective licensors, and your interest therein is only that of having possession of and the right to reproduce the Wiley Materials pursuant to Section 2 herein during the continuance of this Agreement. You agree that you own no right, title or interest in or to the Wiley Materials or any of the intellectual property rights therein. You shall have no rights hereunder other than the license as provided for above in Section 2. No right, license or interest to any trademark, trade name, service mark or other branding ("Marks") of WILEY or its licensors is granted hereunder, and you agree that you shall not assert any such right, license or interest with respect thereto

NEITHER WILEY NOR ITS LICENSORS MAKES ANY WARRANTY OR REPRESENTATION OF ANY KIND TO YOU OR ANY THIRD PARTY, EXPRESS, IMPLIED OR STATUTORY, WITH RESPECT TO THE MATERIALS OR THE ACCURACY OF ANY INFORMATION CONTAINED IN THE MATERIALS, INCLUDING, WITHOUT LIMITATION, ANY IMPLIED WARRANTY OF MERCHANTABILITY, ACCURACY, SATISFACTORY QUALITY, FITNESS FOR A PARTICULAR PURPOSE, USABILITY, INTEGRATION OR NON-INFRINGEMENT AND ALL SUCH WARRANTIES ARE HEREBY EXCLUDED BY WILEY AND ITS LICENSORS AND WAIVED BY YOU.

WILEY shall have the right to terminate this Agreement immediately upon breach of this Agreement by you.

You shall indemnify, defend and hold harmless WILEY, its Licensors and their respective directors, officers, agents and employees, from and against any actual or threatened claims, demands, causes of action or proceedings arising from any breach of this Agreement by you.

IN NO EVENT SHALL WILEY OR ITS LICENSORS BE LIABLE TO YOU OR ANY OTHER PARTY OR ANY OTHER PERSON OR ENTITY FOR ANY SPECIAL, CONSEQUENTIAL, INCIDENTAL, INDIRECT, EXEMPLARY OR PUNITIVE DAMAGES, HOWEVER CAUSED, ARISING OUT OF OR IN CONNECTION WITH THE DOWNLOADING, PROVISIONING, VIEWING OR USE OF THE MATERIALS REGARDLESS OF THE FORM OF ACTION, WHETHER FOR BREACH OF CONTRACT, BREACH OF WARRANTY, TORT, NEGLIGENCE, INFRINGEMENT OR OTHERWISE (INCLUDING, WITHOUT LIMITATION, DAMAGES BASED ON LOSS OF PROFITS, DATA, FILES, USE, BUSINESS OPPORTUNITY OR CLAIMS OF THIRD PARTIES), AND WHETHER OR NOT THE PARTY HAS BEEN ADVISED OF THE POSSIBILITY OF SUCH DAMAGES. THIS LIMITATION SHALL APPLY NOTWITHSTANDING ANY FAILURE OF ESSENTIAL PURPOSE OF ANY LIMITED REMEDY PROVIDED HEREIN.

Should any provision of this Agreement be held by a court of competent jurisdiction to be illegal, invalid, or unenforceable, that provision shall be deemed amended to achieve as nearly as possible the same economic effect as the original provision, and the legality, validity and enforceability of the remaining provisions of this Agreement shall not be affected or impaired thereby.

The failure of either party to enforce any term or condition of this Agreement shall not constitute a waiver of either party's right to enforce each and every term and condition of this Agreement. No breach under this agreement shall be deemed waived or excused by either party unless such waiver or consent is in writing signed by the party granting such waiver or consent. The waiver by or consent of a party to a breach of any provision of this Agreement shall not operate or be construed as a waiver of or consent to any other or subsequent breach by such other party.

This Agreement may not be assigned (including by operation of law or otherwise) by you without WILEY's prior written consent.

Any fee required for this permission shall be non-refundable after thirty (30) days from receipt by the CCC.

These terms and conditions together with CCC's Billing and Payment terms and conditions (which are incorporated herein) form the entire agreement between you and WILEY concerning this licensing transaction and (in the absence of fraud) supersedes all prior agreements and representations of the parties, oral or written. This Agreement may not be amended except in writing signed by both parties. This Agreement shall be binding upon and inure to the benefit of the parties' successors, legal representatives, and authorized assigns.

In the event of any conflict between your obligations established by these terms and conditions and those established by CCC's Billing and Payment terms and conditions, these terms and conditions shall prevail.

WILEY expressly reserves all rights not specifically granted in the combination of (i) the license details provided by you and accepted in the course of this licensing transaction, (ii) these terms and conditions and (iii) CCC's Billing and Payment terms and conditions.

This Agreement will be void if the Type of Use, Format, Circulation, or Requestor Type was misrepresented during the licensing process.

This Agreement shall be governed by and construed in accordance with the laws of the State of New York, USA, without regards to such state's conflict of law rules. Any legal action, suit or proceeding arising out of or relating to these Terms and Conditions or the breach thereof shall be instituted in a court of competent jurisdiction in New York County in the State of New York in the United States of America and each party hereby consents and submits to the personal jurisdiction of such court, waives any objection to venue in such court and consents to service of process by registered or certified mail, return receipt requested, at the last known address of such party.

WILEY OPEN ACCESS TERMS AND CONDITIONS

Wiley Publishes Open Access Articles in fully Open Access Journals and in Subscription journals offering Online Open. Although most of the fully Open Access journals publish open access articles under the terms of the Creative Commons Attribution (CC BY) License only, the subscription journals and a few of the Open Access Journals offer a choice of Creative Commons Licenses. The license type is clearly identified on the article.

The Creative Commons Attribution License

The Creative Commons Attribution License (CC-BY) allows users to copy, distribute and transmit an article, adapt the article and make commercial use of the article. The CC-BY license permits commercial and non-**Creative Commons Attribution Non-Commercial License**

The Creative Commons Attribution Non-Commercial (CC-BY-NC)License permits use, distribution and reproduction in any medium, provided the original work is properly cited and is not used for commercial purposes.(see below)

Creative Commons Attribution-Non-Commercial-NoDerivs License

The Creative Commons Attribution Non-Commercial-NoDerivs License (CC-BY-NC-ND) permits use, distribution and reproduction in any medium, provided the original work is properly cited, is not used for commercial purposes and no modifications or adaptations are made. (see below)

Use by commercial "for-profit" organizations

Use of Wiley Open Access articles for commercial, promotional, or marketing purposes requires further explicit permission from Wiley and will be subject to a fee.

Further details can be found on Wiley Online Library http://olabout.wiley.com/WileyCDA/Section/id-410895.html

- **Reference number 57.**

ELSEVIER LICENSE TERMS AND CONDITIONS

This Agreement between Mahsa Esfahani ("You") and Elsevier ("Elsevier") consists of your license details and the terms and conditions provided by Elsevier and Copyright Clearance Center.

License Number	3967430998541
License date	
Licensed Content Publisher	Elsevier
Licensed Content Publication	Wear
Licensed Content Title	Fretting wear in self-piercing riveted aluminium alloy sheet
Licensed Content Author	Y.K Chen,L Han,A Chrysanthou,J.M O'Sullivan
Licensed Content Date	August–September 2003
Licensed Content Volume	255
Licensed Content Issue	7-12
Licensed Content Pages	8
Start Page	1463
End Page	1470
Type of Use	reuse in a thesis/dissertation
Intended publisher of new work	other
Portion	figures/tables/illustrations
Number of figures/tables/illustrations	5
Format	both print and electronic
Are you the author of this Elsevier article?	No
Will you be translating?	No
Order reference number	
Original figure numbers	Fig. 12, 3, 4,8, 10
Title of your thesis/dissertation	Surface Engineering of Hybrid Joints for sub-assembly
Expected completion date	Oct 2016

Estimated size (number of pages)	250
Elsevier VAT number	GB 494 6272 12
Requestor Location	Mahsa Esfahani John Street Hawthorn Melbourne, VIC 3122 Australia
Total	0.00 AUD

INTRODUCTION

1. The publisher for this copyrighted material is Elsevier. By clicking "accept" in connection with completing this licensing transaction, you agree that the following terms and conditions apply to this transaction (along with the Billing and Payment terms and conditions established by Copyright Clearance Center, Inc. ("CCC"), at the time that you opened your Rightslink account and that are available at any time at http://myaccount.copyright.com).

GENERAL TERMS

2. Elsevier hereby grants you permission to reproduce the aforementioned material subject to the terms and conditions indicated.
3. Acknowledgement: If any part of the material to be used (for example, figures) has appeared in our publication with credit or acknowledgement to another source, permission must also be sought from that source. If such permission is not obtained then that material may not be included in your publication/copies. Suitable acknowledgement to the source must be made, either as a footnote or in a reference list at the end of your publication, as follows:
"Reprinted from Publication title, Vol /edition number, Author(s), Title of article / title of chapter, Pages No., Copyright (Year), with permission from Elsevier [OR APPLICABLE SOCIETY COPYRIGHT OWNER]." Also Lancet special credit - "Reprinted from The Lancet, Vol. number, Author(s), Title of article, Pages No., Copyright (Year), with permission from Elsevier."
4. Reproduction of this material is confined to the purpose and/or media for which permission is hereby given.
5. Altering/Modifying Material: Not Permitted. However figures and illustrations may be altered/adapted minimally to serve your work. Any other abbreviations, additions, deletions and/or any other alterations shall be made only with prior written authorization of Elsevier Ltd. (Please contact Elsevier at permissions@elsevier.com)
6. If the permission fee for the requested use of our material is waived in this instance, please be advised that your future requests for Elsevier materials may attract a fee.
7. Reservation of Rights: Publisher reserves all rights not specifically granted in the combination of (i) the license details provided by you and accepted in the course of this licensing transaction, (ii) these terms and conditions and (iii) CCC's Billing and Payment terms and conditions.
8. License Contingent Upon Payment: While you may exercise the rights licensed immediately upon issuance of the license at the end of the licensing process for the transaction, provided that you have disclosed complete and accurate details of your proposed use, no license is finally effective unless and until full payment is received from you (either by publisher or by CCC) as provided in CCC's Billing and Payment terms and conditions. If full payment is not received on a timely basis, then any license preliminarily granted shall be deemed automatically revoked and shall be void as if never granted. Further, in the event that you breach any of these terms and conditions or any of CCC's Billing and Payment terms and conditions, the license is automatically revoked and shall be void as if never granted. Use of materials as described in a revoked license, as well as any use of the materials beyond the scope of an unrevoked license, may constitute copyright infringement and publisher reserves the right to take any and all action to protect its copyright in the materials.
9. Warranties: Publisher makes no representations or warranties with respect to the licensed material.
10. Indemnity: You hereby indemnify and agree to hold harmless publisher and CCC, and their respective officers, directors, employees and agents, from and against any and all claims arising out of your use of the licensed material other than as specifically authorized pursuant to this license.
11. No Transfer of License: This license is personal to you and may not be sublicensed, assigned, or transferred by you to any other person without publisher's written permission.
12. No Amendment Except in Writing: This license may not be amended except in a writing signed by both parties (or, in the case of publisher, by CCC on publisher's behalf).
13. Objection to Contrary Terms: Publisher hereby objects to any terms contained in any purchase order, acknowledgment, check endorsement or other writing prepared by you, which terms are inconsistent with

these terms and conditions or CCC's Billing and Payment terms and conditions. These terms and conditions, together with CCC's Billing and Payment terms and conditions (which are incorporated herein), comprise the entire agreement between you and publisher (and CCC) concerning this licensing transaction. In the event of any conflict between your obligations established by these terms and conditions and those established by CCC's Billing and Payment terms and conditions, these terms and conditions shall control.

14. Revocation: Elsevier or Copyright Clearance Center may deny the permissions described in this License at their sole discretion, for any reason or no reason, with a full refund payable to you. Notice of such denial will be made using the contact information provided by you. Failure to receive such notice will not alter or invalidate the denial. In no event will Elsevier or Copyright Clearance Center be responsible or liable for any costs, expenses or damage incurred by you as a result of a denial of your permission request, other than a refund of the amount(s) paid by you to Elsevier and/or Copyright Clearance Center for denied permissions.

LIMITED LICENSE

The following terms and conditions apply only to specific license types:

15. **Translation**: This permission is granted for non-exclusive world **English** rights only unless your license was granted for translation rights. If you licensed translation rights you may only translate this content into the languages you requested. A professional translator must perform all translations and reproduce the content word for word preserving the integrity of the article.

16. **Posting licensed content on any Website**: The following terms and conditions apply as follows: Licensing material from an Elsevier journal: All content posted to the web site must maintain the copyright information line on the bottom of each image; A hyper-text must be included to the Homepage of the journal from which you are licensing at http://www.sciencedirect.com/science/journal/xxxxx or the Elsevier homepage for books at http://www.elsevier.com; Central Storage: This license does not include permission for a scanned version of the material to be stored in a central repository such as that provided by Heron/XanEdu.

Licensing material from an Elsevier book: A hyper-text link must be included to the Elsevier homepage at http://www.elsevier.com . All content posted to the web site must maintain the copyright information line on the bottom of each image.

Posting licensed content on Electronic reserve: In addition to the above the following clauses are applicable: The web site must be password-protected and made available only to bona fide students registered on a relevant course. This permission is granted for 1 year only. You may obtain a new license for future website posting.

17. **For journal authors:** the following clauses are applicable in addition to the above:

Preprints:

A preprint is an author's own write-up of research results and analysis, it has not been peer-reviewed, nor has it had any other value added to it by a publisher (such as formatting, copyright, technical enhancement etc.).

Authors can share their preprints anywhere at any time. Preprints should not be added to or enhanced in any way in order to appear more like, or to substitute for, the final versions of articles however authors can update their preprints on arXiv or RePEc with their Accepted Author Manuscript (see below).

If accepted for publication, we encourage authors to link from the preprint to their formal publication via its DOI. Millions of researchers have access to the formal publications on ScienceDirect, and so links will help users to find, access, cite and use the best available version. Please note that Cell Press, The Lancet and some society-owned have different preprint policies. Information on these policies is available on the journal homepage.

Accepted Author Manuscripts: An accepted author manuscript is the manuscript of an article that has been accepted for publication and which typically includes author-incorporated changes suggested during submission, peer review and editor-author communications.

Authors can share their accepted author manuscript:

- \- immediately
    - via their non-commercial person homepage or blog
    - by updating a preprint in arXiv or RePEc with the accepted manuscript
    - via their research institute or institutional repository for internal institutional uses or as part of an invitation-only research collaboration work-group
    - directly by providing copies to their students or to research collaborators for their personal use
    - for private scholarly sharing as part of an invitation-only work group on commercial sites with which Elsevier has an agreement

- after the embargo period
  - via non-commercial hosting platforms such as their institutional repository
  - via commercial sites with which Elsevier has an agreement

In all cases accepted manuscripts should:

- link to the formal publication via its DOI
- bear a CC-BY-NC-ND license - this is easy to do
- if aggregated with other manuscripts, for example in a repository or other site, be shared in alignment with our hosting policy not be added to or enhanced in any way to appear more like, or to substitute for, the published journal article.

Published journal article (JPA): A published journal article (PJA) is the definitive final record of published research that appears or will appear in the journal and embodies all value-adding publishing activities including peer review co-ordination, copy-editing, formatting, (if relevant) pagination and online enrichment.

Policies for sharing publishing journal articles differ for subscription and gold open access articles:

Subscription Articles: If you are an author, please share a link to your article rather than the full-text. Millions of researchers have access to the formal publications on ScienceDirect, and so links will help your users to find, access, cite, and use the best available version.

Theses and dissertations which contain embedded PJAs as part of the formal submission can be posted publicly by the awarding institution with DOI links back to the formal publications on ScienceDirect.

If you are affiliated with a library that subscribes to ScienceDirect you have additional private sharing rights for others' research accessed under that agreement. This includes use for classroom teaching and internal training at the institution (including use in course packs and courseware programs), and inclusion of the article for grant funding purposes.

Gold Open Access Articles: May be shared according to the author-selected end-user license and should contain a CrossMark logo, the end user license, and a DOI link to the formal publication on ScienceDirect.

Please refer to Elsevier's posting policy for further information.

18. **For book authors** the following clauses are applicable in addition to the above: Authors are permitted to place a brief summary of their work online only. You are not allowed to download and post the published electronic version of your chapter, nor may you scan the printed edition to create an electronic version. **Posting to a repository:** Authors are permitted to post a summary of their chapter only in their institution's repository.

19. **Thesis/Dissertation**: If your license is for use in a thesis/dissertation your thesis may be submitted to your institution in either print or electronic form. Should your thesis be published commercially, please reapply for permission. These requirements include permission for the Library and Archives of Canada to supply single copies, on demand, of the complete thesis and include permission for Proquest/UMI to supply single copies, on demand, of the complete thesis. Should your thesis be published commercially, please reapply for permission. Theses and dissertations which contain embedded PJAs as part of the formal submission can be posted publicly by the awarding institution with DOI links back to the formal publications on ScienceDirect.

Elsevier Open Access Terms and Conditions

You can publish open access with Elsevier in hundreds of open access journals or in nearly 2000 established subscription journals that support open access publishing. Permitted third party re-use of these open access articles is defined by the author's choice of Creative Commons user license. See our open access license policy for more information.

Terms & Conditions applicable to all Open Access articles published with Elsevier:

Any reuse of the article must not represent the author as endorsing the adaptation of the article nor should the article be modified in such a way as to damage the author's honour or reputation. If any changes have been made, such changes must be clearly indicated.

The author(s) must be appropriately credited and we ask that you include the end user license and a DOI link to the formal publication on ScienceDirect.

If any part of the material to be used (for example, figures) has appeared in our publication with credit or acknowledgement to another source it is the responsibility of the user to ensure their reuse complies with the terms and conditions determined by the rights holder.

Additional Terms & Conditions applicable to each Creative Commons user license:

CC BY: The CC-BY license allows users to copy, to create extracts, abstracts and new works from the Article, to alter and revise the Article and to make commercial use of the Article (including reuse and/or resale of the Article by commercial entities), provided the user gives appropriate credit (with a link to the formal publication through the relevant DOI), provides a link to the license, indicates if changes were made and the licensor is not represented as endorsing the use made of the work. The full details of the license are available at http://creativecommons.org/licenses/by/4.0.

CC BY NC SA: The CC BY-NC-SA license allows users to copy, to create extracts, abstracts and new works from the Article, to alter and revise the Article, provided this is not done for commercial purposes, and that the user gives appropriate credit (with a link to the formal publication through the relevant DOI), provides a link to the license, indicates if changes were made and the licensor is not represented as endorsing the use made of the work. Further, any new works must be made available on the same conditions. The full details of the license are available at http://creativecommons.org/licenses/by-nc-sa/4.0.

CC BY NC ND: The CC BY-NC-ND license allows users to copy and distribute the Article, provided this is not done for commercial purposes and further does not permit distribution of the Article if it is changed or edited in any way, and provided the user gives appropriate credit (with a link to the formal publication through the relevant DOI), provides a link to the license, and that the licensor is not represented as endorsing the use made of the work. The full details of the license are available at http://creativecommons.org/licenses/by-nc-nd/4.0. Any commercial reuse of Open Access articles published with a CC BY NC SA or CC BY NC ND license requires permission from Elsevier and will be subject to a fee.

Commercial reuse includes:

- - Associating advertising with the full text of the Article
- - Charging fees for document delivery or access
- - Article aggregation
- - Systematic distribution via e-mail lists or share buttons

Posting or linking by commercial companies for use by customers of those companies.

- **Reference number 64.**

ASM International copyright permission

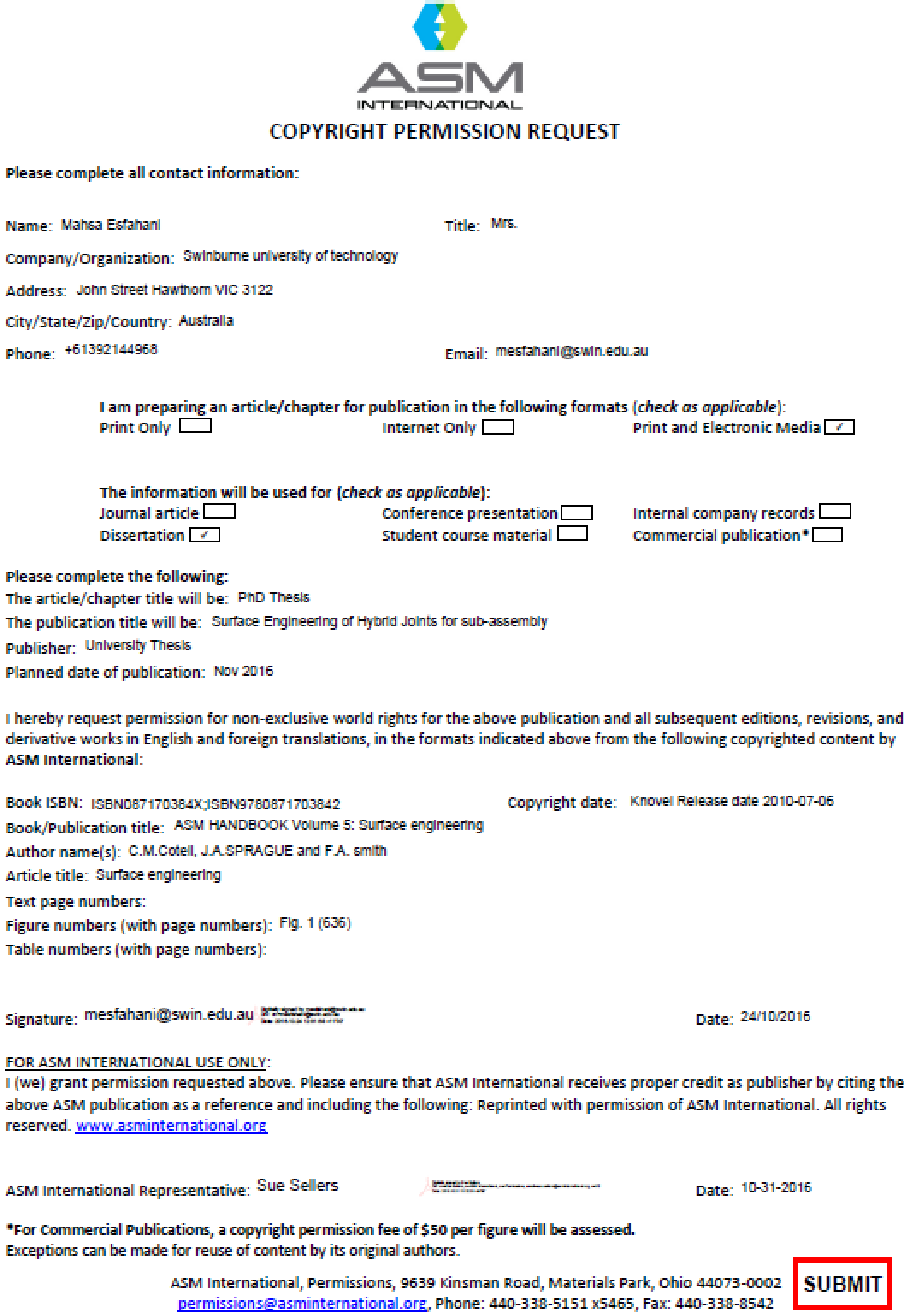

ASM INTERNATIONAL

COPYRIGHT PERMISSION REQUEST

Please complete all contact information:

Name: Mahsa Esfahani Title: Mrs.

Company/Organization: Swinburne university of technology

Address: John Street Hawthorn VIC 3122

City/State/Zip/Country: Australia

Phone: +61392144968 Email: mesfahani@swin.edu.au

I am preparing an article/chapter for publication in the following formats (*check as applicable*):

Print Only ☐ Internet Only ☐ Print and Electronic Media ☑

The information will be used for (*check as applicable*):

Journal article ☐ Conference presentation ☐ Internal company records ☐

Dissertation ☑ Student course material ☐ Commercial publication* ☐

Please complete the following:

The article/chapter title will be: PhD Thesis

The publication title will be: Surface Engineering of Hybrid Joints for sub-assembly

Publisher: University Thesis

Planned date of publication: Nov 2016

I hereby request permission for non-exclusive world rights for the above publication and all subsequent editions, revisions, and derivative works in English and foreign translations, in the formats indicated above from the following copyrighted content by **ASM International**:

Book ISBN: ISBN087170384X;ISBN9780871703842 Copyright date: Knovel Release date 2010-07-06

Book/Publication title: ASM HANDBOOK Volume 5: Surface engineering

Author name(s): C.M.Cotell, J.A.SPRAGUE and F.A. smith

Article title: Surface engineering

Text page numbers:

Figure numbers (with page numbers): Fig. 1 (636)

Table numbers (with page numbers):

Signature: mesfahani@swin.edu.au Date: 24/10/2016

FOR ASM INTERNATIONAL USE ONLY:

I (we) grant permission requested above. Please ensure that ASM International receives proper credit as publisher by citing the above ASM publication as a reference and including the following: Reprinted with permission of ASM International. All rights reserved. www.asminternational.org

ASM International Representative: Sue Sellers Date: 10-31-2016

***For Commercial Publications, a copyright permission fee of $50 per figure will be assessed.**

Exceptions can be made for reuse of content by its original authors.

ASM International, Permissions, 9639 Kinsman Road, Materials Park, Ohio 44073-0002

permissions@asminternational.org, Phone: 440-338-5151 x5465, Fax: 440-338-8542

SUBMIT

- **Reference number 101.**

SPRINGER LICENSE TERMS AND CONDITIONS

This Agreement between Mahsa Esfahani ("You") and Springer ("Springer") consists of your license details and the terms and conditions provided by Springer and Copyright Clearance Center.

License Number	3967880180257
License date	
Licensed Content Publisher	Springer
Licensed Content Publication	Journal of Phase Equilibria
Licensed Content Title	Thermodynamic analysis and phase equilibria calculations of pb-zn, sn-zn, and pb-sn-zn systems
Licensed Content Author	M. Srivastava
Licensed Content Date	Jan 1, 1993
Licensed Content Volume	14
Licensed Content Issue	6
Type of Use	Thesis/Dissertation
Portion	Figures/tables/illustrations
Number of figures/tables/illustrations	1
Author of this Springer article	No
Order reference number	
Original figure numbers	Phase diagram of Sn-Zn
Title of your thesis / dissertation	Surface Engineering of Hybrid Joints for sub-assembly
Expected completion date	Oct 2016
Estimated size(pages)	250
Requestor Location	Mahsa Esfahani John Street Hawthorn Melbourne, VIC 3107 Australia
Total	0.00 AUD
Terms and Conditions	

Introduction
The publisher for this copyrighted material is Springer. By clicking "accept" in connection with completing this licensing transaction, you agree that the following terms and conditions apply to this transaction (along with the Billing and Payment terms and conditions established by Copyright Clearance Center, Inc. ("CCC"), at the time that you opened your Rightslink account and that are available at any time at http://myaccount.copyright.com).

Limited License

With reference to your request to reuse material on which Springer controls the copyright, permission is granted for the use indicated in your enquiry under the following conditions:

- Licenses are for one-time use only with a maximum distribution equal to the number stated in your request.
- Springer material represents original material which does not carry references to other sources. If the material in question appears with a credit to another source, this permission is not valid and authorization has to be obtained from the original copyright holder.
- This permission
• is non-exclusive

- is only valid if no personal rights, trademarks, or competitive products are infringed.
- explicitly excludes the right for derivatives.

- Springer does not supply original artwork or content.

- According to the format which you have selected, the following conditions apply accordingly:

- Print and Electronic: This License include use in electronic form provided it is password protected, on intranet, or CD-Rom/DVD or E-book/E-journal. It may not be republished in electronic open access.
- Print: This License excludes use in electronic form.
- Electronic: This License only pertains to use in electronic form provided it is password protected, on intranet, or CD-Rom/DVD or E-book/E-journal. It may not be republished in electronic open access.

For any electronic use not mentioned, please contact Springer at permissions.springer@spi-global.com.

- Although Springer controls the copyright to the material and is entitled to negotiate on rights, this license is only valid subject to courtesy information to the author (address is given in the article/chapter).

- If you are an STM Signatory or your work will be published by an STM Signatory and you are requesting to reuse figures/tables/illustrations or single text extracts, permission is granted according to STM Permissions Guidelines: http://www.stm-assoc.org/permissions-guidelines/

For any electronic use not mentioned in the Guidelines, please contact Springer at permissions.springer@spi-global.com. If you request to reuse more content than stipulated in the STM Permissions Guidelines, you will be charged a permission fee for the excess content.

Permission is valid upon payment of the fee as indicated in the licensing process. If permission is granted free of charge on this occasion, that does not prejudice any rights we might have to charge for reproduction of our copyrighted material in the future.

-If your request is for reuse in a Thesis, permission is granted free of charge under the following conditions:

This license is valid for one-time use only for the purpose of defending your thesis and with a maximum of 100 extra copies in paper. If the thesis is going to be published, permission needs to be reobtained.

- includes use in an electronic form, provided it is an author-created version of the thesis on his/her own website and his/her university's repository, including UMI (according to the definition on the Sherpa website: http://www.sherpa.ac.uk/romeo/);

- is subject to courtesy information to the co-author or corresponding author.

Geographic Rights: Scope

Licenses may be exercised anywhere in the world.

Altering/Modifying Material: Not Permitted

Figures, tables, and illustrations may be altered minimally to serve your work. You may not alter or modify text in any manner. Abbreviations, additions, deletions and/or any other alterations shall be made only with prior written authorization of the author(s).

Reservation of Rights

Springer reserves all rights not specifically granted in the combination of (i) the license details provided by you and accepted in the course of this licensing transaction and (ii) these terms and conditions and (iii) CCC's Billing and Payment terms and conditions.

License Contingent on Payment

While you may exercise the rights licensed immediately upon issuance of the license at the end of the licensing process for the transaction, provided that you have disclosed complete and accurate details of your proposed use, no license is finally effective unless and until full payment is received from you (either by Springer or by CCC) as provided in CCC's Billing and Payment terms and conditions. If full payment is not received by the date due, then any license preliminarily granted shall be deemed automatically revoked and shall be void as if never granted. Further, in the event that you breach any of these terms and conditions or any of CCC's Billing and Payment terms and conditions, the license is automatically revoked and shall be void as if never granted. Use of materials as described in a revoked license, as well as any use of the materials beyond the scope of an unrevoked license, may constitute copyright infringement and Springer reserves the right to take any and all action to protect its copyright in the materials.

Copyright Notice: Disclaimer

You must include the following copyright and permission notice in connection with any reproduction of the licensed material:

"Springer book/journal title, chapter/article title, volume, year of publication, page, name(s) of author(s), (original copyright notice as given in the publication in which the material was originally published) "With permission of Springer"

In case of use of a graph or illustration, the caption of the graph or illustration must be included, as it is indicated in the original publication.

Warranties: None
Springer makes no representations or warranties with respect to the licensed material and adopts on its own behalf the limitations and disclaimers established by CCC on its behalf in its Billing and Payment terms and conditions for this licensing transaction.
Indemnity
You hereby indemnify and agree to hold harmless Springer and CCC, and their respective officers, directors, employees and agents, from and against any and all claims arising out of your use of the licensed material other than as specifically authorized pursuant to this license.
No Transfer of License
This license is personal to you and may not be sublicensed, assigned, or transferred by you without Springer's written permission.
No Amendment Except in Writing
This license may not be amended except in a writing signed by both parties (or, in the case of Springer, by CCC on Springer's behalf).
Objection to Contrary Terms
Springer hereby objects to any terms contained in any purchase order, acknowledgment, check endorsement or other writing prepared by you, which terms are inconsistent with these terms and conditions or CCC's Billing and Payment terms and conditions. These terms and conditions, together with CCC's Billing and Payment terms and conditions (which are incorporated herein), comprise the entire agreement between you and Springer (and CCC) concerning this licensing transaction. In the event of any conflict between your obligations established by these terms and conditions and those established by CCC's Billing and Payment terms and conditions, these terms and conditions shall control.
Jurisdiction
All disputes that may arise in connection with this present License, or the breach thereof, shall be settled exclusively by arbitration, to be held in the Federal Republic of Germany, in accordance with German law.
Other conditions:
V 12AUG2015

- **Reference number 106.**

Elsevier e-Book Terms and Conditions

elsevier.com/legal/elsevier-website-terms-and-conditions/elsevier-e-book-terms-and-conditions
Elsevier.com Agreement for Perpetual e-Book Access
This agreement ("Agreement") is made by and between Elsevier Ltd., The Boulevard, Langford Lane, Kidlington, Oxford, OX5 1GB, UK ("Elsevier") and the individual (the "Subscriber") identified in the order confirmation ("Order Confirmation") on the website at http://elsevier.com ("Website") as of the date that the Subscriber submits the Order Confirmation by selecting the "Pay" button thereon. This Agreement expressly incorporates by reference and includes the Website's Terms and Conditions, Privacy Policy, and any guidelines, rules or disclaimers that may be posted and updated on specific web pages of the Website or on notices that are sent to
the Subscriber.
The parties hereto agree as follows:
SECTION 1. SUBSCRIPTION
1.1 Subscribed Product
Elsevier hereby grants to the Subscriber the non-exclusive, non-transferable, perpetual right to access and make
personal and non-commercial use of the Elsevier eBooks identified in the Shopping Cart on the Order Confirmation (the "Subscribed Product") and provide the Subscribed Product to the Subscriber subject to the
terms and conditions of this Agreement.
1.2 Authorized Uses
The Subscriber may download, access and view the Subscribed Product by means of a format-compatible electronic reading device or other system. Subscriber is authorized to download additional copies of the

Subscribed Product and to transfer them to other electronic reading devices of the Subscriber, solely for the
Subscriber’s personal use.
Elsevier permits that the Subscriber may copy, paste, and/or print up to a maximum of ten percent (10%) of the Subscribed Product. Elsevier retains the right to amend these percentages at any time with written notice to the Subscriber.

1.3 Restrictions on Use of the Subscribed Product

Except as expressly permitted in writing by Elsevier, the Subscriber may not:
- abridge, modify, translate or create any derivative work based on the Subscribed Product;
- remove, obscure or modify in any way any copyright notices, other notices or disclaimers as they appear in the
Subscribed Product;
- reproduce, distribute, transfer, sell, rent, lease or lend the Subscribed Product; or
- bypass, modify, defeat or circumvent security measures that protect the Subscribed Product.
- **post individual items from the Subscribed Product on social networking sites.**

1.4 Intellectual Property Ownership

The Subscriber acknowledges that all right, title and interest in and to the Subscribed Product remain with Elsevier and its suppliers, except as expressly set forth in this Agreement, and that the redistribution of the
Subscribed Product could materially harm Elsevier and its suppliers.

SECTION 2. ELSEVIER PERFORMANCE OBLIGATIONS

Elsevier will make the Subscribed Product accessible to the Subscriber from the Elsevier Store at
http://elsevier.com. The Subscribed Product will be accessible for download for a period of twelve (12) months
from the date that the Subscriber submits the Order Confirmation by selecting the “Pay” button thereon.

SECTION 3. SUBSCRIBER PERFORMANCE OBLIGATIONS

3.1 Protection from Unauthorized Access and Use

The Subscriber shall use reasonable efforts to:
- ensure that any passwords or credentials used to access the Subscribed Product are used only by
Subscriber for its personal use and Subscriber should not divulge any passwords or credentials to any third party; and
- immediately upon becoming aware of any unauthorized use of the Subscribed Product, inform Elsevier and
take appropriate steps to ensure that such activity ceases and to prevent any recurrence.

3.2 System Requirements

Use of the Subscribed Product requires compatible devices internet access, and certain software (fees may apply); may require periodic updates, and may be affected by the performance of these factors. Subscriber agrees that meeting these requirements, which may change from time to time, is the responsibility of the Subscriber.

SECTION 4. FEES AND PAYMENT TERMS

The Subscriber shall pay to Elsevier the fees (the “Fees”), including any applicable taxes, for access to and use of the Subscribed Product at the rates in effect when the charges were incurred. Refunds are not available in the event of a price reduction or promotional offering. If the Subscribed Product becomes unavailable following a transaction but prior to download, the sole remedy is a refund. If technical problems prevent or unreasonably delay delivery of the Subscribed Product, the exclusive and sole remedy is either replacement or refund of the Fees, as determined by Elsevier.

SECTION 5. TERM AND CANCELLATION

The term of this Agreement shall commence when Elsevier processes the Subscriber’s payment of the Fees, including any applicable taxes, and shall continue to access and use the Subscribed Product in perpetuity in accordance with the usage provisions of this Agreement. The perpetual access granted hereunder for the above .Subscribed Product is subject to payment of a one-time fee as identified in the Shopping Cart on the Order Confirmation. The right of cancellation of this Agreement ends when the Subscriber downloads the Subscribed Product.

SECTION 6. ELSEVIER WARRANTIES AND INDEMNITIES

6.1 Warranties

Elsevier warrants that use of the Subscribed Product in accordance with the terms and conditions herein will not infringe the intellectual property rights of any third party.

6.2 Indemnities

Elsevier shall indemnify, defend and hold harmless the subscriber from and against any loss, damage, costs, liability and expenses (including reasonable attorneys’ fees) arising from or out of any third-party action or claim that use of the Subscribed Product in accordance with the terms and conditions herein infringes the intellectual property rights of such third party. If any such action or claim is made, the Subscriber will promptly notify and cooperate with Elsevier. This indemnity obligation shall survive the termination of this Agreement.

6.3 Disclaimer

EXCEPT FOR THE EXPRESS WARRANTIES AND INDEMNITIES STATED HEREIN AND TO THE EXTENT PERMITTED BY APPLICABLE LAW, ELSEVIER AND ITS SUPPLIERS PROVIDE THE SUBSCRIBED PRODUCT "AS IS" AND MAKE NO REPRESENTATION OR WARRANTY AND EXPRESSLY DISCLAIM ANY LIABILITY FOR ANY CLAIM ARISING FROM OR OUT OF THE SUBSCRIBED PRODUCT, INCLUDING BUT NOT LIMITED TO ANY ERRORS, INACCURACIES, OMISSIONS, OR DEFECTS CONTAINED THEREIN, AND ANY IMPLIED OR EXPRESS WARRANTY AS TO MERCHANTABILITY OR FITNESS FOR A PARTICULAR PURPOSE.

6.4 Limitation of Liability

Except for the express warranties and indemnities stated herein and to the extent permitted by applicable law, in no event shall Elsevier or its suppliers be liable for any indirect, incidental, special, consequential or punitive damages including, but not limited to, loss of data, business interruption or loss of profits, arising out of or in connection with this Agreement, or shall the liability of Elsevier and its suppliers to the Subscriber exceed a sum equal to the Fees paid by the Subscriber hereunder, even if Elsevier or any supplier has been advised of the possibility of such liability or damages.

SECTION 7. RISK OF LOSS

Risk of loss for the Subscribed Product transfers when the Subscriber downloads or accesses the Subscribed Product.

SECTION 8. GENERAL

8.1 Force Majeure

Neither party's delay or failure to perform any provision of this Agreement as a result of circumstances beyond its control (including, but not limited to, war, strikes, fires, floods, governmental restrictions, power failures, telecommunications or Internet failures or damage to or destruction of any network facilities or servers) shall be deemed a breach of this Agreement.

8.2 Severability

The invalidity or unenforceability of any provision of this Agreement shall not affect any other provisions of this Agreement.

8.3 Entire Agreement

This Agreement contains the entire understanding and agreement of the parties and merges and supersedes any and all prior and contemporaneous agreements, communications, proposals and purchase orders, written or oral, between the parties with respect to the subject matter contained herein.

8.4 Governing Law

This Agreement will be governed by and construed in accordance with the laws of England and Wales, without regard to conflict of law principles, and the parties irrevocably consent to the exclusive jurisdiction of the courts located in London, England, with respect to any action or suit arising out of or pertaining to this Agreement (except where local law requires).

8.5 Assignment

The Subscriber shall not assign, transfer or license any of its rights or obligations under this Agreement unless it obtains the prior written consent of Elsevier, which consent shall not unreasonably be withheld.

8.6 Privacy

Elsevier shall not, without the prior written consent of the Subscriber, transfer any personal information of Subscriber to any non-affiliated third party or use it for any purpose other than as described in this Agreementand in the online privacy policy for the relevant online service.

8.7 Notices

All notices given pursuant to this Agreement shall be in writing and, if to Elsevier, delivered to Elsevier Ltd., The Boulevard, Langford Lane, Kidlington, Oxford, OX5 1GB, UK , and if to the Subscriber, delivered to the contact details identified on the Order Confirmation, or to such other address(es) as the party concerned shall have designated by notice hereunder.

Last revised: 23rd February 2016

- **Reference number 122.**

SPRINGER LICENSE TERMS AND CONDITIONS

This Agreement between Mahsa Esfahani ("You") and Springer ("Springer") consists of your license details and the terms and conditions provided by Springer and Copyright Clearance Center.

License Number	3967880627594
License date	
Licensed Content Publisher	Springer
Licensed Content Publication	Journal of Solution Chemistry
Licensed Content Title	Lactonization and Protonation of Gluconic Acid: A Thermodynamic and Kinetic Study by Potentiometry, NMR and ESI-MS
Licensed Content Author	Zhicheng Zhang
Licensed Content Date	Jan 1, 2007
Licensed Content Volume	36
Licensed Content Issue	10
Type of Use	Thesis/Dissertation
Portion	Figures/tables/illustrations
Number of figures/tables/illustrations	1
Author of this Springer article	No
Order reference number	
Original figure numbers	Scheme 1
Title of your thesis / dissertation	Surface Engineering of Hybrid Joints for sub-assembly
Expected completion date	Oct 2016
Estimated size(pages)	250
Requestor Location	Mahsa Esfahani John Street Hawthorn Melbourne, VIC 3122 Australia
Total	0.00 AUD
Terms and Conditions	

Introduction
The publisher for this copyrighted material is Springer. By clicking "accept" in connection with completing this licensing transaction, you agree that the following terms and conditions apply to this transaction (along with the Billing and Payment terms and conditions established by Copyright Clearance Center, Inc. ("CCC"), at the time that you opened your Rightslink account and that are available at any time at http://myaccount.copyright.com).
Limited License
With reference to your request to reuse material on which Springer controls the copyright, permission is granted for the use indicated in your enquiry under the following conditions:
- Licenses are for one-time use only with a maximum distribution equal to the number stated in your request.
- Springer material represents original material which does not carry references to other sources. If the material in question appears with a credit to another source, this permission is not valid and authorization has to be obtained from the original copyright holder.
- This permission
• is non-exclusive

- is only valid if no personal rights, trademarks, or competitive products are infringed.
- explicitly excludes the right for derivatives.

- Springer does not supply original artwork or content.
- According to the format which you have selected, the following conditions apply accordingly:

- **Print and Electronic:** This License include use in electronic form provided it is password protected, on intranet, or CD-Rom/DVD or E-book/E-journal. It may not be republished in electronic open access.
- **Print:** This License excludes use in electronic form.
- **Electronic:** This License only pertains to use in electronic form provided it is password protected, on intranet, or CD-Rom/DVD or E-book/E-journal. It may not be republished in electronic open access.

For any electronic use not mentioned, please contact Springer at permissions.springer@spi-global.com.

- Although Springer controls the copyright to the material and is entitled to negotiate on rights, this license is only valid subject to courtesy information to the author (address is given in the article/chapter).
- If you are an STM Signatory or your work will be published by an STM Signatory and you are requesting to reuse figures/tables/illustrations or single text extracts, permission is granted according to STM Permissions Guidelines: http://www.stm-assoc.org/permissions-guidelines/

For any electronic use not mentioned in the Guidelines, please contact Springer at permissions.springer@spi-global.com. If you request to reuse more content than stipulated in the STM Permissions Guidelines, you will be charged a permission fee for the excess content.

Permission is valid upon payment of the fee as indicated in the licensing process. If permission is granted free of charge on this occasion, that does not prejudice any rights we might have to charge for reproduction of our copyrighted material in the future.

-If your request is for reuse in a Thesis, permission is granted free of charge under the following conditions:

This license is valid for one-time use only for the purpose of defending your thesis and with a maximum of 100 extra copies in paper. If the thesis is going to be published, permission needs to be reobtained.

- includes use in an electronic form, provided it is an author-created version of the thesis on his/her own website and his/her university’s repository, including UMI (according to the definition on the Sherpa website: http://www.sherpa.ac.uk/romeo/);
- is subject to courtesy information to the co-author or corresponding author.

Geographic Rights: Scope

Licenses may be exercised anywhere in the world.

Altering/Modifying Material: Not Permitted

Figures, tables, and illustrations may be altered minimally to serve your work. You may not alter or modify text in any manner. Abbreviations, additions, deletions and/or any other alterations shall be made only with prior written authorization of the author(s).

Reservation of Rights

Springer reserves all rights not specifically granted in the combination of (i) the license details provided by you and accepted in the course of this licensing transaction and (ii) these terms and conditions and (iii) CCC's Billing and Payment terms and conditions.

While you may exercise the rights licensed immediately upon issuance of the license at the end of the licensing process for the transaction, provided that you have disclosed complete and accurate details of your proposed use, no license is finally effective unless and until full payment is received from you (either by Springer or by CCC) as provided in CCC's Billing and Payment terms and conditions. If full payment is not received by the date due, then any license preliminarily granted shall be deemed automatically revoked and shall be void as if never granted. Further, in the event that you breach any of these terms and conditions or any of CCC's Billing and Payment terms and conditions, the license is automatically revoked and shall be void as if never granted. Use of materials as described in a revoked license, as well as any use of the materials beyond the scope of an unrevoked license, may constitute copyright infringement and Springer reserves the right to take any and all action to protect its copyright in the materials.

Copyright Notice: Disclaimer

You must include the following copyright and permission notice in connection with any reproduction of the licensed material:

"Springer book/journal title, chapter/article title, volume, year of publication, page, name(s) of author(s), (original copyright notice as given in the publication in which the material was originally published) "With permission of Springer"

In case of use of a graph or illustration, the caption of the graph or illustration must be included, as it is indicated in the original publication.

Warranties: None

Springer makes no representations or warranties with respect to the licensed material and adopts on its own behalf the limitations and disclaimers established by CCC on its behalf in its Billing and Payment terms and conditions for this licensing transaction.

Indemnity.You hereby indemnify and agree to hold harmless Springer and CCC, and their respective officers, directors, employees and agents, from and against any and all claims arising out of your use of the licensed material other than as specifically authorized pursuant to this license.

No Transfer of License

This license is personal to you and may not be sublicensed, assigned, or transferred by you without Springer's written permission.

No Amendment Except in Writing

This license may not be amended except in a writing signed by both parties (or, in the case of Springer, by CCC on Springer's behalf).

Objection to Contrary Terms

Springer hereby objects to any terms contained in any purchase order, acknowledgment, check endorsement or other writing prepared by you, which terms are inconsistent with these terms and conditions or CCC's Billing and Payment terms and conditions. These terms and conditions, together with CCC's Billing and Payment terms and conditions (which are incorporated herein), comprise the entire agreement between you and Springer (and CCC) concerning this licensing transaction. In the event of any conflict between your obligations established by these terms and conditions and those established by CCC's Billing and Payment terms and conditions, these terms and conditions shall control.

Jurisdiction

All disputes that may arise in connection with this present License, or the breach thereof, shall be settled exclusively by arbitration, to be held in the Federal Republic of Germany, in accordance with German law.

Other conditions:

V 12AUG2015

- **Reference number 141.**

JOHN WILEY AND SONS LICENSE TERMS AND CONDITIONS

This Agreement between Mahsa Esfahani ("You") and John Wiley and Sons ("John Wiley and Sons") consists of your license details and the terms and conditions provided by John Wiley and Sons and Copyright Clearance Center.

License Number	3967881094165
License date	
Licensed Content Publisher	John Wiley and Sons
Licensed Content Publication	Wiley oBooks
Licensed Content Title	Fundamental Considerations
Licensed Content Author	Milan Paunovic,Mordechay Schlesinger,Dexter D. Snyder
Licensed Content Date	Feb 24, 2011
Licensed Content Pages	32
Type of use	Dissertation/Thesis
Requestor type	University/Academic
Format	Print and electronic
Portion	Figure/table
Number of figures/tables	1
Original Wiley figure/table number(s)	Figure 1-15
Will you be translating?	No
Title of your thesis / dissertation	Surface Engineering of Hybrid Joints for sub-assembly
Expected completion date	Oct 2016
Expected size (number of pages)	250

Requestor Location	Mahsa Esfahani John Street Hawthorn, Melbourne, VIC 3122, Australia
Publisher Tax ID	EU826007151
Total	0.00 AUD
Terms and Conditions	

TERMS AND CONDITIONS

This copyrighted material is owned by or exclusively licensed to John Wiley & Sons, Inc. or one of its group companies (each a"Wiley Company") or handled on behalf of a society with which a Wiley Company has exclusive publishing rights in relation to a particular work (collectively "WILEY"). By clicking "accept" in connection with completing this licensing transaction, you agree that the following terms and conditions apply to this transaction (along with the billing and payment terms and conditions established by the Copyright Clearance Center Inc., ("CCC's Billing and Payment terms and conditions"), at the time that you opened your RightsLink account (these are available at any time at http://myaccount.copyright.com).

Terms and Conditions

The materials you have requested permission to reproduce or reuse (the "Wiley Materials") are protected by copyright.

You are hereby granted a personal, non-exclusive, non-sub licensable (on a stand-alone basis), non-transferable, worldwide, limited license to reproduce the Wiley Materials for the purpose specified in the licensing process. This license, **and any CONTENT (PDF or image file) purchased as part of your order,** is for a one-time use only and limited to any maximum distribution number specified in the license. The first instance of republication or reuse granted by this license must be completed within two years of the date of the grant of this license (although copies prepared before the end date may be distributed thereafter). The Wiley Materials shall not be used in any other manner or for any other purpose, beyond what is granted in the license. Permission is granted subject to an appropriate acknowledgement given to the author, title of the material/book/journal and the publisher. You shall also duplicate the copyright notice that appears in the Wiley publication in your use of the Wiley Material. Permission is also granted on the understanding that nowhere in the text is a previously published source acknowledged for all or part of this Wiley Material. Any third party content is expressly excluded from this permission.

With respect to the Wiley Materials, all rights are reserved. Except as expressly granted by the terms of the license, no part of the Wiley Materials may be copied, modified, adapted (except for minor reformatting required by the new Publication), translated, reproduced, transferred or distributed, in any form or by any means, and no derivative works may be made based on the Wiley Materials without the prior permission of the respective copyright owner.**For STM Signatory Publishers clearing permission under the terms of the STM Permissions Guidelines only, the terms of the license are extended to include subsequent editions and for editions in other languages, provided such editions are for the work as a whole in situ and does not involve the separate exploitation of the permitted figures or extracts,** You may not alter, remove or suppress in any manner any copyright, trademark or other notices displayed by the Wiley Materials. You may not license, rent, sell, loan, lease, pledge, offer as security, transfer or assign the Wiley Materials on a stand-alone basis, or any of the rights granted to you hereunder to any other person.

The Wiley Materials and all of the intellectual property rights therein shall at all times remain the exclusive property of John Wiley & Sons Inc, the Wiley Companies, or their respective licensors, and your interest therein is only that of having possession of and the right to reproduce the Wiley Materials pursuant to Section 2 herein during the continuance of this Agreement. You agree that you own no right, title or interest in or to the Wiley Materials or any of the intellectual property rights therein. You shall have no rights hereunder other than the license as provided for above in Section 2. No right, license or interest to any trademark, trade name, service mark or other branding ("Marks") of WILEY or its licensors is granted hereunder, and you agree that you shall not assert any such right, license or interest with respect thereto

NEITHER WILEY NOR ITS LICENSORS MAKES ANY WARRANTY OR REPRESENTATION OF ANY KIND TO YOU OR ANY THIRD PARTY, EXPRESS, IMPLIED OR STATUTORY, WITH RESPECT TO THE MATERIALS OR THE ACCURACY OF ANY INFORMATION CONTAINED IN THE MATERIALS, INCLUDING, WITHOUT LIMITATION, ANY IMPLIED WARRANTY OF MERCHANTABILITY, ACCURACY, SATISFACTORY QUALITY, FITNESS FOR A PARTICULAR PURPOSE, USABILITY, INTEGRATION OR NON-INFRINGEMENT AND ALL

SUCH WARRANTIES ARE HEREBY EXCLUDED BY WILEY AND ITS LICENSORS AND WAIVED BY YOU.

WILEY shall have the right to terminate this Agreement immediately upon breach of this Agreement by you.

You shall indemnify, defend and hold harmless WILEY, its Licensors and their respective directors, officers, agents and employees, from and against any actual or threatened claims, demands, causes of action or proceedings arising from any breach of this Agreement by you.

IN NO EVENT SHALL WILEY OR ITS LICENSORS BE LIABLE TO YOU OR ANY OTHER PARTY OR ANY OTHER PERSON OR ENTITY FOR ANY SPECIAL, CONSEQUENTIAL, INCIDENTAL, INDIRECT, EXEMPLARY OR PUNITIVE DAMAGES, HOWEVER CAUSED, ARISING OUT OF OR IN CONNECTION WITH THE DOWNLOADING, PROVISIONING, VIEWING OR USE OF THE MATERIALS REGARDLESS OF THE FORM OF ACTION, WHETHER FOR BREACH OF CONTRACT, BREACH OF WARRANTY, TORT, NEGLIGENCE, INFRINGEMENT OR OTHERWISE (INCLUDING, WITHOUT LIMITATION, DAMAGES BASED ON LOSS OF PROFITS, DATA, FILES, USE, BUSINESS OPPORTUNITY OR CLAIMS OF THIRD PARTIES), AND WHETHER OR NOT THE PARTY HAS BEEN ADVISED OF THE POSSIBILITY OF SUCH DAMAGES. THIS LIMITATION SHALL APPLY NOTWITHSTANDING ANY FAILURE OF ESSENTIAL PURPOSE OF ANY LIMITED REMEDY PROVIDED HEREIN.

Should any provision of this Agreement be held by a court of competent jurisdiction to be illegal, invalid, or unenforceable, that provision shall be deemed amended to achieve as nearly as possible the same economic effect as the original provision, and the legality, validity and enforceability of the remaining provisions of this Agreement shall not be affected or impaired thereby.

The failure of either party to enforce any term or condition of this Agreement shall not constitute a waiver of either party's right to enforce each and every term and condition of this Agreement. No breach under this agreement shall be deemed waived or excused by either party unless such waiver or consent is in writing signed by the party granting such waiver or consent. The waiver by or consent of a party to a breach of any provision of this Agreement shall not operate or be construed as a waiver of or consent to any other or subsequent breach by such other party.

This Agreement may not be assigned (including by operation of law or otherwise) by you without WILEY's prior written consent.

Any fee required for this permission shall be non-refundable after thirty (30) days from receipt by the CCC.

These terms and conditions together with CCC's Billing and Payment terms and conditions (which are incorporated herein) form the entire agreement between you and WILEY concerning this licensing transaction and (in the absence of fraud) supersedes all prior agreements and representations of the parties, oral or written. This Agreement may not be amended except in writing signed by both parties. This Agreement shall be binding upon and inure to the benefit of the parties' successors, legal representatives, and authorized assigns.

In the event of any conflict between your obligations established by these terms and conditions and those established by CCC's Billing and Payment terms and conditions, these terms and conditions shall prevail.

WILEY expressly reserves all rights not specifically granted in the combination of (i) the license details provided by you and accepted in the course of this licensing transaction, (ii) these terms and conditions and (iii) CCC's Billing and Payment terms and conditions.

This Agreement will be void if the Type of Use, Format, Circulation, or Requestor Type was misrepresented during the licensing process.

This Agreement shall be governed by and construed in accordance with the laws of the State of New York, USA, without regards to such state's conflict of law rules. Any legal action, suit or proceeding arising out of or relating to these Terms and Conditions or the breach thereof shall be instituted in a court of competent jurisdiction in New York County in the State of New York in the United States of America and each party hereby consents and submits to the personal jurisdiction of such court, waives any objection to venue in such court and consents to service of process by registered or certified mail, return receipt requested, at the last known address of such party.

WILEY OPEN ACCESS TERMS AND CONDITIONS

Wiley Publishes Open Access Articles in fully Open Access Journals and in Subscription journals offering Online Open. Although most of the fully Open Access journals publish open access articles under the terms of the Creative Commons Attribution (CC BY) License only, the subscription journals and a few of the Open Access Journals offer a choice of Creative Commons Licenses. The license type is clearly identified on the article.

The Creative Commons Attribution License
The Creative Commons Attribution License (CC-BY) allows users to copy, distribute and transmit an article, adapt the article and make commercial use of the article. The CC-BY license permits commercial and non-

Creative Commons Attribution Non-Commercial License
The Creative Commons Attribution Non-Commercial (CC-BY-NC)License permits use, distribution and reproduction in any medium, provided the original work is properly cited and is not used for commercial purposes.(see below)

Creative Commons Attribution-Non-Commercial-NoDerivs License
The Creative Commons Attribution Non-Commercial-NoDerivs License (CC-BY-NC-ND) permits use, distribution and reproduction in any medium, provided the original work is properly cited, is not used for commercial purposes and no modifications or adaptations are made. (see below)

Use by commercial "for-profit" organizations
Use of Wiley Open Access articles for commercial, promotional, or marketing purposes requires further explicit permission from Wiley and will be subject to a fee.
Further details can be found on Wiley Online Library http://olabout.wiley.com/WileyCDA/Section/id-410895.html

Other Terms and Conditions:

v1.10 Last updated September 2015

- **Reference number 146.**

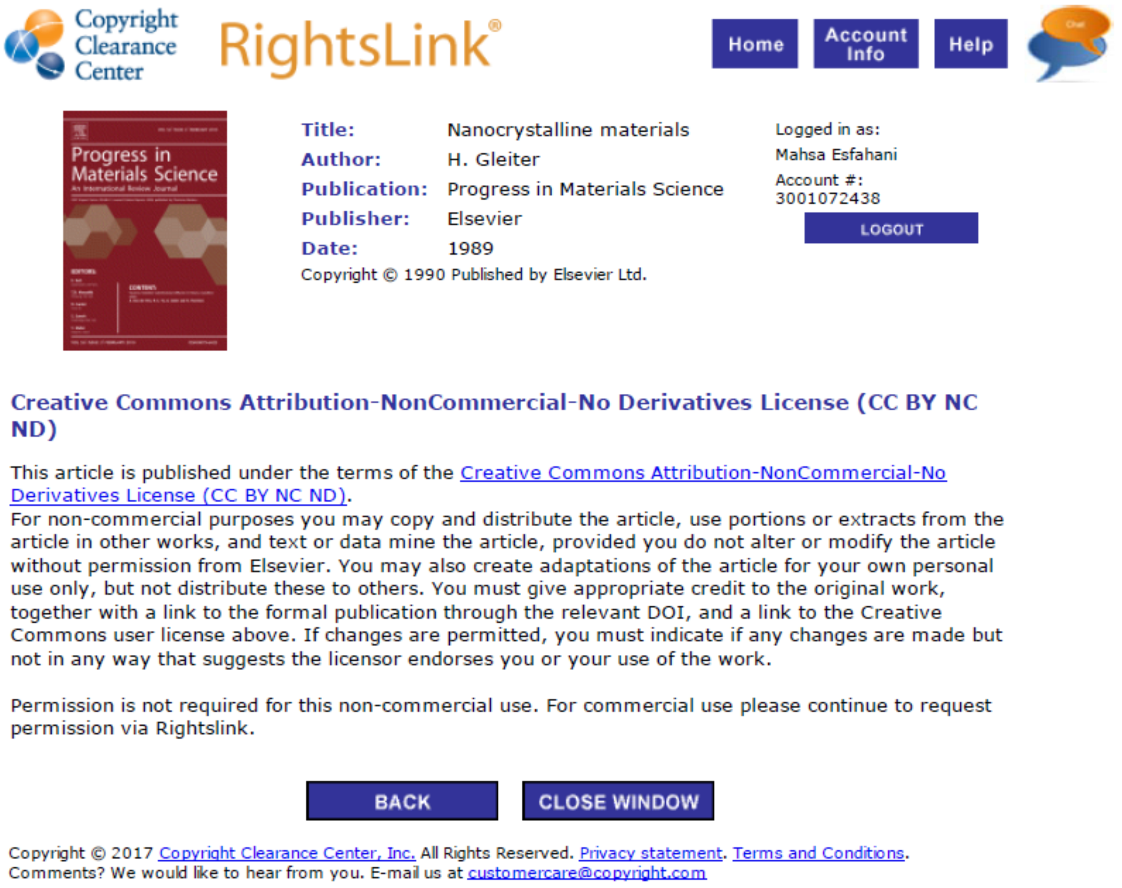

Title: Nanocrystalline materials
Author: H. Gleiter
Publication: Progress in Materials Science
Publisher: Elsevier
Date: 1989
Copyright © 1990 Published by Elsevier Ltd.

Logged in as:
Mahsa Esfahani
Account #:
3001072438

Creative Commons Attribution-NonCommercial-No Derivatives License (CC BY NC ND)

This article is published under the terms of the Creative Commons Attribution-NonCommercial-No Derivatives License (CC BY NC ND).
For non-commercial purposes you may copy and distribute the article, use portions or extracts from the article in other works, and text or data mine the article, provided you do not alter or modify the article without permission from Elsevier. You may also create adaptations of the article for your own personal use only, but not distribute these to others. You must give appropriate credit to the original work, together with a link to the formal publication through the relevant DOI, and a link to the Creative Commons user license above. If changes are permitted, you must indicate if any changes are made but not in any way that suggests the licensor endorses you or your use of the work.

Permission is not required for this non-commercial use. For commercial use please continue to request permission via Rightslink.

Reference number 149.

ELSEVIER LICENSE TERMS AND CONDITIONS

This Agreement between Mahsa Esfahani ("You") and Elsevier ("Elsevier") consists of your license details and the terms and conditions provided by Elsevier and Copyright Clearance Center.

License Number	3967891005057
License date	
Licensed Content Publisher	Elsevier
Licensed Content Publication	Nanostructured Materials
Licensed Content Title	Nanostructured materials: state of the art and perspectives
Licensed Content Author	H. Gleiter
Licensed Content Date	1995
Licensed Content Volume	6
Licensed Content Issue	1-4
Licensed Content Pages	12
Start Page	3
End Page	14
Type of Use	reuse in a thesis/dissertation
Intended publisher of new work	other
Portion	figures/tables/illustrations
Number of figures/tables/illustrations	1
Format	both print and electronic
Are you the author of this Elsevier article?	No
Will you be translating?	No
Order reference number	
Original figure numbers	Fig.1
Title of your thesis/dissertation	Surface Engineering of Hybrid Joints for sub-assembly
Expected completion date	Oct 2016
Estimated size (number of pages)	250
Elsevier VAT number	GB 494 6272 12
Requestor Location	Mahsa Esfahani John Street Hawthorn Melbourne, VIC 3107 Australia
Total	0.00 AUD
Terms and Conditions	

INTRODUCTION

1. The publisher for this copyrighted material is Elsevier. By clicking "accept" in connection with completing this licensing transaction, you agree that the following terms and conditions apply to this transaction (along with the Billing and Payment terms and conditions established by Copyright Clearance Center, Inc. ("CCC"), at the time that you opened your Rightslink account and that are available at any time at http://myaccount.copyright.com).

GENERAL TERMS

2. Elsevier hereby grants you permission to reproduce the aforementioned material subject to the terms and conditions indicated.

3. Acknowledgement: If any part of the material to be used (for example, figures) has appeared in our publication with credit or acknowledgement to another source, permission must also be sought from that source. If such permission is not obtained then that material may not be included in your publication/copies. Suitable acknowledgement to the source must be made, either as a footnote or in a reference list at the end of your publication, as follows:

"Reprinted from Publication title, Vol /edition number, Author(s), Title of article / title of chapter, Pages No., Copyright (Year), with permission from Elsevier [OR APPLICABLE SOCIETY COPYRIGHT OWNER]." Also Lancet special credit - "Reprinted from The Lancet, Vol. number, Author(s), Title of article, Pages No., Copyright (Year), with permission from Elsevier."

4. Reproduction of this material is confined to the purpose and/or media for which permission is hereby given.

5. Altering/Modifying Material: Not Permitted. However figures and illustrations may be altered/adapted minimally to serve your work. Any other abbreviations, additions, deletions and/or any other alterations shall be made only with prior written authorization of Elsevier Ltd. (Please contact Elsevier at permissions@elsevier.com)

6. If the permission fee for the requested use of our material is waived in this instance, please be advised that your future requests for Elsevier materials may attract a fee.

7. Reservation of Rights: Publisher reserves all rights not specifically granted in the combination of (i) the license details provided by you and accepted in the course of this licensing transaction, (ii) these terms and conditions and (iii) CCC's Billing and Payment terms and conditions.

8. License Contingent Upon Payment: While you may exercise the rights licensed immediately upon issuance of the license at the end of the licensing process for the transaction, provided that you have disclosed complete and accurate details of your proposed use, no license is finally effective unless and until full payment is received from you (either by publisher or by CCC) as provided in CCC's Billing and Payment terms and conditions. If full payment is not received on a timely basis, then any license preliminarily granted shall be deemed automatically revoked and shall be void as if never granted. Further, in the event that you breach any of these terms and conditions or any of CCC's Billing and Payment terms and conditions, the license is automatically revoked and shall be void as if never granted. Use of materials as described in a revoked license, as well as any use of the materials beyond the scope of an unrevoked license, may constitute copyright infringement and publisher reserves the right to take any and all action to protect its copyright in the materials.

9. Warranties: Publisher makes no representations or warranties with respect to the licensed material.

10. Indemnity: You hereby indemnify and agree to hold harmless publisher and CCC, and their respective officers, directors, employees and agents, from and against any and all claims arising out of your use of the licensed material other than as specifically authorized pursuant to this license.

11. No Transfer of License: This license is personal to you and may not be sublicensed, assigned, or transferred by you to any other person without publisher's written permission.

12. No Amendment Except in Writing: This license may not be amended except in a writing signed by both parties (or, in the case of publisher, by CCC on publisher's behalf).

13. Objection to Contrary Terms: Publisher hereby objects to any terms contained in any purchase order, acknowledgment, check endorsement or other writing prepared by you, which terms are inconsistent with these terms and conditions or CCC's Billing and Payment terms and conditions. These terms and conditions, together with CCC's Billing and Payment terms and conditions (which are incorporated herein), comprise the entire agreement between you and publisher (and CCC) concerning this licensing transaction. In the event of any conflict between your obligations established by these terms and conditions and those established by CCC's Billing and Payment terms and conditions, these terms and conditions shall control.

14. Revocation: Elsevier or Copyright Clearance Center may deny the permissions described in this License at their sole discretion, for any reason or no reason, with a full refund payable to you. Notice of such denial will be made using the contact information provided by you. Failure to receive such notice will not alter or invalidate the denial. In no event will Elsevier or Copyright Clearance Center be responsible or liable for any costs, expenses or damage incurred by you as a result of a denial of your permission request, other than a refund of the amount(s) paid by you to Elsevier and/or Copyright Clearance Center for denied permissions.

LIMITED LICENSE

The following terms and conditions apply only to specific license types:

15. Translation: This permission is granted for non-exclusive world English rights only unless your license was granted for translation rights. If you licensed translation rights you may only translate this content into the languages you requested. A professional translator must perform all translations and reproduce the content word for word preserving the integrity of the article.

16. Posting licensed content on any Website: The following terms and conditions apply as follows: Licensing material from an Elsevier journal: All content posted to the web site must maintain the copyright information line on the bottom of each image; A hyper-text must be included to the Homepage of the journal from which you are licensing at http://www.sciencedirect.com/science/journal/xxxxx or the Elsevier homepage for books at http://www.elsevier.com; Central Storage: This license does not include

permission for a scanned version of the material to be stored in a central repository such as that provided by Heron/XanEdu.

Licensing material from an Elsevier book: A hyper-text link must be included to the Elsevier homepage at http://www.elsevier.com . All content posted to the web site must maintain the copyright information line on the bottom of each image.

Posting licensed content on Electronic reserve: In addition to the above the following clauses are applicable: The web site must be password-protected and made available only to bona fide students registered on a relevant course. This permission is granted for 1 year only. You may obtain a new license for future website posting.

17. For journal authors: the following clauses are applicable in addition to the above:

Preprints:

A preprint is an author's own write-up of research results and analysis, it has not been peer-reviewed, nor has it had any other value added to it by a publisher (such as formatting, copyright, technical enhancement etc.).

Authors can share their preprints anywhere at any time. Preprints should not be added to or enhanced in any way in order to appear more like, or to substitute for, the final versions of articles however authors can update their preprints on arXiv or RePEc with their Accepted Author Manuscript (see below).

If accepted for publication, we encourage authors to link from the preprint to their formal publication via its DOI. Millions of researchers have access to the formal publications on ScienceDirect, and so links will help users to find, access, cite and use the best available version. Please note that Cell Press, The Lancet and some society-owned have different preprint policies. Information on these policies is available on the journal homepage.

Accepted Author Manuscripts: An accepted author manuscript is the manuscript of an article that has been accepted for publication and which typically includes author-incorporated changes suggested during submission, peer review and editor-author communications.

Authors can share their accepted author manuscript:

- immediately

via their non-commercial person homepage or blog

by updating a preprint in arXiv or RePEc with the accepted manuscript

via their research institute or institutional repository for internal institutional uses or as part of an invitation-only research collaboration work-group

directly by providing copies to their students or to research collaborators for their personal use

for private scholarly sharing as part of an invitation-only work group on commercial sites with which Elsevier has an agreement

- after the embargo period

via non-commercial hosting platforms such as their institutional repository

via commercial sites with which Elsevier has an agreement

In all cases accepted manuscripts should:

- link to the formal publication via its DOI
- bear a CC-BY-NC-ND license - this is easy to do
- if aggregated with other manuscripts, for example in a repository or other site, be shared in alignment with our hosting policy not be added to or enhanced in any way to appear more like, or to substitute for, the published journal article.

Published journal article (JPA): A published journal article (PJA) is the definitive final record of published research that appears or will appear in the journal and embodies all value-adding publishing activities including peer review co-ordination, copy-editing, formatting, (if relevant) pagination and online enrichment.

Policies for sharing publishing journal articles differ for subscription and gold open access articles:

Subscription Articles: If you are an author, please share a link to your article rather than the full-text. Millions of researchers have access to the formal publications on ScienceDirect, and so links will help your users to find, access, cite, and use the best available version.

Theses and dissertations which contain embedded PJAs as part of the formal submission can be posted publicly by the awarding institution with DOI links back to the formal publications on ScienceDirect.

If you are affiliated with a library that subscribes to ScienceDirect you have additional private sharing rights for others' research accessed under that agreement. This includes use for classroom teaching and internal training at the institution (including use in course packs and courseware programs), and inclusion of the article for grant funding purposes.

Gold Open Access Articles: May be shared according to the author-selected end-user license and should contain a CrossMark logo, the end user license, and a DOI link to the formal publication on ScienceDirect. Please refer to Elsevier's posting policy for further information.
18. For book authors the following clauses are applicable in addition to the above: Authors are permitted to place a brief summary of their work online only. You are not allowed to download and post the published electronic version of your chapter, nor may you scan the printed edition to create an electronic version. Posting to a repository: Authors are permitted to post a summary of their chapter only in their institution's repository.
19. Thesis/Dissertation: If your license is for use in a thesis/dissertation your thesis may be submitted to your institution in either print or electronic form. Should your thesis be published commercially, please reapply for permission. These requirements include permission for the Library and Archives of Canada to supply single copies, on demand, of the complete thesis and include permission for Proquest/UMI to supply single copies, on demand, of the complete thesis. Should your thesis be published commercially, please reapply for permission. Theses and dissertations which contain embedded PJAs as part of the formal submission can be posted publicly by the awarding institution with DOI links back to the formal publications on ScienceDirect.

Elsevier Open Access Terms and Conditions
You can publish open access with Elsevier in hundreds of open access journals or in nearly 2000 established subscription journals that support open access publishing. Permitted third party re-use of these open access articles is defined by the author's choice of Creative Commons user license. See our open access license policy for more information.
Terms & Conditions applicable to all Open Access articles published with Elsevier:
Any reuse of the article must not represent the author as endorsing the adaptation of the article nor should the article be modified in such a way as to damage the author's honour or reputation. If any changes have been made, such changes must be clearly indicated.
The author(s) must be appropriately credited and we ask that you include the end user license and a DOI link to the formal publication on ScienceDirect.
If any part of the material to be used (for example, figures) has appeared in our publication with credit or acknowledgement to another source it is the responsibility of the user to ensure their reuse complies with the terms and conditions determined by the rights holder.
Additional Terms & Conditions applicable to each Creative Commons user license:
CC BY: The CC-BY license allows users to copy, to create extracts, abstracts and new works from the Article, to alter and revise the Article and to make commercial use of the Article (including reuse and/or resale of the Article by commercial entities), provided the user gives appropriate credit (with a link to the formal publication through the relevant DOI), provides a link to the license, indicates if changes were made and the licensor is not represented as endorsing the use made of the work. The full details of the license are available at http://creativecommons.org/licenses/by/4.0.
CC BY NC SA: The CC BY-NC-SA license allows users to copy, to create extracts, abstracts and new works from the Article, to alter and revise the Article, provided this is not done for commercial purposes, and that the user gives appropriate credit (with a link to the formal publication through the relevant DOI), provides a link to the license, indicates if changes were made and the licensor is not represented as endorsing the use made of the work. Further, any new works must be made available on the same conditions. The full details of the license are available at http://creativecommons.org/licenses/by-nc-sa/4.0.
CC BY NC ND: The CC BY-NC-ND license allows users to copy and distribute the Article, provided this is not done for commercial purposes and further does not permit distribution of the Article if it is changed or edited in any way, and provided the user gives appropriate credit (with a link to the formal publication through the relevant DOI), provides a link to the license, and that the licensor is not represented as endorsing the use made of the work. The full details of the license are available at http://creativecommons.org/licenses/by-nc-nd/4.0. Any commercial reuse of Open Access articles published with a CC BY NC SA or CC BY NC ND license requires permission from Elsevier and will be subject to a fee.
Commercial reuse includes:

- Associating advertising with the full text of the Article
- Charging fees for document delivery or access
- Article aggregation
- Systematic distribution via e-mail lists or share buttons

Posting or linking by commercial companies for use by customers of those companies.

- **Chapter 4**

Trans Tech Publications Ltd LICENSE TERMS AND CONDITIONS

This is a License Agreement between Mahsa Esfahani ("You") and Trans Tech Publications Ltd ("Trans Tech Publications Ltd") provided by Copyright Clearance Center ("CCC"). The license consists of your order details, the terms and conditions provided by Trans Tech Publications Ltd, and the payment terms and conditions.

All payments must be made in full to CCC. For payment instructions, please see information listed at the bottom of this form.

License Number	3981001330779
License date	Nov 02, 2016
Licensed content publisher	Trans Tech Publications Ltd
Licensed content title	Key Engineering Materials II
Licensed content date	Jan 1, 2012
Type of Use	Thesis/Dissertation
Requestor type	Author of requested content
Format	Print, Electronic
Portion	chapter/article
Number of pages in chapter/article	5
Title or numeric reference of the portion(s)	PAGE 1501-1505
Title of the article or chapter the portion is from	Effect of joining process on the coatings of self-piercing rivets
Editor of portion(s)	Fan/ Wu
Author of portion(s)	Mahsa Esfahani
Volume of serial or monograph.	488-489
Page range of the portion	1501-1505
Publication date of portion	2012
Rights for	Main product
Duration of use	Life of current edition
Creation of copies for the disabled	no
With minor editing privileges	yes
For distribution to	Worldwide
In the following language(s)	Original language of publication
With incidental promotional use	no
The lifetime unit quantity of new product	Up to 4,999
Made available in the following markets	Academic
The requesting person/organization is:	Mahsa Esfahani/ Swinburne University
Order reference number	
Author/Editor	Mahsa Esfahani
The standard identifier of New Work	PhD Thesis
The proposed price	Zero
Title of New Work	Surface Engineering of Hybrid Joints for Sub-Assembly
Publisher of New Work	Swinburne university of technology
Expected publication date	Dec 2016
Estimated size (pages)	245
Total (may include CCC user fee)	0.00 USD

TERMS AND CONDITIONS

The following terms are individual to this publisher:

None

Other Terms and Conditions:

STANDARD TERMS AND CONDITIONS

1. Description of Service; Defined Terms. This Republication License enables the User to obtain licenses for republication of one or more copyrighted works as described in detail on the relevant Order Confirmation (the “Work(s)”). Copyright Clearance Center, Inc. (“CCC”) grants licenses through the Service on behalf of the rightsholder identified on the Order Confirmation (the “Rightsholder”). “Republication”, as used herein, generally means the inclusion of a Work, in whole or in part, in a new work or works, also as described on the Order Confirmation. “User”, as used herein, means the person or entity making such republication.

2. The terms set forth in the relevant Order Confirmation, and any terms set by the Rightsholder with respect to a particular Work, govern the terms of use of Works in connection with the Service. By using the Service, the person transacting for a republication license on behalf of the User represents and warrants that he/she/it (a) has been duly authorized by the User to accept, and hereby does accept, all such terms and conditions on behalf of User, and (b) shall inform User of all such terms and conditions. In the event such person is a “freelancer” or other third party independent of User and CCC, such party shall be deemed jointly a “User” for purposes of these terms and conditions. In any event, User shall be deemed to have accepted and agreed to all such terms and conditions if User republishes the Work in any fashion.

3. Scope of License; Limitations and Obligations.

3.1 All Works and all rights therein, including copyright rights, remain the sole and exclusive property of the Rightsholder. The license created by the exchange of an Order Confirmation (and/or any invoice) and payment by User of the full amount set forth on that document includes only those rights expressly set forth in the Order Confirmation and in these terms and conditions, and conveys no other rights in the Work(s) to User. All rights not expressly granted are hereby reserved.

3.2 General Payment Terms: You may pay by credit card or through an account with us payable at the end of the month. If you and we agree that you may establish a standing account with CCC, then the following terms apply: Remit Payment to: Copyright Clearance Center, Dept 001, P.O. Box 843006, Boston, MA 02284-3006. Payments Due: Invoices are payable upon their delivery to you (or upon our notice to you that they are available to you for downloading). After 30 days, outstanding amounts will be subject to a service charge of 1-1/2% per month or, if less, the maximum rate allowed by applicable law. Unless otherwise specifically set forth in the Order Confirmation or in a separate written agreement signed by CCC, invoices are due and payable on “net 30” terms. While User may exercise the rights licensed immediately upon issuance of the Order Confirmation, the license is automatically revoked and is null and void, as if it had never been issued, if complete payment for the license is not received on a timely basis either from User directly or through a payment agent, such as a credit card company.

3.3 Unless otherwise provided in the Order Confirmation, any grant of rights to User (i) is “one-time” (including the editions and product family specified in the license), (ii) is non-exclusive and non-transferable and (iii) is subject to any and all limitations and restrictions (such as, but not limited to, limitations on duration of use or circulation) included in the Order Confirmation or invoice and/or in these terms and conditions. Upon completion of the licensed use, User shall either secure a new permission for further use of the Work(s) or immediately cease any new use of the Work(s) and shall render inaccessible (such as by deleting or by removing or severing links or other locators) any further copies of the Work (except for copies printed on paper in accordance with this license and still in User's stock at the end of such period).

3.4 In the event that the material for which a republication license is sought includes third party materials (such as photographs, illustrations, graphs, inserts and similar materials) which are identified in such material as having been used by permission, User is responsible for identifying, and seeking separate licenses (under this Service or otherwise) for, any of such third party materials; without a separate license, such third party materials may not be used.

3.5 Use of proper copyright notice for a Work is required as a condition of any license granted under the Service. Unless otherwise provided in the Order Confirmation, a proper copyright notice will read substantially as follows: “Republished with permission of [Rightsholder’s name], from [Work's title, author, volume, edition number and year of copyright]; permission conveyed through Copyright Clearance Center, Inc. ” Such notice must be provided in a reasonably legible font size and must be placed either immediately adjacent to the Work as used (for example, as part of a by-line or footnote but not as a separate electronic link) or in the place where substantially all other credits or notices for the new work containing the republished Work are located. Failure to include the required notice results in loss to the Rightsholder and CCC, and the User shall be liable to pay liquidated damages for each such failure equal to twice the use fee specified in the Order Confirmation, in addition to the use fee itself and any other fees and charges specified.

3.6 User may only make alterations to the Work if and as expressly set forth in the Order Confirmation. No Work may be used in any way that is defamatory, violates the rights of third parties (including such third parties' rights of copyright, privacy, publicity, or other tangible or intangible property), or is otherwise illegal, sexually explicit or obscene. In addition, User may not conjoin a Work with any other material that may result in damage to the reputation of the Rightsholder. User agrees to inform CCC if it becomes aware of any infringement of any rights in a Work and to cooperate with any reasonable request of CCC or the Rightsholder in connection therewith.

4. Indemnity. User hereby indemnifies and agrees to defend the Rightsholder and CCC, and their respective employees and directors, against all claims, liability, damages, costs and expenses, including legal fees and expenses, arising out of any use of a Work beyond the scope of the rights granted herein, or any use of a Work which has been altered in any unauthorized way by User, including claims of defamation or infringement of rights of copyright, publicity, privacy or other tangible or intangible property.

5. Limitation of Liability. UNDER NO CIRCUMSTANCES WILL CCC OR THE RIGHTSHOLDER BE LIABLE FOR ANY DIRECT, INDIRECT, CONSEQUENTIAL OR INCIDENTAL DAMAGES (INCLUDING WITHOUT LIMITATION DAMAGES FOR LOSS OF BUSINESS PROFITS OR INFORMATION, OR FOR BUSINESS INTERRUPTION) ARISING OUT OF THE USE OR INABILITY TO USE A WORK, EVEN IF ONE OF THEM HAS BEEN ADVISED OF THE POSSIBILITY OF SUCH DAMAGES. In any event, the total liability of the Rightsholder and CCC (including their respective employees and directors) shall not exceed the total amount actually paid by User for this license. User assumes full liability for the actions and omissions of its principals, employees, agents, affiliates, successors and assigns.

6. Limited Warranties. THE WORK(S) AND RIGHT(S) ARE PROVIDED “AS IS”. CCC HAS THE RIGHT TO GRANT TO USER THE RIGHTS GRANTED IN THE ORDER CONFIRMATION DOCUMENT. CCC AND THE RIGHTSHOLDER DISCLAIM ALL OTHER WARRANTIES RELATING TO THE WORK(S) AND RIGHT(S), EITHER EXPRESS OR IMPLIED, INCLUDING WITHOUT LIMITATION IMPLIED WARRANTIES OF MERCHANTABILITY OR FITNESS FOR A PARTICULAR PURPOSE. ADDITIONAL RIGHTS MAY BE REQUIRED TO USE ILLUSTRATIONS, GRAPHS, PHOTOGRAPHS, ABSTRACTS, INSERTS OR OTHER PORTIONS OF THE WORK (AS OPPOSED TO THE ENTIRE WORK) IN A MANNER CONTEMPLATED BY USER; USER UNDERSTANDS AND AGREES THAT NEITHER CCC NOR THE RIGHTSHOLDER MAY HAVE SUCH ADDITIONAL RIGHTS TO GRANT.

7. Effect of Breach. Any failure by User to pay any amount when due, or any use by User of a Work beyond the scope of the license set forth in the Order Confirmation and/or these terms and conditions, shall be a material breach of the license created by the Order Confirmation and these terms and conditions. Any breach not cured within 30 days of written notice thereof shall result in immediate termination of such license without further notice. Any unauthorized (but licensable) use of a Work that is terminated immediately upon notice thereof may be liquidated by payment of the Rightsholder's ordinary license price therefor; any unauthorized (and unlicensable) use that is not terminated immediately for any reason (including, for example, because materials containing the Work cannot reasonably be recalled) will be subject to all remedies available at law or in equity, but in no event to a payment of less than three times the Rightsholder's ordinary license price for the most closely analogous licensable use plus Rightsholder's and/or CCC's costs and expenses incurred in collecting such payment.

8. **Miscellaneous.**

8.1 User acknowledges that CCC may, from time to time, make changes or additions to the Service or to these terms and conditions, and CCC reserves the right to send notice to the User by electronic mail or otherwise for the purposes of notifying User of such changes or additions; provided that any such changes or additions shall not apply to permissions already secured and paid for.

8.2 Use of User-related information collected through the Service is governed by CCC’s privacy policy, available online here: http://www.copyright.com/content/cc3/en/tools/footer/privacypolicy.html.

8.3 The licensing transaction described in the Order Confirmation is personal to User. Therefore, User may not assign or transfer to any other person (whether a natural person or an organization of any kind) the license created by the Order Confirmation and these terms and conditions or any rights granted hereunder; provided, however, that User may assign such license in its entirety on written notice to CCC in the event of a transfer of all or substantially all of User’s rights in the new material which includes the Work(s) licensed under this Service.

8.4 No amendment or waiver of any terms is binding unless set forth in writing and signed by the parties. The Rightsholder and CCC hereby object to any terms contained in any writing prepared by the User or its principals, employees, agents or affiliates and purporting to govern or otherwise relate to the licensing transaction described in the Order Confirmation, which terms are in any way inconsistent with any terms set forth in the Order Confirmation and/or in these terms and conditions or CCC's standard operating procedures, whether such writing is prepared prior to, simultaneously with or subsequent to the Order Confirmation, and whether such writing appears on a copy of the Order Confirmation or in a separate instrument.

8.5 The licensing transaction described in the Order Confirmation document shall be governed by and construed under the law of the State of New York, USA, without regard to the principles thereof of conflicts of law. Any case, controversy, suit, action, or proceeding arising out of, in connection with, or related to such licensing transaction shall be brought, at CCC's sole discretion, in any federal or state court located in the County of New York, State of New York, USA, or in any federal or state court whose geographical jurisdiction covers the location of the Rightsholder set forth in the Order Confirmation. The parties expressly submit to the personal jurisdiction and venue of each such federal or state court.If you have any comments or questions about the Service or Copyright Clearance Center, please contact us at 978-750-8400 or send an e-mail to info@copyright.com.

v 1.1

- **Chapter 5**

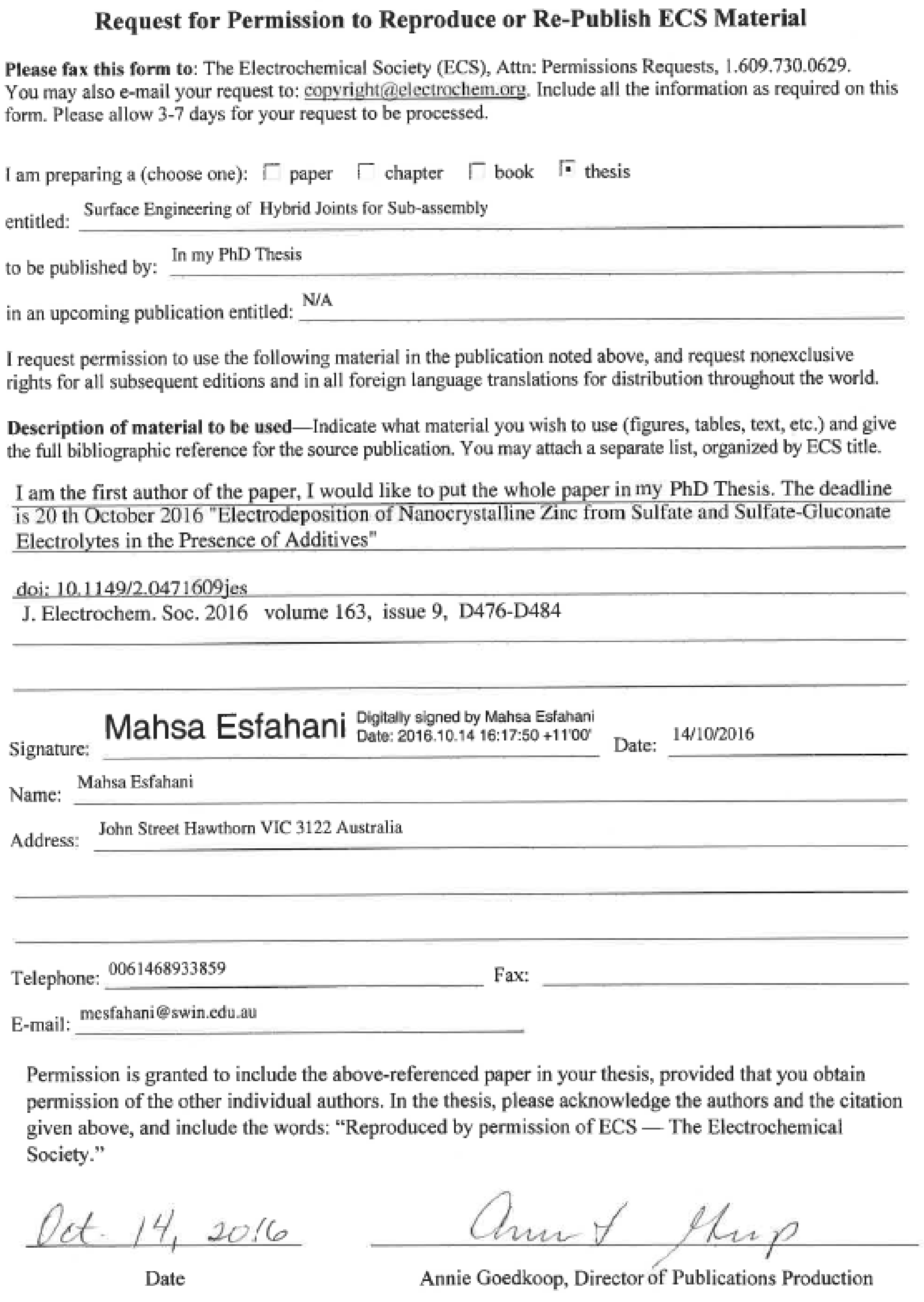

Request for Permission to Reproduce or Re-Publish ECS Material

Please fax this form to: The Electrochemical Society (ECS), Attn: Permissions Requests, 1.609.730.0629. You may also e-mail your request to: copyright@electrochem.org. Include all the information as required on this form. Please allow 3-7 days for your request to be processed.

I am preparing a (choose one): ☐ paper ☐ chapter ☐ book ☒ thesis

entitled: Surface Engineering of Hybrid Joints for Sub-assembly

to be published by: In my PhD Thesis

in an upcoming publication entitled: N/A

I request permission to use the following material in the publication noted above, and request nonexclusive rights for all subsequent editions and in all foreign language translations for distribution throughout the world.

Description of material to be used—Indicate what material you wish to use (figures, tables, text, etc.) and give the full bibliographic reference for the source publication. You may attach a separate list, organized by ECS title.

I am the first author of the paper, I would like to put the whole paper in my PhD Thesis. The deadline is 20 th October 2016 "Electrodeposition of Nanocrystalline Zinc from Sulfate and Sulfate-Gluconate Electrolytes in the Presence of Additives"

doi: 10.1149/2.0471609jes
J. Electrochem. Soc. 2016 volume 163, issue 9, D476-D484

Signature: Mahsa Esfahani Digitally signed by Mahsa Esfahani Date: 2016.10.14 16:17:50 +11'00' Date: 14/10/2016

Name: Mahsa Esfahani

Address: John Street Hawthorn VIC 3122 Australia

Telephone: 0061468933859 Fax:

E-mail: mesfahani@swin.edu.au

Permission is granted to include the above-referenced paper in your thesis, provided that you obtain permission of the other individual authors. In the thesis, please acknowledge the authors and the citation given above, and include the words: "Reproduced by permission of ECS — The Electrochemical Society."

Oct. 14, 2016
Date

Annie Goedkoop, Director of Publications Production

List of Publications

- M. Esfahani, J. Zhang, Y. Durandet, J. Wang, and Y. C. Wong, "Electrodeposition of nanocrystalline zinc from sulfate and sulfate-gluconate electrolytes in the presence of additives", Journal of the Electrochemical Society, vol. 163, pp. D476-D484, 2016.

- M. Esfahani, J. Zhang, Y. Durandet, J. Wang, and Y. C. Wong, "Effect of thiourea on the structure and corrosion properties of electrodeposited Zn-Sn", Annual Conference of the Australian Corrosion Association 2014: Corrosion and Prevention 2014.

- M. Esfahani, Y. Durandet, J. Wang, and Y. C. Won, "Effect of joining process on the coatings of self-piercing rivets", Advanced Materials Research, vol.488- 489, pp.1501-1505,2012.